DNA Nanotech: Expanding the repertoire of DNA for the assembly of nanoscale objects and electrical devices.

by

Richard P. Fahlman

B.Sc. (Honors), Simon Fraser University, 1996

THESIS SUBMITTED IN PARTIAL FULFILLMENT OF THE REQUIREMENTS FOR THE DEGREE OF DOCTOR OF PHILOSOPHY

in the Department of Molecular Biology and Biochemistry

SIMON FRASER UNIVERSITY

August 2001

Abstract

Much recent interest has focused on DNA as a material for the construction of objects and the templating of other materials on the nanometer to micrometer scale. Such constructions have made use of the recognition of "complementary" nucleotide sequence by single-stranded stretches of DNA in the formation of double helices. The ability of DNA double helices to act as a semi-conductor for electron transfer has opened more opportunities for using DNA in nanoscale devices. This work describes several advancements involving structural and functional aspect of DNA based nanotechnologies.

We have developed a new approach to assemble DNA nanostructures in a cation dependent manner. Association is via the formation of guanine quartets from two G·G mismatch domains within a duplex DNA framework. Association can be regulated by the addition or removal of cation species that promote guanine quartet formation (i.e. K^+ or Sr^{2+}). We have also demonstrated that these domains can be 'programmed' to be self-specific in mixed solutions by patterning the G·G mismatches into distinct domains.

We have evaluated the process of charge transfer through immobile DNA junctions. This work compares anthraquinone- and rhodium-based methods to induce charge transfer through DNA and identifies some pitfalls in one of the prominently used systems.

We have also demonstrated that the conformational transitions of folded DNA structures, more complex than simple double helical DNA, can be utilized in regulating charge transfer. We have successfully constructed 'electrical on/off switches' composed of DNA, which are modulated by the presence or absence of particular compounds in solution. Switches that are modulated by the small molecule adenosine and as well as ones modulated by short oligonucleotides have been assembled. The construction and demonstration of their operation now opens a new window of opportunity for the development of DNA detector systems, which could be directly coupled to microchips. Direct detection of molecules and nucleic acids in this fashion would result in techniques where target molecules can be immediately detected with very high sensitivity and specificity.

Dedication

To my family, my wife Dana and sons Richard and Orion for their motivation and patience.

Acknowledgments

I would like to express my appreciation and thanks to Dr. Dipankar Sen, for his support, passion for discovery and a willingness for endeavors outside of our research expertise.

I would also like to thank my supervisory committee, Dr. G. Agnes and J.W. Thewalt for their suggestions and advice throughout my degree.

I would like to thank the following for their contributions to this thesis.

Edward Venczel and Ron Geyer for there experience and training when I was starting on this whole endeavor.

Other past and present Sen Lab members for friendship, useful discussions and providing a fun and stimulating work place. Thanks, Dennis Wang, Anat Feldman, Dan Chinnapen, Paola Travascio and Ying Fu Li-*jeff*.

Carlo Sankar for his contributions with working on the cofactor independent DNAzyme, Na-8, in chapter 5.
Micheal Hsing and Caroline Sporer-Tuhten for there work on synapsable duplexes in chapter 4.

Dr. P. Wilson for providing space in his laboratory as well as helping with the synthesis of the compounds iisted in chapter 6.
I would also like to thank the members of the Wilson lab, especially Jay Cadiex for their help when I had difficulties with during synthesis.

Dr. R.D. Sharma and Dr. R.K. Pomeroy for useful discussions for the synthetic strategies for the assembly of the ruthenium and rhodium organo-metallic complexes.

Marcy Tracy for her help with NMR, and Kent Verge for running MS samples for me on his own time.

I would like to acknowledge the following for funding throughout my degree:

The Department of Molecular Biology and Biochemistry
Simon Fraser University
Natural Sciences and Engineering Research Council of Canada (NSERC).

Finally I would like to thank Dana Fahlman for her help in preparing this thesis.

Table of Contents

Page

List of Tables

List of Figures

Chapter 3: Self-Selective Synapsable Duplexes

Chapter 5: A New Secondary Model for the Na-8 DNAzyme

Chapter 6: Electron Transfer Agents

Part I

Introduction

"It has not escaped our notice that the specific pairing we have postulated immediately suggests a possible copying mechanism for the genetic material."

Watson & Crick (1953)

-From the original manuscript presenting the structure of double helical DNA

Chapter 1

Introduction – Thesis Overview

1. Central Role of DNA

The discovery of the structure of the DNA double helix by Watson and Crick outlined the role of DNA in modern life (Watson & Crick, 1953). The complementary nature of the base pairing between adenine and thymine (A-T) as well as guanine and cytosine (G-C), shown in figure 1-1, is the central basis for the replication of DNA double helices as well as for the transcription of RNA. The rules of complementary base pairing are such that each strand of a DNA double helix contains the 'blueprint' for the other. During DNA replication, the strands are separated and individual strands act as a template for the replication machinery in the formation of new complementary sequences. This ability makes DNA ideally suited as the heritable storage molecule for genetic information. Templating for nascent strand formation also allows information to be read from the DNA sequences by the translation of short sections of the genome (genes) into RNA, which is coded for in the same fashion as DNA with the exception of uracil replacing thymine, i.e. in A-U base pairs. Typically DNA in modern biology can be envisioned as long static strands of double helices, punctuated by episodes of replication, transcription, and recombination.

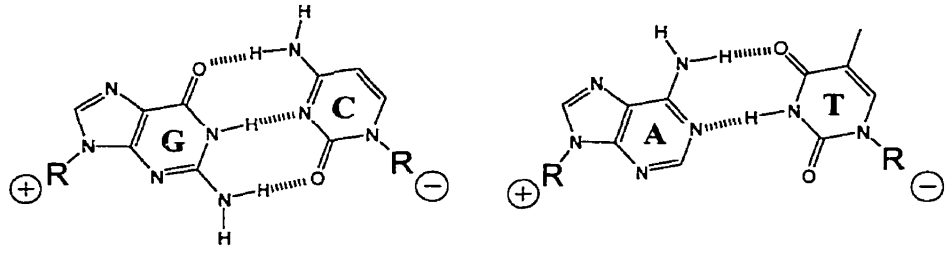

Figure 1-1. Watson and Crick base pairing. Strand polarity is indicated as (+) or (-), which represent the backbone going into or coming out of the plane, respectively.

1.1 Beyond the Gene

DNA, as a polymer, has the potential for a great deal more than simply being a depository of genetic material. If one extracts DNA from its evolutionarily determined role as the genetic storehouse of living organisms, its remarkable and novel properties can be realized and exploited *in vitro*. Given the opportunity, DNA can fold into complex structures and assemble into multi-unit assemblies and arrays. This ability of DNA to form complex tertiary structures has been applied in a variety of research areas. DNA sequences have been isolated that can fold into complex structures that possess catalytic (DNAzymes) and ligand binding (aptamers) abilities. DNA has also been utilized in the assembly of nano-scale objects: construction of various DNA-based three-dimensional objects of defined topology has been achieved (reviewed by Seeman, 1998). The property of sequence-complementarity recognition by individual DNA single-strands has been used to facilitate the organization of other materials, such as gold microbeads and quantum dots, into near-crystalline arrays (Mirkin *et al*, 1996; Alivisatos *et al*, 1996; Mucic *et al*, 1998; Loweth *et al*, 1999; Mitchell *et al*, 1999), and the targeting of

materials to surfaces that have been 'templated' with target DNA sequences (Taton *et al,* 2000). Two fundamental properties of DNA have made it especially suitable as a raw material for such nano-scale constructions: (a) highly specific recognition of sequence complementarity by individual DNA strands, and the assembly on that basis of two complementary strands into double helices, and (b) the fact that in aqueous solutions a DNA double helix (of < 150 base pairs) has the physical and hydrodynamic properties of a rigid rod.

Beyond the employment of DNA in the construction of structurally static objects and arrays, is a potential to generate structures with conformational variability. The potential for utilization of DNA structures capable of conformational changes has just recently been realized. The foundation of this methodology is based upon the influence of environmental conditions on DNA structures. Particular structures are only stable under specific solution conditions or in the presence of some type of regulator molecule. In cases where this is taken advantage of, DNA structures undergo a conformational change upon the addition or removal of appropriate stimuli. This structural 'switching' nature of DNA is now just beginning to be used in the development of various types of DNA-based sensors and mechanical devices. Currently this strategy has been successfully used in allosteric nucleic acid enzymes (reviewed by Soukup & Breaker, 2000) and for a B- to Z-DNA-based mechanical switch (described below).

The formation of useful (functional) DNA is profitably achieved by combining some common and not so common structural motifs. Examples of common DNA structural motifs, as well as some of their dynamic features, are summarized in the following section.

This thesis 'presents' DNA as the biopolymer of choice, but in most cases the related molecule, RNA, can be used. For technical reasons, DNA is the focus of this work.

2. DNA Structure

2.1 Structure of Double Helical DNA

As previously mentioned, in 'normal' situations (such as within a cell) DNA is found as double helices stabilized by Watson-Crick hydrogen bonding and by base stacking interactions. Double helical DNA itself has some degrees of structural variability. Under typical conditions of neutral pH and moderate (~physiological) salt concentrations, double helical DNA is typically a right-handed B-type helix, shown in figure 1-2. The B-type double helix is relatively sequence independent in that all DNA sequences can form it when the appropriate complementary sequence is available. All B-type helices possess relatively similar structures, but the micro details of these structures do vary and are typically responsible for the ability of DNA binding proteins to recognize particular DNA sequences. A few DNA sequences cause larger anomalies to the structure of B-type helices, such as intrinsic kinks or bends (reviewed by Crothers *et al,* 1990).

Another type of right-handed double helix that can be formed by DNA, which is also typical when DNA is hybridized to RNA, is the A-type helix. As seen in figure 1-2, this helix type is stouter than the B-type helix and there is an actual hole down the center of the helix. Another gross structural difference that can be seen in figure 1-2 is that the plane that the base pairs form is not at a 90° angle relative to the axis of the helix.

A third type of double helix, Z-DNA, is distinct from A and B –type helices because of its being left-handed (figure 1-2). Z-type helices require particular sequences, such as alternating purine-pyrimidine repeats, under relatively high ionic strength conditions in order to form (reviewed by Herbert & Rich, 1999). Z-type helices can also form under lower ionic strength conditions with certain chemically modified DNA sequences (Behe & Felsenfeld, 1981).

Under conditions that do not promote Z-type helix formation, a particular double helix will simply adopt a B-type conformation. The salt-dependent transition of B- to Z-DNA has been exploited in the construction of a DNA mechanical switch (Mao *et al,* 1999b). The basis of the structure was two DNA domains composing of double crossovers (double crossovers are discussed below) separated by a single connecting double helix consisting of GC^{5Me} (C^{5Me}- 5-methyl cytosine) repeats. The addition of sufficient Mg^{2+} or $Co(NH_3)_6^{3+}$ causes the conversion of the connecting right-handed B-DNA duplex into a left-handed Z-DNA duplex. Globally, this transition resulted in the two terminal double-crossover domains to rotate approximately 3.5 revolutions with respect to one another. This process was also shown to be reversible upon the removal of the inducing cation species.

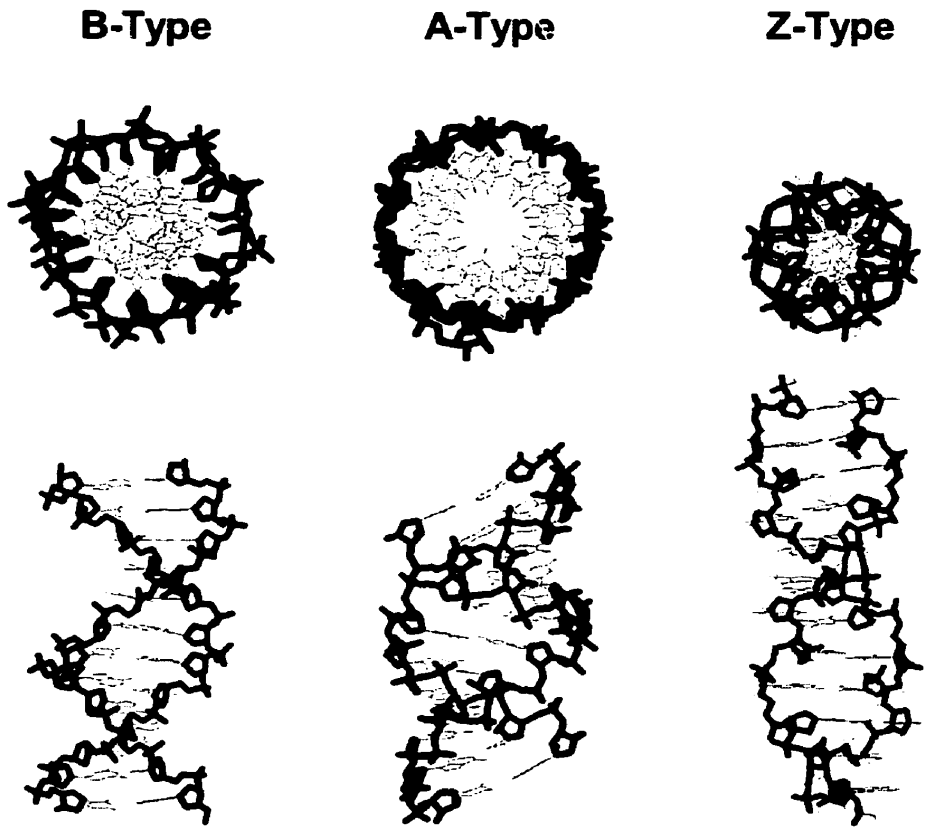

Figure 1-2. Structures of double stranded DNA. Backbones are highlighted to emphasize the contours of each type of double helix. Models were built from pdb files from the nucleic acid structure database[1].

Despite double stranded DNA not being one of the more complex and interesting structures that DNA can adopt, it is still the core structural unit for all alternative uses of DNA. Fundamentals of double helical DNA structure make it an ideal polymer in the design and assembly of nanostructures. The ability of single stranded DNA sequences to specifically and reliably self assemble into double helices, irrespective of nucleotide sequence, allows for enormous variability in the choices of sequences available in designing DNA-based structures.

[1] *(http://ndb.sdsc.edu/NDB/)*. Diagrams were constructed using these files on the freeware program RasMol *(http://www.umass.edu/microbio/rasmol/)*.

The rigidity of double helices also makes them well suited for the assembly of nanostructures. Rigidity allows duplex DNA to be used over appropriate distances. In aqueous solutions a DNA double helix has the physical and hydrodynamic properties of a rigid rod, with a persistence length of 28-35 nm (80-100 base pairs) in 1M sodium chloride [and substantially longer persistence lengths at lower salt (Hagerman, 1988)].

The localization of the bases in a continual stack in double helical DNA has also been demonstrated to facilitate the process of charge transfer down the double helix. The phenomena of charge transfer through double stranded DNA allows it to be used, potentially, as a 'nano-wire' of sorts.

2.2 DNA Structures of Higher Complexity

The double helical nature of DNA is the most globally known of its structures, and is described in detail in virtually all introductory biochemistry textbooks. Inclusion of mismatch base pairs, bulged bases, branched DNA structures and other conformations resulting from the folding of single stranded DNA, and the hybridization of partially complementary sequence, however result in an enormous variety of structures that DNA can in fact adopt.

Generally, such diverse and complex structures have been associated with cellular RNA. In the cell, RNAs are found as single stranded molecules, which fold to form various complex structures possessing a variety of functions, such as tRNA and ribosomal RNA. DNA is also capable of enormous structural diversity, provided it is given the opportunity. It has often been discussed that RNA has the potential to form more complex and functional structures than DNA because of the extra 2' -OH group on

RNA. The 2' -OH is indeed used is some structural motifs, but on a global scale RNA is yet to be proven to be superior in accomplishing particular tasks (ie catalysts and aptamers). In cases where comparable examples exist for each polymer that accomplish the same task, neither appears superior despite the use different folded structures to accomplish the given task. RNA and DNA aptamers that bind ATP have been reported which exhibit comparable binding affinities (Sassanfar & Szostack, 1993; Huizenga & Szostack, 1995). Rare examples also exist where the same sequence, either as RNA or DNA, performs the same function, as demonstrated with a sequence by Travascio *et al,* (1999) where a particular nucleotide sequence can assume the role of either a ribozyme or a DNAyme, both of which possess peroxidase activity. At the functional architectural level it has been shown that DNA can mimic some key biologically relevant RNA structures. One example involves the reconstruction of the $tRNA^{Phe}$ stem-loop using DNA (Basti *et al,* 1996). The sequence did require 2 modified bases in order to create the Mg^{2+} binding site and support successful binding to the ribosome. Modifications included a m^1G, which replaced the Y base in the tRNA stem loop, and a m^5C to complete the magnesium binding site. A requirement for modified bases to mimic the RNA structure did not in itself indicate a lack of ability on the part of DNA, given that tRNA possesses many modified bases itself. Some of these modifications include pseudouridine and inosine.

The folding of long single-stranded DNA sequences, as well as the association of partially complementary strands, can result in a variety of structures with diverse topologies. Samples of some common structural motifs are shown in figure 1-3.

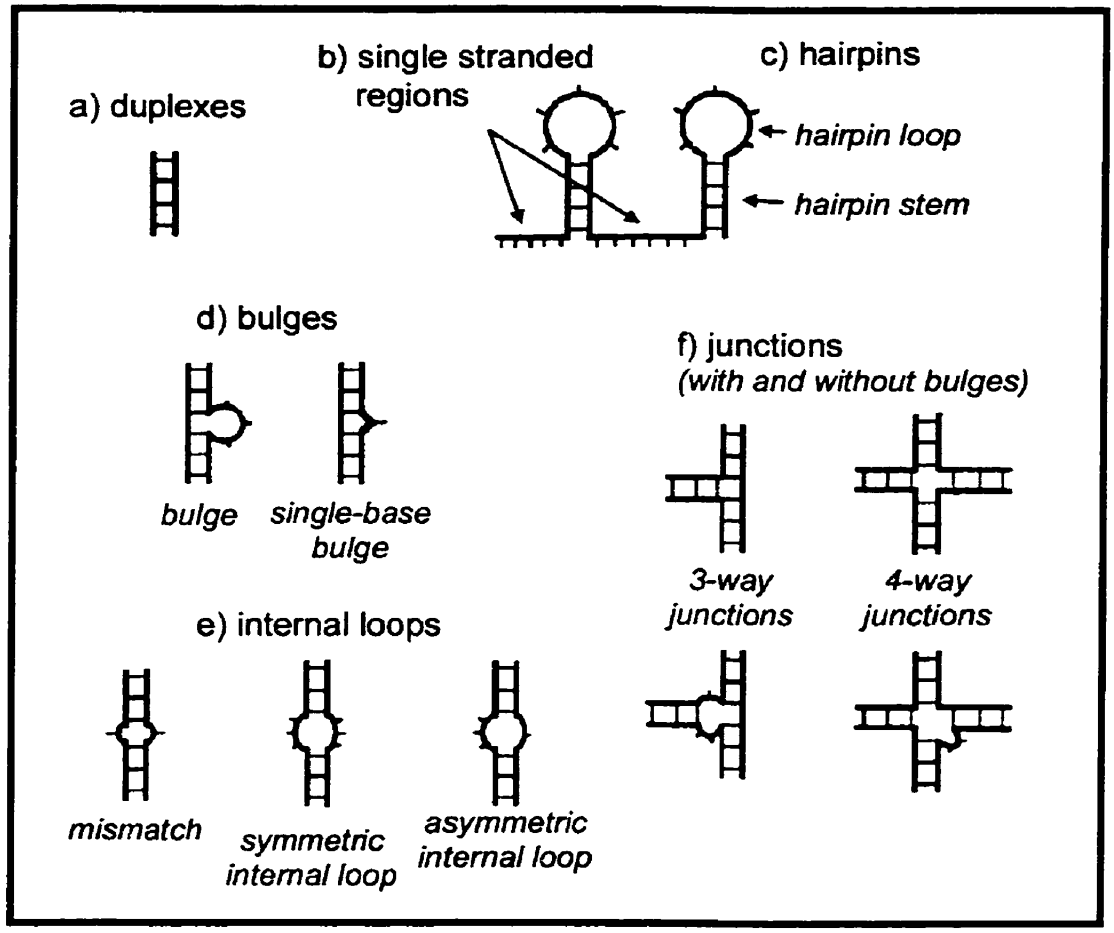

Figure 1-3. Some common DNA (and RNA) structural motifs. Structures depicted in d)-f) do not necessarily have to result from the association of multiple strands. The sequences can be linked by the incorporation of hairpin loops at the ends of duplex regions.

2.2.1 Hairpins and Single Stranded Regions

Single-stranded regions, as the name implies, are regions not involved in base pairing. Some single-stranded-regions that occur in particular contexts are classified as specific secondary structures or motifs such as loops and bulges described below. Other single-stranded regions that do not fall into discreet classes, or simply serve to separate various other domains (figure 1-3(b)), are simply referred to as single-stranded regions.

Beginning a brief examination of some common ways in which single-stranded DNA (or RNA) can fold, an obvious first way is when a single stranded sequence folds to form a duplex sequence with itself. This can occur when a sequence contains complementary regions. The resulting duplex possesses a turn or a fold back loop, which is typically termed a hairpin loop (figure 1-3c). The particular sequence in the hairpin loop can influence the stability of the adjoining duplex by forming a structurally stable hairpin loop stabilized by intra-loop hydrogen bonds and stacking interactions or not. Examples of such stable loops are "tetra loops". One class of stable tetra loops are composed of the 5'-YYYR-3' sequence.

2.2.2 Mismatches, Internal Loops and Bulges

The ability of single stranded DNA to form double helices when the two sequences are not perfectly complementary can result in a variety of structures. The duplex resulting from such an association may contain mismatch base pairs, bulges, or internal loops.

In the realm of biology, mismatches occasionally occur in a variety of mutagenic processes and cells have a variety of enzymatic systems to correct these, to reduce the frequency of deleterious affects caused by mismatches in genomic DNA (Mol *et al,* 1999; Aquilina & Bignami, 2001). In synthetic DNA constructs mismatches are interesting and prove useful in a variety of tasks.

Mismatches, as the name implies, are base pairs not of the correct Watson and Crick type. These typically perturb the structure of the B-type helix and destabilize the structure to some degree, depending on the identity of the mismatch. It is not that the

bases in a mismatch pair do not interact, but do so less efficiently than Watson and Crick base pairs. The base-base interactions that do form are typically called non-Watson-Crick base pairs. Several non-Watson-Crick base pairs are shown in figure 1-3, to demonstrate some of the variety possible in base-base interactions. A large variety of base-base interactions as well as base-sugar interactions have been documented in the analysis of complex RNA and DNA structures.

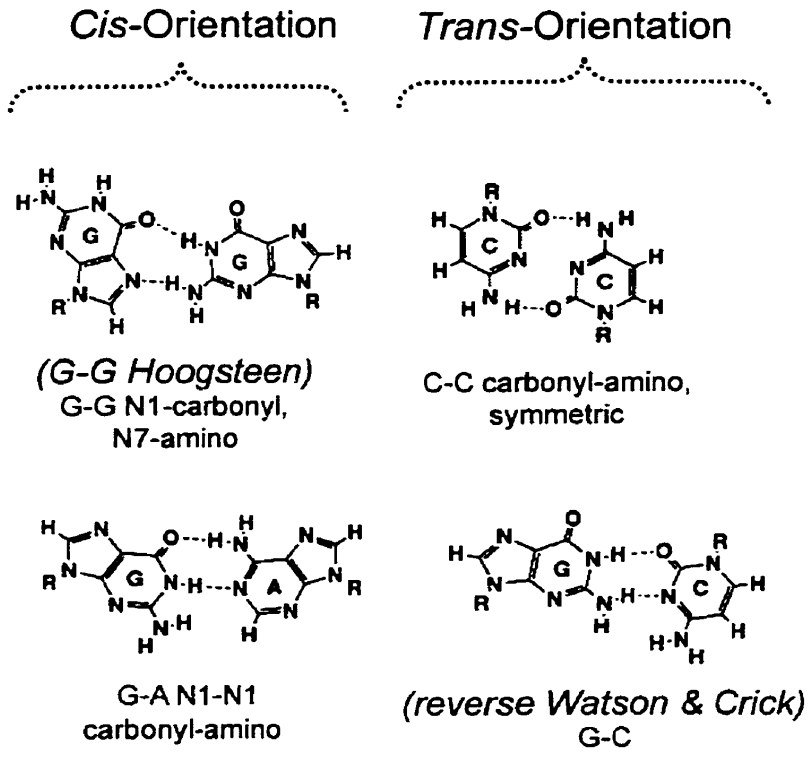

Figure 1-4. Examples of non-Watson & Crick base pairs. The non-conical base pairs can be in *cis* or *trans* configuration with respect to the position of the glycosidic bond relative to a line drawn parallel to the base-to-base hydrogen bonds. Structures from Tinoco (1993).

With the large variety known base interactions a new nomenclature system has been recently proposed in order to classify each type in order to aid in structure comparisons (Leontis & Westhof, 2001). The proposed nomenclature system is targeted

towards RNA but should apply directly to the description of DNA structures (with the obvious exceptions of structures that use the RNA's 2' hydroxy group).

With non-Watson-Crick base pairs and other DNA structures such as triplexes, the rotation of the glycosidic bond becomes important. The conventional base pairing in B-type DNA always ensures *anti* glycosidic bond conformations (figure 1-5) but in some mismatches and the left handed Z-type DNA, the *syn* conformation is also found. The variability of glycosidic bond conformation allows the base to use a non-Watson-Crick base pairing face to be used in base-pairing (ie in the G·G Hoogsteen base pair shown in figure 1-4) and for other interactions.

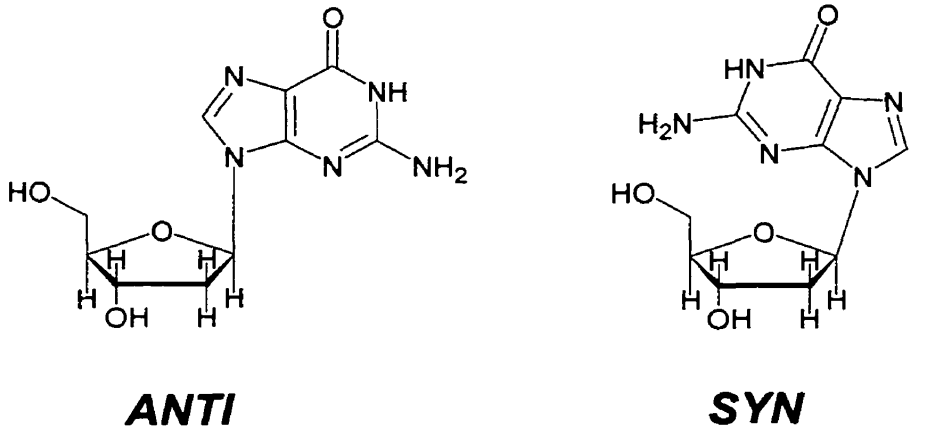

Figure 1-5. **Variability of the glycosidic bond angle. The normal orientation for Watson & Crick base pairs is having the base in the *anti* conformation.**

A mismatch does not have to be restricted to a single base pair within a double helix. More than one simple non-Watson-Crick base pair can be arranged in tandem, such that there are in equal or unequal numbers on each strand of the mismatch region. These regions of contiguous non-Watson and Crick base pairs are typically referred to as

a symmetric internal loop (figure 1-3(e)). In cases where one participating DNA strand contains more bases in the loop than the other strand, an asymmetric loop is formed (figure 1-3(e)). Depending on the sequence content of the loops they can introduce functionality to a duplex.

In chapters 2 to 4, I have utilized DNA duplexes that contain tandem guanine-guanine (G·G) and thymine-thymine (T·T) mismatches in internal loops. These G·G mismatches allow the duplexes to dimerize and form 'synapsed' duplexes. Another DNA construct utilized in chapter 7 that possesses an internal loop is the ATP aptamer. This DNA sequence binds adenosine and ATP with high affinity.

A variation in internal loops occurs when one of the two strands possesses no unpaired bases, so that the loop consists of bases from only one strand. In essence, the resulting structure is an asymmetric internal loop but this special case is termed a DNA bulge (figure 1-3b). The additional base(s) on the one strand causes the helix to bend in a predictable manner, depending on the number of bases in the bulge (reviewed in Lilley, 1995). Incorporation of bulged DNA allows for predictable kinks to form in the DNA double helix, which also disrupts the base stacking through the helix at the kinked site.

2.2.3 Branched DNA

An alternative to sequences that form double helices with internal disruptions, such as loops and bulges, is where only one end of a sequence base pairs with another sequence. The remaining non-base paired region is then free to base pair with a third sequence. If this third sequence is capable of forming double helical regions with both of

the two original sequences, then a 3-Way junction can be formed (figure 1-3f). This strategy can be applied also to construct 4-Way and higher order junctions.

Four-way junctions are intermediates in genetic recombination, known as Holliday junctions (Holliday, 1964). The branch points in these biologically relevant junctions are flanked by sequences of homologous symmetry. This symmetry permits an isomerization event known as branch migration (Hsieh & Panyutin, 1995).

Instability of the branch point locus in natural four-way junctions impedes their use for stable nanoscale constructions. To circumvent this problem it has been necessary to eliminate symmetry within the system, thus immobilizing the locus of the junction (Seeman, 1982).

In moderate ionic strength solutions the extended 4-way junction structure (figure 1-6a) folds such that the arms stack to give two coaxially stacked helices, structures b) - d). Typically parallel structures, like 1-6b, or the alternate variant in which arms α and γ along with β and χ form the stacked pairs, do not form unless the structure is constrained to prevent the formation of anti-parallel structures. Examples of how 4-way junctions can be constrained in the different conformations were demonstrated by Kimball *et al* (1990). A particular junction prefers one of the two anti-parallel junction conformers, c) or d), depending on the particular bases located at the junction (Duckett *et al*, 1988).

The tertiary structure of these junctions resembles an 'X'-like shape, as demonstrated in the insert of figure 1-6.

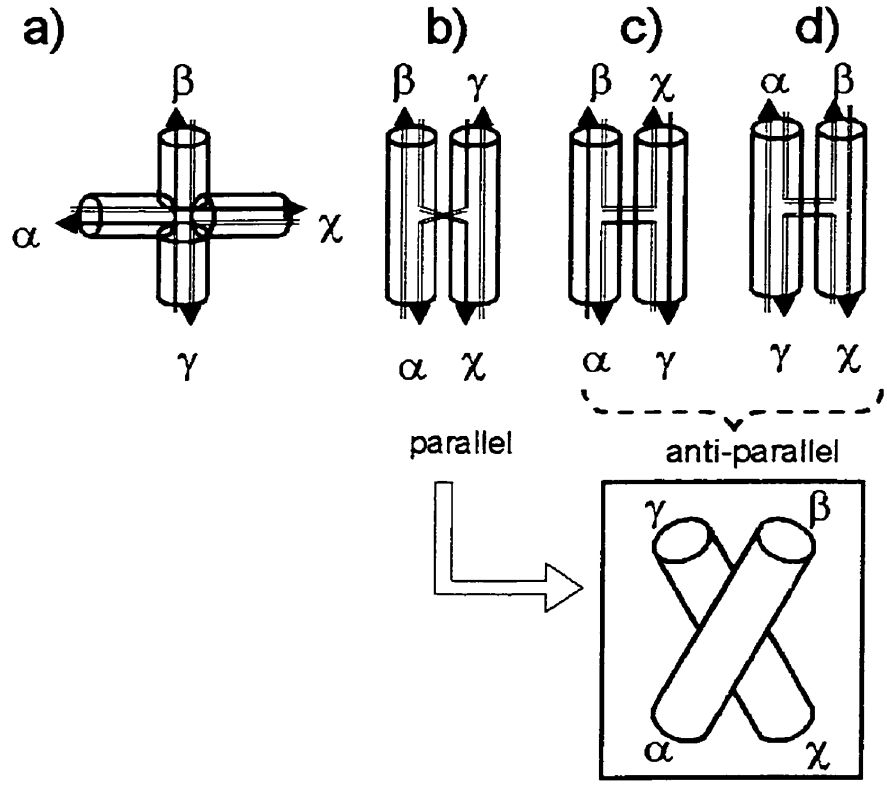

Figure 1-6. Stacking in 4-Way Junctions. a) A 4-way junction in an open conformation. In the presence of appropriate cation concentrations the structure folds such that the arms of the junction coaxially stack to form favorable base stacking interactions. Various parallel (b) and anti-parallel junctions (c&d) exist. Typically 4-way junctions form anti-parallel structures unless forced by some other constraint. The resulting stacking c) vs d) depend upon the specific sequence composition at the junction. The lower insert is to indicate that even though the figures show the 4-way junctions with the coaxially stacked arms in parallel, they are in fact at an angle to each other, in an 'X' like structure.

The use of DNA in the construction of geometric objects has been pioneered by Seeman (for an account of this work see the article by Nadrian Seeman (2000)), who has described objects with the topologies of, for instance, a tetrahedron (Chen & Seeman, 1991), a truncated octahedron (Zhang & Seeman, 1994), and Borromean rings (Mao *et al,* 1997). The modules for such constructions were stable three-way and four-way

immobile junctions of DNA duplexes where they play the role of vertices in the structures. Each double helical arm of such a junction terminated in a short stretch of single-stranded DNA of defined sequence (a "sticky end"), which was used to bind, on the basis of precise sequence complementarity, to the sticky ends of other three- or four-way junctions. More recently, Seeman has utilized a more rigid structural unit, the DNA "double-crossover", composed of two closely spaced four-way junctions (figure 1-7), to assemble two-dimensional quasi-crystalline arrays (Winfree *et al,* 1998; Liu *et al,* 1999; Mao *et al,* 1999).

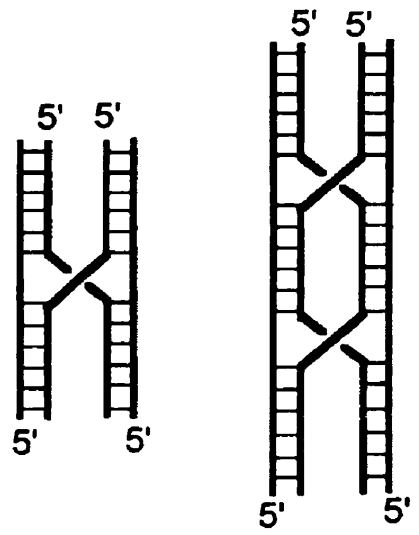

Figure 1-7. Structure of double crossovers. On the left is a traditional four-way junction and on the right is the stable double crossover, which is the fusion of two four-way junctions.

2.2.4 Other Structures

The previously mentioned structures are but a sampling of the defined structures that different DNA (& RNA) can adopt. Other associations, or structural motifs, not mentioned in this manuscript include triplexes, i-tetraplexes and pseudoknots, to name a few.

2.3 Guanine Quartets

Another alternate form of base-base interaction, which is particularly relevant to this work, are guanine quartets (G-quartets). G-quartets result from the ability of guanine bases to self-associate to form a very stable planar structure. The arrangement is of four guanine bases in a plane, held together by Hoogsteen bonding to form a guanine quartet (G-quartet), as shown in figure 1-8a. G-quartets are known to form from various guanine rich DNA (Sen & Gilbert, 1988; Williamson *et al*, 1989) and RNA (Kim *et al*, 1991) sequences. Two such contiguous G-quartets form a central cation-binding site that must be occupied to stabilize the structure (figure 1-8(b)). Guanine quartets thus have the unusual property among nucleic acid higher-order structures that they require specific group Ia or IIa metal ions to support their formation. This is due to a requirement for size-specific binding of an appropriate monovalent or divalent cation into the cavity between successive layers of G-quartets (reviewed by Williamson, 1994; Wellinger & Sen, 1997), where the metal ion coordinates in an eight-fold fashion to keto-oxygen atoms from the two participating guanine quartets. The ease with which a given cation fits into the above-mentioned cavity reflects a balance between the ease of desolvation of the ion and the favorable interactions formed between the ion and the keto-ligands from

the quartets (Hud *et al.*, 1996). Of the group Ia and IIa cations, K^+ and Sr^+ function most optimally to stabilize G-quartets, whereas Na^+, Rb^+, Ca^{2+} and Ba^{2+} are less optimal (and Li^+, Mg^{2+}, and Cs^+ are generally ineffective). The thalious ion, Tl^+, has also been demonstrated to support the formation of G-quartets (Basu *et al*, 2000), and there is also evidence for the lead cation, Pb^{2+} as well (Smirnov & Shafer, 2000).

The requirement for specific ion species to facilitate the formation of guanine quadruplex structures gives us a handle to regulate their formation. Controlling formation or disassociation by adding or removing specific cation species makes quadruplexes attractive elements to be used in nanoscale assemblies.

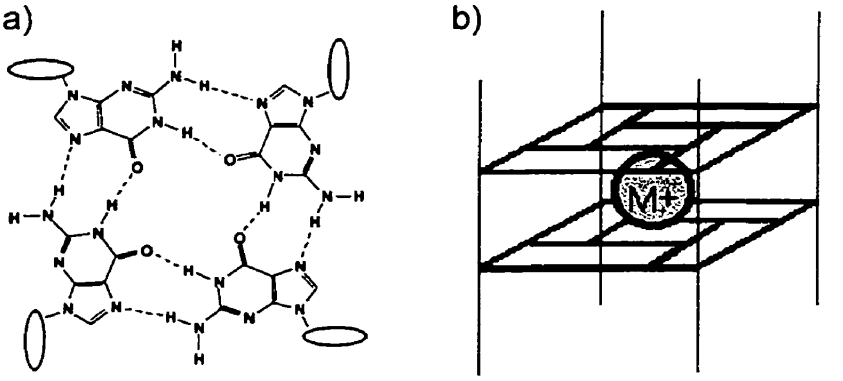

Figure 1-8. Guanine quartets. a) Diagram of a guanine quartet demonstrating the H-bonding between guanines. The sugar phosphate backbones are indicated as ovoid shaped. b) A schematic demonstrating the cation-binding site formed between two successive G-quartets.

Guanine quadruplexes, extended helical structures containing G-quartets, can be structurally diverse (reviewed by Simonsson, 2001). As seen in figure 1-9, the same sequence can form a variety of different quadruplex conformers. The sequence

GGGTTTGGG is capable of forming tetramers with all of the stands in a parallel orientation with respect to their sugar phosphate backbones as depicted in figure 1-9(a). The same sequence is also capable of forming a variety of dimer species, with the backbones of the strands in a variety of anti-parallel orientations, structures b) - d). In certain cases solution conditions can dictate the preference of one structure over another, as observed by Sen & Gilbert (1990). Longer single stranded sequences containing several guanine repeats are also capable of forming a variety of intra-molecular G-quadruplexes, structures e) - g). Again, the variability of these sequences arise from the directionality of the DNA backbone.

Of all the diverse possibilities of G-quadruplex structures that can potentially form from some sequences, the all-parallel structure (figure 1-9a) is the most thermodynamically favorable (Sen & Gilbert, 1990). The other various anti-parallel structures arise because they are stable kinetic traps that form more quickly than the all-parallel structures. Parallel structures require the association of four strands while the other types are dimers or intra-molecular structures.

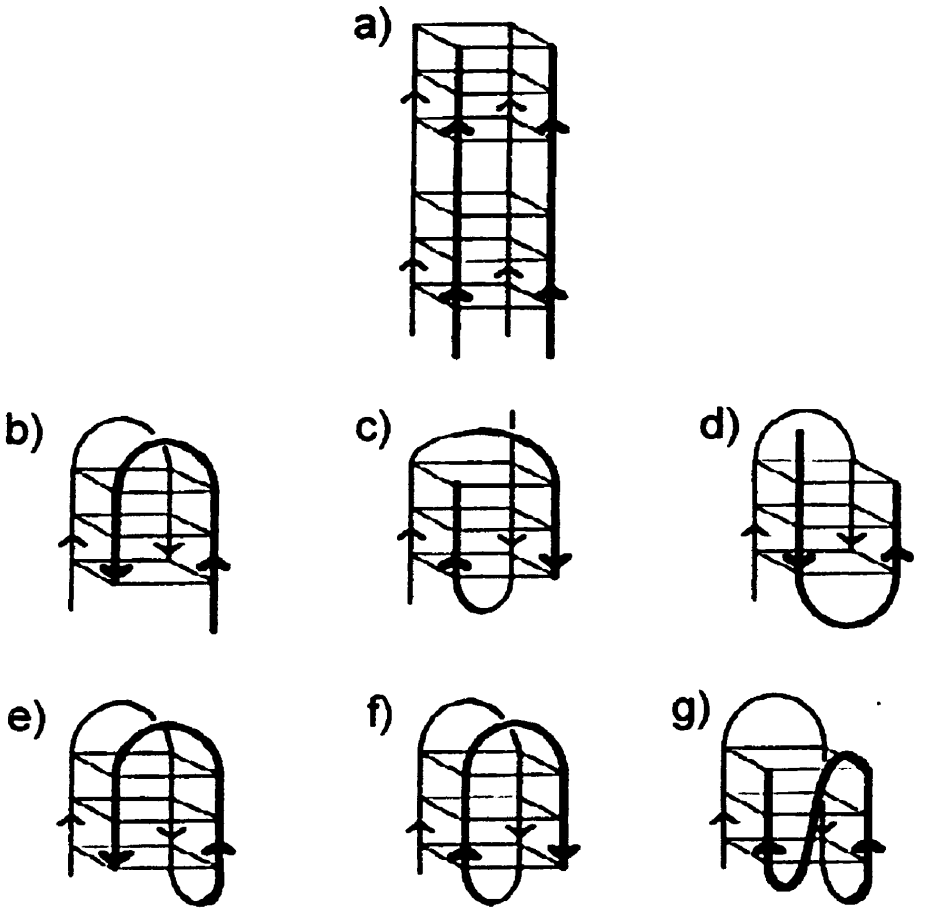

Figure 1-9. **Structural diversity of guanine quadruplexes (Wellinger & Sen, 1997). a) An all-parallel guanine quadruplex. b) - d) Anti-parallel guanine quadruplex structures. e) - g) Structures containing intra-molecular G-quartets.**

3. Thesis overview

This manuscript is composed of five parts, with this general introduction and conclusion constituting two of the parts. Parts II-IV are composed of a compilation of research from three distinct research areas. The underlying theme, is that all three parts describe novel, and non-genetic applications of DNA

Three 'alternative' roles of DNA covered in this manuscript include: 1) DNA nanostructures, 2) Catalytic DNA or DNAzymes and 3) Electron transfer through DNA.

Part II includes a body of work pertaining to the construction of nano-scale objects from DNA. In particular, this work revolves around the formation of nanostructures utilizing a guanine-quartet (G-quartet) framework. The system we have been working with are "synapsable duplexes", which are double stranded DNA constructs containing G·G mismatches. The mismatches can be induced to form G-quartets by the addition of appropriate cations to the solution. Work on this system has been aimed at the development of *self*-selectivity in the system. Most of the information in chapters two and three has been published at the time of writing this thesis (Fahlman & Sen, 1998 & 1999), while the work in chapter four is currently unpublished work.

Part III is a brief section on catalytic DNA. I have been involved in refining the secondary structure of a DNAzyme known as Na-8. Na-8 was originally isolated and reported by a former student in our laboratory, Ron Geyer (Geyer & Sen, 1997). This section gives a brief introduction to catalytic DNA as well as the presentation of a new proposed secondary structure model for the Na-8 DNAzme.

Part IV covers our work on charge transfer through DNA. The main objective of our work in this area is the examination of charge transfer through branched DNA

structures as well as the development of DNA assemblies that can regulate the process of charge transfer. This aspect significantly contrasts with the work of others, who mainly examine the process of charge transfer through double stranded DNA in trying to determine the much disputed mechanism and efficiency of the process through DNA.

Part II

'Synapsable' DNA
Guanine Quartet Based Nanostructures

Chapter 2

Cation Specific Synapsable Duplexes

1. Introduction

1.1 Alternate DNA Nanostructure Design

A majority of the published work on using DNA as a material in nanostructure construction is based upon two main designs as discussed in chapter 1. *1)* The association of single stranded DNA sequences into double helices. *2)* Branch points or structural junctions based upon immobile junctions.

There has been some pursuit of other strategies or structural motifs in the assembly of DNA and RNA superstructures. The development and evaluation of other methods can greatly increase the variety and complexity of DNA structures that can be designed and assembled. Tertiary structural motifs found in the naturally occurring ribozymes have been shown to be effective in RNA based assemblies (Jaeger & Leontis, 2000; Jaeger *et al*, 2001). The *self*-association of guanine bases in the formation of G-quartets (figure 2-1a) has also been shown to form long linear polymeric structures (Sen & Gilbert, 1992; Marsh & Henderson, 1994) and higher order arrays (Chen, 1995).

1.2 Synapsable DNA

We have recently described a quite different paradigm for the stable self-association of two DNA double helices, that does not exploit sticky-end complementarity. This methodology involves a side-by-side association, or "synapsis", of two DNA duplexes, at pre-determined "synapsable" sites constructed within them

(Figure 2-1(a)). Unlike single-stranded DNA, standard DNA duplexes have little ability to interact with one another. Two duplexes do not have significant shape complementarity; and the DNA bases with their hydrogen-bonding and π-stacking ability, are fully base-paired in a Watson Crick sense (A=T; G≡C) in the interior of the double helix; and that the sugar-phosphate backbones of duplexes possess high (and therefore mutually repulsive) negative charge densities. However, the simple innovation of introducing a stretch of contiguous guanine-guanine mismatch base-pairs (called a "G-G domain") into an otherwise standard Watson-Crick base-paired duplex (shown schematically in figure 2-1(a)) has been shown to enable a stable side-to-side association and binding of two such duplexes, under physiological and near-physiological conditions of temperature and salt (Venczel & Sen, 1996). A DNA duplex incorporating a G-G domain is referred to as a "synapsable" DNA duplex. Two such duplexes are able to dimerize via synapsis of their respective G-G domains to form "duplex dimers", held together by the very stable hydrogen-bonded arrangement of guanine bases in G-quartets (Figure 2-1b) (Venczel & Sen, 1996).

Utilization of G-quartets in the framework of double stranded DNA limits the potential conformations of G-quadruplex structures that form. This restriction allows for a more predictable formation and allows for the use of G-quartets in more highly defined structures than previously reported.

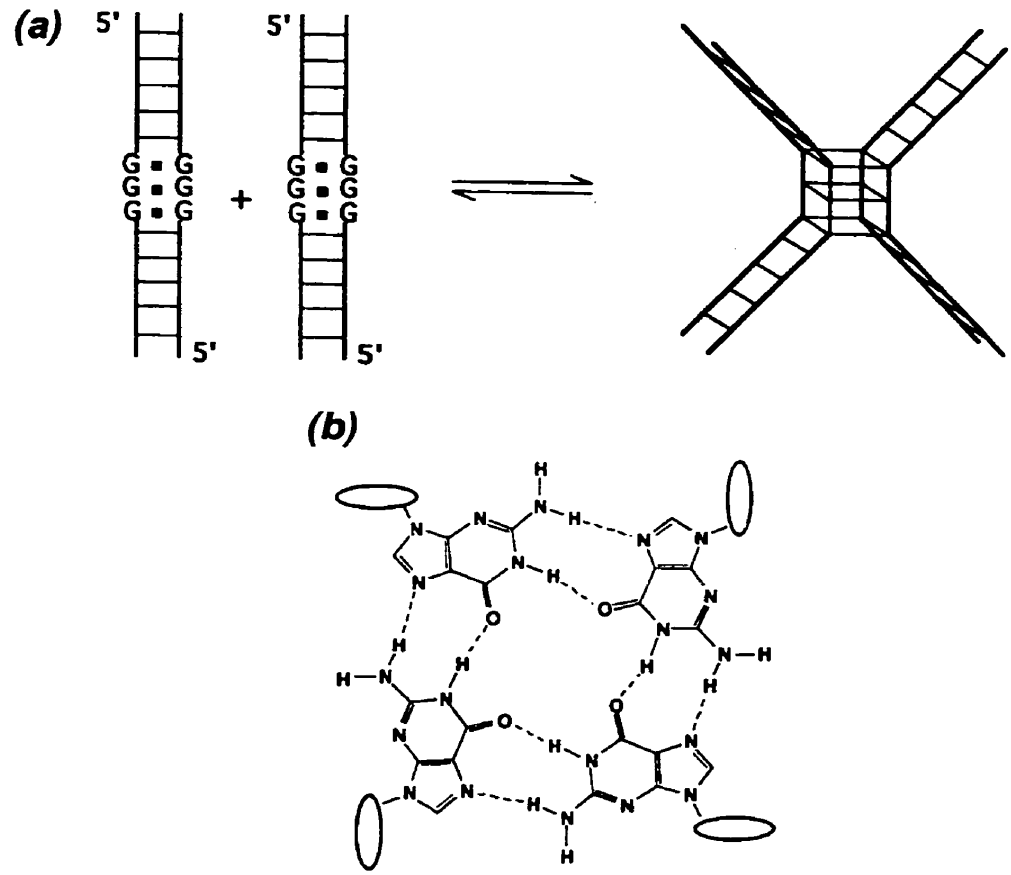

Figure 2-1. Synapsable DNA. (a) Schematic of the dimerization of two duplexes containing G·G mismatches in the formation of a synapsed duplex. (b) A guanine quartet, the structure responsible for the association of the synapsable duplex.

In other contexts, the formation of guanine-quartets and guanine-quadruplexes (DNA structures composed of, or containing, guanine-quartets) in aqueous solutions has been shown to be favored by the presence of specific Group IA and IIA cations, notably potassium and strontium (and, less effectively, by sodium and rubidium; calcium and barium), which bind within the cavity formed between two adjacent guanine-quartets (Williamson, 1994; Wellinger & Sen, 1997). The dimerization of synapsable duplexes

was also found to follow this general trend (Venczel & Sen, 1996). Given that different Group IA and IIA cations differentially stabilized the duplex-dimers (for instance potassium was strongly stabilizing; whereas lithium was not), the assembly and disassembly of superstructures built with duplex-dimer modules might in principle be achievable by simply changing the cation present in solution - for instance, replacing 0.5 M Li^+ for 0.5 M K^+, and *vice versa*.

1.3 Parallel G·G Domains

We wished to investigate whether it might be possible to generate more than one class of synapsable domain within duplexes, such that each class was able to distinguish "self" from "non-self". This was one major goal of my thesis work in order to design domains that would recognize their correct pair even in mixed solutions, such that multiple domains could be used in the assembly of DNA nanostructures.

The original synapsable domain, A·B, shown in figure 2-2(a) has strands running conventionally anti-parallel to each other. The anti-parallel G·G mismatch containing duplex was originally used by Venczel & Sen (1996) in the initial demonstration of the formation of synapsed duplexes. The dimerization of A·B would necessarily have strand orientations in $(A{\cdot}B)_2$, that were anti-parallel (figure 2-2(b), structure *j*), or partially anti-parallel (structure *k*).

As previously mentioned in chapter 1, it has been found as a rule that G-quadruplexes in which all four participating strands lie in a parallel orientation are more thermodynamically stable than complexes that have their strands in an antiparallel or partially antiparallel orientation (Sen & Gilbert, 1990; Lu *et al*, 1993). If it were possible

to generate a synapsed complex with a purely parallel orientation of strands in the synapsed region, such a complex may have superior stability to that of $(A{\cdot}B)_2$.

We chose to generate a parallel strand- orientation of the G·G mismatch base pairs within an otherwise anti-parallel Watson and Crick duplex by introducing 5'-5' and 3'-3' phosphodiester linkages at the borders of the guanine-motif within one of the constituent strands (strand β) in the duplex. The resulting duplex, A·β, is shown in figure 2-2(a). The synapsed complex produced by the A·β duplex would be expected to have parallel quadruplex strand orientations, as shown for structure *l* in figure 2-2(b) (in theory, a partially parallel complex, similar to structure *k*, could form, but we would expect the purely parallel quadruplex to form from thermodynamic considerations). Our goals were therefore to determine whether the duplex A·β would indeed dimerize or synapse to form $(A{\cdot}\beta)_2$ and whether the conditions for such synapsis would be different from that found for A·B. A comparison of the relative stabilities of the complex $(A{\cdot}B)_2$ and that of the putative $(A{\cdot}\beta)_2$ was done to determine whether $(A{\cdot}\beta)_2$ was indeed more stable than $(A{\cdot}B)_2$. Finally, we wished to determine whether the synapsis of A·B and potential synapsis of A·β were selective in mixed solutions.

(a)

Duplex A·B

5′ GTGACTCGAGAAGCTCCTGAGGGGGGGGGTGTGGTTCAAGGATCCACAG
CACTGAGCTCTTCGAGGACTGGGGGGGGGACACCAAGTTCCTAGGTGTC5′

Duplex A·β

5′GTGACTCGAGAAGCTCCTGA-----GGGGGGGG-----TGTGGTTCAAGGATCCACAG
CACTGAGCTCTTCGAGGACT5′-5′GGGGGGGG3′-3′ACACCAAGTTCCTAGGTGTC5′

(b)

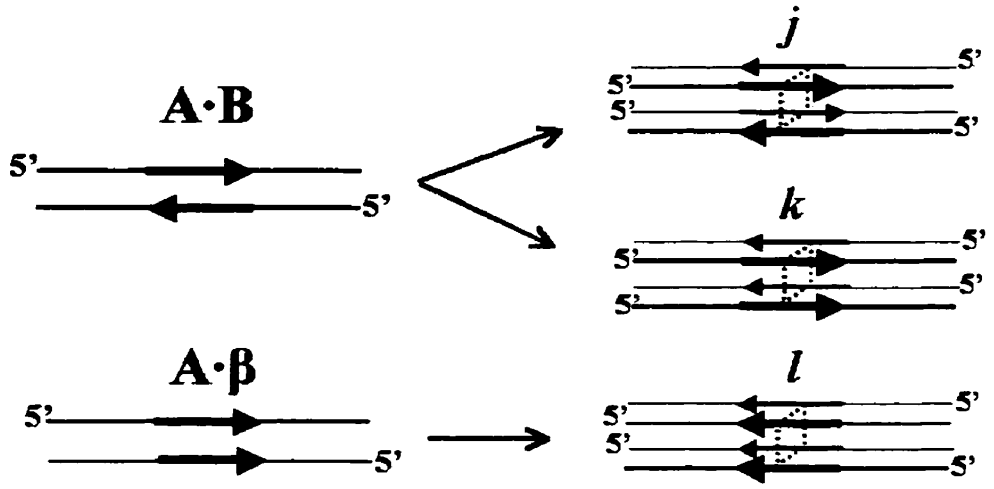

Figure 2-2. **Synapsable duplex design. (a) Sequences for the synapsable duplexes A·B and A·β. (b) Anticipated strand orientations for the synapsed duplexes $(A{\cdot}B)_2$ and $(A{\cdot}\beta)_2$. Arrows in the synapsable domains indicate strand polarity (5' → 3').**

2. Materials and Methods

2.1 DNA Synthesis and Purification

The three DNA sequences used to construct the two duplexes, A·B and A,·β, are shown in figure 2-2(a). The oligomers were synthesized at the University of Calgary Core DNA Services; the dG-5'-CE phosphoramadite for the eight "reversed polarity" guanine resides in the β strand were purchased from Glen Research. The oligomers were dissolved in 35 µl of denaturing gel loading buffer plus 5 µl 80 mM LiOH, and treated at 95°C for three minutes to break down any pre-formed G-quadraplex complexes. The oligomers were then size-purified in 8% (w/v) denaturing polyacrylamide gels. Eluted samples were filtered through 0.2 µm micro filters and then desalted and concentrated using C-18 Spice Columns (Analtech). The lyophilized, pure DNA pellets were finally suspended in 50 µl TE (10 mM Tris-Cl, pH 8.0, and 0.1 mM EDTA) buffer. The 5' end-labeling with [γ-^{32}P]ATP was done using standard kinasing procedures. Ethanol precipitations, were they carried out, always were made up to 0.3 M LiCl (rather than NaCl) to discourage the formation of G-quadraplex structures.

2.2 Double-Stranded DNA Preparation

The duplexes, A·B and A·β, were assembled by mixing in water at room temperature, 500 pmol of a given oligomer with 470 pmol of unlabeled and 20 pmol of a ^{32}P-labeled complimentary sequence. The combined oligomers were then made to 50 mM tetramethyl ammonium chloride (TMACl), heated to 95°C, and allowed to cool slowly to 30°C. The crude duplex samples were loaded in an 8% native polyacrylamide gel, run in 50 mM Tris-borate, (pH 8.0), 1 mM $MgCl_2$, and 10 mM TMACl, at room temperature.

Duplex bands were detected by autoradiography, cut out, and eluted over night with TMACl buffer (50 mM TMACl, 10 mM Tris-Cl buffer, (pH 7.5), and 0.1 mM EDTA).

2.3 Formation of Synapsed Duplexes

Double-stranded DNA samples, as prepared above, were diluted with TMACl buffer to a final concentration of 5 μM duplex. Samples (5 μl) of such DNA duplex solutions were combined with 5 μl of various salt solutions and incubated at 37°C for 20 hours. Tightly sealed tubes were used throughout and the tubes were fully submerged in water during incubations to prevent changes in the sample volume from evaporation and condensation. Aliquots from each sample were then removed, combined with standard non-denaturing loading buffers and run in 8% native polyacrylamide gels in KMg buffer (50 mM Tris-Borate, (pH 8.0), 1 mM $MgCl_2$, and 10 mM KCl), run at 6 W. The gels were dried, radioactive bands visualized and assayed using a BioRad GS-250 Molecular Imager.

2.4 Methylation Protection Assays

DNA samples (10 μl) were incubated as described above in 2.3, to produce mixtures of both duplexes and synapsed duplexes, in buffers containing, respectively, 50 mM TMACl buffer, 25 mM TMACl buffer containing 10mM Mg^{2+}, 10 mM Sr^{2+}, or 35 mM Ca^{2+}. Following overnight incubations at 37°C, the samples were each combined with 200 mM lithium cacodylate, and were made up to 0.1% (v/v) dimethyl sulphate. Methylation was allowed to proceed at 37°C for 30 minutes. Samples were then loaded on 8% native gels run in KMg buffer (see above). The wet gel was exposed to X-ray film

and bands corresponding to DNA duplexes and synapsed duplexes were cut out of the gel, eluted into 100 µl TMACl buffer overnight, and purified by ethanol precipitation. DNA pellets were then dissolved in 50 µl of 10% (v/v) piperidine and heated at 90°C for 20 minutes. Following lyophilization and dissolution in denaturing loading buffer, equal counts from different samples were loaded on a 10% sequencing gel, run at 20 W. The gel was dried prior to visualization on a BioRad GS-250 Molecular Imager.

2.5 Melting Point Assays

Synapsed duplex samples were prepared as described above, with prolonged periods of incubation (up to six days) to ensure the equilibrium (and hence maximal yield of duplex dimers) had been reached. Samples were then diluted to 0.1 µM DNA, and the solutions were adjusted to have final concentrations of both 10 mM Ca^{2+} and 10 mM Sr^{2+} in a buffer containing TMACl buffer. The diluted samples were equilibriated for two hours at 37°C, and then subjected to a routine where they were heated for 15 minutes each at a series of progressively increasing temperatures, from 70 to 90°C, in 2.5°C steps. Following incubations at given temperatures, 10 µl aliquots were removed and mixed into 5 µl of non-denaturing dye solutions on ice. After brief cooling, each sample was loaded on an 8% native gel run in KMg buffer (see above).

2.6 Cross Reactivity

Testing for reactivity between the dimerization domains was done with A·B or A·β along with a DNA hairpin sequence, mH8, shown in figure 2-6. Experiments were done identically to procedures listed in 2.3 in forming synapsed complexes, with one

exception. In cross reactivity reactions 5 μl of a solution containing 2.5 μM of each DNA constructed was mixed with 5 μl salt containing samples and incubated and treated as mentioned in 2.3 above.

3. Results and Discussion

3.1 Ion Requirements

We wished to investigate the following: (a) whether the duplex A·β, in the presence of appropriate group Ia or group IIa cations, were able to synapse to form $(A{\cdot}\beta)_2$ in the manner of A·B forming $(A{\cdot}B)_2$; and (b) whether the cation dependence of $(A{\cdot}B)_2$ (and, $(A{\cdot}\beta)_2$, if formed) followed the conventional pattern for the formation of G-quartets in general.

3.1.1 Monovalent Cations

Figure 2-3(a) shows the results of incubating gel-purified A·B and A·β duplexes in the presence of different alkali chlorides. The incubations were done in 1M salt (much higher than required for A·B synapses) so that low concentrations of the starting duplexes might be used. A striking observation from these experiments was that A·B and A·β formed synapsed complexes with vastly differing efficiencies. The yields of synapsed complexes in these 24 hour incubations were found to be within 10 to 15% of the yields at equilibrium, and were measured to be ~60% $(A{\cdot}B)_2$ in potassium and rubidium, where as the highest yield of $(A{\cdot}\beta)_2$ was < 20% (in sodium). The yield of $(A{\cdot}B)_2$ with the different cations followed the conventional order of K>Rb>Na>Li, Cs, that has been

observed with most G-quartet complexes (reviewed by Williamson, 1994; Wellinger & Sen, 1997).

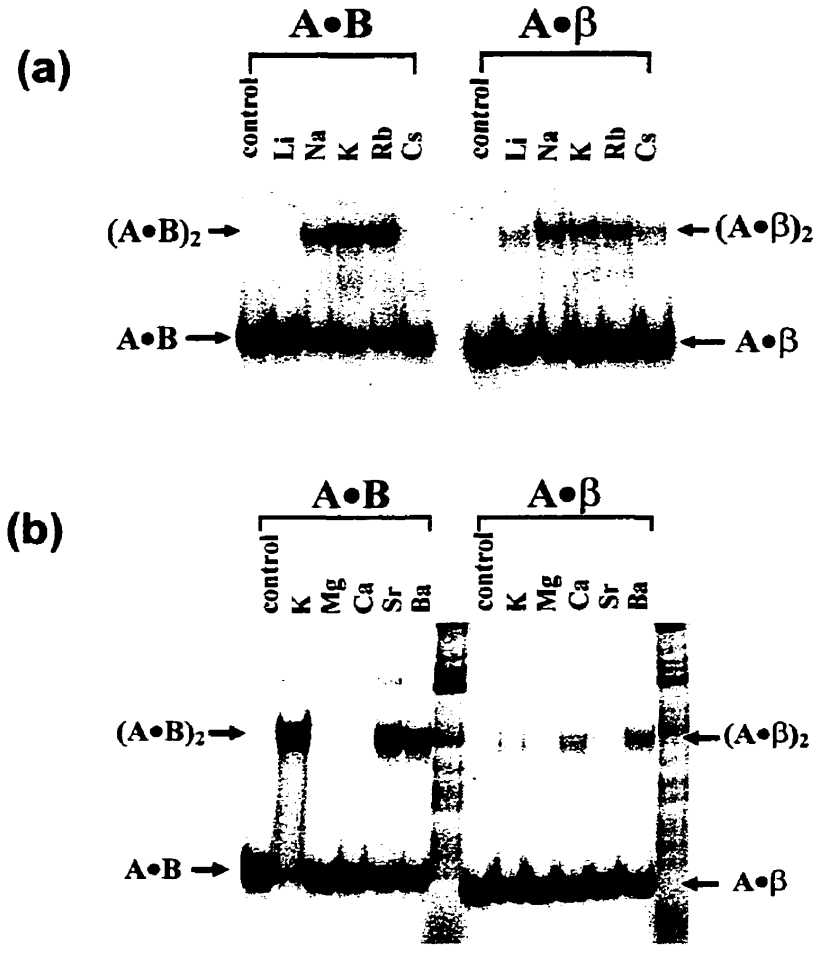

Figure 2-3. **(a) The influence of monovalent cations on the formation of $(A{\cdot}B)_2$ and $(A{\cdot}\beta)$ synapsed duplexes. Samples of 2.5 μM duplex DNA (A·B and A·β) were incubated separately for 20 hours at 37°C in the presence of the different alkali chlorides. Controls contained 50 mM TMACl buffer, whereas the samples contained 1M XCl (X = Li, Na, K, Rb or Cs) and 25 mM TMACl buffer. (b) The influence of divalent cations on the formation of $(A{\cdot}B)_2$ and $(A{\cdot}\beta)_2$ synapsed duplexes. Incubation conditions are identical to a) with the exception of 10 XCl_2 (X = Mg, Ca, Sr or Ba) are used in replacement to the alkali chlorides. Nagative controls contained 50 mM TMACl buffer only, and a positive control (K) contained 1 M KCl in 25 mM TMACl buffer.**

A likely explanation for poor yields of $(A{\cdot}\beta)_2$ from $A{\cdot}\beta$ was that the guanine mismatches within $A{\cdot}\beta$ were not substantially hydrogen-bonded in Hoogsteein base-pairs, which are necessary precursors to the formation of G-quartets. Alternatively, in the event of conformational and hydrogen-bonding fluxionality in the G·G mismatch region of $A{\cdot}\beta$, the mismatches only transiently adopted Hoogsteen base pairs. In the A·B duplexes, by contrast, the mismatches appeared to form Hoogsteen G·G base pairs with a higher frequency. Interestingly, a study by Suda *et al.* (1995) on single-stranded oligomers of the sequence $(dGGA)_9$ found that these oligomers dimerized to form parallel-stranded duplexes in a pH-independent manner. Probing of this unusual parallel duplex indicated the existence of G·G base pairs probably of the reverse Watson & Crick variety. These findings are certainly consistent with the poor ability of the parallel G·G mismatches in $A{\cdot}\beta$ to synapse to give rise to $(A{\cdot}\beta)_2$ complexes.

3.1.2 Divalent Cations

Figure 2-3(b) shows the results of incubating gel-purified A·B and $A{\cdot}\beta$ duplexes with 10 mM of the group IIa metal chlorides, from $MgCl_2$ to $BaCl_2$. The first major observation with these incubations was with the monovalent ion incubations (above), $(A{\cdot}B)_2$ formed far more efficiently than did the $(A{\cdot}\beta)_2$. Once again, A·B showed the expected cation requirement for dimerization in the presence of 10 mM M^{2+}, with the order of efficiency of Sr > Ba > Ca > Mg (Chen, 1992; Venczel & Sen, 1993). $A{\cdot}\beta$ duplexes, however, showed a very different ion preference: Ba > Ca > Sr > Mg, which was not at all characteristic for the formation of most G-quartet structures. For instance, results from previous studies (Chen, 1992; Venczel & Sen, 1993) had indicated that of

the group IIa cations, Sr^{2+} was the most efficient at supporting guanine quartet formation by single-stranded sequences containing a single stretch of guanine residues; Sr^{2+} was found also to stabilize G-quartets more strongly than the other group IIa cations. We carried out incubations of the single strand B and, separately, β, in the presence of Sr^{2+}; and, separately, 10 mM Ca^{2+}. B and β showed similar patterns of G-quartet formation in the presence of each of these two cations (data not shown), with Ca^{2+} weakly supporting the formation of B_4 and β_4; and, Sr^{2+} robustly supporting the formation of hairpin dimmers of both B and β. Therefore, the unusual, and mutually different, cation preferences shown by A·B and A·β are unique to those synapsed duplexes, and not properties of B and β *per se.*

To explain the above results regarding $(A\cdot\beta)_2$, we set out a hypothesis that the failure of Sr^{2+} to support $(A\cdot\beta)_2$ formation had a kinetic, rather than thermodynamic basis.

3.1.3 Examining Conditions for Efficient Formation of $(A\cdot\beta)_2$

We wished to establish first whether any salt conditions could be found for efficient production of $(A\cdot\beta)_2$ (~8% yield with 10 mM Ca^{2+}, incubated for 20 hours at 37°C). Contrastingly, Ca^{2+} was poor in supporting the formation of $(A\cdot B)_2$. We therefore carried out experiments to determine whether incubation with higher concentrations of calcium would result in more substantial yields of $(A\cdot\beta)_2$. Figure 2-4 shows the results of incubating gel-purified A·β duplexes and, separately, A·B duplexes (2.5 μM for each duplex) in the presence of 0, 10, 20, 35, 50 mM $CaCl_2$, respectively. The 50 mM incubation gave $(A\cdot\beta)_2$ at a ~50% yield (*en route* to an equilibrium yield of 77%,

measured following six days of incubation). The A·B duplex, incubated under the same conditions, gave less than 2% yield of the $(A \cdot B)_2$ complex.

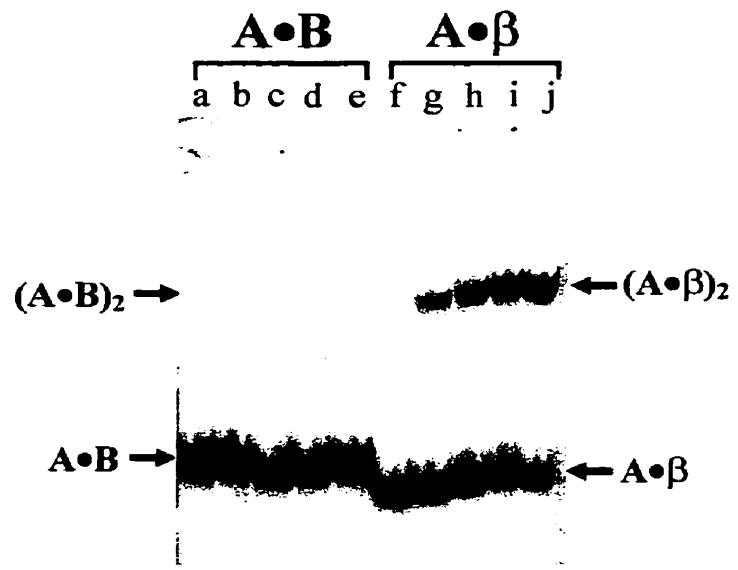

Figure 2-4. The effect of calcium concentration on the formation of $(A \cdot B)_2$ and $(A \cdot \beta)_2$ synapsed duplexes. Samples of 2.5 µM duplex DNA (A·B or A· β) were incubated for 20 hours at 37°C in different concentrations of $CaCl_2$. Lanes a and f, negative controls, containing 50 mM TMACl buffer. The remaining lanes contain 25 mM TMACl buffer and the following $CaCl_2$ concentrations: lanes b and g, 10 mM Ca^{2+}; lanes c and h, 20 mM Ca^{2+}; lanes d and i, 35 mM Ca^{2+}; lanes e and j, 50 mM Ca^{2+}.

3.2 Mechanism of Ion Selectivity

To test how many of the eight G·G mismatches in the A·B and A·β duplexes actually participated in synapsis *via* the formation of a short stretch of inter-duplex G-quartets, we carried out methylation protection experiments. Treatment of DNA with dimethyl sulphate (DMS) preferentially methylates the N-7 position of guanine (figure 2-5). The site of modification on the DNA can be determined by heating the sample in

basic solution, which results in strand scission at the methylated guanine (Maxim & Gilbert, 1977).

Other positions and bases also react with DMS but these modifications are not sensitive to cleavage upon treatment with hot piperidine.

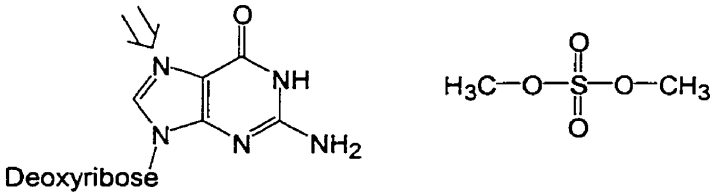

Figure 2-5. Methylation of guanine. The N-7 site on guanine, indicated by an arrow, can be methylated by DMS.

In a G·G Hoogsteen base pair, one of the two participating guanine residues is protected from methylation at its N-7 position, whereas the other is methylatable. G·G Hoogsteen pairs that participate in the formation of G-quartets would, by contrast, be fully protected from methylation, since every N-7 position in a G-quartet is involved in hydrogen bonding. In an earlier study (Venczel & Sen, 1996), methylation protection had been used as a sensitive probe for determining which guanine Hoogsteen pairs dimerized to give guanine quartets. Here, methylation protection was also a potentially important tool for determining whether in the presence of strontium the A·β duplex (but not the A·B duplex) formed some alternative guanine-mediated structure, which was kinetically unable to dimerize to form the $(A{\cdot}B)_2$ synapsed complex.

Figure 2-6 shows methylation protection patterns for the undimerized duplexes A·B and A·β (with strand A 5'-labeled in each case) in TMACl buffer (lanes a and e), calcium (lanes b and f), and strontium ions (lanes c and g), respectively, as well as protection patterns for the synapsed complexes $(A{\cdot}B)_2$ (lane d), and $(A{\cdot}\beta)_2$ (lane h). In

the presence of TMACl or Ca^{2+} (or, Mg^{2+} data not shown) the eight-guanine residues (G1 to G8) in the G·G mismatch domains of both A·B and A·β were methylated relatively uniformly. In the two synapsed complexes (lanes d and h), by contrast, all but the 3' and 5'- most guanine residues (G1 and G8) were protected, consistent with the notion in these complexes approximately six guanine quartets were forming in each synapsed region. Analogous experiments carried out with strand B or β being 5'-labeled, instead of strand A, gave data that were fully consistent with the above.

However, methylation patterns of unsynapsed A·B and A·β in the presence of Sr^{2+} (Sr-A·B {lane c} and Sr-A·β {lane g}), showed important differences between them. Whereas the pattern of Sr-A·B (lane c) resembled those of Ca-A·B, Sr-A·β (lane g) showed a unique methylation pattern, in which G1 and G8 were strongly methylated (as above); G2, G3, G6 and G7 were protected, as they might be if they might be forming G-quartets; however, the two most central guanines, G4 and G5 (indicated with arrows) were strongly methylated (a pattern similar to this was found also with Ca-A·β at low temperatures but not at 37°C).

This data is consistent with a particular conformation of duplex Sr-A·β shown in figure 2-7, a 'pinched' duplex, in which two intra-duplex guanine quartets have formed. Analysis of the methylation pattern of Sr-A·β with strand β labeled instead of strand A showed a similar but somewhat more complex pattern (data not shown), which, together with the data from strand A suggested the existence of two similar pinched duplexes, shown in figure 2-7(a) and 2-7(b) respectively (in model b, the asymmetry of guanine-participation from strand β is a consequence of the shorter than usual separation of

adjacent nucleotides across the 3'-3' linkage, and larger than usual separation of adjacent nucleotides across the 5'-5' linkage).

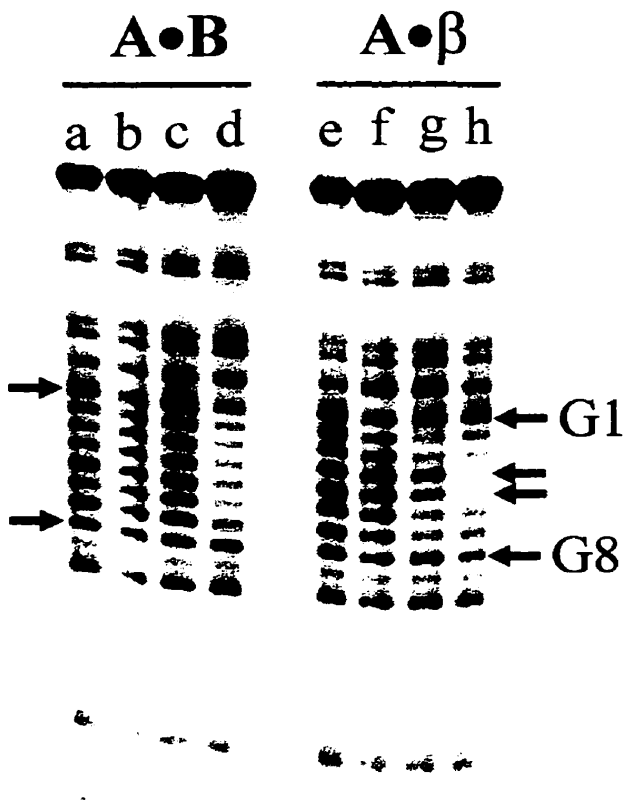

Figure 2-6. **Methylation protection studies on A·B, A·β, and their respective synapsed complexes. Methylation protection patterns with the A·B duplex. Lanes a to c are protection patterns of the undimerized A·B duplex after incubating for 20 hours at 37°C. Lane a) is in the presence of 50 mM TMACl buffer; lane b) is in the presence of 35 mM Ca^{2+}; and lane c) is in the presence of 10 mM Sr^{2+}. Lane d) shows the protection pattern of the $(A·B)_2$ complex, formed from the dimerization of A·B in the presence of 10 mM Sr^{2+}. Methylation protection patterns of the A·β duplex, under identical conditions to the A·B duplex. Lanes e) to g) are of the undimerized duplex in TMACl buffer, 35 mM Ca^{2+}, and 10 mM Sr^{2+}, respectively. Lane h) is of $(A·β)_2$, from dimerization of the A·β in the presence of 35 mM Ca^{2+}.**

The formation of two putative intra-molecular G-quartets by the Sr-A·β pinched duplex (but not by the Sr-A·B duplex) explains why the formation of $(A \cdot B)_2$ is favored by the strongly stabilizing Sr^{2+}, but not the formation of the likewise six-quartet containing $(A \cdot \beta)_2$. A Sr-A·β "pinched" duplex forms as kinetic by-product, resulting in an inability to dimerize to form $(A \cdot \beta)_2$. Strontium appears to stabilize the intra-molecular G-quartets of the pinched A·β duplex sufficiently to allow them to endure. Presumably, this stabilization is greater than that for the putative intra-duplex quartets that might form in A·B. A reason for this difference may lie in the strand orientations of intra-duplex quartet regions of Sr-A·B and Sr-A·β. In Sr-A·β pinched duplexes the stand orientation is unavoidably partially parallel, which may be a thermodynamically favored arrangement compared to the antiparallel strand orientations in a hypothetical A·B pinched duplex.

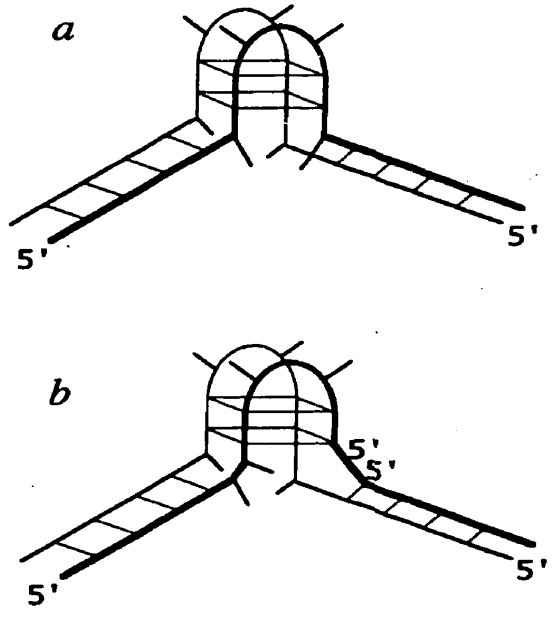

Figure 2-7. Two models for a "pinched" duplex. Formation is a consequence of intra-molecular G-quartets, formed by the A·β duplex in the presence of Sr^{2+}.

Interestingly, a somewhat parallel situation for the existence of a kinetic barrier to the formation of a thermodynamically preferred G-quadruplex complex, had been reported by Sen & Gilbert (1990) for the formation of parallel quadruplexes from single stranded DNA molecules containing multiple guanine motifs. In that study the apparent paradox was presented that in buffers containing the highly G-quartet stabilizing cation K^+, the thermodynamically preferred product, the parallel quadruplex, did not form at all. In the presence of the less stabilizing Na^+ and Rb^+ cations, however, the parallel quadruplex formed well. The explanation for that phenomenon was similar to the one described above, namely that in the presence of potassium (but not in the presence of sodium or rubidium), alternative G-quadruplex structures (antiparallel hairpin dimers) were stabilized so well that the kinetics of parallel quadruplex formation were severely compromised.

3.3 Stability of Synapsed Duplexes

Is $(A{\cdot}\beta)_2$, a synapsed duplex expected to contain a parallel-stranded G-quadruplex, more stable than $(A{\cdot}B)_2$, whose quadruplex could only contain purely antiparallel or partially antiparallel strand orientations? Melting experiments designed to test the above hypothesis were carried out as follows. Pre-formed $(A{\cdot}B)_2$ and $(A{\cdot}\beta)_2$ complexes were first equilibrated, separately, for 2.5 hours at 37°C under conditions of identical ionic strength in a buffer of 10 mM Tris (pH 7.5), 25 mM TMACl, 10 mM $CaCl_2$, 10 mM $SrCl_2$. Melting experiments were then carried out as described in Materials and Methods, and the results were analyzed using gel electrophoresis. For both

complexes the melting behavior appeared to be non-cooperative, with "melting" of the synapsed duplexes occurring over fairly broad temperature ranges. The midpoints of the two melting transitions, however, were: $(A{\cdot}B)_2$ at 87.5°C; and $(A{\cdot}\beta)_2$ at 97.5°C (data not shown). Therefore, the expected order of stability seen with broad classes of G-quadruplex structures (parallel more stable than antiparallel) was true for these synapsed duplexes as well.

The formation constants for both classes of synapsed duplexes were also notably lower than those measured by Lu *et al.* (1993) for the dimerization of G·G base-pair-containing DNA hairpins to form antiparallel quadruplexes. Lu *et al.* studied the thermodynamics of G-quadruplex formation by hairpin dimers formed by the oligomers 5'-dGGGGTTTTGGGG-3' and 5'-dGGGGTT3'-3'TTGGGG-5', and obtained formation constants of 6.5×10^8 M^{-1} and 9.4×10^{12} M^{-1}, respectively (measured in 200 mM NaCl solututions). The formation constants of $(A{\cdot}B)_2$ and $(A{\cdot}\beta)_2$ forming from A·B (in 10 mM $SrCl_2$), and A·β (in 35 mM $CaCl_2$), respectively, were estimated from equilibrium distributions of the free and synapsed duplexes to lie between 10^5 and 10^6 M^{-1}. It is likely that higher charge repulsion between individual A·B (or A·β) duplexes, as well as steric problems with the formation of $(A{\cdot}B)_2$ and $(A{\cdot}\beta)_2$ relative to the formation of the small hairpin-based quadruplexes described by Lu *et al.*, accounts for their stability differences.

3.4 Cross Reactivity

Variable conditions for the formation of $(A{\cdot}B)_2$ and $(A{\cdot}\beta)_2$ synapsed duplexes suggested these duplexes may be *self*-selective in dimerization. We wanted to determine whether a solution containing both A·B and A·β could be selectively induced to form

only $(A{\cdot}B)_2$ or $(A{\cdot}\beta)_2$ by the addition of $SrCl_2$ or $CaCl_2$, respectfully. This could not be tested with the two duplexes being used because of their identical sizes. A new DNA sequence was made, mH8, to test for selectivity in dimerization. The mH8 DNA construct shown in figure 2-8 contains the same 8 G-G mismatch domain possessed by the A·B duplex. This mH8 DNA has the same dimerization properties as the A·B duplex, such as ion preference (data not shown), but the synapsed product has a higher electrophoretic gel mobility in comparison to $(A{\cdot}B)_2$ and $(A{\cdot}\beta)_2$.

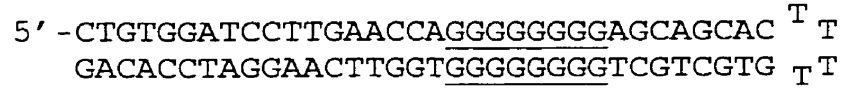

Figure 2-8. Structure of mH8. The mH8 construct that contains the conventional eight G·G mismatch domain, as in the A·B duplex.

Cross reactivity of A·B or A·β with mH8 can be seen on a native gel as a synapsed product with intermediate gel mobility in comparison to mH8 and the duplex being tested. Figure 2-9(a) demonstrates the cross reactivity between mH8 and A·B. The hybrid product mH8-A·B along with the pure dimers of $(mH8)_2$ and $(A{\cdot}B)_2$ can be observed in the presence of Sr^{2+} and Ba^{2+}. This cross reactivity is expected, as the two constructs possess identical dimerization domains.

When A·β duplexes are incubated in combination with mH8 a peculiar cross reactivity is observed. As seen in figure 2-9(b) the hybrid synapsed complexes are formed in Ca^{2+}, Sr^{2+} and Ba^{2+} containing samples. The presence of cations in which a homo-synapsed product does not form (i.e. A·B in Ca^{2+}), still results in a hybrid synapsed complex.

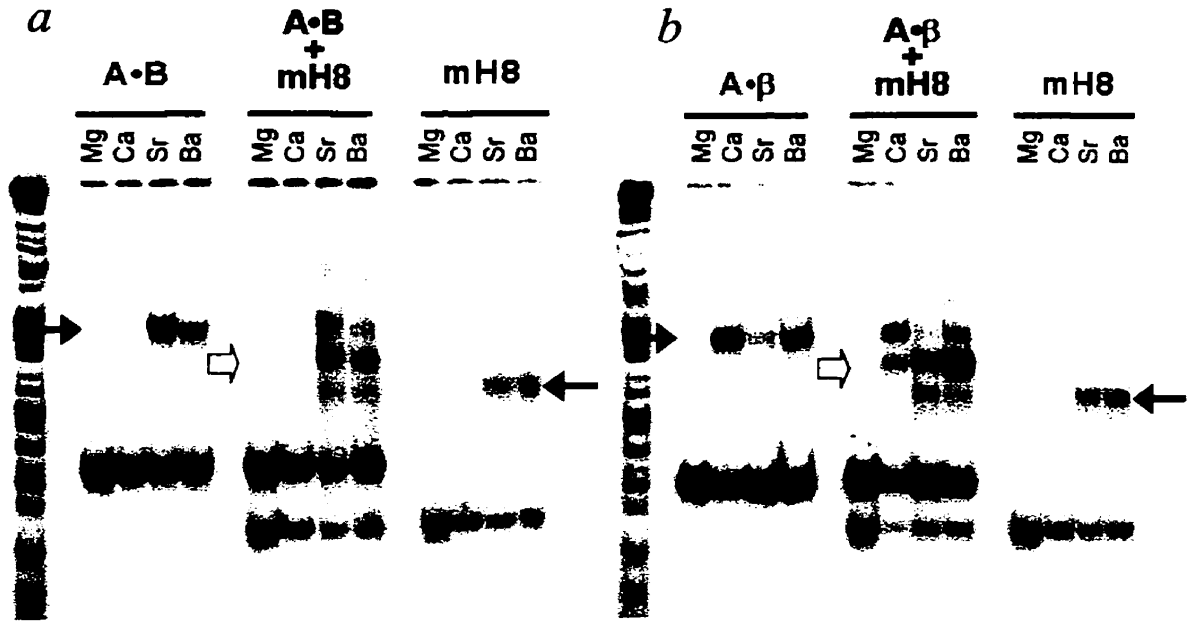

Figure 2-9. **Cross dimerization of synaptic domains. (a) Cross dimerization between A·B duplexes. Samples of 1.25 μM duplex DNA (A·B and mH8) were incubated separately or as a mixture for 20 hours at 37°C in the presence of the four indicated divalent cations. Final cation concentrations of the chloride salts was 10 mM with the exception of $CaCl_2$ which was 35 mM. Black arrows indicate the homo-synapsed duplexes while open white arrows indicate the hybrid (mH8)·(A·B) dimer. (b) Cross dimerization of A·β. Samples are identical to those in (a), but A·β rplacing A·B in all cases.**

3.4.1 Unusual Structure of the Hybrid Synapsed Duplex

Formation of the (A·β)·(mH8) hybrid results in a peculiar quadruplex. The directionality of the backbones of the G·G mismatch domains in the duplexes dictates that the quadruplex has to have three backbone strands in one orientation, while a single strand being anti-parallel to the others as shown in figure 2-10(a). This strand orientation has been observed a couple of times in G-quadruplex structures formed from *Tetrahymena* (Wang & Patel, 1994) and *Oxytricha* (Wang & Patel, 1995) telomeric repeats under some conditions. The formation of the hybrid structure (A·β)·(mH8) now

demonstrates a new way to assemble G-quadruplexes with this relatively unusual strand polarity.

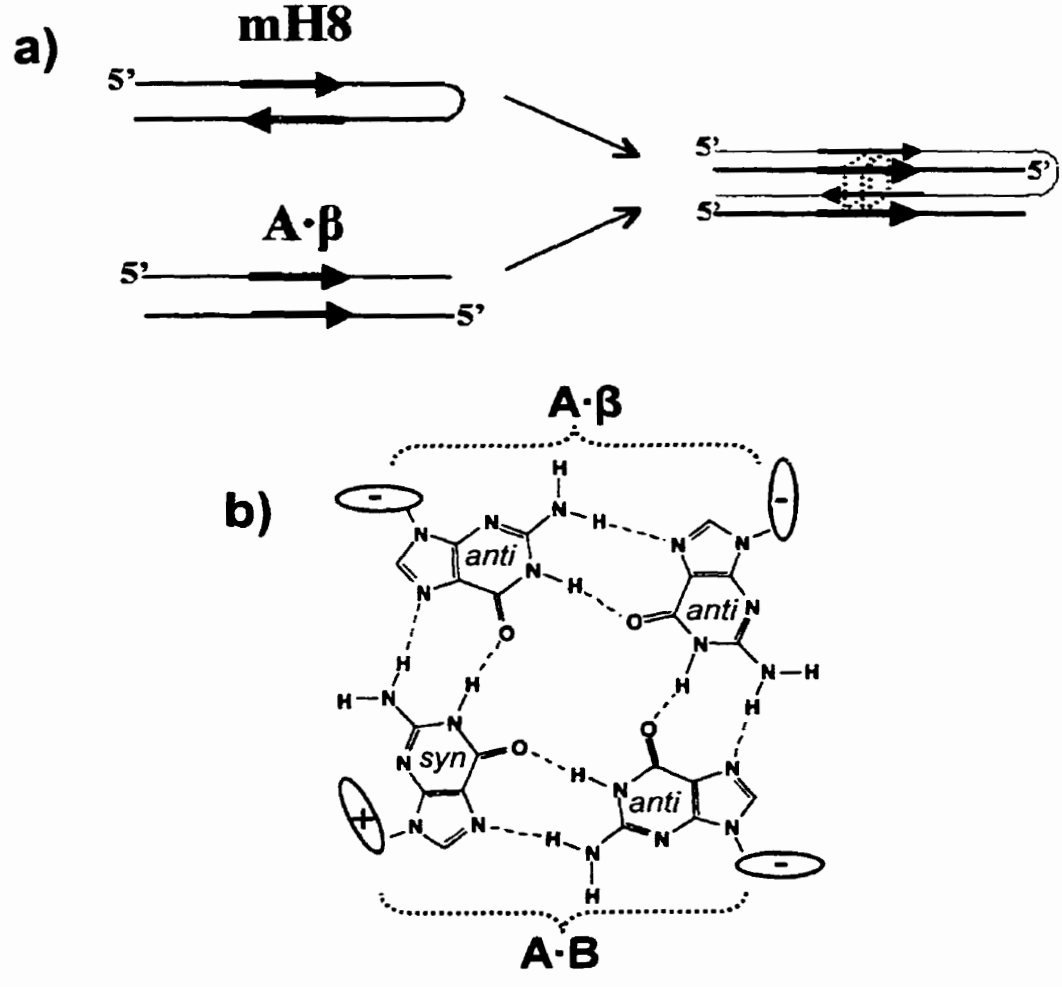

Figure 2-10. **(A·β)·(mH8) synapsed hybrid. (a) Formation of the (A·β)·(mH8) hybrid results in a quadruplex that have three strands with their backbones in parallel. (b) Proposed glycosidic bond orientations participating guanines in the G-quartets of the synapsed hybrid quadruplex. Symbols (+) and (-) indicate strand directionalities of into or out of the page, respectively.**

The ability of this class of quadruplex (three parallel strands) to form in Ca^{2+} solutions while the anti-parallel types formed from A·B do not, is indicative of a greater thermodynamic stability in comparison with typical anti-parallel quadruplex structures. A reason for this may be due to the fact that in three of the participating strands, the guanine bases can be in the *anti*-conformation while the fourth anti-parallel strand the guanine would adopt a *syn*-position (see figure 2-10(b)).

4. Conclusions

This work introduces the notion of cation selectivity into the processes of guanine-mediated synapsis of "synapsable" DNA duplexes. We have described two different kinds of synapsable DNA duplexes, A·B and A·β, which have different salt and cation requirements for the formation of their respective synapsed complexes. The synapsable duplexes do not exhibit self-selectivity in mixed solutions, so these constructs did not achieve our initial goal. Still, these duplexes exhibit a peculiar *partial*-selectivity, where only one of the homo synapsed products (the identity of which depends on whether Ca^{2+} or Sr^{2+} are present in solution) and always the mixed product are observed. Future work could potentially examine whether variations of solution conditions could favor *self*-selectivity, like temperature, alternate ion species and concentrations.

Our efforts have continued to define types of "self-recognizing" synapsable motifs, involving the introduction of non-G-quartet forming bases, such as thymine, into the G·G mismatch domains as described in chapter three.

Guanine-mediated synapsis, as described above, is unique in that it provides a means for the self-recognition and supramolecular assembly by intact, unmelted DNA

double helices under low temperature conditions. Such site-specific stable associations of two or more DNA duplexes are of potential utility both in the investigation of *in vivo* molecular biological phenomena, such as in distinguishing between "looping" *versus* "tracking" motions of DNA-binding proteins on DNA duplexes (reviewed by Schleif, 1992), as well as in a variety of *in vitro* applications such as the creation of quasi-crystalline DNA or DNA-protein arrays for structural studies (Seeman, 1985), or in novel signal-amplification devices (Venczel & Sen, 1996). The possible use of two distinct kinds of synapsable domains described above will only contribute to the richness of potential applications of these unique DNA structures.

Chapter 3

Self-Selective Synapsable Duplexes

1. Introduction

The work presented with the A·B and A·β duplexes, in chapter 2, fell short of our original objective of designing synapsable duplexes that exhibit self-selectivity in dimerization. For instance, in the simplest case, whether from a mixed solution of duplexes containing synapsable domains *"a"* and *"b"*, only the a_2 and b_2, and not the *a.b* types of synapsed duplex-dimers might be obtained.

An alternate strategy in the design of G·G mismatch domains was pursued and is described in this chapter. Spacing the G·G mismatches into patterns, by disrupting contiguous runs of G·G mismatches with T·T mismatches, we postulated that different patterns would not have their respective G·G mismatches in correct alignment for optimal G-quartet formation. With this strategy, *self-* or *homo*-dimerization would result in a greater number of G-quartets than with cross-dimerization. Minimal G-quartet formation with *cross-* or *hetero*-dimer products would yield a thermodynamic preference for self-selectivity.

In this chapter we demonstrate that it is indeed possible to design such non-equivalent synapsable G-G domains, which have the property of "self"-synapsis. We also demonstrate that from a solution containing a mixture of *a* and *b*, it is possible, utilizing small variations in the incubation conditions, to generate the a_2 and b_2 complexes simultaneously; a_2 alone; and b_2 alone. In none of the above incubations is the *a.b* product observed.

Utilization of synapsable domains until now has only been to associate simple DNA duplexes. We have also, for this first time used synapsable domains in the assembly of a more complex structure.

2. Materials and Methods

2.1 DNA Synthesis and Purification

The two DNA oligomers used to construct the J•K duplex had the following sequences (the underlined sequences indicate the bases designated to form its G-G domain in the assembled duplex):

J: 5'-GTGAC TCGAG AAGCT CCTGA TTGGT TGGGG GTTTG TGGTT CAAGG ATCCA CAG and

K: 5'-CTGTG GATCC TTGAA CCACA TTGGG GGTTG GTTTC AGGAG CTTCT CGAGT CAC, respectively.

The oligomers for the L•M duplex were:

L: 5'-CTCGA GAAGC TCCTG ATTGG GTGGG TTTGT GGTTC AAGGA TCC, and

M: 5'-GGATC CTTGA ACCAC ATTGG GTGGG TTTCA GGAGC TTCTC GAG.

The oligomers for the H•I duplex were:

H: 5'-TGACT CGAGA AGCTC CTGAT TGGGG GTTTG TGGTT CAAGG ATCCA CA, and

I: 5'-TGTGG ATCCT TGAAC CACAT TGGGG GTTTC AGGAG CTTCT CGAGT CA.

The oligomers for the three-way junction were:

W(H•I)T(L•M): 5'-TGCAG TTGAG TTGGG TGGGT TCTGG CGAAC GGACG TTGCA GGCTT TTGCC TGCCA CCGGC GGAAG CTCTT GGGGG TTGCG ACGAT GG,

and

C(H•I)T(L•M): 5'-CCATC GTCGC TTGGG GGTTG AGCTT CCGCC GGTGC GTCCG TTCGC CAGTT GGGTG GGTTC TCAAC TGCA.

All oligomers were synthesized at the University of Calgary Core DNA Services. Crude oligomer samples were dissolved in 50 µl of denaturing gel-loading buffer (0.25% bromophenol blue; 0.5% xylene cyanol FF, 30% glycerol; 10 mM Tris-Cl, pH 7.5), heated at 95° C for 3 minutes to break down any pre-formed G-quadraplex complexes, and size-fractionated in 8% (w/v) denaturing polyacrylamide gels. The DNA bands in the gel were visualized by UV-shadowing, excised, and the DNA recovered by overnight elution into TE buffer (10 mM Tris, pH 7.9; 0.1 mM EDTA). The DNA solutions were filtered through 0.2 µm micro filters (Gelman Sciences) and desalted and concentrated using C-18 Spice Columns (Analtech). The lyophilized pellets of purified DNA were finally dissolved in 50 µl of TE buffer. 5' end-labeling with [γ-^{32}P] ATP was carried out using standard kinasing protocols (Sambrook, 1989). Ethanol precipitations of the DNA, where necessary, were carried out by adding 2.5 volumes of EtOH to aqueous DNA solutions made up to 0.8 M LiCl.

2.2 Preparation of Double Stranded DNA

All duplexes and the three-way junction were assembled by mixing in water at room temperature 500 pmoles of a given oligomer with 500 pmoles (470 pmoles of unlabeled and 30 pmoles of 5'-^{32}P-labeled) of its complementary oligomer. The oligomer mixtures were made up to TMACl buffer [100 mM tetramethylammonium chloride (TMACl); 10 mM Tris, pH 7.9], heated to 95° C for 2 min, and allowed to cool slowly to 30° C. The resulting duplex DNA samples were purified by loading in 8% non-denaturing polyacrylamide gels, which were electrophoresed in TBT buffer (50 mM Tris borate, pH 8.0; 10 mM TMACl) at 6W at room temperature. Bands of duplex DNA in the gel were detected by autoradiography, excised, and the DNA eluted into two times TMACl buffer. Eluted samples were concentrated using Microcon microconcentrators (Amicon) with a 10 kD molecular weight cut-off.

2.3 Formation of Synapsed Duplex-Dimers and Three-way Junction Dimers

Duplex DNA samples, as prepared above, were diluted with two times TMACl buffer to two times the final DNA concentration to be used for dimerizations. Samples containing more than one duplex were also prepared in this fashion. 5 μl aliquots of such duplex DNA solutions were combined with 5 μl of various salt solutions and incubated at 37° C for different times. Tightly sealed 100 μl tubes were used throughout and the tubes were completely immersed in a water bath at 37° C to prevent changes in the sample volume from evaporation and condensation. For analysis aliquots were removed from each sample, combined with non-denaturing gel-loading buffer and run in 8% non-

denaturing polyacrylamide gels (6% gels were used for the three-way junction sequences) run in KMg buffer (50 mM Tris-borate, pH 8.0; 10 mM KCl; 2mM $MgCl_2$), at 6W at 4° C, unless stated otherwise. Gels were then dried and radioactive bands visualized and assayed using a BioRad GS-250 Molecular Imager.

2.4 Melting Point Determinations

Melting points of duplex DNA samples were determined spectrophotometrically using a Cary 300 Bio UV-Visible Spectrophotometer with a temperature controller (Varian). The absorbance at 260 nm of 0.3 μM samples of duplex DNA were monitored from 37° C - 90° C, with a heating rate of 0.1° C / min. Absorbance profiles were analyzed with the Cary Thermal Software v1.00(6).

The melting behavior of synapsed duplex-dimers was followed most accurately by electrophoretic methods. Samples were prepared as described above, with prolonged incubations to ensure that equilibrium had been reached in the formation of synapsed duplex-dimers. Samples were then diluted to 0.1 μM total DNA, while keeping the salt concentration (1M KCl, in TMACl buffer) constant. The diluted samples were incubated at 37° C for one hour, and then subjected to a routine where they were heated for 15 minutes each at a series of progressively increasing temperatures, from 50° to 95° C, in 5° C steps. Following each incubation at a given temperature, 2 μl aliquots were removed and mixed into 3 μl of non-denaturing gel-loading buffer solution on ice. After being left on ice for three minutes, each sample was loaded into an 8% non-denaturing gel run in KMg buffer (see above) for analysis.

2.5 Methylation-Protection Assays

Methylation experiments were carried out using a modified version of the DNA sequencing procedure of Maxam and Gilbert, 1977. DNA samples (10 μl; 5 μM final) were incubated in solutions containing 1M LiCl in TMACl buffer (where synapsis was not desired), or in 1M KCl in TMACl buffer (where synapsis was desired). Following overnight incubations at 37° C, each sample was combined with 3.3 μl of 200 mM lithium cacodylate (pH 7.5), and made up to 0.1-0.4% (v/v) dimethyl sulfate (DMS). Methylation was allowed to proceed at 37° C for 30 minutes, and each sample was then combined with 5 μl of non-denaturing loading buffer and run in 8% non-denaturing gels run in KMg buffer (see above). The wet gels were exposed to X-ray film and bands corresponding to DNA duplexes and synapsed duplex-dimers were cut out of the gel. The DNA from all excised gel bands was eluted into 300 μl TE buffer overnight, and recovered by ethanol precipitation (see above). The purified and washed DNA pellets were dissolved in 50 μl of 10% (v/v) piperidine in water and heated at 90° C in sealed tubes for 30 minutes. Following this treatment the samples were lyophilized to remove water and piperidine, and the DNA dissolved in denaturing gel-loading buffer. Samples containing equal counts of radioactivity were loaded and run in 10% sequencing gels run at 25W. The gels were dried, and the radioactive DNA bands visualized using a BioRad GS-250 Molecular Imager.

3. Results and Discussion

3.1 The Design of Self-Selective Synapsable DNA Duplexes

Prior studies on synapsable DNA duplexes had utilized duplexes that contained stretches of eight contiguous G-G mismatches within their synapsable G-G domains (Venczel & Sen, 1996; Fahlman & Sen, 1998). These experiments left open the question whether more than one kind of G-G domain, say, *a*, *b*, and *c*, could be used for synapsis, such that domain *a* was specific for synapsing only with another *a*, and not with *b* or *c*. We therefore designed two divergent G-G domains by interspersing T-T base mismatches among the G-G mismatches to spatially separate contiguous G-G domains. T-T mismatches were chosen in part because prior work (Venczel & Sen, 1996) had indicated that their presence at the ends of G-G domains did not interfere with the latters' synaptic properties. Along with internal interrupting T·T mismatches, two T·T mismatches on either side of the synapsable domain were included to provide conformational flexibility between the synapsable domain and the double stranded arms. Two different synapsable duplexes, J·K and L·M, were thus created (figure 3-1).

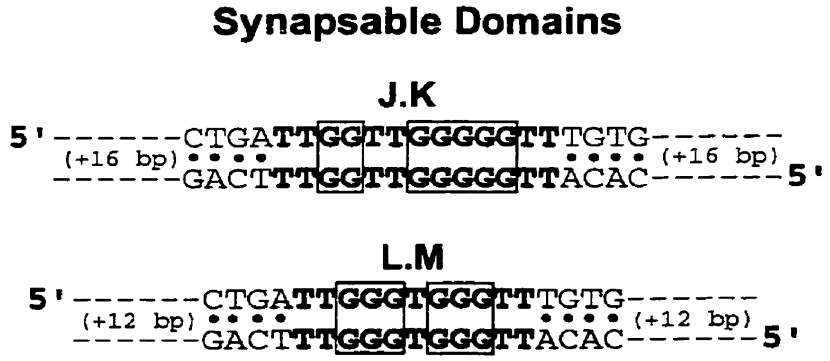

Figure 3-1. G-G domains of synapsable duplexes J·K and L·M. The highlighted bases constitute the G-G domains, and boxes surround G-G mismatch base pairs.

We postulated that *self-* or *homo*-synapsis by each of these duplexes would potentially form a larger number of guanine quartets [up to seven in $(J{\cdot}K)_2$; and, six in $(L{\cdot}M)_2$] than might form from *cross-* or *hetero*-dimerization of the duplexes [at best, five quartets in the heterosynapse (J·K)·(L·M)]. We therefore surmised that at equilibrium, the greater predicted thermodynamic stability of the two homo-synapsed dimers might lead to their accumulation relative to the hetero-synapsed dimer.

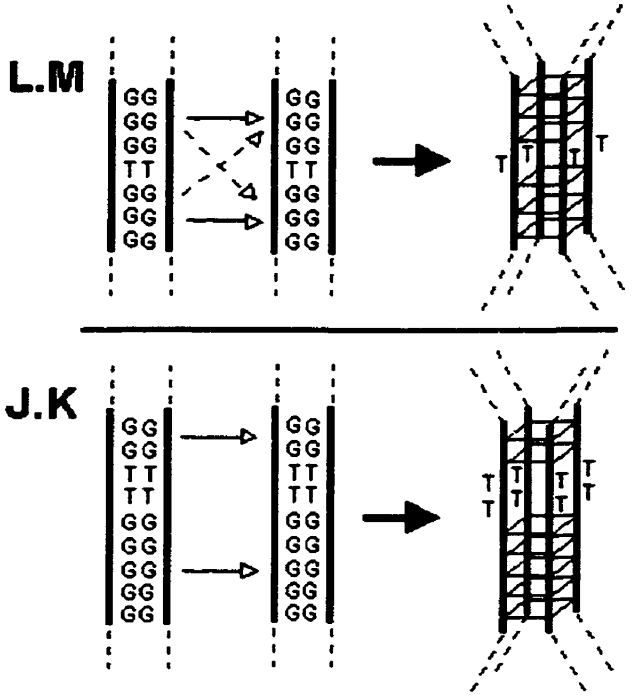

Figure 3-2. Symmetry of L·M and J·K dimerization domains. The symmetry of the L·M dimerization domain results in two possible orientations for dimerization that would result in maximal G-quartet formation. In comparison the non-symetric J·K domain only has one orientation.

Only the dimerization domain of L·M is symmetrical, which results in two possible orientations for dimerization that maximized G-quartet formation (figure 3-2). This aspect should have no influencing affect on selectivity, but should result in a modest increase in the rate of dimerization in comparison to J·K. A possibly detrimental affect of using symmetrical domains is in the assembly of constructs of higher complexity, as in section 3-6 of this chapter.

3.2 Synapatic-Dimerization of J•K and L•M Duplexes.

The individual abilities of the duplexes J·K and L·M to dimerize via synapsis was examined in the presence of 1M of different alkali cations, at 37° C. Conventionally, G-quadruplex formation (whether starting with single-stranded DNA, or with synapsable duplexes) follows the ion preference of $K^+ > Rb^+$, $Na^+ >> Li^+$, Cs^+ (Williamson, 1994; Wellinger & Sen, 1997). Figure 3-3 shows that L·M exhibited the above cation preference for its dimerization. However, an anomalous cation preference was observed for the dimerization of the J·K duplex, with both Na^+ and Rb^+ supporting a larger yield of dimerized product than K^+ (Figure 3-3). Such anomalous cation preferences for the formation of certain specific G-quadruplex structures have been reported (Sen & Gilbert, 1990; Fahlman & Sen, 1998), and are generally the consequence of the formation and stabilization by the highly-stabilizing potassium ion of alternative G-quadruplex complexes. A mechanistic model for the observed anomalous ion dependence for the formation of $(J·K)_2$ is given below in section 3.5.

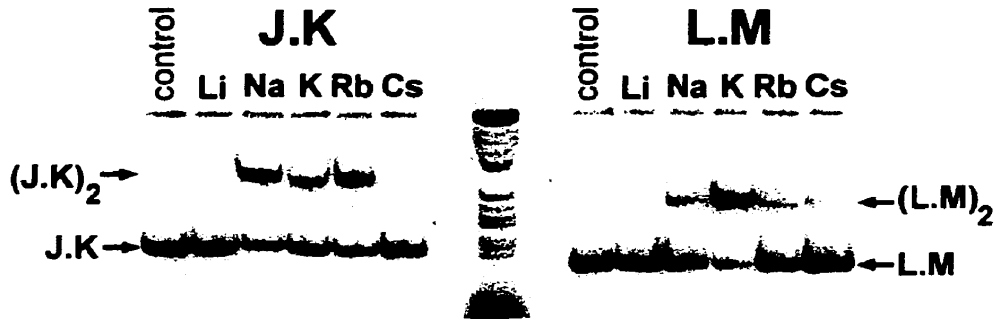

Figure 3-3. Nondenaturing polyacrylamide gels showing the influence of the different alkali cations on the synaptic dimerization of the J·K and L·M duplexes. Samples of 2.0 μM duplex DNA (J·K and L·M) were incubated at 37°C for 48 h in the presence of different alkali chlorides. Control samples contained 100 mM TMACl and 10 mM Tris (pH 7.9), while the other samples were incubated in 1 M XCl (where X = Li, Na, K, Rb or Cs), 100mM TMACl, and 10 mM Tris (pH 7.9)

In addition to the divergent alkali cation-dependences for the formation of $(J{\cdot}K)_2$ and $(L{\cdot}M)_2$, the rates of formation of these two complexes was found to be remarkably different. Figure 3-4 shows that the synaptic dimerization of 0.5 μM L·M reached equilibrium almost 1000 times faster than that of 2.5 μM J·K, when both were measured under standardized dimerization conditions (1M KCl in TMACl buffer, at 37° C). The dimerization of duplex L·M followed second-order kinetics, with an observed rate constant of $1.5 \pm 0.3 \times 10^5$ M^{-1} min^{-1} under the above standard conditions (average of four experiments). Using the K_d value of 130 ± 70 nM computed from the equilibrium distribution of L·M and $(L{\cdot}M)_2$ under these conditions, a dissociation rate constant for $(L{\cdot}M)_2$ to L·M of 0.025 ± 0.014 min^{-1} was calculated. A comparison of the rate of L·M dimerization with that of the formation of duplexes from single-stranded DNA (2.6×10^8 $M^{-1}min^{-1}$ at 32.5° C and 1.14×10^8 M^{-1} min^{-1} at 40.2° C) (Porschke & Eigen, 1971),

indicated that the L·M duplex dimerizes about three orders of magnitude slower than duplex-formation by single-stranded DNA. In contrast, other G-quartet forming sequences exhibit significantly slower kinetics of formation than the dimerization of L·M, with typical rates of between 6-300 M^{-1} min^{-1} (Guo *et al,* 1992; Guo, Liu & Kallenbach, 1992; Fang & Cech, 1993).

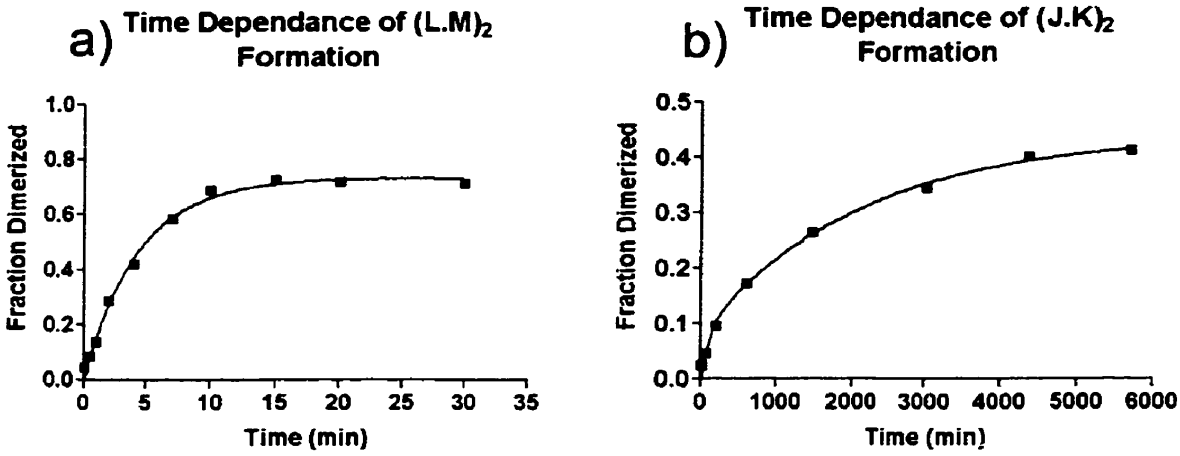

Figure 3-4. Time dependences for the synaptic dimerization of L·M (a) and J·K (b) into their respective duplex dimers. The duplex concentrations used were 0.5 μM for L·M and 2.5 μM for J·K. Samples were incubated in 1 M KCl, 100 mM TMACl, 10 mM Tris (pH 7.9) at 37°C.

The dimerization of the J·K duplex did not follow simple second-order kinetics. The formation curve for $(J{\cdot}K)_2$ formation (Figure 3-4(b)) showed at least two components. We postulated that this complexity of kinetics was related to this duplex's unusual ion preference for dimerization (Figure 3-3). A possibility was that the J·K duplex, in the presence of potassium, existed in two interchanging conformational forms, J·K and J·K', of which J·K' perhaps was incapable of synaptic dimerization (owing possibly to the presence of *intra*molecular G-quartets within its own structure).

Experiments to determine the existence and nature of such a putative J·K' conformer are described below.

3.3 Duplex-Dimer Stability

The thermal stabilities of the synapsable duplexes J·K and L·M duplexes were measured in 1M LiCl in TMACl buffer, using standard UV-spectrophotometric techniques. Figure 3-5 shows the absorbance data for the two duplexes as functions of temperature. The melting points of the duplexes were determined to be 80.4° and 74.4° C, respectively, and the melting behavior of both duplexes was cooperative, as is found for standard DNA duplexes.

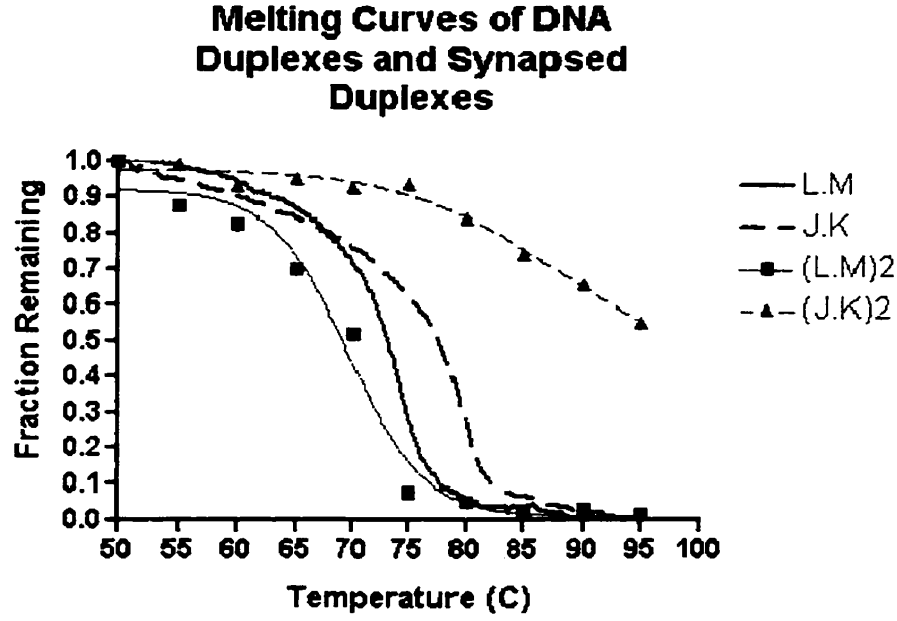

Figure 3-5. Thermal melting profiles of the duplexes J·K and L·M and of their duplex dimers.

The melting behavior of the duplex-dimers $(J{\cdot}K)_2$ and $(L{\cdot}M)_2$ was most conveniently measured using gel-electrophoretic techniques (Venczel & Sen, 1996; Fahlman & Sen, 1998). Owing to the high double-stranded DNA content (relative to quadruplex content) of both $(J{\cdot}K)_2$ and $(L{\cdot}M)_2$, the dimer dissociation is difficult to monitor spectroscopically, owing to the large spectroscopic contribution of those double-stranded arms. Pre-formed duplex-dimer samples were diluted to lower their DNA concentration to <100 nM, such that a re-association of dissociated duplex dimers was essentially undetectable within the experimental timescale. The samples' ionic strength was maintained at 1M KCl in TMACl buffer. The melting behaviors of $(J{\cdot}K)_2$ and $(L{\cdot}M)_2$ were then measured as described in Materials and Methods. Figure 3-5 shows that the $(L{\cdot}M)_2$ to L·M transition was cooperative and had a midpoint of ~ 71 ± 2° C. The $(J{\cdot}K)_2$ complex was, by contrast, more stable, and did not describe a complete melting curve by 95° C. In fact, the broad initial phase (from 75° - 95°) of $(J{\cdot}K)_2$ breakdown may represent the breakdown of a proportion of $(J{\cdot}K)_2$ complexes containing fewer G-quartets than the bulk of the $(J{\cdot}K)_2$ complexes (from a "slipped" or imperfectly aligned side-by-side arrangement of the two participating J·K duplexes). Alternatively, this initial phase of $(J{\cdot}K)_2$ breakdown may reflect very slow kinetics of dissociation (on the experimental timescale) of the $(J{\cdot}K)_2$ complex. In either event, it was clear that the $(J{\cdot}K)_2$ dimer was significantly more stable than the $(L{\cdot}M)_2$ dimer.

3.4 Self-Selectivity of Synaptic Dimerizations

To determine whether the duplexes would cross-react to form *hetero*-dimers, solutions containing both duplexes, J·K and L·M, were incubated under standard

dimerization conditions (see above). Figure 3-6 shows these results. It had been previously demonstrated that if two synapsable duplexes, say A·B and mH8, containing the *same* synapsable G-G domain, but being of different overall lengths (and therefore having different electrophoretic mobilities) were allowed to dimerize together, a hetero-dimer (A·B)·(mH8) formed, in addition to the $(A{\cdot}B)_2$ and $(mH8)_2$ homodimers. Being of intermediate molecular weight the (A·B)·(mH8) complex ran in the gel between the $(A{\cdot}B)_2$ and $(mH8)_2$ complexes; in other words, a total of three product bands was seen (Venczel & Sen, 1996). Figure 3-6, lane C, shows that when a dimerization mixture containing J·K and L·M was allowed to reach equilibrium in 1M KCl at 37° C, only the two bands corresponding to the homo-dimer products $(J{\cdot}K)_2$ and $(L{\cdot}M)_2$ were observed. Therefore, dimerization by these two duplexes appeared to be *self*-specific.

Furthermore, if the same dimerization mixture was incubated briefly (~ 20 minutes), such that equilibrium was not reached, only the $(L{\cdot}M)_2$ product was observed (Figure 3-6, lane B). Therefore, the rapid kinetics of $(L{\cdot}M)_2$ formation could be exploited to obtain just this dimer out of a J·K and L·M mixture. Analogously, we found that the greater thermodynamic stability of $(J{\cdot}K)_2$ could be taken advantage of to obtain only the $(J{\cdot}K)_2$ complex out of the same dimerization mixture. If the 1M ionic strength of a solution containing an equilibrium distribution of J·K, L·M, $(J{\cdot}K)_2$ and $(L{\cdot}M)_2$ was diluted to a final salt concentration of 10 mM KCl in TMACl-buffer, and the diluted solution incubated at 37° C for 20 min, $(L{\cdot}M)_2$ was found selectively to dissociate (Figure 3-6, lane D). Lane E shows that under these low salt conditions for the selective breakdown of $(L{\cdot}M)_2$ neither J·K nor L·M were able to dimerize, even after 3 days of incubation.

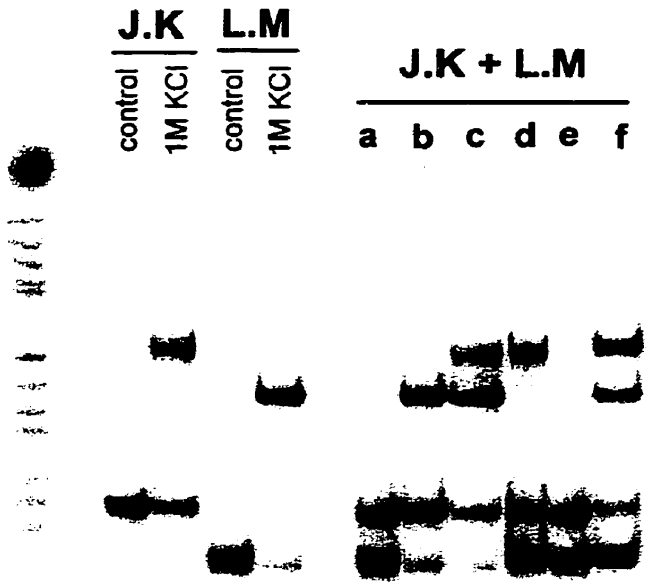

Figure 3-6. **Self-selectivity of J·K and L·M dimerization. Samples of J·K and L·M alone (left panel) contain 2.0 μM dsDNA in TMACl buffer (100mM TMACl) and 10 mM Tris (pH 7.9), with and without 1 M KCl. These samples were incubated at 37°C for 72 h. Mixed samples containing 2.0 μM each of the J·K and L·M duplexes are shown in lanes a-f, in all cases incubated in TMACl buffer. Lanes b and c, incubations in TMACl buffer containing 1 M KCl; lane b shows a 20-min incubation, lane c shows a 72-h incubation. Lane d, the effect of diluting a preincubated sample (as in lane c) to a KCl concentration of 10 mM. Lane c, incubation in 10 mM KCl. Lane f, incubation in 1 M NaCl.**

The above experiments demonstrated the high versatility of this system; such that from a single starting solution containing the J·K and L·M duplexes, we were able to obtain at will a $(J{\cdot}K)_2$ synapsis, a $(L{\cdot}M)_2$ synapsis, or both synapses at the same time. Control incubations with single-stranded J and L oligomers carried out in 1M KCl at 37° C indicated that these oligomers formed J_4 and L_4 quadruplexes, as expected, but also cross-associated, to give the series of complexes J_3L, J_2L_2, etc (data not shown).

Therefore, the specificity of self-association described above was unique to the J·K and L·M *duplexes*, and not to their component single-strands. This example of self-selectivity by G-quadruplex-forming DNA species is currently unique.

3.5 The duplex J•K forms a dimerization-incompetent conformer, J•K'

In order to understand the molecular events that permitted self-selective synaptic dimerizations by J·K and L·M to occur out of mixtures of the two duplexes, it was necessary to examine both the anomalous kinetics and cation-preference observed for the formation of $(J{\cdot}K)_2$. To do this we examined precisely which of the guanines in J·K were, under different solution conditions, involved in G-quartet formation-- to determine whether *intra*-molecular G-quartets could form in the undimerized J·K duplex. The technique used for this investigation was methylation-protection. Guanines that are involved in G-quartet formation (unlike those that are either not base-paired or are involved in Watson-Crick G≡C base-pairs) are resistant to methylation by dimethyl sulfate (DMS) at their N-7 positions, and this "protection" from methylation can be used to pinpoint those guanines in a synaspable duplex or in a synapsed duplex-dimer that are participating in a guanine-quartet (Sen & Gilbert, 1988).

The results of the DMS probing of J, L, J·K, L·M, $(J{\cdot}K)_2$, and $(L{\cdot}M)_2$ are shown in Figure 3-7 as sequencing gels, with the guanines in strands J and L, respectively, being examined in all cases. As expected, in the duplex dimers $(J{\cdot}K)_2$ and $(L{\cdot}M)_2$, the guanines in the respective G-G domains (indicated within brackets) showed methylation protection of all or some of the guanines within the domains, relative to the duplex samples methylated in LiCl. The $(L{\cdot}M)_2$ duplex dimer exhibited complete protection of its

mismatch guanines while $(J{\cdot}K)_2$ exhibited only a partial protection of 5 of its 7 mismatch guanines. It was the J·K and the L·M samples in potassium solutions that showed the most revealing results. Whereas the L·M duplex showed similar methylation patterns of its G-G domain guanines in both lithium and potassium solutions [the slight protection of all the domain guanines in potassium was probably due to a partial interconversion of L·M and $(L{\cdot}M)_2$ within the methylation timescale], the J·K duplex in potassium solution showed a quite different protection pattern from its counterpart in lithium solution. In the J·K sample in potassium the two isolated guanines of its motif TTGGTTGGGGGTT were fully methylation-protected along with two of the guanines out of the remaining stretch of five. This protection pattern was highly suggestive of the possibility that even in its duplex form J·K formed a significant conformer, J·K', which already contained (intramolecular) G-quartets, thus rendering this conformer incapable of dimerizing to $(J{\cdot}K)_2$. A schematic diagram for the structure of the conformer J·K', which we term a "pinched" duplex, is given in Figure 3-8.

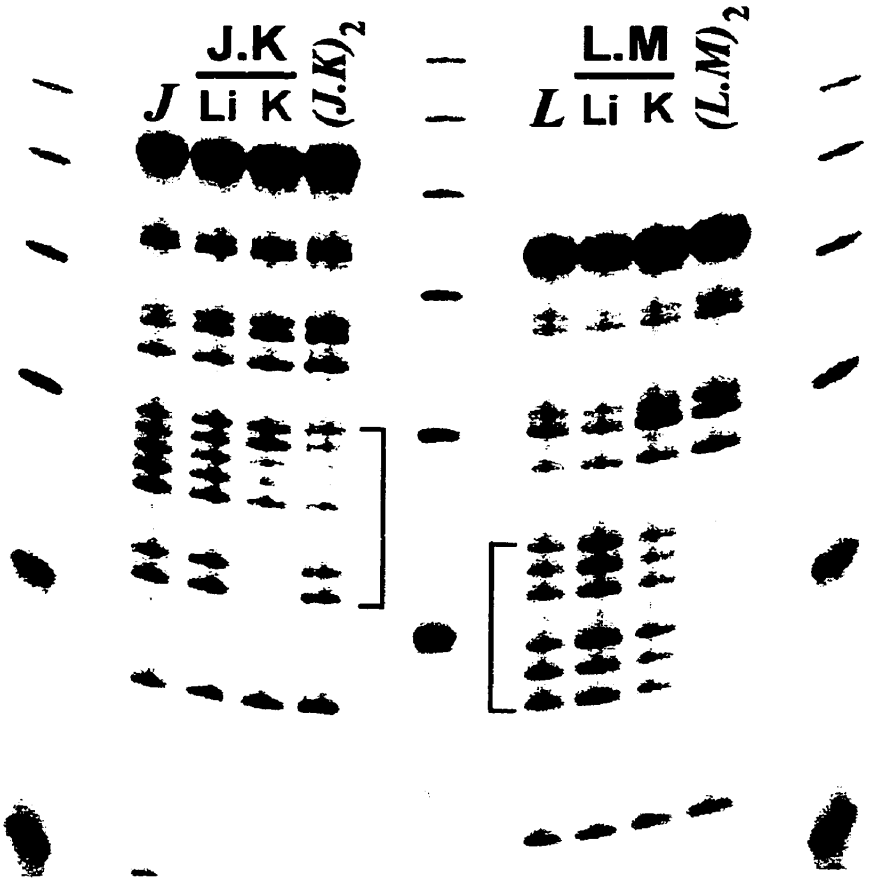

Figure 3-7. **Sequencing gels showing Methylation protection patterns of the L·M and J·K duplexes. DNA samples were partially methylated by DMS and cleaved at methylated guanine bases with piperdine as described in the Materials and Methods section. All Methylation reactions wee carried out in TMACl buffer at 37°C. Lanes J and L display the patterns of the single-stranded DNA sequences J and L methylated in 1 M LiCl. Lanes containing the duplex DNA samples, J·K and L·M, were methylated either in 1 M LiCl or in 1 M KCl (as indicated). Methylation of the duplex dimers, lanes $(J{\cdot}K)_2$ and $(L{\cdot}M)_2$, was carried out in 1 M KCl.**

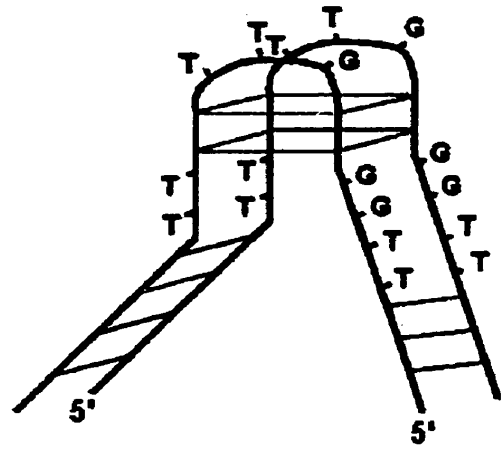

Figure 3-8. Model for the potassium confomer of J·K, the J·K' "pinched" duplex.

3.5.1 H·I a Minimized form of the J·K Domain

To test our hypothesis that the above model was true, a simplified version of the J·K G-G domain was created. The new duplex, H·I, had the domain sequence of TTGGGGGTT, which would be expected to lack the ability to fold back to form intramolecular G-quartets, such as found within J·K. The removal of the extra doublet of G-G mismatches of the J·K domain rid of all indications of a 'pinched' duplex. As predicted, the H·I duplex exhibited a normal preference shown in figure 3-9 for the alkali cations: $K^+ > Na^+ \sim Rb^+ > Li^+ \sim Cs^+$, unlike J·K but similar to L·M.

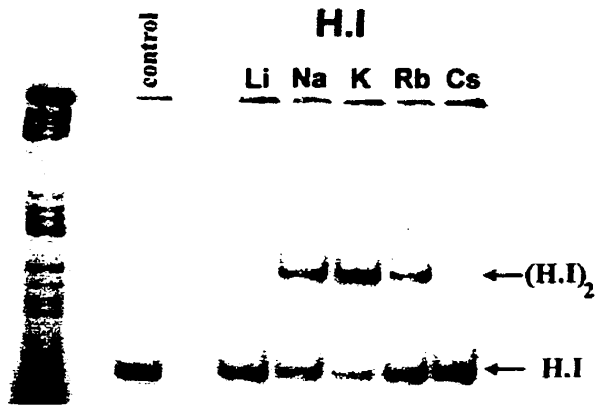

Figure 3-9. **H·I Dimerization. Nondenaturing polyacrylamide gels showing the influence of the different alkali cations on the synaptic dimerization of the H·I duplex. Samples of 2.0 μM duplex DNA were incubated at 37°C for 48 h in the presence of different alkali chlorides. Control samples contained 100 mM TMACl and 10 mM Tris (pH 7.9), while the other samples were incubated in 1 M XCl (where X = Li, Na, K, Rb or Cs), 100mM TMACl, and 10 mM Tris (pH 7.9)**

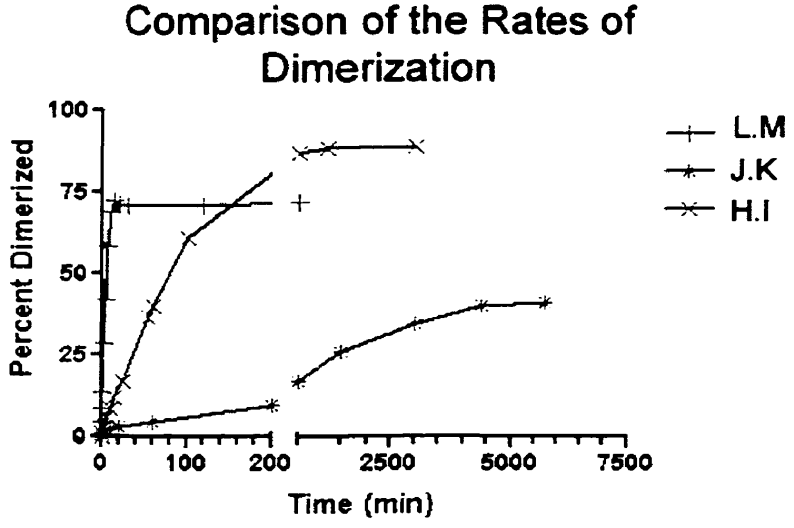

Figure 3-10. **Comparison of the time dependence of dimerization of the three duplexes: L·M, H·I and J·K. Duplex concentrations are 0.5, 1.0, and 2.5 uM respectively. Samples were incubated in 1M KCl, 100 mM TMACl, 10 mM Tris (pH 7.9) at 37°C.**

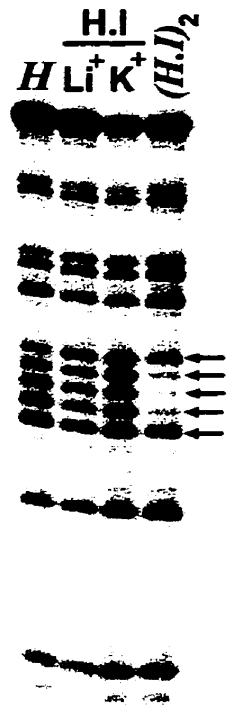

Figure 3-11. Methylation protection of the H·I duplex. DNA samples were partially methylated by DMS and cleaved at methylated sites with piperdine as described in the Materials and Methods section. All Methylation reactions were carried out in TMACl buffer at 37°C. Lane H displays the patterns of the single-stranded DNA sequence H methylated in 1 M LiCl. Lanes containing the duplex DNA samples, labeled H·I, were methylated either in 1 M LiCl or in 1 M KCl (as indicated). Methylation of the duplex dimer, lanes $(H{\cdot}I)_2$, was carried out in 1 M KCl. Arrows indicate the 5 G·G mismatches in the dimerization domain.

Duplex H·I also dimerizes significantly faster than J·K and in contrast exhibited second-order kinetics with a rate constant of $3.3 \times 10^3 \pm 0.8 \times 10^3$ M^{-1} min^{-1} at 37° C in 1M KCl. The rate constant was determined by triplicate experiments using different DNA concentrations. As shown in figure 3-10, the H·I duplex still dimerizes significantly slower than L·M suggesting another phenomena may also be occurring other than a 'pinched' duplex structure. The dissociation constant for the $(H{\cdot}I)_2$ dimer was determined to be 76 ± 40 nM under these same conditions. Thermal denaturation

experiments revealed a melting temperature for the synapsed $(H{\cdot}I)_2$ product of 88 $\pm$ 2° C under the same conditions used in examining J·K and L·M in section 3.3 above.

Methylation studies shown in figure 3-11 of the H·I duplex also showed, predictably, that the reactivity pattern of domain guanines in un-dimerized H·I duplexes were equivalent in lithium and potassium solutions. As with the $(J{\cdot}K)_2$ synapsed duplexes and the $(A{\cdot}B)_2$ and $(A{\cdot}\beta)_2$ synapsed duplexes discussed in chapter 2 section 3.2, the periphery G·G mismatches do not exhibit methylation protection as opposed to the observation for $(L{\cdot}M)_2$ in figure 3-7. The T·T mismatches that flank the G·G mismatches provide enough conformational flexibility to allow for a G-quartet to double helix transition (otherwise the same observation would have been made for $(L{\cdot}M)_2$). A potential explanation is that a significant proportion of H·I dimerizes out of phase, such that only 4 G-quartets form. This would result in only partial protection of the terminal guanines (partial because guanines on either end would be randomly excluded from G-quartet participation). This explanation cannot completely explain the results as the methylation of the terminal guanines is more than 50% of those in the double helical arms, so other factors must also be involved.

To test whether the self-selectivity of synapsis that we had observed from mixtures of J·K and L·M also occurred in mixtures of H·I and L·M, incubations for dimerization of mixed samples in 1M KCl were carried out (figure 3-12). As with the J·K and L·M combination no heterodimer product (H·I)·(L·M) was observed, even when incubations were carried out at the permissive temperature of 4° C in 1M KCl (data not shown).

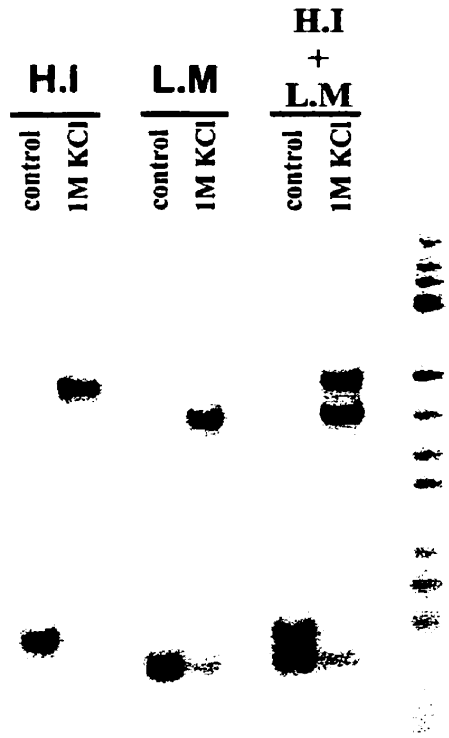

Figure 3-12. Selectivity between H·I and L·M. Samples containing 1 μM of the indicated dsDNA where incubated overnight at 37°C in TMACl buffer and with or without 1 M KCl. No hybrid dimer is observed, indicating that the H·I and L·M domains exhibit self-selectivity upon dimerization.

3.6 The Assembly of More Sophisticated DNA Superstructures.

3.6.1 Design of 3-Way Junction Containing L·M and H·I Dimerization Domains

We constructed a 3-way junction of DNA duplexes, (H·I)T(L·M), two of whose arms contained, respectively, the G-G domains of H·I and L·M (*"h·i"* and *"l·m"*, Figure 3-13(a)). A known stable 3-way junction was used as the core of the structure that had two bulged thymines at the junction. Incorporation of extra bases and the junction of 3-way junctions is known to increase the stability of these structures (Leontis *et al*, 1991; Stuhmeier *et al*, 1997). The core 3-way junction we chose to use has been studied by high-resolution NMR by Leontis *et al*, 1993, who found that it preferred to adopt a "T"-

like conformation of the three arms (rather than a "Y"-like conformation observed with 3-way junctions with no extra bases at the junction). The structure of this 3-way junction is shown in figure 3-13(b). Extra sequences were added to the ends of the arms of this core structure to form the final (H·I)T(L·M) construct. The spacing of the synapsable domains from the junction was such that their major grooves would be on the opposite side of that of the third arm of the junction. The (H·I)T(L·M) construct was simply constructed by annealing together the two synthetic single-stranded DNA oligomers (see Materials & Methods). Only two sequences where required because as indicated schematically in figure 3-13(a), two of the sequences were linked by a hairpin loop at the end of one of the arms of the 3-way junction.

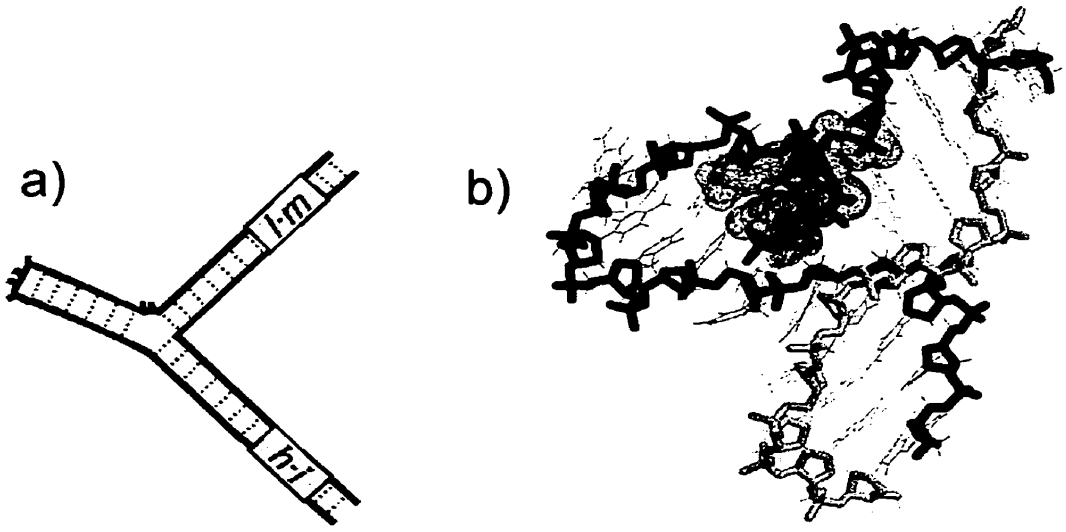

Figure 3-13. **a) Depiction of (H·I)T(L·M). The three-way junction is assembled from two DNA sequences by the use of a hairpin loop in the short double stranded arm. b) The NMR structure of the 3-way junction published by Leontis *et al* (1993)[1] that the (H·I)T(L·M) construct was based on. The DNA backbone is highlighted to emphasize the overall directionality of the helices. Orientation of the structure is matched to the diagram in a). The two bulged bases at the junction are shaded in as a space-filling model.**

[1] Protein Structure Database (www.rcsb.org/pdb/) PDB ID: 1EKW.

3.6.2 Dimerization of the 3-Way Junction

Upon dimerization of the domains of (H·I)T(L·M) there are two potential results. Two constructs can dimerize by matching up both of their H·I and L·M domains with each other's as depicted in figure 3-14(a). The alignment of the synapsable domains such that the proximal ends, with respect to the junction, of each domain are associated is termed a 'head to head' association. Directionality of association must be described because of the symmetry of the synapsable domains. Alternatively each domain of an (H·I)T(L·M) construct may dimerize with a domain on two different (H·I)T(L·M) constructs. In this case the domains are associated in a 'head to tail' orientation. In the second case of association the result would be a linear (in the sense of connectivity) polymeric assembly of unpredictable unit length (figure 3-14(b)). This scenario would result in a 'ladder' of slow migrating bands in electrophoresis experiments. The dimer would predictably run as a single entity but the end to end polymeric assembly would be observed as multiple species, each corresponding to a specific unit length of the assembly.

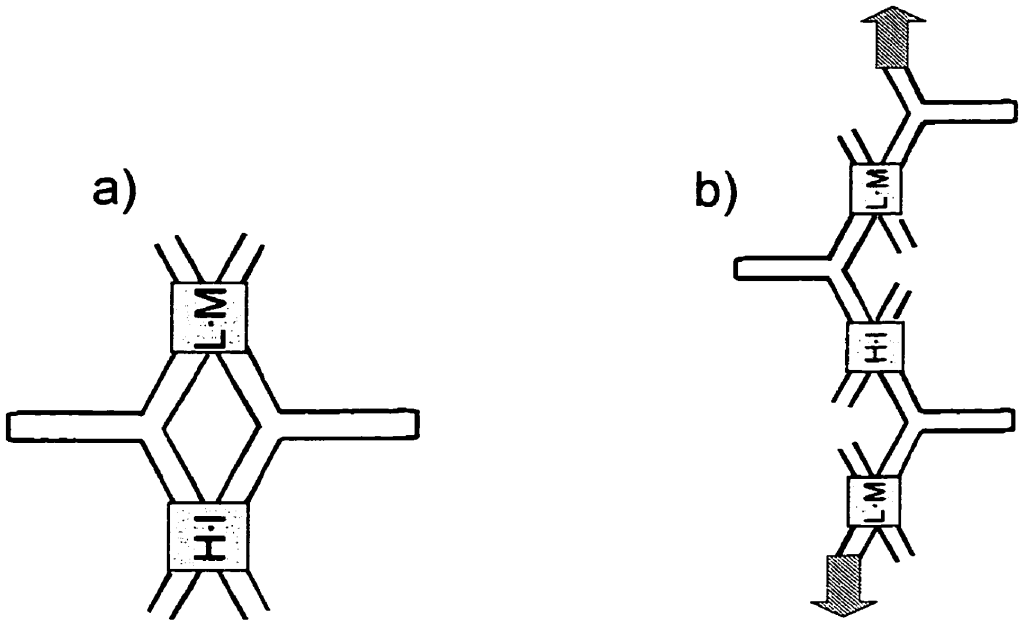

Figure 3-14. Models for the association of (H·I)T(L·M). a) A dimeric structure where association at the synapsed sites is to the same (H·I)T(L·M) construct. B) A polymeric assembly of (H·I)T(L·M), where each domain associates to a different (H·I)T(L·M) construct.

On incubation of (H·I)T(L·M) with potassium a single predominant higher-order complex formed rapidly and almost quantitatively (figure 3-15). A single major product indicates that both postulated products in figure 3-14 do not form, and the identity of this product was pursued. The simplest explanation for the formation of a single product species is that it is a dimer. Whether it is the dimer shown in figure 3-14(a) or whether it is a dimer that utilizes only one dimerization domain could not be established with out further examination.

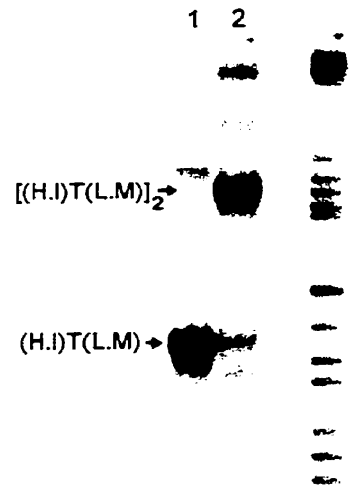

Figure 3-15. Dimerization of the (H·I)T(L·M) three-way junction. Samples containing 1.0 μM (H·I)T(L·M) were incubated in TMACl buffer (lane 1) and in TMACl buffer containing 1 M KCl (lane 2). Samples were incubated for 3 h at 37°C. The lane on the right shows DNA size markers.

Evidence that the major product was a dimeric product, $[(H{\cdot}I)T(L{\cdot}M)]_2$, (such as shown schematically in figure 3-14(a)) was obtained from methylation-protection experiments (figure 3-16). This experiment revealed that both the $h{\cdot}i$ and $l{\cdot}m$ domains showed the methylation-protection patterns characteristic of their having undergone synapsis. When methylation-protection experiments were carried out in a time-dependent manner, it was found that, as expected, that the $l{\cdot}m$ domain synapsed first, in the first 10 minutes, followed by the $h{\cdot}i$ domain (data not shown). Further evidence that $[(H{\cdot}I)T(L{\cdot}M)]_2$ was held together at both the H·I and L·M synaptic sites was suggested further by the fact that this complex was fully stable to melting even at 95° C, at which temperature the individual $(H{\cdot}I)_2$ and $(L{\cdot}M)_2$ duplex-dimers had melted (see previous section 3.3 and 3.5.1).

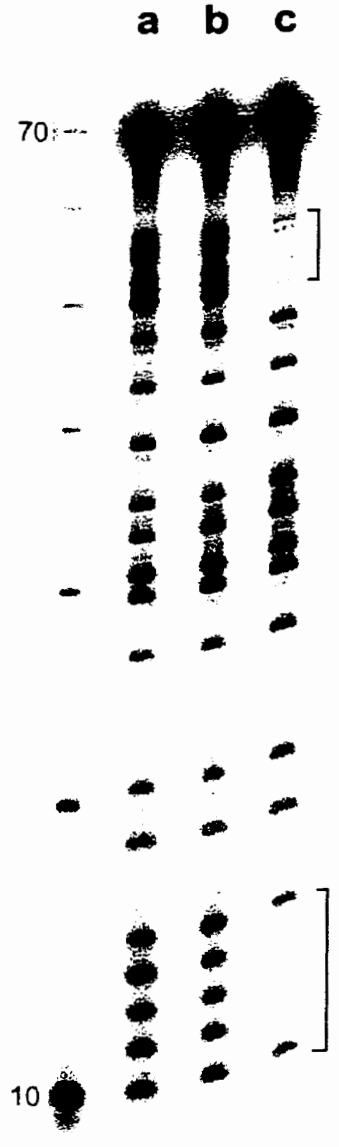

Figure 3-16. **Sequencing gel showing Methylation protection of guanine bases. DNA samples were partially methylated by DMS and cleaved at methylated sites with piperdine as described in the Materials and Methods section. All Methylation reactions wee carried out in TMACl buffer at 37°C after a 2hour pre-incubation in the appropriate salt solution. Lanes (a) and (b) show the probing pattern of undimerized (H·I)T(L·M) in 1M LiCl or KCl respectively. Methylation of the dimer, lane (c), was carried out in 1 M KCl. Square brackets indicate the two dimerization domains, *I.m* upper and *h.i* lower.**

The absence of polymeric association of (H·I)T(L·M) is peculiar. There should be no steric interference to prevent association. The double stranded region distal to the dimerization domains, with respect to the junction, is shorter (10 bp) in comparison to the proximal double stranded region (15 & 14 bp). These distances prevent the ends of the arms of two different constructs from interfering with each other during association with the same (H·I)T(L·M) construct. Despite the fact that the dimeric structure is predicted to be thermodynamically more stable, with two synapsed sites maintaining association, the association constants measured for individual L·M and H·I duplexes indicate favorable enough association to allow the polymeric assemblies to persist in solution to a reasonable extent.

3.6.3 An Alternate Dimeric Structure for (H·I)T(L·M)

The pursuit of a explanation of why (H·I)T(L·M) does not form polymeric assemblies led to the realization of an alternate dimeric structure to that original shown in figure 3-14(a). If two constructs associate in a 'head to tail' fashion as would occur in the formation of polymeric assemblies an alternate outcome could occur. The flexibility of the two T·T linker mismatches flanking each domain and the parameter that G-quartet structures are right handed helical structures with a rotation of ~30° a quartet (Kang *et al,* 1992) would allow for the undimerized domains to also come in contact with each other and also dimerize as indicated in figure 3-17. The determination of what kind of dimer product forms cannot be determined by the data on hand. There is also a possibility of mixed types where one domain is associated in a 'head to head' fashion while the other is in a 'head to tail' orientation in the dimer structure. The degree of variability in the

different modes of association will in essence be dependent on the flexibility of the junctions and linker sequences.

This type of unpredictability in the structure of dimerization would be prevented by the use of synapsed domains that cannot dimerize in a symmetrical fashion. The designs of such synapsable domains are described in section 3.7.

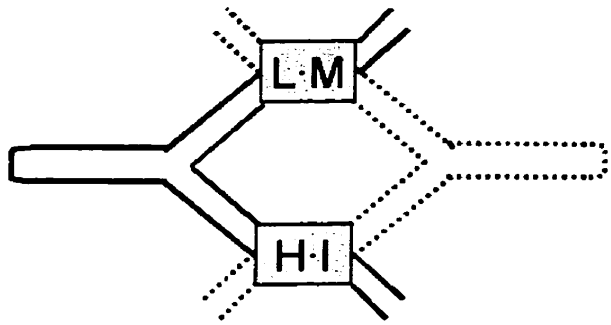

Figure 3-17. An alternate structure for (H·I)T(L·M). Individual (H·I)T(L·M) constructs are indicated as either a solid or a dashed line. The symmetry of the H·I and L·M domains also allows for a 'head to tail' type of association along with the 'head to head' type association depicted in figure 3-14(a).

3.6.4 Higher Order Assemblies

Constructs like $[(H{\cdot}I)T(L{\cdot}M)]_2$ may be regarded as a structural "tile" for the assembly of DNA superstructures and, as shown in figure 3-18(A), it is a structural analogue of the double-crossover complex (figure 3-18(B)) used as a construction "tile" by Seeman and coworkers (Winfree *et al*, 1998; Liu *et al*, 1999; Mao *et al*, 1999b). A key difference between the two "tiles" is that constructs like the $[(H{\cdot}I)T(L{\cdot}M)]_2$ tile may be broken down and reconstructed from its synaptic precursor (H·I)T(L·M) by controlling solution conditions (i.e. by adding or removing potassium), and without the need for a topological untangling of strands as might be required for the double-crossover. In order to have precise control over the way synapsable domains associate, non-symmetrical

domains would have to be used for the reasons observed in section 3.6.2. In the case of higher order DNA assemblies, synapsable domains described in section 3.7 would have to be used.

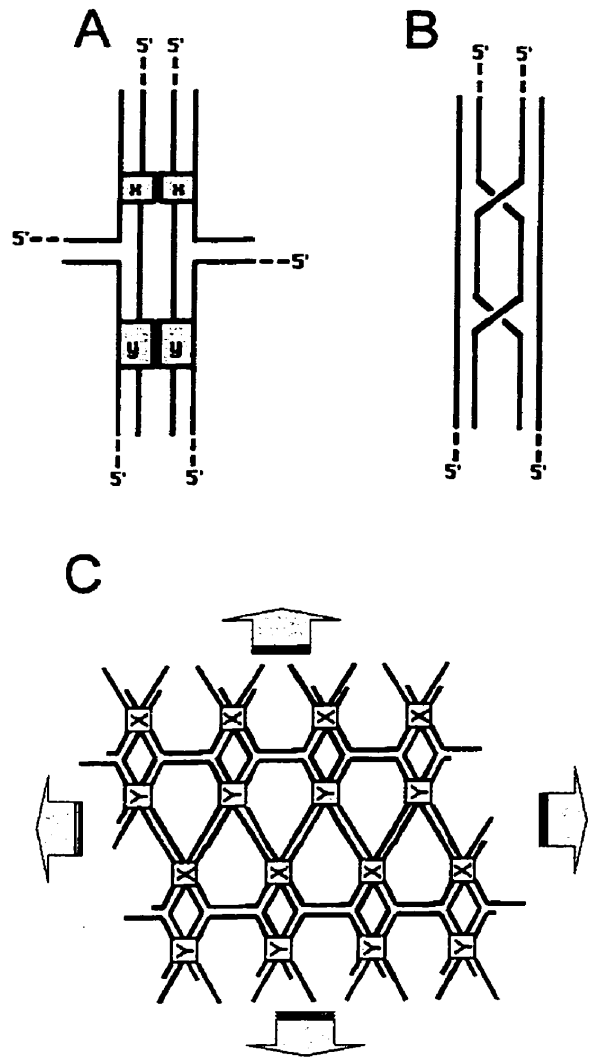

Figure 3-18. **Using (H·I)T(L·M) 'like' constructs as 'tiles' in 2-dimensional arrays. A) Three-way junction construct containing synapsable domains can potentially associate into higher-order structures by the use of sticky end methodologies. B) For comparison the double crossover is shown to indicate similarities between the structures. C) Proposed schematic for a two-dimensional array associated by synapsable domains and sticky ends.**

Figure 3-18(A) shows schematically that either two, four, or six unique sticky-end sequences can be associated with the $[(H{\cdot}I)T(L{\cdot}M)]_2$ tile, in a predetermined orientational relationships to one another. Such a tile, either by itself, or in combination with double-crossover tiles, could be used to generate a variety of repeating structural arrays. A schematic diagram of 'tile' structures, using postulated X and Y synapsable domains, is associated in a two dimensional array by association six sticky end sequences in shown in figure 3-18(C). An interesting new flexibility in assembling DNA superstructures or repeating arrays using both the $[(H{\cdot}I)T(L{\cdot}M)]_2$-like and double-crossover modules might be that assembly could be carried out in two different sequential orders, depending on the superstructure being assembled. For instance, the sticky-end annealing processes of the double-crossovers (which are favored by the overall solution ionic strength, but not by specific Group IA or IIA cations) could either precede or follow the G-G domain-mediated synaptic annealing (which are favored specifically by potassium ions and disfavored by lithium ions).

3.7 Future Design on Non-Symmetrical Domains

We have determined that for efficient and detailed control of DNA nanostructure assembly using synapsable DNA we need more that specificity in dimerization. A second component for dimerization is also essential. Precise and predictable orientational association is also critical to make synapsable DNA methodologies practical for nanostructure assembly.

It should be possible to design synapsable domains that exhibit specificity as the domains we have discussed in this chapter that also only dimerize in one orientation. Domains like J·K could be used, but I think this motif is also impractical because of extremely low rates of dimerization.

Taking what we have learned in this chapter and chapter 2, we can apply this to systems that include the self-association of other bases. Of particular interest is isoguanine (figure 3-19(A)), which can also associate into quartet structures in a cation dependent manner as shown in figure 3-19(B) (Seela *et al*, 1996; Tirumala & Davis, 1997). The properties of isoguanine have had significantly less investigated than G-quartets, but it is known that they exhibit a similar cation preference of $K^+ > Na^+$ (Roberts *et al*, 1997).

What makes isoguanine potentially better suited for our task is that isoguanine has been reported to only form quadruplex structures with their backbones in an all-parallel orientation (Roberts *et al*, 1997). Formation of only all parallel structures also holds true in quadruplex structures containing quartets composed of guanine and isoguanine bases. The incorporation of isoguanine bases along with guanines in reverse polarity, synapsable domains can be constructed like L·M and H·I, which should only be able to dimerize in one orientation as in figure 3-19(C). By incorporating the different designs highly selective synapsable domains with a precise directional alignment upon dimerization should be readily obtainable.

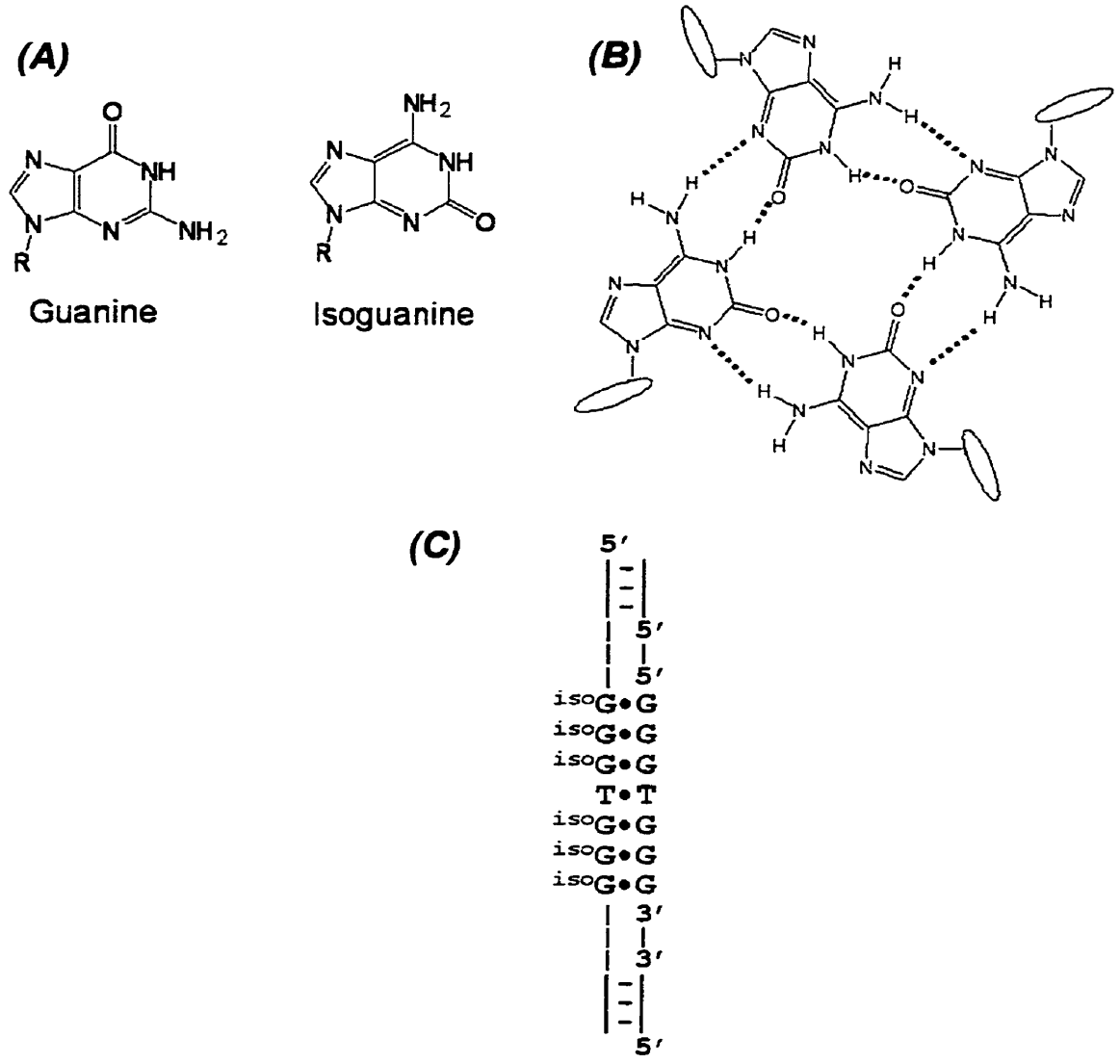

Figure 3-19. **Isoguanine quartets. A) Comparison of guanine and isoguanine bases. B) Proposed structure of an isoguanine quartet. C) A synapsable domain using isoguanine that mimics the structure of LMTT-0 (L·M) but should posses a single orientation in dimerization.**

4. Conclusions

A key result reported in this chapter is the property of synaptic specificity, observable in solution mixtures of two synapsable duplexes with non-identical G-G domains. We have shown that experimental conditions can be established in which (a) two non-identical synapsable duplexes both dimerize by synapsis, but overwhelmingly to *self* (simultaneous specificity); and (b) one duplex at a time dimerizes selectively to give its homosynapsed dimer; whereas the other duplex remains undimerized (individual specificity). Undoubtedly many more such self-specific G-G domains can be designed. The availability of a number of such domains will facilitate the self-assembly of complex DNA superstructures. In this paper we have demonstrated a simple example of the utility of the simultaneous specificity scheme, whereby two different G-G mismatch domains incorporated into the arms of a 3-way junction DNA molecule, (H·I)T(L·M), were able to synapse, upon the addition of an stabilizing cation (potassium), to form a the dimer, $[(H{\cdot}I)T(L{\cdot}M)]_2$. The use and versatility of controlled individual dimerization of G-G domains within a single molecule may be particularly useful in the construction of complex objects.

Chapter 4

Effects of T·T Spacers on 'Synapsable' DNA Duplexes

1. Introduction

We have previously examined the affect of arranging the G·G mismatches into 'patterns' by incorporating interrupting thymine – thymine (T·T) mismatches within contiguous stretches of G·G mismatches. This approach discussed in chapter 3), demonstrated that 'patterned' G·G mismatches could be made self-selective, in that one 'pattern' or domain selectively dimerizes with similar domains even in mixed solutions (Fahlman & Sen, 1999).

Unexplained observations arose in this study of domains containing T·T mismatches. The L·M duplex dimerized significantly faster than the H·I duplex, while neither were identified to form an inhibitory pinched duplex as seen previously with the A·β and J·K duplexes.

In this chapter an examination of the dimerization properties were done on a G·G mismatch domain while systematically varying the number of T·T spacer mismatches between the G·G mismatches. The basic design we chose to examine was the originally designed L·M duplex. We chose this construct because of its simple symmetrical design and its unusually fast rate of dimerization (observed second order rate constant of 1.5×10^5 $M^{-1}min^{-1}$ (Fahlman & Sen, 1999)

The original L.M. domain had a single T-T mismatch spacing two G-G mismatch triplets. To examine the affects of this T-T spacer, we varied this internal T-T mismatch from 0 to 3 T-T mismatches as depicted in figure 4-1. To examine whether potential base pairs in place of the T·T mismatches have any affect, duplexes containing AT base pairs

(figure 4-5) where also examined. For consistency, the original L.M duplex is re-named LMTT-1 in this manuscript.

With this study we hoped to gain some insight into what is required for specificity. Do the slightest differences cause the synapsable domains be selective or are significant differences in the designs required.

2. Materials and Methods

2.1 DNA Sequences

All oligonucleotides were purchased from Sigma Genosys, except L-0, M-0, L-1T and L-2T, which were synthesized at the University of Calgary Core Services. DNA samples were resuspended in TE buffer and gel purified as described in chapter 3. Final concentrations of samples were determined by measuring optical densities of the solutions.

The following sequences were used in the assembly of the indicated synapsable duplexes. Underlined sequences indicate the sequences that make up the synapsable domain when the duplexes are assembled.

Duplex **LM-0** (43 bp).

L-0: 5'-CCTCGAGAAGCTCCTGATTGGGGGGTTTGTGGTTCAAGGATCC-3'

M-0: 5'-GGATCCTTGAACCACATTGGGGGGTTTCAGGAGCTTCTCGAGG-3'

Duplex **LMTT-1** (43 bp) - *the original L·M duplex from chapter 3.*

L-T: 5'-CTCGAGAAGCTCCTGATTGGGTGGGTTTGTGGTTCAAGGATCC-3'

M-T: 5'-GGATCCTTGAACCACATTGGGTGGGTTTCAGGAGCTTCTCGAG-3'

Duplex **LMTT-2** (43 bp)

L-2T: 5'-TCGAGAAGCTCCTGATTGGGTTGGGTTTGTGGTTCAAGGATCC-3'

M-2T: 5'-GGATCCTTGAACCACATTGGGTTGGGTTTCAGGAGCTTCTCGA-3'

Duplex **LMTT-3** (43 bp)

L-3T: 5'-TCGAGAAGCTCCTGATTGGGTTTGGGTTTGTGGTTCAAGGATC-3'

M-3T: 5'-GATCCTTGAACCACATTGGGTTTGGGTTTCAGGAGCTTCTCGA-3'

Duplex **LMTT-1** ***L*** (53 bp)

L-1T ***L***:

5'-AGTGACTCGAGAAGCTCCTGATTGGGTGGGTTTGTGGTTCAAGGATCCACAGT-3'

M-1T ***L***:

5'-ACTGTGGATCCTTGAACCACATTGGGTGGGTTTCAGGAGCTTCTCGAGTCACT-3'

Duplex **LMTT-2** ***L*** (53 bp)

L-2T ***L***:

5'-GTGACTCGAGAAGCTCCTGATTGGGTTGGGTTTGTGGTTCAAGGATCCACAGT-3'

M-2T ***L***:

5'-ACTGTGGATCCTTGAACCACATTGGGTTGGGTTTCAGGAGCTTCTCGAGTCAC-3'

Duplex **LMAT-1** ***L*** (53 bp)

L-1T*L*: sequence shown above.

M-1A ***L***:

5'-ACTGTGGATCCTTGAACCACATTGGGAGGGTTTCAGGAGCTTCTCGAGTCACT-3'

Duplex **LMAT-2** (43 bp)

L-2T: sequence shown above.

M-2A: 5'-GGATCCTTGAACCACATTGGGAAGGGTTTCAGGAGCTTCTCGA-3'

Duplex **LMAT-2** ***L*** (53 bp)

L-2T ***L***: sequence shown above.

M-2A ***L***:

5'-ACTGTGGATCCTTGAACCACATTGGGAAGGGTTTCAGGAGCTTCTCGAGTCAC-3'

Duplex **LMAT-3** ***L*** (53 bp)

L-3T ***L***:

5'-GTGACTCGAGAAGCTCCTGATTGGGTTTGGGTTTGTGGTTCAAGGATCCACAG-3'

M-3A ***L***:

5'-CTGTGGATCCTTGAACCACATTGGGAAAGGGTTTCAGGAGCTTCTCGAGTCAC-3'

2.2 Duplex Assembly

One strand of a duplex was radio-labeled at 5'- phosphate by T4 kinase and γ-^{32}P-ATP. The labeled DNA was then ethanol precipitated by mixing with 300 mM sodium acetate and 3× volume of EtOH. The precipitated DNA was resuspended in 20 µl of TE buffer.

Formation of double stranded DNA was carried out by mixing 1 nmol of one unlabeled strand with 0.9 nmol of the complementary unlabeled strand plus 0.1 nmol of its labeled strand in 1 µl of 1× TMACl [100 mM tetramethylammonium chloride (TMACl); 10 mM Tris, pH 7.9]. The solution was heated to 95 °C for one minute and allowed to cool to 37 °C. The DNA duplex formed was gel purified in 8% non-

denaturing polyacrylamide gel, which was electrophoresed in TBT buffer (50 mM Tris-borate, pH 8.0; 10mM TMACl) at 9W at room temperature. Bands of DNA duplex were visualized by autoradiography, excised and eluted into 500 µl of 2× TMACl buffer. The eluted DNA samples were concentrated by Micron Microconcentrators (Amicon) if it was necessary.

2.3 Formation of duplex dimers

2.3.1 Kinetic of Dimerization

The concentrations of the eluted DNA duplexes were determined by optical densities. 40 µl of one DNA duplex sample was mixed with 40 µl of 2 M KCl at 37 °C. The final concentration of the DNA was therefore 1/2 of the initial concentration. Small aliquots were then removed from the mix at different time points and loaded on a 8% non-denaturing polyacrylamide gel, which was electrophoresed in KMg buffer (50mM Tris-borate, pH 8.0; 10 mM KCl; 2 mM $MgCl_2$) at 6W at room temperature. The gels were dried and the bands were visualized on a phosphoimager (BioRad G5-250). The intensities of the bands representing the duplexes and the dimers were quantitated and compared.

2.3.2 Cross-reactivity of Dimerization

The concentration of each DNA duplex was determined, and aliquots were made so that each had the same concentration (1.46 µM). 2.5 ul of one short duplex (43 bp) was mixed with 2.5 µl of one long duplex (53 bp), combined with 5 µl of 2 M KCL and 1 µl of 10 mM EDTA. Therefore, the final concentration of one duplex was roughly ¼ of the

initial concentration. The mixtures were incubated in 37 °C for 26 hours. The samples were loaded on a 8% non-denaturing polyacrylamide gel, which was electrophoresed in KMg buffer (50mM Tris-borate, pH 8.0; 10 mM KCl; 2 mM $MgCl_2$) at 6W at room temperature. The gels were dried and the bands were visualized on a phosphoimager (BioRad G5-250).

2.4 Chemical Probing

Methylation protection, permanganate oxidation and diethyl pyrocarbonate assays

All three assays were utilized to study the tertiary structure of LM3TA-L in the presence of K^+ ion. In this experiment, single stranded DNA (L3T-L and M3A-L) was first treated with 10% piperdine and incubated at 90 °C for 30 minute and then lyophilized. The purpose of this initial piperdine treatment was to remove damaged DNA. The single stranded DNA was then radio-labeled by the standard kinasing protocols described above, followed by ethanol precipitation. The DNA sample was gel purified on 8% denaturing polyacrylamide gel, which was electrophoresed in TBE buffer (50mM Tris-borate, pH 8.0; 10mM EDTA) at 20 W at room temperature. Bands closet to the top of gel were excised and eluted into 300 µl of 300mM sodium acetate. It was followed by another ethanol precipitation. Formation of double stranded DNA was carried out by mixing 500 pmol of one unlabeled strand with 450 pmol of the complementary unlabeled strand plus 50 pmol of its labeled strand in 2× TMACl [200 mM tetramethylammonium chloride (TMACl); 20 mM Tris, pH 7.9].

The DNA duplex prepared was mixed with 1× volume of either 2M KCl (where synapsis was desired) or 2M LiCl (where synapsis was not desired), the mixtures were

incubated in 37°C for 30 minutes. The solutions were equally divided into three 9 µl of aliquots, and each aliquots was treated by dimethyl sulphate (DMS), permanganate (MnO_4^-) or Diethyl Pyrocarbonate (DEPC).

2.4.1 Methylation protection assay

DMS methylates guanines (Sambrook et al, 1989), and therefore, it was used to characterize the G-G mismatch region on LM3TA-L. 2 µl of 1.2% DMS was added into 9 µl of the aliquots, and the mixture was allowed to stand at room temperature for 17 minutes. 3 µl of stop solution (Sambrook et al, 1989, pg. 13.84) was added to quench the reaction, followed by the addition of 10ul of 300mM sodium acetate and 3× volume of 100% ethanol.

2.4.2 Permanganate oxidation assay

The reaction to oxidize thymines with single stranded charater was similar to that previously described Nielsen (1990). Aliquots of 9µl containing the DNA and appropriate salts were mixed with 1 µl of 1.2mM of $KMnO_4$ and incubated at room temperature for 2 minutes. The reaction was stopped by the addition of 1 µl of allyl alcohol followed by 39 µl of 0.3 M sodium acetate (pH 7.5) and 3× volumes of 100% ethanol. Samples were then precipitated, washed 1× with 100 µl 70 EtOH then resuspended in 100 µl 10% piperidine. Resuspended samples were then heated to 90°C for 30 minutes the dried under vacuum. The samples were then resuspended in 50 µl ddH_20, then dried again. Finally the samples where dissolved in denaturing loading buffer and loaded on a 10%

sequencing gel. The gel was dried and the bands were visualized on a phosphoimager (BioRad G5-250).

2.4.3 Diethyl pyrocarbonate assay

DEPC carboxylates the N-6 and N-7 positions of adenines (Kohwi-Shigematsu & Kohwi, 1992) and was used to probe the behavior of adenines at the linker site of LM3TA-L. The 9 µl aliquot was incubated with 1 µl of 100% DEPC at room temperature for one hour, followed by the addition of 60 µl of 0.3 M sodium acetate (pH 7.5) and 3× volume of 100% ethanol (The addition of 1 µl DEPC is excessive and will not all dissolved, but what is desired is a saturating solution of DEPC for the assay). Samples were then precipitated, washed 1× with 100 µl 70 EtOH then resuspended in 100 µl 10% piperidine. Resuspended samples were then heated to 90°C for 30 minutes the dried under vacuum. The samples were then resuspended in 50 µl ddH_20, then dried again. Finally the samples where dissolved in denaturing loading buffer and loaded on a 10% sequencing gel. The gel was dried and the bands were visualized on a phosphoimager (BioRad G5-250).

2.5 Reversibility of Sr^{2+}Induced Pinched Duplex Formation of LMAT-3

This experiment followed the same protocols as those described in the "Methylation protection, permanganate oxidation and diethyl pyrocarbonate assays" section, with several differences. Firstly 1× TMACl was used instead of 2× during the formation of LMAT-3*L* duplex. Secondly 0.5× volumes of 15 mM of $SrCl_2$ (where synapsis was desired) and 0.5× volumes of 15 mM of $MgCl_2$ (where synapsis was not desired) have

replaced 1× volume of 2M KCl and 2M LiCl in the 30 minutes incubation. For example, 20 µl of LMAT-3*L* duplex was mixed with 10 µl of 15 mM $SrCl_2$ or with 10 µl of 15 mM $MgCl_2$. Thirdly, after the 30 minute incubation, the mixture was equally divided into half; while half of the sample was added with 1/3× volume of 100 mM EDTA, the other half was added with 1/3× volume of dH_20. For example, 15 µl of the sample, already containing the duplex and the ion, was mixed with 5 µl of 100 mM EDTA or 5 µl of dH_2O. Both of the samples were allowed to stand at room temperature overnight. The rest of steps in the experiment were carried out using the same protocols.

3. Results & Discussion:

3.1 Sequence Design

As previously mentioned all duplexes where designed around the originally characterized L·M synapsable duplex. In all cases two flanking T·T mismatches were retained on either side of the dimerization domain (figures 4-1(a) and 4-5(a)). These flanking mismatches appear to aid the dimerization of the duplexes into 'synapsed' dimers by providing a transition region between the double helices and G-quartets (Venczel & Sen, 1996)

3.2 T-T Domain Dimerization

The first question we wanted to address was whether all of the domains listed in figure 4-1(a), could dimerize and whether they exhibit any selectivity in dimerization. Incubating duplexes possessing dimerization domains in K^+ containing solutions results in synapsed duplex dimer, which possesses a characteristically reduced mobility in a non-

denaturing acrylamide gel. Incubating long DNA duplexes containing dimerization domains with short duplexes containing dimerization domains results in observed synapsed duplex dimers with varying gel mobility. If the domains in the long and short duplexes can cross-react to form a *hetero*-synapsed duplex, it is observed as a species with intermediate gel mobility in comparison to *homo*-synapsed duplex products. Two experiments shown in figure 4-1(b) and 4-1(c), were conducted using long DNA duplexes (53 bp) containing either LMTT-1 (figure 4-1(b)) or LMTT-2 (figure 4-1(c)) domains, which were incubated with short duplexes (43 bp) containing one of the four different LMTT dimerization domains.

Examination of figure 4-1(b) shows that long duplexes containing LMTT-1 do not cross-hybridize with duplexes containing LM-0. This demonstrates self-selectivity between the LMTT1 and LM-0 domains. Cross-hybridization is observed with short duplexes containing LMTT-1 (as expected) and LMTT-2 domains. This observation indicates there is no selectivity between LMTT-1 and LMTT-2 domains. The sample containing short duplexes with LMTT-3 domain indicates that this duplex does not form a 'synapsed' duplex at all. Duplexes containing the LMTT-3 domain have been incubated in 1M KCl for over 48 hours at 37°C with no significant dimer product (< 1%) observed (data not shown).

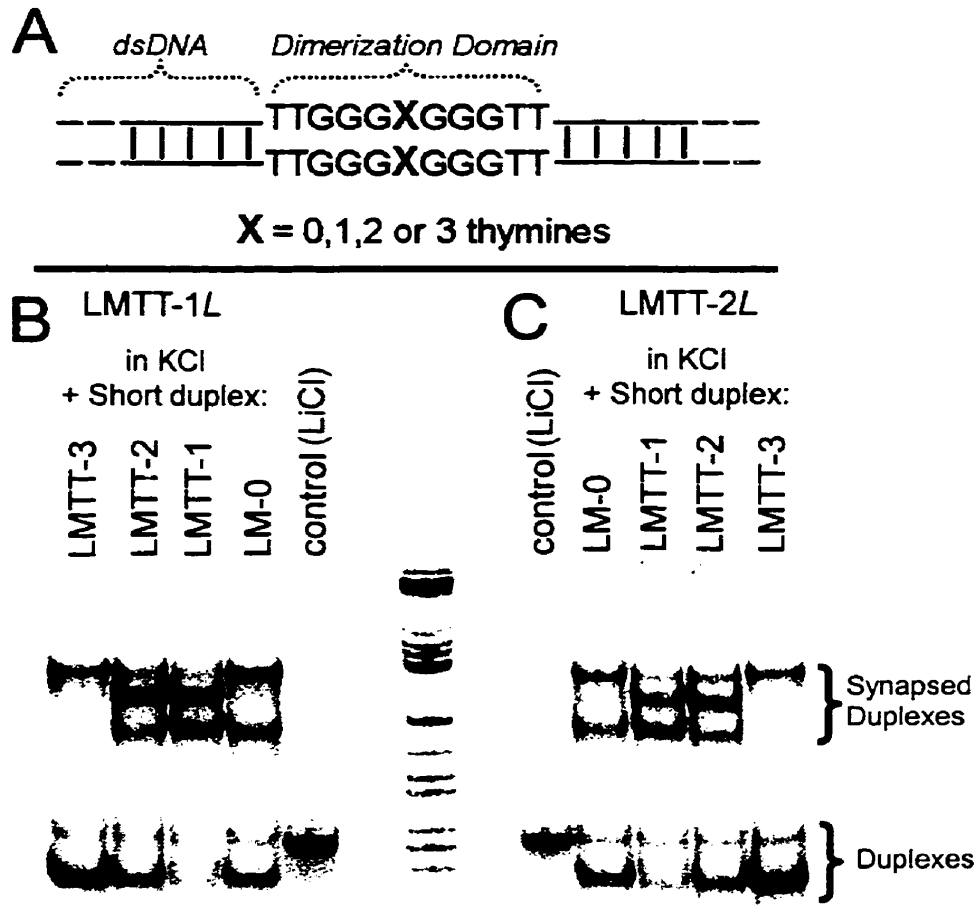

Figure 4-1. **Affects of T·T Spacers on Dimerization. (A) G-G mismatch domains tested for dimerization and specificity. The mismatch domains contain a central spacer that contains from 0 to 3 T-T mismatches. The domains are termed; LM-0 for no mismatches, LMTT-1 for one T-T mismatches and so forth. The domains where contained in either short or long duplexes with lengths of either 43 or 53 base pairs. (B) Incubation of long duplexes containing the LMTT-1 domain with short duplexes containing one of the four-dimerization domains. Samples of 1 μM duplexes in 1M KCl (other than the LiCl control) were incubated for over 20 hours at 37°C then resolved on a native gel as described in the materials and methods. (C) The same as B, but the long duplex contains the LMTT-2 dimerization domain.**

Figure 4-1(c) shows complimentary observations to figure 4-1(b). When long duplexes containing the LMTT-2 domain are used, self-selectivity is observed when incubated with short sequences containing the LM-0 domain. Consistently no selectivity is observed between LMTT-1 and LMTT-2 domains. Again no dimerization is observed with duplexes containing LMTT-3.

Disrupting a run of six G-G mismatches in dimerization domain by a T-T mismatch results in self-selectivity between the two domains. A second T-T mismatch remains selective against 6 contiguous G-G mismatch domain while it exhibits no selectivity to a domain containing a single T-T mismatch. These two observations may be partially explained from a thermodynamic perspective. Optimal dimerization of LM-0 results in 6 continuous G-quartets while LMTT-1 will result in two runs of three. Considering a simple alignment of the domains:

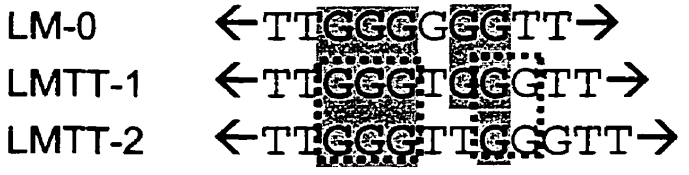

Figure 4-2. Alignment of synapsable Domains. Individual strands of the mismatch domains are shown for a simple alignment of the G·G mismatches.

The formation of cross products or hetro-dimers between LM-0 and LMTT-1 will only form 5 G-quartets, which results in a thermodynamically less stable complex. Alignment of the LMTT-1 and LMTT-2 domains results in a similar calculation, but selectivity is not observed. This is likely due to the flexibility of the T-T mismatch

'spacers', which could take on a conformation to allow the G-G mismatches to align 'in phase' to maximize G-quartet formation. The extent that the T·T mismatches will space the two G·G domains is hard to predict. There is some evidence that intervening bases between G-quartets can be extruded out of the structure to possibly allow the G-quartets to form a continuous stack (Chen, 1995).

The absence of a 'synapsed' dimer for the LMTT-3 domains is likely due to the formation of intra-molecular G-quartets. Three T-T mismatches appear to have enough freedom of motion to allow the duplex to fold back upon itself forming a 'pinched' duplex. Other duplexes containing G-G mismatches have also previously been shown to form 'pinched' duplexes in the previous two chapters (Fahlman & Sen, 1998, 1999). Determination of the existence of this product follows.

3.3 Probing the LMTT-3 Structure

Chemical probing was used to determine whether the inability of LMTT-3 domains to dimerize is due to the formation of *intra*-molecular G-quartets. The protocol is dependent on the observation that G-quartets render the participating guanines to be resistant to methylation at N-7 (Sen & Gilbert, 1988). DNA methylation can be visualized due to N-7 methyl guanine being susceptible to cleavage in hot piperidine. Figure 4-3 demonstrates that in the presence of 1M KCl, the guanines in the dimerization domain become resistant to methylation in comparison to the other guanines in the double-stranded arms. The same guanines exhibit no protection in the presence of 1 M LiCl. Methylation protection in the presence of potassium and not in lithium is highly indicative of G-quartets because ions such as lithium do not promote their formation.

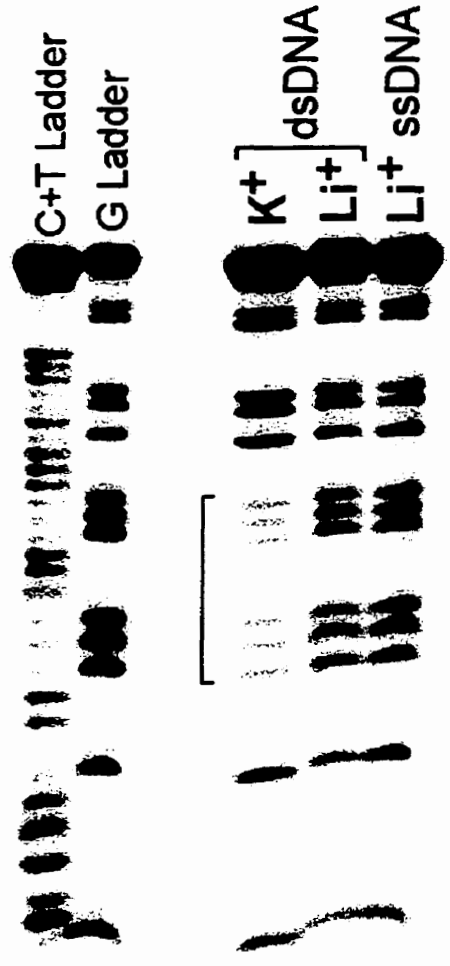

Figure 4-3.

Methylation protection of duplexes containing the LMTT-3 domain. DNA samples were partially methylated with DMS and then cleaved at methylated sites with piperidine as described in the materials and methods. G and C+T ladders are Maxim and Gilbert sequencing reaction products (Maxim & Gilbert, 1977). As ssDNA or dsDNA there is not apparent protection to methyation to any of the guanines in 1M LiCl. When the duplex is in 1M KCl the central guanines (highlighted by a square bracket) become highly resistant to methylation.

A structural model for a 'pinched' duplex of LMTT-3 with the G-G mismatches participating in intramolecular G-quartets is depicted in figure 4-4. The same DNA construct was also probed with potassium permanganate ($KMnO_4$), which reacts with un-stacked or single stranded thymines, see section 3.6.1 of this chapter. Mismatch thymines (linker and spacer) all exhibit relatively similar reactivity to $KMnO_4$ in either Li^+ or K^+ solutions (data not shown). This suggests that in either the 'open' or 'pinched' duplex, the T-T mismatches are not stacked in the structure. So these regions are most likely relatively unstructured.

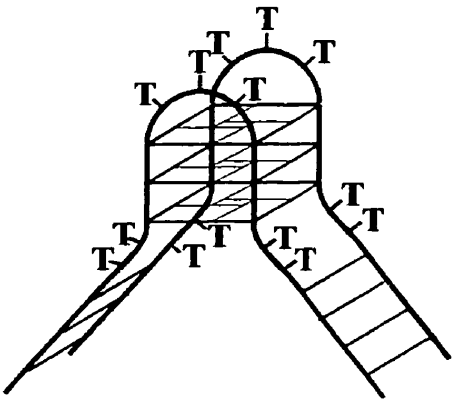

Figure 4-4. Model for the 'pinched' duplex formed by LMTT-3 that results in the inability of the duplex to dimerize.

3.4 Kinetics of Dimerization

The rates of dimerization of the different duplex dimers where determined for short duplexes (43 bp) containing either the LM-0, LMTT-1 or LMTT-2 domains. Rates were measured under standard conditions of 1 M KCl, 50 mM TMACl and 50 mM Tris-Cl (pH 7.9) at 37°C. A summary of the results is shown in table 1. Reported constants are an average from at least three different experiments. Each experimental run was performed at different concentrations (i.e. 0.25, 0.60 and 1.25 uM for LMTT-1) to

confirm dimerization is obeying second order kinetics. A remarkable trend is observed, with the LMTT-1 & 2 domains possessing rate constants almost two orders of magnitude higher than that of LM-0.

Table 4-1 Rates of Dimerization by LMTT-type Duplexes

Dimerization Domain	Rate Constant ($M^{-1}min^{-1}$)
LM-0	$4.9(\pm1.3)\times10^{3}$
LMTT-1	$1.5(\pm0.3)\times10^{5}$
LMTT-2	$1.1(\pm0.2)\times10^{5}$
LMTT-3	< 0.05 *

Second order association rate constants where determined at 37°C in solutions containing 1 M KCl and 50 mM TMACl buffer. Numbers reported are averages of at least three experiments. * No significant dimerization is observed but an upper limit has been determined.

The first key point that can be made from kinetic observations is that for 'pinched' duplexes to form a spacer of at least 3 bases is required to allow the duplex to stably fold back upon itself. This is with the observation that LMTT-3 does not dimerize, while both LMTT-1 & 2 both rapidly dimerize with similar rates.

The trend breaking observation of the rate of dimerization of duplexes containing LM-0 domains is more difficult to interpret. We have also previously reported similar reduced rates with another domain, H·I, which contained 5 continuous G-G mismatches (LM-0 has 6), where the observed second order rate constant was found to be $(3.3\pm0.8)\times10^{3}$ $M^{-1}min^{-1}$ (Fahlman & Sen, 1999). There appears to be another inhibitory aspect to longer continuous stretches of G-G mismatches, which is disrupted by the interrupting internal T-T mismatches as in LMTT-1 & -2. Methylation studies of

duplexes containing continuous stretches of G-G mismatches do not present any evidence for an alternate structure where the guanines in the synapsable domain exhibit the same reactivity as the guanines in the double stranded arms of the duplex (data not shown, but similar probing patterns are shown for H·I in figure 3-11 in chapter 3). So it is speculated that if the G·G mismatches are participating in so other type of stable interaction which prevents the formation of G-quartets, it does not involve the use of the N-7 of the participating guanines.

3.5 Dimerization of A·T Spacer Containing Duplexes

Flexibility of T-T mismatches of the spacer are potentially responsible for the cross reactivity between LMTT-1 and LMTT-2 domains as well as for the formation of the 'pinched' duplex of LMTT-3. We wanted to determine whether replacing the T-T mismatches with Watson & Crick A·T base pairs, as depicted in figure 4-5(A), could reduce the flexibility of the spacer. We hoped that a reduction in the flexibility could allow the LMAT-3 structure to dimerize as well as allow for specific dimerization between LMAT-1 and -2.

It was unknown at this point whether that these short runs of A·T base pairs would even form in the contexts of long mismatch domains. A series of mixtures of long and short duplexes were tested to determine the ability of the LMAT domains to dimerize along with their specificity of dimerization. As shown in figure 4-5(B), the results are identical to those of the LMTT domains. In the presence of 1M KCl, the LMAT 1 & 2 domains display selectivity towards LM-0, while exhibiting no selectivity to one another.

Again no synasped product is observed with LMAT-3, suggesting the formation of a 'pinched' duplex.

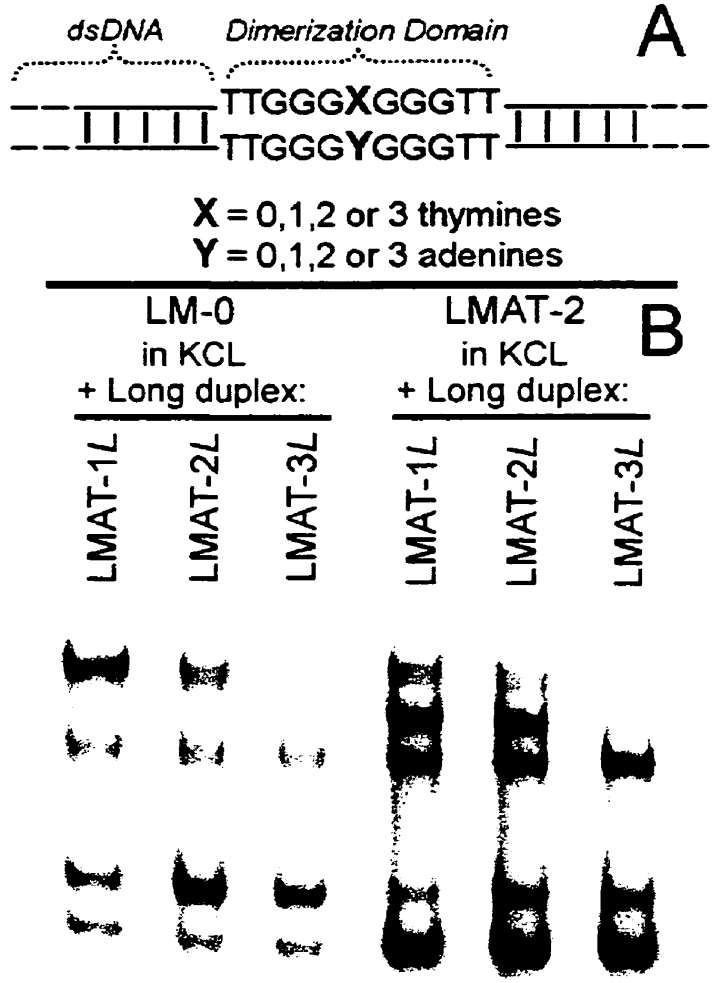

Figure 4-5. **(A) G-G mismatch domains containing A·T spacers. The mismatch domains contain a central spacer that contains from 0 to 3 A·T base pairs. Domain LM-0 remains the same with no spacer sequence. The domains are termed; LMAT-1, LMAT-2 and LMAT-3 for 1, 2 or three A·T base pairs respectively. The domains were within either short or long duplexes with lengths of either 43 or 53 base pairs. (B) Incubation of short duplexes containing the LM-0 domain with long duplexes containing either LMAT-1, 2 or 3. Samples were 1 μM for each duplex in 1M KCl and were incubated for over 20 hours at 37°C then resolved on a native gel as described in the materials and methods. (C) The same as B, but the short duplexes contain the LMAT-2 dimerization domain.**

3.6 Chemical Probing of LMAT-3

With no product formation with LMAT-3, we wanted to test whether again a pinched duplex was forming and whether the 3 potential A-T base pairs were in fact forming. For this we resorted to chemical probing; of particular interest was a reaction with diethyl pyrocarbonate (DEPC). DEPC is known to specifically react with single stranded adenines at N-7 positions (figure 4-6(A)). Specificity for ssDNA results from DEPC being too large to access the N-7 of adenine through the major groove of the double helix so disruptions in the helix's structure allow for DEPC reactivity (McCarthy *et al*, 1990). DEPC can also react with N-6 of adenine but only the modification at N-7 results in a base labile product that allows for detection by electrophoresis.

3.6.1 Probing the M-A3 Strand

When the strand containing the 3 adenines of interest (strand M-A3) was P32-end labeled, contrasting results were observed in Li^+ and K^+ containing solutions. Reactivity to DMS mirrors that of the LMTT-3 duplex where the G-G mismatches become resistant to methylation in K^+ containing solutions as seen in figure 4-7(A). What make the LMAT-3 duplex results different is with the DEPC reaction, where in Li^+ solutions the 3 adenines are resistant to DEPC. This protection would suggest that these adenines are involved in a 'mini'-helix under these conditions. If Li^+ is replaced with K^+, a remarkable hyper-reactivity is observed with the two 5' most adenines of the spacer region. A remarkable change in reactivity is observed in K^+, again suggesting the formation of a 'pinched' duplex as shown in figure 4-8.

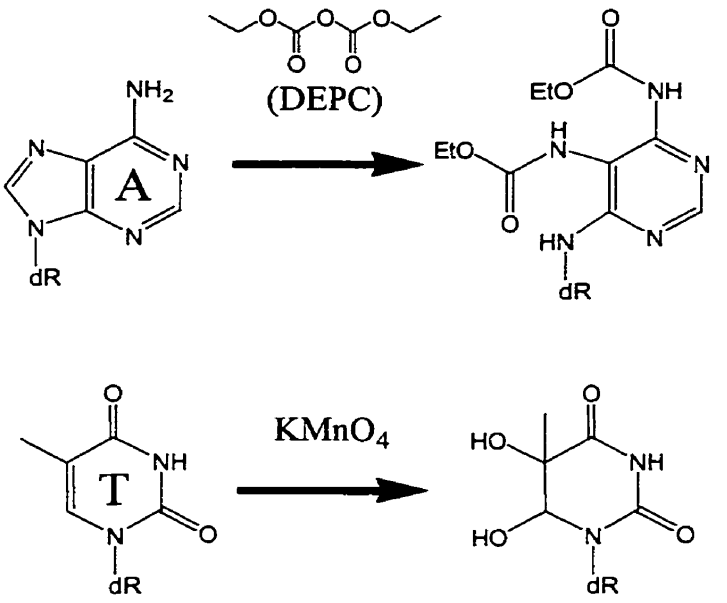

Figure 4-6. Adenine and thymine specific chemical probing reactions. A) Reaction of DEPC with the N-7 adenine gives the depicted product. The site of modification can be determined by treatment with hot piperidine, which causes strand cleavage at the site of modification. B) Oxidation of thymine by $KMnO_4$ results in the removal of the 5-6 double bond. The resulting product is also susceptible to strand cleavage by hot piperidine treatment.

Potassium permanganate is known to oxidize thymines forming a thymine diol (figure 4-6(A). The participation in the base stack in double helical DNA prevents accessibility of the 5,6 double bond to reaction, so only thymines not in B-DNA are reactive to permanganate (Jeppesen & Nielson, 1989 & 1989; Fox & Grigg, 1988).

3.6.2 Probing the L-T3 Strand

Experiments using the strand with the thymines in the spacer (strand L-T3) do not show completely complimentary results. As seen in figure 4-7(B), the G-G mismatches exhibit identical results with respect to DMS protection in the presence of K^+. The reaction with $KMnO_4$ shows somewhat contrasting results in comparison to the DEPC

results above. With $KMnO_4$ the thymines in the spacer exhibit reactivity in samples in Li^+ solutions as seen in figure 4-7(B), which would suggest the bases are not stably base-paired to the adenines in the 'mini'-helix. When the duplex is in K^+ containing solutions there is an enhancement to the reactivity with $KMnO_4$ to the 5' most thymine in the spacer. The change in reactivity when samples in Li^+ and K^+ are compared also suggests a conformational difference between the two samples.

Discrepancies on the status of an A·T 'mini'-helix in Li^+ containing solution determined by DEPC and $KMnO_4$ probing reflect the different accessibilities of the two compounds. DEPC is a larger compound that requires sufficient space in order to react with the N-7 of adenines, so a lack of reaction suggests that the region of the spacer does not open up sufficiently to expose the adenines to attack by DEPC. In contrast MnO_4^- is much smaller, fits more readily in the groove of the DNA helix, and can react with thymines that become exposed or un-stacked during minor perturbances in the structure. These contrasting observations between reactivities of the two compounds suggest that on a global scale the LMAT-3 domain probably remains relatively linear but minor deformations in the helix are continually occurring. These perturbances are to be expected because if the linear structure were very stable, the pinched duplex would not be expected to form at all.

The suggestion of the LMAT-3 domain being relatively linear in Li^+ containing solution while $KMnO_4$ reactivity persists opens the possibility that the LMTT-3 domain could also possibly be linear.

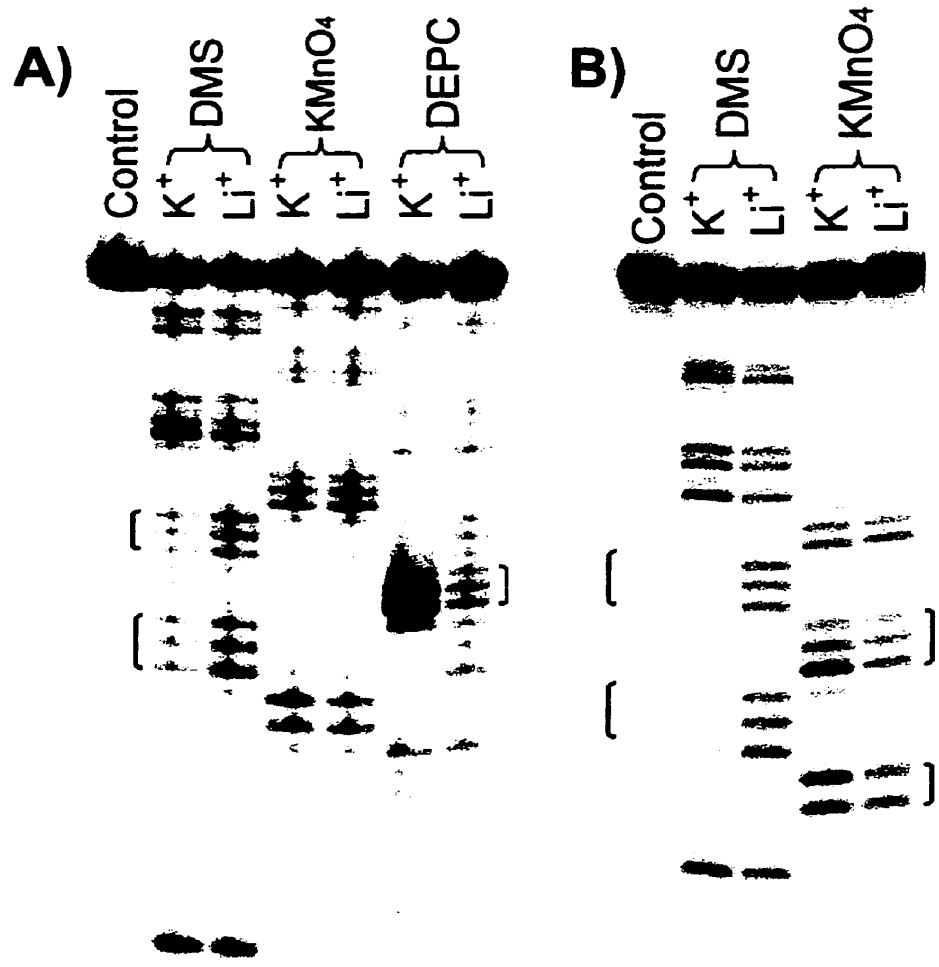

Figure 4-7. **Chemical probing of duplexes containing the LMAT-3 G-G mismatch domain. (A) The P32-endlabelled strand contains the adenines in the spacer sequence (strand M-3A). Duplexes were partially modified with DMS, $KMnO_4$ or DEPC in either 1M LiCl or 1M KCl. Sites of modification are cleaved by piperidine treatment as described in the Materials and Methods. The control lane is of duplex DNA only treated with piperidine. Brackets indicate regions with variable probing between Li+ and K+ conditions. (B) The P32-endlabelled strand is complimentary (L-3T) to that in A, and contains the thymines in the spacer sequence. Duplexes were partially modified with DMS or $KMnO_4$ as in A. Brackets indicate regions of variable reactivity between Li+ and K+ solution conditions.**

3.6.3 The LMAT-3 Pinched Duplex

Chemical probing data as discussed suggest that the LMAT-3 duplex forms the pinched duplex shown in figure 4-8. Other observations in the chemical probing of this structure beyond the support of its existence are also noteworthy. The probing patterns of both M-3A (figure 4-7(A)) and L-3T (figure 4-7(B)) exhibited unusual features of the bases in the spacer region in the pinched duplex structure (K^+ samples). In the case of probing LMAT-3 when M-3A is end-labeled, the 3' most adenine in the spacer does not become reactive to DEPC in the pinched duplex structure like the other two bases in the spacer. Likewise, experiments where L-3T is end-labeled show the 3' most thymine becoming hyper reactive in the pinched duplex in comparison to the other thymines in the spacer sequence. The positions of these protected and hyper reactive bases are indicated on the schematic structure shown in figure 4-8.

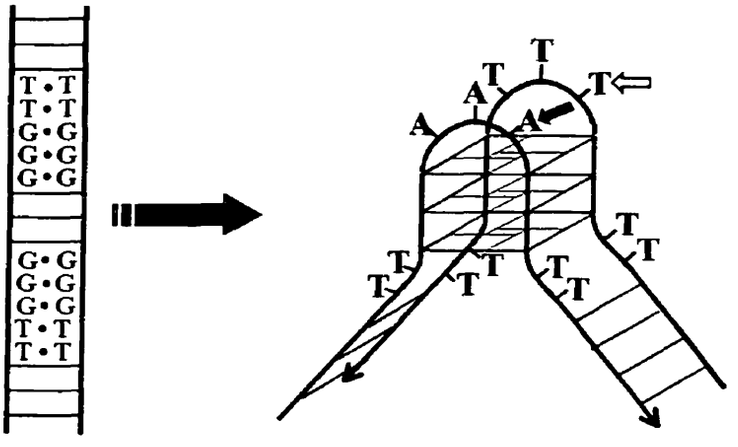

Figure 4-8. Model of the folding of LMAT-3 in the presence of KCl, which disrupts the 'mini'-helix of the three A-T base pair spacer. Protected adenine is indicated with a black arrow while the hyper reactive thymine is indicated with a white arrow.

Observations suggest the spacer sequences that form the loop are forming some sort of defined structure and not simply extended into the solvent in a random way. The detailed structure of this loop cannot be determined by chemical probing alone. Other methods that can examine molecular detail would have to be used.

3.7 Comparison of Pinched Duplexes

Over the course of this work we have observed the formation of pinched duplexes on several occasions. Synapsable domains constructed with normal anti parallel DNA duplexes all required loops of three bases in order to fold back upon itself to form a pinched duplex (i.e. J·K, LMTT-3 & LMAT-3). Contrasting this observation were the results in chapter 2 with the A·B duplex, which possessed 2 bases in the loops of the pinched duplex. An explanation for this difference most likely resides in the type quadruplex structure of these pinched duplexes. As a necessity the pinched duplexes like LMTT-3 are all anti-parallel. In contrast the A·β duplex has its G·G mismatches in a parallel orientation, so when the duplex folds to a pinched duplex the resulting quadruplex will be partially parallel as discussed in chapter 2).

As suggested the partially parallel structure seems to be more stable so it may allow for a strained loop in the pinched complex.

3.8 Reversible Formation of the Pinched Duplex Structure

The ability of the pinched duplex to form at the expense of the 'mini'-helix led us to the idea that this system might be used as a salt induced conformational switch. Under inert solution conditions the duplex remains relatively linear, but upon the addition of the appropriate cation species, the duplex folds back upon itself to form the pinched duplex.

This gives us a two state system that can be modulated by controlling the cation species present in solution. The LMAT-3 domain is more applicable for conformational changes that the other duplexes in this manuscript that have also been shown to form pinched duplexes. The duplexes A·β and J·K are both capable of dimerizing, so in a system where only the pinched duplex is desired, dimerization can result in unwanted association of structures. For a more practical use the dynamic change in structure has to be reversible, so we examined alternate conditions to induce the formation of the LMAT-3 pinched duplex. Instead of using K^+ to induce G-quartet formation, we used Sr^{2+}, which can me readily removed by the addition of chelators such as EDTA.

Figure 4-9 shows the results of chemical probing of LMAT-3 with DMS and DEPC when the samples are treated with Sr^{2+} or Mg^{2+}. If the presence of Sr^{2+} alone the DMS and DEPC probing patterns are indicative of the formation of the pinched duplex. When this same sample is then treated with a five-fold excess of EDTA all probing patterns resemble that of Mg^{2+} containing samples. The Mg^{2+} samples are control samples since Mg^{2+} does not promote G-quartet formation and allows the LMAT-3 duplex to remain linear while accounting for the ionic strength of Sr^{2+}. The results show that the formation of the pinched LMAT-3 structure is completely reversible in solution.

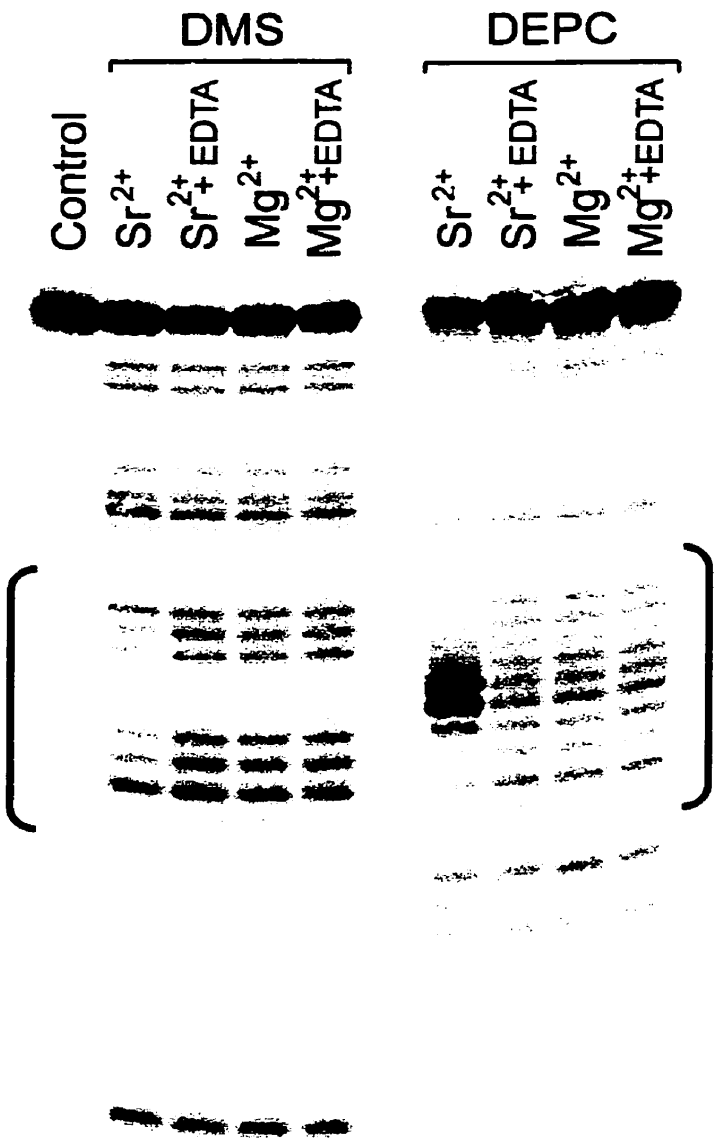

Figure 4-9. **Reversibility in the formation of a pinched duplex. Chemical probing with DMS and DEPC were performed on LMAT-3 incubated in the presence of divalent cations. Samples were incubated in the presence of 5 μM XCl_2 and 50 mM TMACl buffer for 30 minutes at 37°C. The sample was then treated with DMS or DEPC immediately or EDTA was added to a final concentration of 25 μM and incubated for several hours then treated with the chemical agents. After treatment with DMS or DEPC samples are piperidine treated before loading. Control lane is a DNA sample only treated with piperidine. Brackets indicate bases participating in the synapsable domain.**

3.9 Large Scale Conformational Changes Using Pinched Duplexes

A potential use of the formation of pinched duplex structures is in conformational changes in DNA constructs. Controlling which cations are present in solution can then regulate the conformation of the structure. Domains such as LMTT-3 and LMAT-3 are the best suited for this type of task because of their lack of ability to dimerize with other domains.

A relatively simple example of a structure that can potentially demonstrate this effect is with the retractable scaffolding shown in figure 4-10. This structure incorporates G·G mismatch domains that can form pinched structures as well as 4-way junctions.

The basis of the design of a retractable scaffolding structure is that under solution conditions that do not promote G-quartet formation (i.e. no K^+ or Sr^{2+}), the 4-way junctions adopt the preferred 'X' conformation. For more details on the stacking preference see section 2.2.3 in chapter one. In this conformation the DNA adopts an extended structure as shown in figure 4-10.

The addition of G-quartet promoting cations (like Sr^{2+}) induced the G·G mismatch domain (a LMAT-3 like domain) to form a pinched complex. Formation of the pinched duplex would then cause the structure to shorten as shown in figure 4-10, as the 4-way junctions are forced from their preferred stacked structure. Guanine quartets are significantly more stable than the 4-way junction so there is a large energetic driving force for this transition. Forced from its preferred stacked configuration the junction is likely to form less favorable coaxially stacked pairs between the arms of the structure.

The structure can then be returned to its original state by the removal of the cations that induced the structural change.

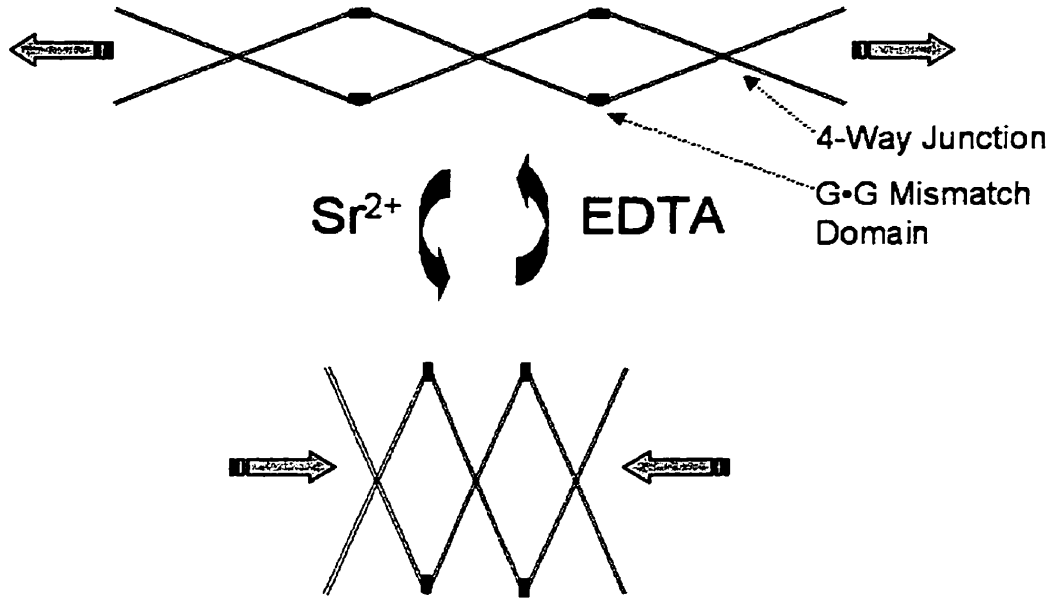

Figure 4-10. Large scale conformational changes using pinched duplexes. A model of a proposed retractable scaffolding complex composed of conventional 4-way junctions and synapsable domains that form pinched duplexes. Regulation of the structure would be by controlling whether cations that promote G-quartets are in solution or not.

Conclusions

This chapter demonstrates the inclusion of spacer mismatch bases within contiguous runs of G·G mismatches is all that is required for synaptic specificity. Additional unpaired bases beyond a single mismatch or base pair does not add another degree of specificity, which is apparently due to the flexibility of the spacer.

Introduction of spacer sequences of one or two base-pairs or mismatches drastically increase the rate of dimerization of the synapsable domain. The mechanism of this still eludes us but it does not involve the formation of pinched duplexes.

We have demonstrated that for the synapsable domains constructed of conventional anti-parallel domains will prefer the fold-back structure of a pinched duplexes when the G·G mismatch domains are separated by spacer sequences of at least 3 mismatches or base pairs. When such duplexes contain 3 G·G mismatches on either side of the spacer region (LMAT-3 and LMTT-3 versus J·K) the duplex becomes incompetent to dimerize. We have postulated that these domains that can only form pinched duplexes may be used in conformational changes in latter generations of DNA nanostructures.

Part III

Catalytic DNA

"Chance is the only source of true novelty."

[From Life Itself, 1982]
Francis Crick

Chapter 5

A New Secondary Model for the Na-8 DNAzyme

1. Introduction

1.1 The RNA World

The discovery of the ability of RNA molecules to catalyze chemical reactions *(ribozymes)* (Kruger *et al,* 1982; Guerrier-Takada *et al,* 1983) brought to light that proteins were not the only biopolymer that can fold into complex shapes to form enzymatic active sites. The number of different types of naturally occurring ribozymes is still rather small, now being eight with the ribosome just being added to the list (Ban *et al,* 2000; Nissen *et al,* 2000; a perspective on this work has been written on this by Thomas R. Cech, 2000). The initial discovery of the ability of RNA to catalyse chemical reactions brought support to the notion of the *RNA World Hypothesis* (White, 1976; Gilbert, 1986; Benner *et al,* 1989) soon after the original discovery of ribozymes. This hypothesis suggests that early life forms lacked proteins and these organisms relied on RNA for enzymatic catalysis and other functions. The appeal of RNA as the first complex biopolymer comes from its ability to code for genetic information through Watson and Crick base pairing and potentially catalyze all the reactions required for a metabolism. In some opinions, modern naturally occurring ribozymes are vestiges or the prior RNA world. The process of evolution would have replaced most of the original of RNA in the early organisms by the evolutionarily later biopolymer - *proteins.*

The success of the *RNA World Hypothesis* depends on demonstrating the ability of RNA to be able to catalyze a variety of chemical reactions that would be required for even a very simple metabolisim. The small variety of extant ribozymes does not give an

adequate picture of the repertoire of chemical reactions RNA can catalyze. The majority of reactions catalysed by ribozymes include RNA processing reactions, like RNA cleavage, splicing and ligation, with the exception of the peptidyl transferase function of the ribosome.

1.2 *In Vitro* Selection

In vitro selection methods have been developed that allow for the successful isolation of new ribozymes. This method is an iterative procedure that enriches and eventually isolates nucleic acid sequences with desired properties from an initial large randomized pool of sequences, typically $<10^{16}$ variants (Ellington & Szostack, 1990; Kinzler & Vogelstein, 1990; Robertson & Joyce, 1990; Tuerk & Gold, 1990).

In vitro selection has resulted in a number of different ribozymes, which have demonstrated a greatly diversified catalytic repertoire for this class of enzymes (for reviews see Joyce, 1994; Lorsch & Szostack, 1996; Breaker 1996). Some recent novel ribozyme that have been selected for, that would be relevant to an RNA world, include: ribozymes catalyzing the Diels-Alder reaction (Seelig & Jaschke, 1999; Tarasow *et al*, 1997), self-alkylation (Wilson & Szostack, 1995), nucleotide synthesis (Unrau & Bartel, 1998) and, recently, an RNA polymerse (Johnston *et al,* 2001).

Beyond using *in vitro* selection to identify ribozymes this methodology has also been applied in the identification of RNA molecules with other functions, including aptamers (RNA sequences that bind particular ligands). Unusual examples of non-catalytic RNAs that have been isolated, which may also have relevance to an RNA World, are RNAs that bind and permeate lipid membranes (Khvorova *et al,* 1999).

1.3 Catalytic DNA

The selection of new ribozymes through *in vitro* selection suggested the possibility of isolating catalytic DNA molecules (DNAzymes or deoxyribozymes). No known catalytic DNA sequences are known in nature, but the development of selection methodologies opened the opportunity to identify DNAzymes de *novo*. The structural similarities between RNA and DNA polymers are such that if RNA is capable of folding into complex catalytic structures, DNA would also be predicted to have a similar ability. An early attempt at isolating novel DNAzymes using *in vitro* selection was successful, with the original DNAzyme being a lead depended RNA phosphodiester cleaving enzyme (Breaker & Joyce, 1994). Since this first example several other types DNAzymes have also been selected (for reviews see Breaker, 1997; Sen & Geyer, 1998; Li & Breaker, 1999).

1.4 A Co-Factor Independent DNAzyme

Original work with the naturally occurring ribozymes suggested that they were all metalloenzymes. The lack of chemical functional groups for acid-base chemistry led to hypothesis that all nucleic acid enzymes were metalloenzymes and folded into structures to optimally position metal cations to catalyze a reaction (Yarus, 1993; Pyle, 1993).

An *in vitro* selection experiment by Ron Geyer, a previous member of our laboratory, demonstrated that DNA can catalyze the cleavage of an RNA phosphodiester bond in the absence of di- or tri-valent cations or any other cofactors (Geyer & Sen, 1997). After this reported cofactor independence of this family of catalytic DNA

sequences, several of the naturally occurring ribozymes where re-examined and where also found to be functional in the absence of metal cofactors (Murray *et al,* 1998).

The original selection for DNA sequences that catalyze the cleavage of RNA phosphodiester bond in the absence of a co-factor resulted in a few families of enzymes. A representative clone, G3, from one of the families was used, by Ron Geyer in the construction of a mutagenized library for a secondary selection. The mutagenized library contained sequences similar to the parental G3 sequence, but each position in the original random region was mutagenized with a frequency of 15%. After six rounds of selection the secondary selection resulted in a number of related sequences. The sequences shown in figure 5-1 summarize the "Na"-family of sequences from this secondary selection. This figure also shows the regions of conservation between the sequences, compared to the parental G3.

Of the regions of conservation a long invariant sequence 5'-CCCAAGAAGGG-3' is of particular interest. The manifested high degree of conservation is bolstered by the fact that this domain also emerged in another selection for RNA cleaving DNAzymes by Faulhammer & Famulok (1997). The occurrence of this conserved sequence from two independent selections is highly supportive of a critical catalytic role for the sequence. The sequences selected by Faulhammer & Famulok (1997), were never tested for cofactor independence but were found to be active under low magnesium concentrations.

```
G3    TTT--ACCCAAGAAGGGGTGCG--TAC-TAT--GC-T-ACCTTATT-AAC---G-
Na1   TTTGTACCCAAGAAGGGGTG--A-TAC-TA-G-GC-T-ACCGTGTT-ACC---G-
Na2   TTT--ACCCAAGAAGGGGTGC--CTAC-TTT--GCC--ACCATATT--------
Na3   TTT--ACCCAAGAAGGGGTGCG--TTCA-AT--GC-T-ACCTTATT-AAC-----
Na4   TTT--ACCCAAGAAGGGGTG-GACT--G-A-GCGCCT-ACCC-AG-CAGA---G-
Na6   TTT--ACCCAAGAAGGGGTGC---TAC-TAT--G-TT-ACCTTATT-A-C---G-
Na9   TTT--ACCCAAGAAGGGGTGCTTC-AC-TAT--GC-T-ACGTAATT-AAC-----
Na10  TTT--ACCCAAGAAGGGGTGCG--TAC-TAT-AGCG--ACCGTATT-AAC-----
Na13  TTT--ACCCAAGAAGGGGTGCG-C-AC-TA-GA-C-T-ACCTTAT--AACT----
Na14  TTT--ACCCAAGAAGGGGTGC---TAC--AT--G--T-AC-TTAT--AACTTCGA
Na15  TTT--ACCCAAGAAGGGGTGCGG--AC-T-TG-GCTT--CATTATT-AATT--GA
Na16  ------CCCAAGAAGGGGTGCG--TAAA-CT--GC-T-ACCCTATT-AACCT--A
Na17  TT---ACCCAAGAAGGGGTGC--CTA-AT-T--GC-T-AC-TCACA-AAC-----
Na18  TTTG-ACCCAAGAAGGGGTGC-A-TAC-T-T-AGC-TGACCTTATTCAAC-----
Na19  TTT--ACCCAAGAAGGGGTGC---TAC-TA--AGCCT-ACTTTATT-ACC-----
Na22  TTT--ACCCAAGAAGGGGTGC--CTACA-AT--GC-T-ACCCTGTT-CAC---G-
Na23  TTT--ACCCAATAAGGGGTGC--CTAC-TCT--GC-T-ACGTTATTTAAC---G-
Na24  TTT--ACCCAAGAAGGGGTGCAAC--C--AT-TGCCTAACCTAAT-CACC---G-
Na8   TT-G-ACCCAAGAAGGGGTG--ACTAC-TTT--GC-T-ACGTTATTCCAC-----
      ------------------------------------------------------
      TTT--ACCCAAGAAGGGGTG------------GC-T-AC---AT----------
```

Figure 5-1. The Na-family of sequences. Comparison of the randomized regions of the clones isolated after the selection with the randomized sequence of G3 (Geyer & Sen, 1997). The bottom line shows the consensus sequence.

A structural model for the Na-family was proposed based upon sequence homologies and limited chemical and enzymatic probing. The proposed secondary model is shown in figure 5-2.

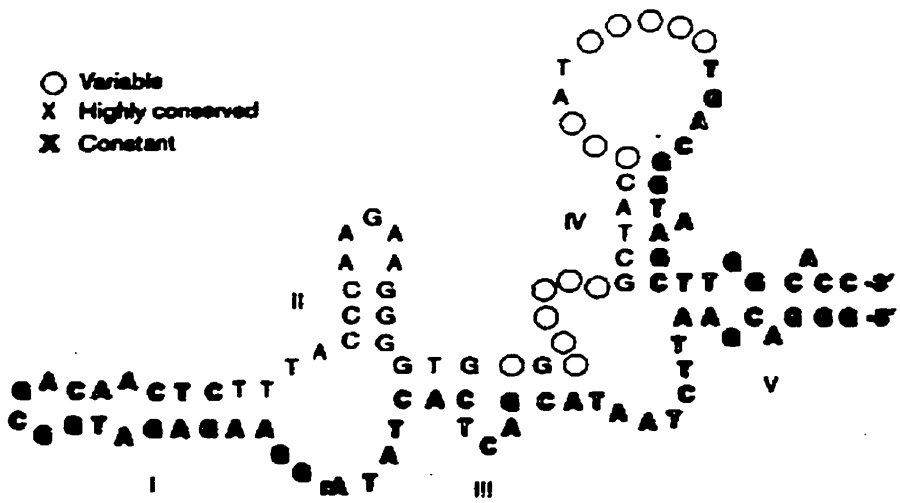

Figure 5-2. **Structural model for the Na-family of *self*-cleaving cofactor dependant DNAzymes (Geyer & Sen, 1997). Site of *self*-cleavage (RNA phosphodiester) is shown as *rA*. Double helical regions are numbered I-V for positional reference.**

1.5 Chapter Overview

This chapter is a reevaluation of the secondary structure of an individual clone of the Na-family, Na-8. My work is part of a long-term project of the lab of trying to understand, mechanistically, how this DNAzyme can catalyze the cleavage of an RNA phosphodiester bond in the absence of a cofactor.

2. Materials and Methods

2.1 DNA Sequences and Preparation

All DNA sequences were purchased from the University of Calgary Core DNA services and upon arrival were suspended in denaturing buffer (10mM Tris-Cl, pH 8.0, 1 mM EDTA, 95% formamide), heated to 90°C for 2 minutes, and purified on an 8% denaturing gel (8.4 M urea, 0.5× TBE). Bands were visualized by UV-shadowing and the gel containing the DNA was excised and crushed. The DNA was passively eluted with shaking in 300 mM NaOAc, pH 7.5. After elution the supernatant was filtered on 0.2 μm syringe filters the loaded on C-18 *Spice Columns.* Once the DNA was loaded on the column it was washed extensively with ddH_2O; the passing of 30% acetonitrile through the column then eluted the DNA. Samples were then evaporated to dryness under vacuum, and then resuspended in 100 μl TE (10 mM Tris-Cl, pH 7.5, 0.1 mM EDTA). Concentrations of DNA samples were then determined by measuring optical densities at 260 nm, and using the simple conversion of 1 OD = 0.033 μg/μl of single stranded DNA.

The following is a list of the sequences used:

Primers for generating Na-8 or dNa-8.

JDP1:

5'-GGT GCC AAG CTT ACC GTC

JDP2:

5'-CTG CAG AAT TCT AAT ACG ACT CAC TAT AGG AAG AGA TGG CGA C

JDP1bio:

5'-biotin-GGT GCC AAG CTT ACC GTC

rAP4:

5'-GGG ACG AAT CTT AAT ACG ACT CAC TAT **rA**

Where rA has a ribose sugar (RNA) not a deoxyribose.

dAP4:

5'-GGG ACG AAT CTT AAT ACG ACT CAC TAT A

Mutant primers:

JDP1-V':

5'-biotin-CCC TGC AAG CTT ACC GTC AGT GAA

dAPL-V':

5'-CCA CGG AAT TCT AAT ACG ACT CAC TAT A

2.2 Preparation of Na-8 Samples

The Na-8 single-stranded oligomers were generated by PCR amplification using the JDP1 and JDP2 primers and the plasmid containing the original cloned sequence. After PCR, the DNA was gel purified on an 8% non-denaturing gel (1× TBE) and a second PCR was performed using a second set of primers, depending on the desired final sequence ('wild type' or mutant). In the generation of the wild type Na-8 the following primers were used; (a) rAP4, to introduce the single ribonucleotide, and (b) JDP1bio, to introduce the 5' biotin. The generation of Na-8 mutants different primers were used at this step to incorporate the desired modifications. The PCR products were ethanol precipitated, and then dissolved in binding buffer (50 mM Hepes, pH 7.0, 0.5 M NaCl, 5 mM EDTA) and applied to a streptavidin column. The column was washed to remove unbound DNA, and the catalytic strand of DNA (not biotinylated) eluted from the column using 3 × 100 µl of 0.2 N NaOH. Following neutralization with 60 µl of 3 M NaOAc, pH 6.5, the DNA was precipitated by the addition of 1 ml EtOH. Following suspension of

the pellet in TE, the DNA molecules were kinased using T4 polynucleotide kinase and γ-^{32}P-ATP. The kinased DNA molecules were ethanol precipitated and resuspended in denaturing loading buffer and purified on 8% denaturing gel. The product was visualized by exposing the wet gel to X-ray film and the corresponding band was cut out and eluted in 400 µl TE buffer. After eluting the DNA from the gel the DNA was ethanol precipitated and resuspended in 50 µl 50 mM Hepes, pH 7.0, and stored at -80°C until use. Note, when handling the sample as single stranded DNA all steps must be done quickly, and on ice, if possible, because otherwise the Na-8 molecules will begin self-cleavage during many of these steps.

2.3 Kinetic Analysis

Standard self-cleavage assays were carried out in the following Reaction Buffer: 50 mM Hepes, pH 7.0, 1 mM EDTA, 0.5 M NaCl, and 0.1-µg/µl glycogen. All reactions were carried out at 22°. First, the DNA was dissolved in the above buffer (minus NaCl), then heated to 92°C for 1 minute followed by slow cooling to room temperature. The cleavage reactions were initiated by the addition of NaCl from a stock to a final concentration of 0.5 M, and the reaction was quenched by a 5 × dilution into denaturing loading buffer and placed on dry ice until electrophoresis. After all time points are collected samples are placed in a boiling water bath for 1-2 minutes and loaded on a 8% denaturing gel, and the bands were quantified using a BioRad GS-350 Phosphoimager.

2.4 Chemical Probing

Structural probing experiments were performed on Na-8 that was generated with the dAP4 primer in place of the rAP4 primer. This dAP4 primer replaces the single ribose with a deoxyribose in what would otherwise form the cleavage site in the mature Na-8. The generated dNa-8 is not enzymatically active but allows the sequence to be put through various probing protocols that would otherwise cleave the ribose substrate.

2.4.1 Methylation

A sample of dNa-8 was prepared as described above then folded as described for kinetic analysis. To a sample of 10 µl was added 2 µl 1.2% DMS (v/v), and the solution incubated for 20 minutes, followed by ethanol precipitation.

2.4.2 Permanganate

To 10 µl samples of dNa-8 folded with or without Reaction Buffer *(see 2.3 above)*, was added 2 µl of 12 mM $KMnO_4$, the reaction mixture was then incubated for 5 minutes at room temperature. The reaction was quenched by the addition of 1 µl allyl alcohol, the sample was then brought to a total volume of 100 µl with 0.3 M NaOAc, pH 7.5. The sample was then precipitated by the addition of 300 µl cold 100% EtOH. The resulting pellet was suspended in 100 µl 10% piperidine and heated at 90°C for 30 minutes. After piperidine treatment the sample was dried under vacuum, resuspended in 50 µl H_2O and dried again. The pellet was suspended in denaturing loading buffer and then loaded on a denaturing gel.

2.4.3 Diethyl Pyrocarbonate

To 50 µl samples of dNa-8 folded with or without Reaction Buffer *(see 2.3 above)*, was added 1 µl DEPC and incubated for 35 minutes. The sample was brought to a total volume of 100 µl with 0.6 M NaOAc, pH 7.5. The sample was then precipitated by the addition of 300 µl cold 100% EtOH. The collected pellet was suspended in 100 µl 10% piperidine and heated at 90°C for 30 minutes. Following the piperidine treatment the sample was dried under vacuum, resuspended in 50 µl H_2O, and dried again. The pellet was suspended in denaturing loading buffer and can then be loaded on a denaturing gel.

2.4.4 Hydroxylamine

To 10 µl samples of dNa-8 in reaction buffer was added 20 µl of 4 M hydroxylamine (pH 6.0). The samples are incubated for 20 minutes at room temperature. Addition or absence of salt does not have an affect on the experiment because the 4 M hydroxylamine is enough to fold the DNA without NaCl. After the incubation the sample, it was brought to a total volume of 300 µl with 0.3 M NaOAc, pH 7.5. The sample was then precipitated by the addition of 900 µl cold 100% EtOH. The collected pellet was suspended in 100 µl 10% piperidine and heated at 90°C for 30 minutes. After the piperidine treatment the sample was dried under vacuum, resuspended in 50 µl H_2O and dried again. The pellet was suspended in denaturing loading buffer and can then be loaded on a denaturing gel.

3. Results and Discussion

Based on sequence comparison and limited chemical and enzymatic probing the Na-8 DNAzyme was postulated by Geyer & Sen (1997) to have the secondary structure as shown in figure 5-3. We wanted to evaluate the structure by a more complete survey of adenine, thymine and cytosine modifications, using specific reagents.

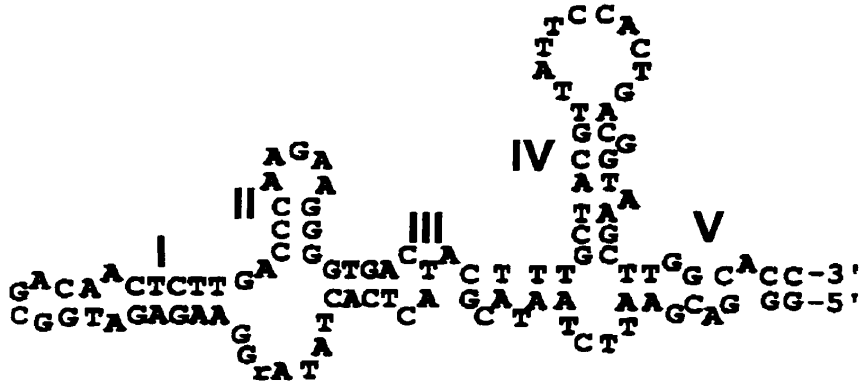

Figure 5-3. **Proposed secondary model for the Na-8 DNAzyme as presented by Geyer (1998). Double stranded stems are numbered with roman numerals.**

3.1 Chemical Probing

Samples of dNa-8 were prepared and were treated with a variety of chemicals that react with DNA in a structurally dependent manner. In all cases the dNa-8 version of the enzyme was utilized since the treatment step to determine the site of chemical modification, heating in 10% piperidine, cleaves the internal ribose cleavage site. Otherwise, if Na-8 were used, only sites of modification 5' of the ribose cleavage site can be determined. We have done these probing experiments on Na-8, but results are not shown as they show identical probing patterns to that of dNa-8 discussed below.

Preparation of dNa-8 is accomplished by using dAP4 and JDP1bio primers during PCR, as described in the materials and methods.

Samples of dNa-8 were treated with potassium permanganate, DEPC, or hydroxylamine. These chemicals preferentially react with thymines, adenines, and cytosines, respectively, when the bases are in a single stranded and unstacked conformation. The reactions of potassium permanganate and DEPC have been described in chapter 4. The reaction of hydroxylamine with cytosine, is shown in figure 5-4, leads to piperdine sensitive modifications.

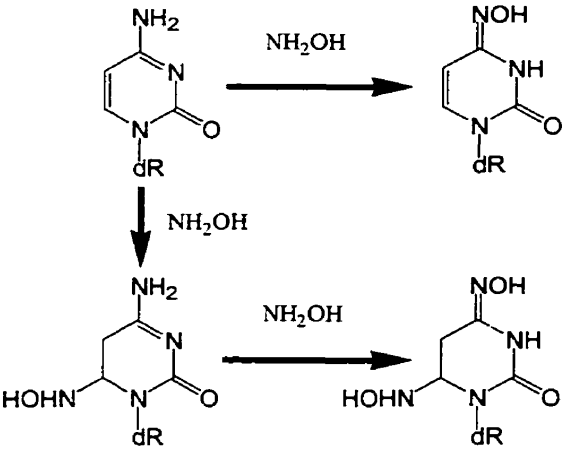

Figure 5-4. Reaction of cytosine with hydroxylamine. Two products form during the reaction, depending on at which site the reaction occurs first. Both products are sensitive to strand cleavage by hot piperidine treatment.

As mentioned above, selectivity for single strands by these reagents is not exclusive; some bases in non-double stranded regions are also resistant to these chemical agents. Also, some mismatch base pairs and some hairpin loops can provide environments for an "unpaired" base such that chemical susceptibility to the chemical used is abrogated. A general rule of thumb when interpreting the modification data with

these chemicals is that bases that are reactive are not in a double stranded context while bases that show protection may be double stranded or in some other compact structure.

Figure 5-5 shows the results of dNa-8 being treated with the three previously mentioned reagents. In the cases of permanganate (T-rxn), and DEPC (A-rxn), reactions were done in the presence or absence of Reaction Buffer to allow a comparison of folded and unfolded protection patterns of the thymines and adenines. In some cases, even under the absence of additional salt, some bases are protected, suggesting areas that fold into stable secondary structures under low ionic strength conditions. The cytosine specific reaction could not effectively be carried out under high and low ionic strength conditions, since 2.7 M hydroxylamine results in a complete folding of the DNA sample, resulting in identical results for the "low salt" and "high salt" samples (data not shown).

Samples of dNA-8 were also probed with DMS in the presence and absence of Reaction Buffer, with essentially no protection being observed on any guanines (data not shown). This indicated that no N-7 of guanines were involved in stable hydrogen bonded interactions within the folded structure.

Along with the evaluation of secondary structure, figure 5-5 shows a sequencing error that occurred in the original characterization of Na-8. Brackets in figure 5-5 indicate a CAC sequence that is reported as CCAC just inside of the JDP1 primer binding sequence. This error is most likely not significant as it is not conserved within the family, but the CAC sequence will be used in the remainder of this manuscript.

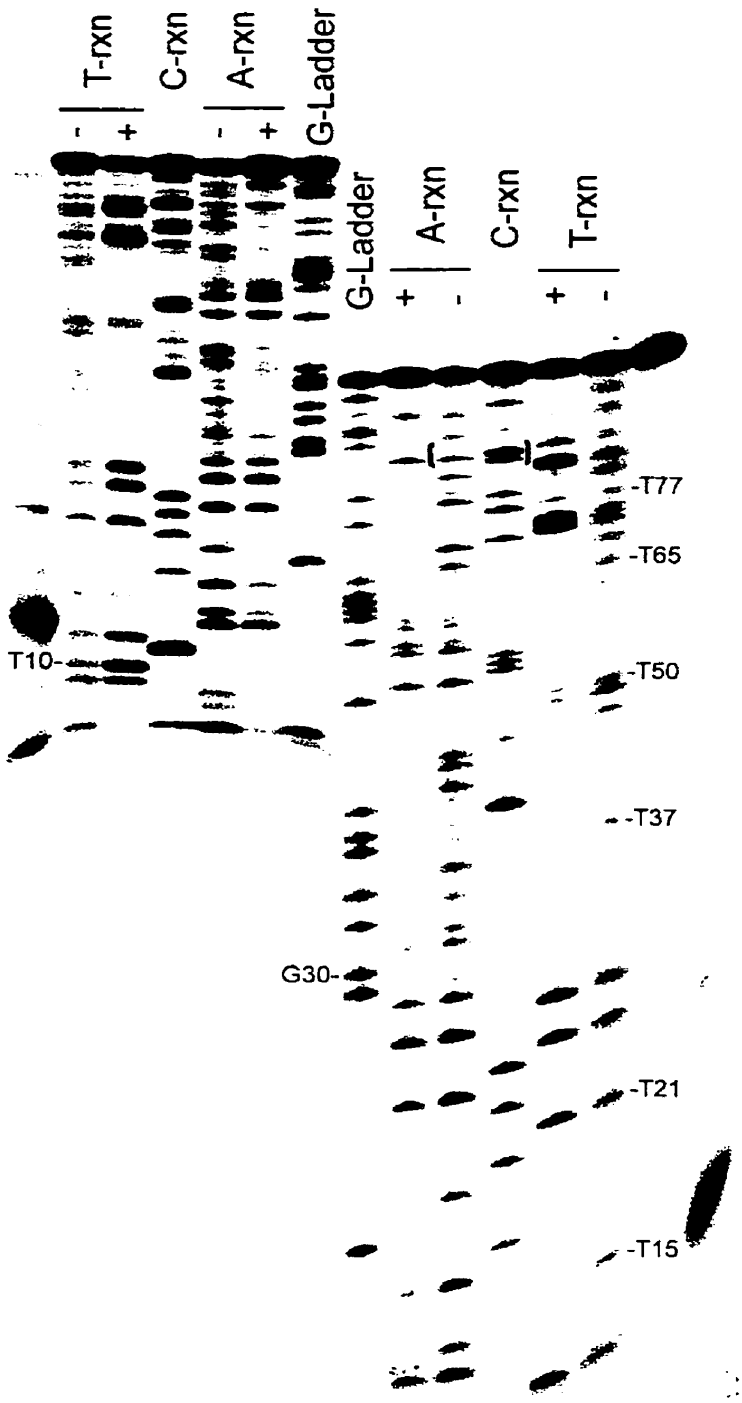

Figure 5-5. **Sequencing gel showing chemical probing patterns on the dNa-8 construct. Left and right lanes contain repeat samples which were staggered in the time of loading on the gel in order to better visualize 5' and 3' ends. T-rxn, C-rxn and A-rxn are sample that were treated with permanganate, hydroxylamine and DEPC respectfully. In the cases of the thymine and adenine reactions the +/- indicate whether the samples where treated in the presence of 0.5 M NaCl. The C-rxn, hydroxylamine, cannot be done at low and high salt conditions for the reason described in the text.**

Each of the three bases, A, T and C, along the Na-8 sequence, were designated as "protected" or "reactive" to the various reagents and are indicated as such on the proposed secondary structure of Na-8. Positions that were difficult to assign were not used in structural interpretations. No simple equivalent reaction exists for guanine bases so they were not examined in this fashion, but DMS has been used as discussed above. As seen in figure 5-6(a), the data agree with the proposed structure in regions of the proposed structure like stems I and IV. Other regions like stem III do not correspond to the chemical probing data. This first suggestion of a problem with the pre-existing Na-8 model (Geyer & Sen, 1997) led to a re-evaluation of the secondary structure.

3.2 Re-evaluating the Secondary Structure of Na-8

Ambiguous fitting of the chemical probing data with the previously proposed model for Na-8 (figure 5-6(a)) led me to re-evaluate the structure. Two different models for the secondary structure were created to better fit the chemical data. The first model, Model B, had stem III shifted to be consistent with the chemical protection data, while the chemically reactive sequences were placed in single stranded environments (figure 5-6(b)). While this model closely fits the original, along with fitting the new chemical probing data, it is problematic in that there is no obvious reason why stem III should actually form. There is almost a complete absence of Watson & Crick base pairing in the stem. Alternative association may be involved; however, other structural models were also investigated.

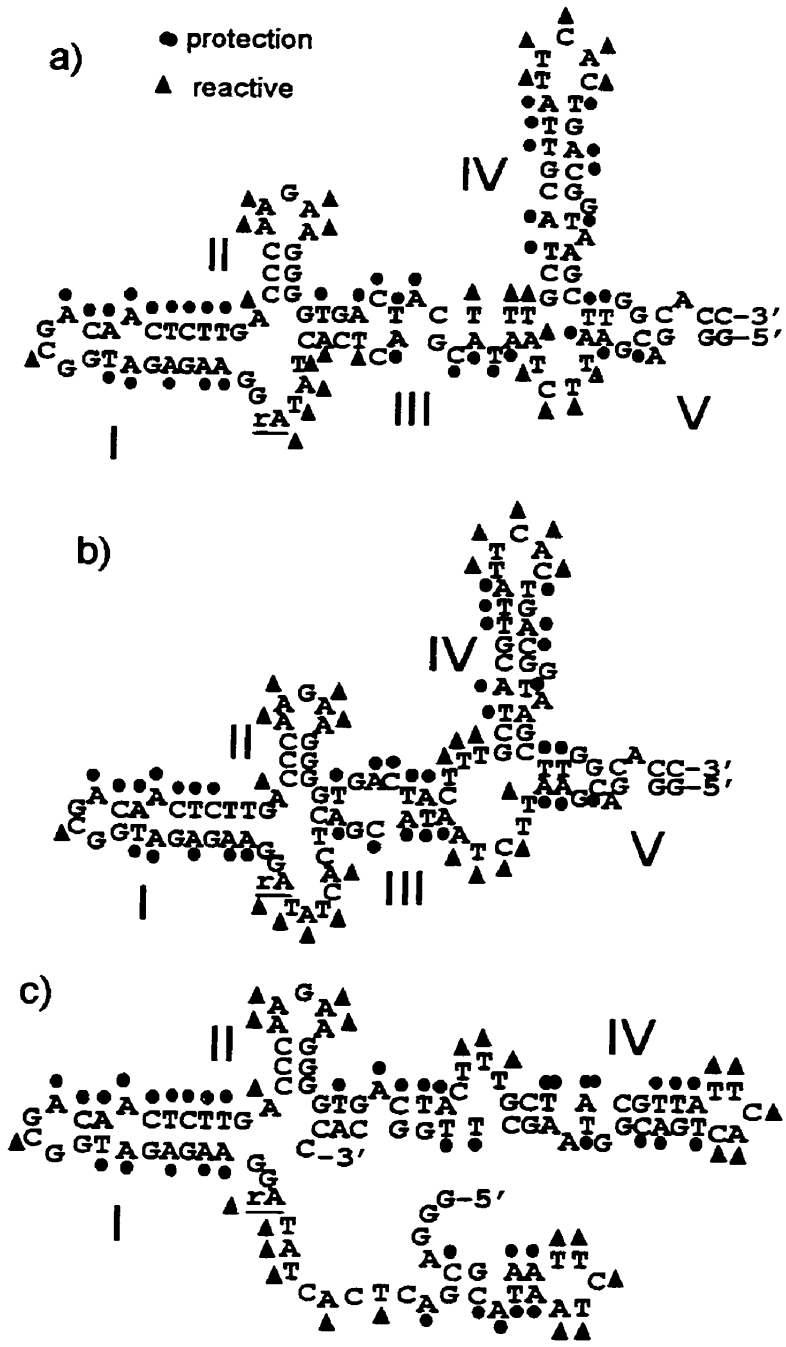

Figure 5-6. **Secondary structure models for Na-8. Models for Na-8 highlighted with the chemical probing data from figure 5-5. (a) Initial proposed model for Na-8. (b) Postulated Model B. (c) Postulated Model C.**

An entirely new model was constructed *de novo,* such that it would not be biased by the original structure. The MFOLD program for predicting DNA secondary structures (SantaLucia, 1998) was used while using constraints for folding such that bases that were chemically reactive were not involved in Watson-Crick base pairs. Regions of protection were not used as constraints because chemically protected bases are not always in Watson-Crick base pairs, as previously mentioned. The final result is a significantly different structure that agrees with the chemical probing data (figure 5-6(c)). A couple of the stems are conserved: stems I, II and IV, while new helices replace III and V. The most obvious difference in the proposed models is that in model C, the 5' and 3' ends of the DNA molecule are no longer associated.

3.3 Secondary Model Evaluation

To determine which model, B or C, is the more likely secondary structure for Na-8, three different mutants of Na-8 were synthesized and assayed for catalytic ability along with the wild type Na-8 DNAzyme. The structural impact on Na-8 of these mutations is outlined in figure 5-7. Mutations Va and Vb would both disrupt the putative stem V in model B (or A) and inactivate the enzyme. In combination, these mutations would re-form the double helix of stem V and presumably allow for enzymatic function if model B were correct. In the case of model C, alternate but less predictable observations are expected.

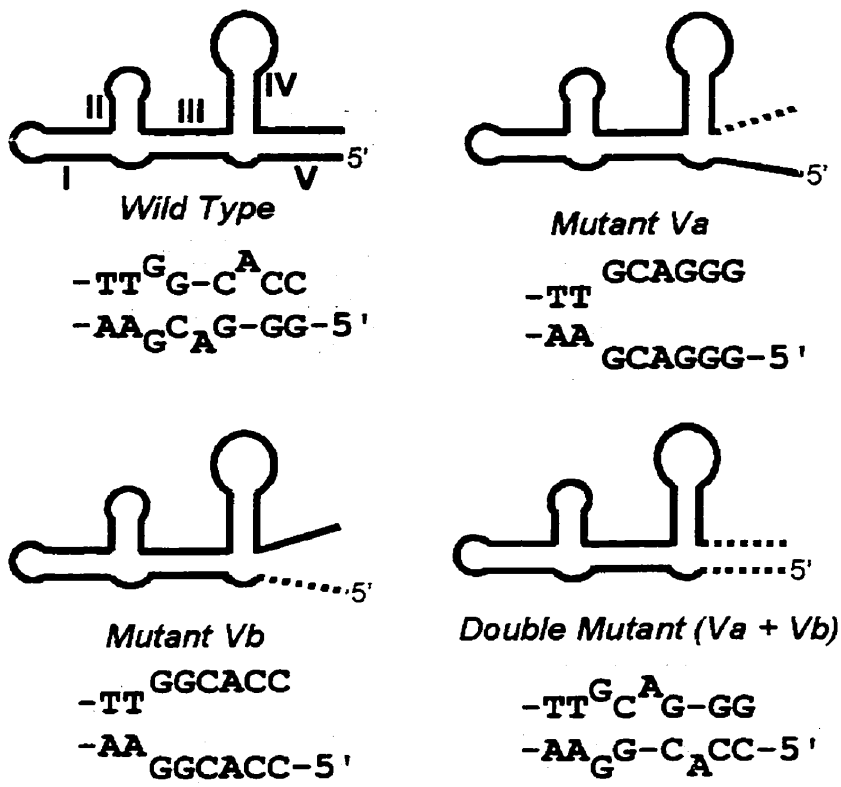

Figure 5-7. **Structural mutations of Na-8. A schematic drawing of the three mutations tested: Va, Vb and the double mutant. Roman numerals label each stem on the diagram of the wild type Na-8 enzyme. All three mutants affect the postulated stem V of the Na-8 model. Sequences in the shaded boxes below each structure show the composition of the bases in the stem V region in each particular case.**

The results of the self-cleaving assays of the three mutants in comparison with the wild type enzymes is shown in figure 5-8, while numerical parameters from the experiments are summarized in table 5-1.

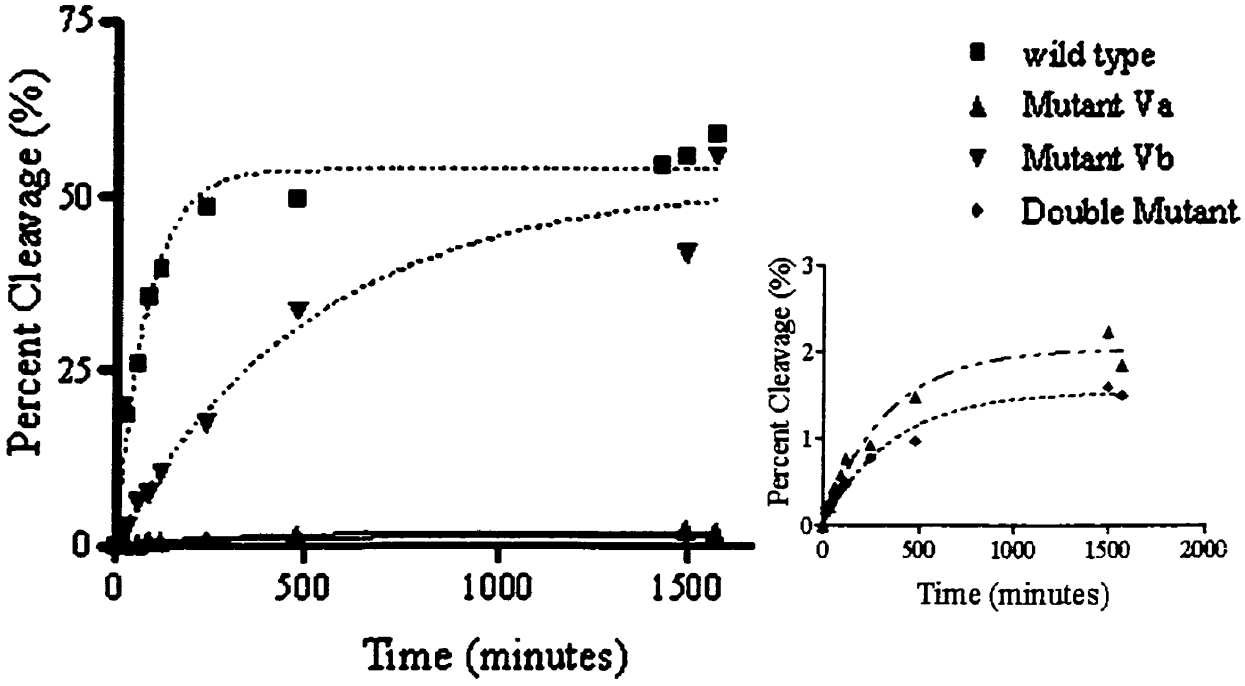

Figure 5-8. Rates of self-cleavage of Na-8 mutants. Kinetic assays were performed at 22°C in 500 mM NaCl, 50 mM HEPES (pH 7.0), 10 mM EDTA.

As shown in figure 5-8 and table 5-1 both mutant Va and the double mutant exhibit very low total yields of self-cleavage, about 5% of the "wild-type". The mutations also exhibit a 3-fold drop in the observed rate of the reaction. In comparison, mutant Vb shows significantly different results. With this mutant the total maximal cleavage remains approximately the same as the wild type enzyme, while a comparable drop in the rate of self-cleavage with respect to mutant Va and the double mutant is also observed.

Table 5-1

Enzyme	k_{obs} (min^{-1})	Maximal Cleavage (%)
Wild Type Na-8	0.012±0.004	54 ± 5
Mutant Va	0.0031±0.0011	2.0 ± 0.3
Mutant Vb	0.0019±0.0009	53 ±10
Double Mutant (Va & Vb)	0.0029 ±0.0010	1.5 ± 0.3

Kinetic parameters of Na-8 mutants. A summary of the kinetic parameters from the experiments in figure 5-8.

This indicates that the 3' end of Na-8 appears to be very critical for proper folding, as improperly folded sequences will not cleave at all. These results strongly favor the new model C over either model A or B, since the enzyme is active in the absence of stem V.

Further insight is also gained by the examination of the results on the mutants. In all cases the mutants have a significant catalytic activity. The background, unanalyzed rate of this self-cleavage reaction cannot be measured directly because it is too slow for accurate measurements. It has been estimated, however, to be 6×10^{-8} min^{-1} (Li & Breaker, 1999b) under our experimental conditions. Enzymatic activity of the mutants tells us that the sequences that we mutated in fact do not compose critical bases in the catalytic core, so are likely to be only important for the effective and efficient folding to the active structure of Na-8. Mutant Vb is of particular interest because it allows for the same degree of cleavage as the wild type enzyme, while only reducing the rate of cleavage. The K_{obs} of Mutant Vb is comparable to that of the parental G3 enzyme [k_{obs} = 0.003 min^{-1} (Geyer & Sen, 1997)]. This mutated region of Vb may thus be involved in structural interactions that allow the Na-8 to have a higher rate of cleavage than G3. Still,

the mutations seem to perform a subtle supplementary role to the enzymes function, indicating to us that the 5' region may be a target for future deletion studies in trying to minimize the structure of the enzyme.

4. Conclusions

We have proposed a new secondary structure model for the Na-8 DNAzyme that better fits the data from chemical probing experiments compared to the original proposed model. This model in figure 5-9 fits all of the chemical and enzymatic probing data obtained to date. It is apparent that this is still not the "minimized" structure of the enzyme, as part of the 5' end of the sequence appears somewhat dispensable. The 3' end of the enzyme also appears to be important for proper folding of the enzyme to an active structure. Future work with Na-8 should determine how much of the 5' sequence can be removed without disabling the catalytic activity.

This new insight to the secondary structure of the enzyme may also allow for other work on the Na-8 enzyme. Previous work failed to separate the Na-8 sequence into catalytic and substrate components such that a true enzyme could be constructed, that possessed the ability to cleave multiple substrate sequences. Original attempts were based on the assumption of the formation of stem III. Material presented here indicates that stem III does not form, which would explain the failure of those original attempts. With the new secondary model the conversion of Na-8 into a true enzyme may be achievable, which would aid in mechanistic studies of the system.

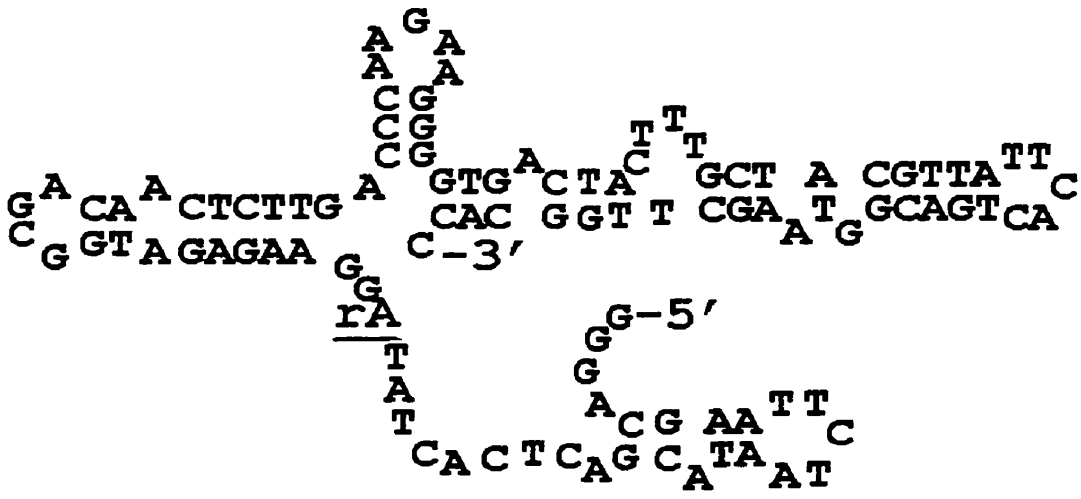

Figure 5-9. **Proposed secondary model of Na-8. The single ribose base cleavage site is indicated as rA.**

This work is a small part of a long term goal of trying to understand how this DNA sequence can catalyze the cleavage of an RNA phosphodiester bond in the absence of a cofactor with a rate enhancement of approximately $\sim 10^7$.

Part IV

Charge Transfer in DNA

Chapter 6

Electron Transfer Agents

1. Introduction

The question of whether and how electrons (or electron holes) may migrate over long distances through DNA was raised almost 40 years ago (Eley & Spivey, 1962; Hoffman & Ladik, 1964). Experiments in the 1990s led to various contradictory conclusions about the efficiency and rate of the process of electron transfer through DNA. Reports on DNA acting as an efficient electron carrier through the aromatic base stacks of duplex DNA, where the term 'π-way' was used to describe an efficient DNA conduction system (Arkin *et al,* 1996; Murphy *et al*, 1993). Other groups reported contradictory results, where DNA was determined to act as an insulator (Lewis *et al*, 1997; Debije *et al,* 1999). A heated debate has persisted over the interpretation and validity of various results (Dotse *et al*, 2000; Wilson, 1997).

Recently, a larger variety of experiments have been done, including direct measurements on 600 nm-long 'ropes' of intertwined, desiccated DNA (Fink & Schonenberger, 1999); and, through individual DNA duplexes (Porath *et al,* 2000), the consensus seems to be that both sides of the debate are correct - to some degree. This unintuitive conclusion arises because of the complex nature of the charge transfer process, which appears to depend on several factors, such as nucleotide sequence, the driving force of the reaction and, interaction, or π-overlap, of the electron donor/acceptor with the DNA base stacks.

The understanding of the fundamental mechanisms of charge migration in DNA is pertinent to current developments in DNA-based molecular electronics,

electrochemistry-based DNA chip technology (Wang, 2000; Boon *et al,* 2000), as well as biologically relevant genomic DNA damage (Burrows & Muller, 1998).

In addition to studies on electrical conduction through DNA, DNA has been used to form other kinds of conducting structures. DNA has been used to template the growth of nanoscale silver wires (Braun *et al,* 1998), and the electrical properties of DNA assembled gold colloids has also been examined (Park *et al,* 2000). A novel metal-DNA complex, known as M-DNA, has also been reported to act as an efficient electrical wire (Aich *et al,* 1999).

1.1 Mechanisms of Charge Transport

Several mechanisms for charge transport through DNA have been reported; however, there is still no generally accepted mechanism for the process (Grinstaff, 1999). The two most prevalent models are the unistep superexchange mechanism and the multistep hole hopping mechanism. These contrasting mechanisms are believed to occur in different situations depending on the specific details of the system being examined, particularly, the charge separations, between the donor, acceptor and bridging sequences (Jortner *et al,* 1998). A third mechanism, that is somewhat related to the hopping model, is the phonon assisted polaron like hopping model. In addition to these three models, others have been proposed, but the above three are the most commonly discussed in the literature. These different mechanisms predict significantly different rates for charge transport as well as different distance and sequence dependences for the process. It is unlikely that only one of the models is correct, as experimental evidence suggests that the mechanism of charge transfer through DNA changes depending on the

driving force of the reaction as well as on the DNA sequence being tested. For a more detailed discussion on the process of charge transport, review articles by Schuster (2000), Giese (2000) and Turro & Barton (1998) are suggested.

1.1.1 Unistep Superexchange

In the unistep superexchange model, the DNA behaves as a molecular wire having a continuous delocalized molecular orbital. In this orbital each base pair is in electronic contact with every other. This allows transfer of an electron from the donor to acceptor in a single step (Murphy *et al,* 1993; Turro & Barton, 1998), allowing for very rapid electron transfer. This system of charge transfer is believed to occur in systems where the electron acceptor and donor are incapable of oxidizing or reducing the bridging DNA sequences. This process is expected to be highly distance dependent, exhibiting an exponential decay as a function of distance (inasmuch as long stretches of duplex DNA are not static, i.e. are not characterized by continual base stacks). The DNA double helix is quite dynamic, with motions in the structure occurring at timescales as short as 30 pico seconds (Borer *et al*, 1994).

1.1.2 Multistep Hole Hopping Mechanism

The hole hopping mechanism is thought to be pertinent to long-range charge transfer through DNA, and is the mechanism currently the most widely supported (Nunez *et al,* 1999; Henderson *et al*, 1999; Meggers *et al*, 1998b; Nakatani *et al*, 1999; Grozema, 2000). In this mechanism an electron hole is created by an initial oxidation event, where a guanine radical cation ($G^{\bullet+}$) is formed. This process requires the original

oxidizing agent to be strong enough to oxidize guanine, in order to initiate the process. The guanine radical cation so formed is unable to oxidize any of the other three bases, owing to their higher ionization potentials, but is able to oxidize other guanines. The oxidation potential of guanine is 1.34 eV while the oxidation potential of adenine [the base with the next highest potential with an oxidation potential of 1.42 eV (Seidel *et al*, 1996; Steenken & Jovanovic, 1997)]. These values are for the free nucleobases. Values in duplex DNA are specific to a sequence context, but the general trend is maintained *($G < A < C \approx T$)*.

The ability of the guanine radical cation to oxidize a nearby guanine allows the electron hole to hop from guanine to guanine by a thermally activated process in a random walk (Ly *et al*, 1996). The process occurs until a side reaction such as the formation of an oxidized guanine, terminates it.

Some difficulties with this mechanism arise in cases where two GG or GGG runs are separated by a sequence that contains isolated guanines. A $G^{\bullet+}$ is capable of oxidizing the 5'-most guanines in these GG or GGG runs because of their lower ionization potential (see below), but once a $G^{\bullet+}G$ is formed it should be incapable of oxidizing an isolated guanine, while remaining capable of oxidizing another GG run. Nevertheless, charge migration is still observed to proceed, even to the most distal GG run. In such a situation it is believed that the central, isolated, guanine does not get oxidized, while forming a 'stepping stone' that acts to reduce the ionization potential of the bridge and allow superexchange to occur between the two GG runs (Nakatani *et al*, 2000).

1.1.3 Phonon Assisted Polaron Like Hopping

This model also relies on the formation of a radical cation or electron hole in the duplex. Such a base radical cation is electron deficient, and the local structure of the DNA distorts to stabilize this deficiency by delocalization onto adjacent bases. Structural changes that could accomplish this include a local partial unwinding of the helix to increase base overlap, or a change in the inclination angle of neighboring bases to bring them closer together.

Such a structural distortion of the duplex around the radical cation has been described as a 'polaron-like species' (Jortner *et al*, 1998). The definition of a polaron is a 'self-trap' of a radical cation within its containing medium. The inability of the structural distortions to continue indefinitely down the helix, as well as the sequence dependences of the structural distortion are such to prevent the distortions in the DNA from being classified as a true polaron (hence the name of polaron-like hopping).

Polaron formation provides a means to average out the ionization potentials of adjacent sequences and allow for efficient migration of the electron hole. Movement of the polaron, like the hopping mechanism, is a thermal (phonon) activated process. The thermal activation will cause base pairs in or near the polaron to leave or join the polaron, with the net result of migration down the DNA duplex. A review article by Schuster (2000) is suggested for a more detailed discussion of this process.

1.1.4 Other Mechanisms

In addition to the theory of long range hole hopping, a coupled proton transfer in the G·C base pair has been proposed (Steenken, 1997). In contrast to the migration of

radical cations or electron holes, negative charge or electron transport has been suggested for some cases (Bixon *et al*, 1999). In the case of electron transfer it is expected to proceed via the reduction of the pyrimidines. Cytosine and thymine are the most readily reduced bases, with both having similar reduction potentials (Seidel *et al*, 1996; Steenken & Jovanovic, 1997). The existence of a pyrimidine in each Watson-Crick base pair would allow for efficient electron transfer with little if any sequence dependence.

1.2 Monitoring Charge Transport

Several methods have been developed to monitor the process of charge transport. Ideally, direct measurements are optimal but currently technical limitations prevent direct measurements at an atomically defined level. A cathode and anode cannot be attached to DNA at defined spots on a particular DNA molecule. Direct measurements are also limited to long DNA double helices because of the limitations of reliably making anode and cathode contacts only a few nanometers apart.

The preferred methods of monitoring charge transport through DNA are to use DNA that has been covalently modified at a defined position(s) with an oxidizing and/or reducing agent. Typically, such chemical functionalities are light sensitive; such that the process of charge transport can be initiated at will by irradiating the sample with the correct wavelength of light.

Several different compounds have been incorporated into DNA in order to monitor charge transport (reviewed by Grinstaff, 1999). Depending on the process one wishes to monitor, i.e. fast superexchange or long-range 'hole' hopping, different

chemical groups are used. Monitoring the short-range superexchange process usually entails the use of fluorescent compounds that can be quenched by an electron transfer event through the DNA. See the above-mentioned review for a summary of compounds that have been utilized, along with a survey of the results obtained with these types of compounds.

1.2.1 Monitoring Electron Hole Migration

Monitoring long distance hole hopping (or phonon assisted polaron like hopping) is typically performed by utilizing of a light sensitive oxidizing agent that will produce a radical cation or electron hole in the DNA upon photo-irradiation. Once formed the migration of the radical cation is determined by the occurrence of a side reaction where the $G^{\bullet+}$ forms an irreversible oxidized adduct by reaction with water or O_2. Compounds that have been covalently attached to a DNA construct for these types of experiments include an anthraquinone derivative and an organo-metallic rhodium(III) complex, both of which are used in this work, as well as several others listed by Grinstaff (1999).

A simple schematic for the process of monitoring cation hole migration is depicted in figure 7-1. Photo-excitation of the tethered oxidizing agent (Ox, i.e. anthraquinone) leads to an excited singlet state (Ox^*). In the case of some oxidizing agents such as anthraquinone, an intersystem crossing to the triplet state may then follow. The DNA may then react with either the singlet or triplet excited state of anthraquinone. This reaction yields a radical cation or electron hole in the DNA ($G^{\bullet+}$), with an efficiency and rate expressed as k_{et}. Whether this radical cation exists on the first purine or guanine is debatable depending on whether the Multistep Hopping

mechanism or the Polaron-Like Hopping mechanisms are being discussed. For simplicity the Multistep hole hopping mechanism is depicted in figure 6-1. Initially formed, the guanine radical cation can undergo several side reactions (Meggers *et al,* 1998; Meggers *et al*, 1998b; Giese *et al,* 1999). Of the possible reactions the two of greatest interest are described below.

The first outcome is a simple back reaction, where the singlet (or triplet) radical ion $Ox^{\bullet-}$ and $G^{\bullet+}$ undergo an electron exchange that results in the original ground state of the system (Ox & G). This process occurs at a particular efficiency and rate described by k_{back}. It has been proposed that this back reaction can be minimized by the exclusion of a guanine base in the first three base pairs at the end of the helix to which the oxidizing agent has been tethered (Sanii & Schuster, 2000). The evidence for this arises from the observation that on DNA duplexes of such design require 1-5% of the irradiation time needed to observe comparable guanine damage at distant sites along the duplex.

The second outcome following the formation of the $Ox^{\bullet-}$ and $G^{\bullet+}$ is where the $Ox^{\bullet-}$ is returned to the ground state by a reaction with O_2, which leads to the formation of superoxide. At the same time the radical cation $G^{\bullet+}$ can undergo a reaction with another base (G), resulting in the movement, or hopping, of the radical cation's position along the duplex. This $G^{\bullet+}$ to G reaction allows the radical cation to randomly 'diffuse' up and down the helix until a terminating reaction occurs. The termination of cation migration happens when a side reaction occurs between the radical cation and either oxygen or water to form a base-labile guanine oxidation product.

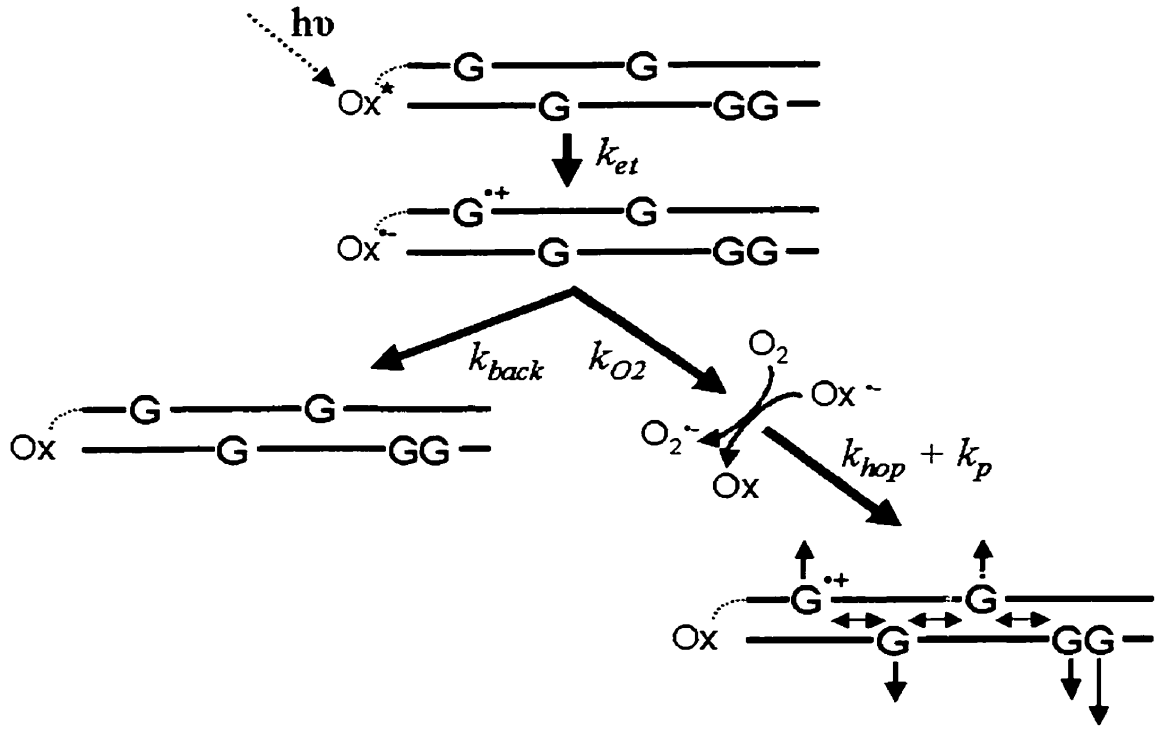

Figure 6-1. A simplified scheme for hole hopping. Photo-excitation of the oxidizing agent leads to radical ion formation on the DNA and oxidizing agent. Two possible outcomes can then occur; a back reaction which results in no net reaction, or charge migration can occur if the oxidizing agent is returned to the ground state by a side reaction with oxygen.

Experimental evidence also has shown that not all guanines react equally well during this oxidized product formation. It has been demonstrated that in Watson-Crick double stranded sequences containing 5'-GG-3', the 5' guanine is the most electron donating and is more readily oxidized in comparison to the 3' guanine or any other isolated guanines in the helix (Saito *et al,* 1995). Such a 5' G reactivity is also supported by theoretical calculations (Sugiyama & Saito, 1996). In addition to the 5' positional effect on the ionization potential of guanine, other sequence contexts influence the oxidation of the 5' guanine. It has been experimentally shown that the

efficiency of GG cleavage occurs in the following order: GGG > CGG > AGG = TGG > TGT (Saito *et al*, 1998).

The actual identity of the resulting oxidized guanine product has also been of some debate. Initially the major oxidation product was believed to be 8-oxo-guanine (Hall *et al,* 1996), but it was later shown that 8-oxoG containing sequences are not efficiently cleaved in hot piperidine (Cullis *et al,* 1996), which is the process to detect guanine oxidation. Later evidence suggested that the major oxidized guanine product in these photo-oxidation experiments was 2-aminoimidazolone (Spassky & Angelov, 1997; Cullis *et al,* 1996; Kino & Saito, 1998). Recently, this has been disputed again by work from Kan & Schuster (1999), where it is has been suggested that 8-oxo-7,8-dihydro-2'-deoxyguanosine is the major oxidation product (susceptible to the piperidine-dependent cleavage) in double stranded DNA, while 2-aminoimidazolone may be the product of oxidation in single stranded DNA.

1.3 Chapter Overview

A major section of this chapter is The Materials and Methods, which includes the synthesis of and derivatization of DNA with anthraquinone; a rhodium complex; and, a ruthenium complex, all of which can be used in monitoring charge transport through DNA. Synthesis was carried out as described in various published articles but in several cases a diversity of published methods had to be attempted to achieve adequate yields. All steps are provided in detail here as a 'manual' for future students continuing on the project, while only partial product characterization is provided, as the remaining characterization is reported in the relevant references.

Originally, our goal, when we set out to explore the process of electron transfer in DNA, was to use the rhodium complex $(Rh(phi)_2(byp')^{3+}$ (-see description below) described by Barton's group at Caltech (Hall *et al,* 1996) to monitor charge transfer through a variety of DNA structures. Initial experiments with this compound resulted in expected results in double stranded DNA samples, but when attempting to use the compound with more complex DNA structures (3 & 4-Way Junctions), confounding and unexplainable results were observed. Given the difficulties with the rhodium complex, we then tried a different system developed by Schuster's group (Gasper & Schuster, 1997). This was using an anthraquinone tethered to the end of a DNA duplex to form radical cations in the DNA upon photo-irradiation, in an analogous manner to that of the rhodium complex. Anthraquinone-DNA adducts yielded data that varied significantly from those obtained from the rhodium complex when examining 4-way junctions. This is not the first time these two adducts have given conflicting results, as can be seen in two different published manuscripts about the repair of thymine dimers via long range electron transfer in duplex DNA (Dandliker *et al,* 1997; Dotse *et al,* 2000)

This chapter provides a comparison of results obtained when the rhodium adduct, as compared to the anthraquinone adduct, was used to monitor charge transport through 4-Way junctions.

2. Materials and Methods

2.1 DNA Derivatization

All chemicals were purchased for Sigma-Aldrich unless stated otherwise. Solvents were all purchased from BDH. DNA sequences with the 5' C6 amino functionality were purchased from the University of Calgary Core DNA services. Unmodified oligos where purchased from either Sigma-Genosys or the University of Calgary Core DNA services.

2.1.1 Derivatization of DNA with a Rhodium Complex

The rhodium complex to be tethered to the 5' end of a DNA sequence required complete synthesis, as it is not commercially available. The compound $Rh(phi)_2(byp')Cl_3$ [phi:9,10 diaminophenanthrene; byp': 4-(4-carboxybutyl)-4'methyl-2,2'-bipyridine] that we synthesized is shown in figure 6-2. This compound is analogous to the rhodium compounds used by Jaqueline Barton's group at Caltech, which has done a significant proportion of all published work on charge transfer through DNA. Their synthesis protocols have been reported, but unfortunately the purification procedures where often omitted so we had to work through many of these steps ourselves. The difference between our compound and those used by Barton's group is that the 'linker' separating the bipyridal and the carboxylic acid is of an intermediate length to those used (Hall *et al,* 1996; Murphy *et al,* 1993).

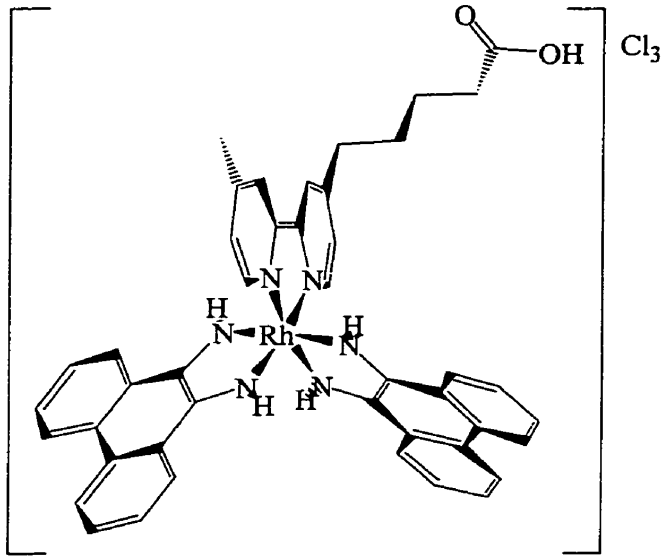

Figure 6-2. Structure of $[Rh(phi)_2(byp')]Cl_3$. Only the Δ isomer is shown.

2.1.1.1 Synthesis of 4-(4-carboxybutyl)-4'methyl-2,2'-bipyridine (byp')

The first step in the synthesis of the $[Rh(phi)_2(byp')]Cl_3$ compound was the synthesis of the bidentate 4-(4-carboxybutyl)-4'methyl-2,2'-bipyridine (byp') ligand. The synthetic route to make this compound is outlined in figure 6-3.

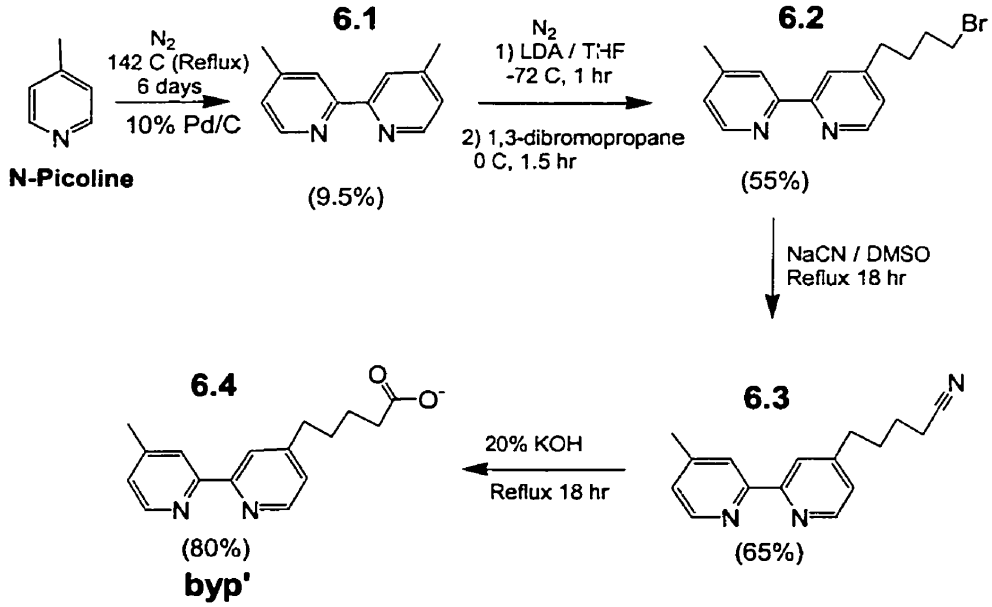

Figure 6-3. Synthetic outline for the byp' ligand.

2.1.1.1.1 Synthesis of 4,4'-dimethyl-2,2'-bipyridine *(6.1)*

The reaction to synthesize 4,4'-dimethyl-2,2'-bipyridine (compound *6.1*) was performed as essentially described by Ghosh & Spiro (1990). To a round bottom flask containing 91.5 g N-picline (0.983 moles) was added 3.57 g 10% Pd/C. The slurry was heated to reflux for 6 days with constant stirring while under a nitrogen atmosphere. The solution was then hot filtered to remove the Pd/C catalyst, upon cooling the crystalline product is observed in the solution of N-picoline. The solution was reduced in volume under vacuum to ~30 ml, to which 75 ml ethyl acetate was added. The solution was heated to dissolve the crystalline product, hot filtered, then placed at room temperature to allow recrystalization. Crystals were collected by filtration and then re-crystalized 2× from 90 ml of ethyl acetate. Final crystals yielded 8.57 g of *6.2* (9.5% yield).

^{1}H NMR (400 MHz, $CDCl_3$): δ 8.57 (d, J = 5.0 Hz, 2 H), 8.36 (s, 2 H), 7.20 (d, J = 5.0 Hz, 2 H), 2.49 (s, 6 H).

2.1.1.1.2 Synthesis of 4-(4-bromobutyl)-4'-methyl-2,2'-bypyridine *(6.2)*

The reaction to synthesize 4-(4-bromobutyl)-4'-methyl-2,2'-bipyridine (compound *6.2*) was performed as essentially described by Yonemoto *et al* (1994). All steps are under a nitrogen atmoshere unless stated otherwise. A 3.0 ml solution of 2.5 M butyl lithium (7.4 mmole) in THF was added to a solution of 1.1 ml diisopropylamine (7.8 mmole) in 15 ml THF with constant stirring on an ice bath. The mixture was stirred for 15 minutes; at this point the solution was orange-brown in color. The flask was then

transferred to a dry ice acetone bath and stirred. After cooling for ~10 minutes a solution of 1.38 g of *6.1* (7.4 mmole) in 35 ml THF was slowly added (over 20 minute period). At this point the solution became dark brown in color. A solution of 1.5 ml dibromopentane (14 mmole) in 15 ml THF was added rapidly (important). After 30 minutes the solution is then transferred back to an ice bath and the reaction was allowed to proceed for another hour. During the course of this reaction the solution goes blue then finally yellow in color. After the reaction was competed it was quenched by the addition of 2.5 ml of water.

The sample was then brought to room temperature and opened to the atmosphere. A concentrated phosphate buffer solution (25 ml-pH 7.0) was then added to the sample. The sample is then extracted with 3 volumes of diethyl ether. The organic phase was then washed 3× with water then dried over sodium sulphate (do not use magnesium sulphate because the product chelates magnesium!). The solution was then filtered and the diethyl ether removed under vacuum (do not heat as the product is temperature sensitive). The residual yellow-brown oil was suspended in a few milliliters of chloroform and loaded on a short silica column (5-7 cm) to remove base line impurities. The yellow product was eluted with ether. Collected fractions were combined and dried under vacuum yielding 1.24 g of *6.2* (55% yield).

^{1}H NMR (400 MHz, CD_2Cl_2): δ 8.53 (dd, J = 5.0, 0.7 Hz, 1 H), 8.50 (dd, J = 5.0, 2.3 Hz, 1 H), 8.26 (m, 2 H), 7.14 (m, 2 H), 3.46 (t, J = 6.5 Hz, 2 H), 2.76 (t, J = 7.5 Hz, 2 H), 2.43 (s, 3 H), 1.92 (m, 2 H), 1.85 (m, 2 H).

2.1.1.1.3 Synthesis of 4-(4-cyanobutyl)-4'-methyl-2,2'-bipyridine *(6.3)*

The reaction to synthesize 4-(4-cyanobutyl)-4'-methyl-2,2'-bipyridine (compound *6.3*) was performed as essentially described by Nubbaumer *et al* (1988). A sample of *2.1*, 0.50 g (1.6 mmole) was dissolved in 10 ml DMSO and added drop by drop to a suspension of 0.8 g NaCN in 2.5 ml DMSO and stirred overnight. During the reaction the solution went orange then finally yellow. The mixture was then poured into a 50 ml solution containing 9.9 g K_2CO_3 and 0.33 g KOH in 81.5 ml distilled water. Once mixed the combined solution goes milky white. The solution was extracted repeatedly with small volumes of diethyl ether (5× 25 ml). Extracts were then washed with several small volumes of water (4× 15 ml). The pale yellow organic solution was dried over Na_2SO_4 then evaporated to dryness, yielding 270 mg of *6.3* as a yellow solid (65% yield).

^{1}H NMR (400 MHz, $CDCl_3$): δ 8.59 (d, 1 H), 8.56 (dd, 1 H), 8.28 (s, 1 H), 8.18 (s, 1 H), 7.15 (m, 2 H), 2.75 (t, 2 H), 2.46 (s, 3 H), 2.4 (t, 2 H), 1.88 (m, 2 H), 1.74 (m 2 H).

2.1.1.1.4 Synthesis of BYP' *(6.4)*

The reaction to synthesize 4-(4-carboxybutyl)-4'-methyl-2,2'-bipyridine (compound *6.4*) was performed as essentially described by Nubbaumer *et al* (1988). A 250 mg sample of *6.3* was dissolved in 20 ml of 20% KOH and refluxed overnight (~18 hours). The sample was then cooled to room temperature and neutralized with concentrated HCl (test pH with pH paper). The sample was then extracted with five volumes of diethyl ether. The extract was washed with charcoal and dried over Na_2SO_4.

The sample was dried down under vacuum and crystallized from a 1:1 benzene:petroleum ether solution. The resulting fine white crystals of *6.4* weighed 215 mg (80% yield).

^{1}H NMR (400 MHz, $CDCl_3$): δ 8.57 (m, 2 H), 8.27 (s, 2 H), 7.15 (m, 2 H), 2.73 (m, 2 H), 2.43 (s, 3 H), 2.4 (t, 2 H), 1.75 (m, 4 H).

2.1.1.2 Synthesis of $Rh(phi)_2(byp')\ Cl_3$

The route of synthesis for the organo-metallic $Rh(phi)_2(byp')\ Cl_3$ used is outlined in figure 6-4.

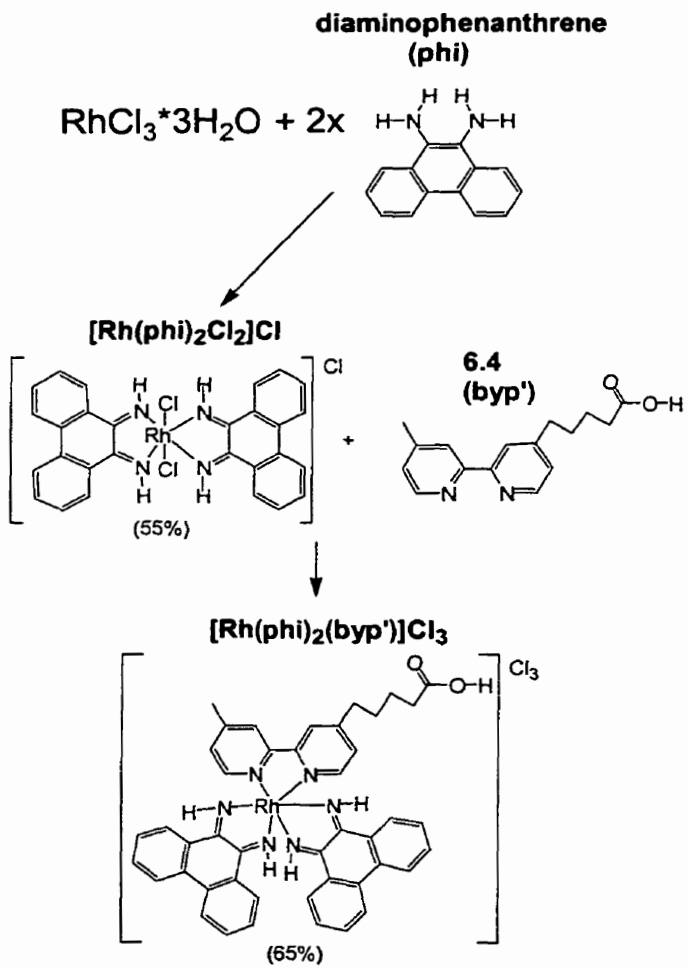

Figure 6-4. **Synthetic outline for the synthesis of $Rh(phi)_2(byp')\ Cl_3$.**

2.1.1.2.1 Synthesis if $[Rh(phi)_2Cl_2]Cl$

This reaction was essentially as described by Pyle *et al* (1990). A sample of 0.100 g $RhCl_3$ hydrate (Pressure Chemicals) was dried under high vacuum for 2 hours. At this point 5 ml anahydrous ethanol was added, and the $RhCl_3$ was dissolved with gentle heating. After dissolution the deep burgundy solution was purged with nitrogen for one hour.

In another flask, 188 mg of 9,10-diaminophenanthrene and 5.6 mg hydrazine dihydrate was dried under high vacuum for 2 hours. The solid was then dissolved in 15 ml dry DMF and the yellow solution was purged with nitrogen for one hour with constant stirring.

The solutions were combined under a nitrogen atmosphere. The combined solutions were then heated to reflux for 5 hours. The brown solution was then cooled to room temperature then opened to air where it goes an olive green color. The solution was then stirred overnight at room temperature. This mixing was done open to the air and away from direct light. The solid product was filtered and washed with diethyl ether, yielding 150.5 mg racemic $[Rh(phi)_2Cl_2]Cl$ (55% yield). MOLDI-TOF: m/z $Rh(phi)_2Cl_2^+$: 293.3 (calculated 293.16).

2.1.1.2.2 Synthesis if $[Rh(phi)_2(byp')]Cl_3$

The reaction conditions in this synthesis are the same as described by Pyle *et al* (1990), but the carboxylic acid functionality on the byp' linker requires different separation methods than that used for an added simple bipyridine described by the authors.

In a 100 ml round bottom flask 49.8 mg $[Rh(phi)_2Cl_2]Cl$ (0.080 mmole) and 26.9 mg byp' (0.1 mmole) were dissolved in 30 ml DMSO with gentle heating. After dissolution 10 ml of water containing 1.1 mg hydrazine hydrate (0.01 mmole) was added dropwise to the warm solution. The solution was then heated to 100°C for 8 hours.

The solution was evaporated to dryness with a high vacuum roto-vap. The solid was then resuspended in a minimal volume of 1:1 water:acetonitrile. The sample was loaded on a silica column and eluted with 1:1 200 mM NaCl: acetonitrile. Fractions containing the desired orange product were combined and reduced in volume to ~10%, then water was added to the solution to a final volume of 20 ml. The product was then selectively precipitated by the addition of 5 ml of a 10% $NaBF_4$. The solid was collected by centrifugation and washed 2× with 10 ml 1% $NaBF_4$, and 1× with 10 ml water. The remaining solid was suspended in 20 ml of acetone and the product was precipitated by the addition of 10% tetraethylamine chloride in acetone. The precipitate was washed 3× with 15 ml aliquots of acetone. The sample was then dried yielding 46.5 mg of racemic $[Rh(phi)_2(byp')]Cl_3$ (65% yield). Analysis by electrospray MS gives m/z of 393 where the predicted value for $Rh(phi)_2(byp')^{2+}$ is 392.9. The observed reduction of rhodium(III) to rhodium (II) is typical in mass spectroscopy (Pyle *et al*, 1990). The product also exhibited identical pH dependant spectroscopic properties as described by Pyle *et al* (1990). Isomers were not separated as both Δ and Λ both work with charge transfer experiments in DNA (Hall *et al,* 1996).

When using the compound for labeling DNA, small amounts are approximately weighed out and dissolved in water. Accurate concentrations can be determined by measuring the samples absorbance at 378 and 292 nm where the complex has extinction

coefficients (ε) of 28,200 and 43,200 $M^{-1}cm^{-1}$ respectively at pH 7.0. Both readings are usually done because discrepancies in the concentrations determined by the two methods are indicative of impurities or non-neutral pH.

2.1.1.3 Preparation of Rhodium Labeled DNA (Rh-DNA)

DNA with 5'-C6- amino label was purchased from University of Calgary Core DNA Services. Upon arrival, the DNA is treated to remove nitrogenous contaminants from the DNA synthesis procedures. The dried DNA sample was first suspended in 100 µl ddH_2O, followed by three consecutive 100 µl extractions with $CHCl_3$. The DNA remaining in the aqueous phase was then precipitated by the addition of 30 µl 1M NaCl and 340 µl 100% EtOH. After mixing the sample, it was placed on dry ice for ~10 minutes followed by centrifugation at 13,000 *g* for 20 minutes to pellet the DNA. The pellet was washed 1× with 150 µl 70% EtOH (v/v). After brief drying the pellet was re-suspended in 100 µl ddH_2O and the concentration determined by UV spectroscopy.

In a 0.5 ml eppendorf tube is added: 15 µl 1 mM $Rh(phi)_2(byp')Cl_3$, 2.5 µl 1M MES (pH 5.75), 2.5 µl *N*-hydroxysulfosuccinimide sodium salt (25 µg/µl in H_20) and 2.5 µl of freshly dissolved EDAC (20 µg/µl in H_20). The sample was incubated at room temperature for 10-15 minutes. To the sample was added 15 µg 5'-amino-DNA as prepared above. After the addition of DNA, 2.5 µl of 50 mM $MgCl_2$ is added. The sample was then wrapped in aluminum foil and placed on a shaker overnight at room temperature. The sample was then ethanol precipitated and rinsed 1× with 100%

ethanol. The pellet was dissolved in 25 μl TE, then purified by reverse phase chromatography on an HPLC using a C18 Deltpack column (Waters).

HPLC protocol is as follows: the solvent flow was continuously 0.75 ml/minute and the column was heated to 65°C. The initial conditions were 100% Solvent A, changing to 30% Solvent B over 30 minutes with a linear gradient. Following this period, the solvent was then rapidly changed to a 100% B for 15 minutes before reconditioning the column to the original conditions. Solvent A was (20:1) 100 mM triethylamine acetate (pH 6.85-7.4): acetonitrile and solvent B is 100% acetonitrile. Typical uncoupled DNA sequences have a retention time of 17 minutes, while the rhodium modified DNA has a retention time of 20 minutes. Retention times vary somewhat for different sequences depending on base length. Ammonium acetate (50 mM, pH 6.0) has also been successfully used as previously reported (Holmlin *et al,* 1999), and results in a similar resolution of product separation.

Fractions containing the product are lyophilized, then resuspended in 100 μl water and lyophilized again. This process was repeated at least three times. The sample was then suspended in 100 μl 300 mM sodium acetate (containing 10 μg of glycogen), then precipitated by the addition of 300 μl 100% ethanol. After chilling on dry ice for at least ten minutes, the samples were then centrifuged at ~10,000 g for 20 minutes. The supernatant was then discarded and the pellet was washed with 70% ethanol. The pellet was dried then suspended in 75 μl TE. The concentration of the sample was determined by measuring the optical density of the sample at 390 nm. At this wavelength the rhodium complex absorbs (ε = 19,000) (Nunez *et al,* 1999).

2.1.2 Derivatization of DNA with a Ruthenium Complex

Another metal complex that was synthesized was [Ru(dppz)(phen)(byp')]Cl_2 (dppz: dipyrido [3,2-a:2',3'-c]phenazine; phen: 1,10-phenanthroline) (figure 6-5). This compound has been described as a 'molecular light switch' for DNA, as it will not fluoresce in aqueous solutions in the absence of DNA (Friedman *et al*, 1990; Jenkins & Barton, 1992; Hiort *et al*, 1993). This compound has also been used in experiments in fluorescent based systems to monitor superexchange charge transfer in DNA (Murphy *et al*,1993; Arkin *et* al, 1996; Holmlin *et al*, 1998; Stemp *et al*, 2000). Even though synthesis was accomplished, the utilization of the compound in our DNA constructs to monitor reactions was problematic. No results utilizing this compound are presented in this manuscript, but its synthesis is reported for anyone wanting to repeat the work to try and get ae fluorescence-based system working.

Of the three ligands in the compound only one has to be synthesized, as phen is commercially available and byp' has already been synthesized for use in the rhodium complex above.

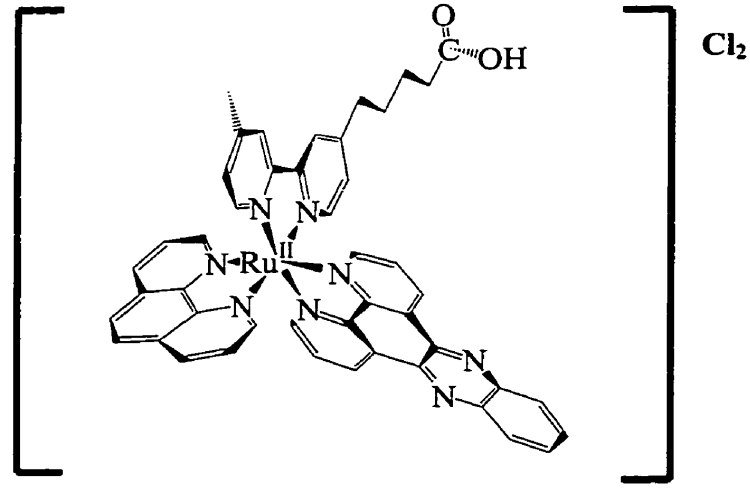

Figure 6-5. Structure of [Ru(phen)(dppz)(byp')] Cl_2. Only the Δ isomer is shown.

2.1.2.1 Synthesis of Δ dipyrido [3,2-a:2',3'-c]phenazine (dppz)

The synthesis of dipyrido [3,2-a:2',3'-c] phenazine (dppz) was synthesized using the scheme outline in figure 6-6.

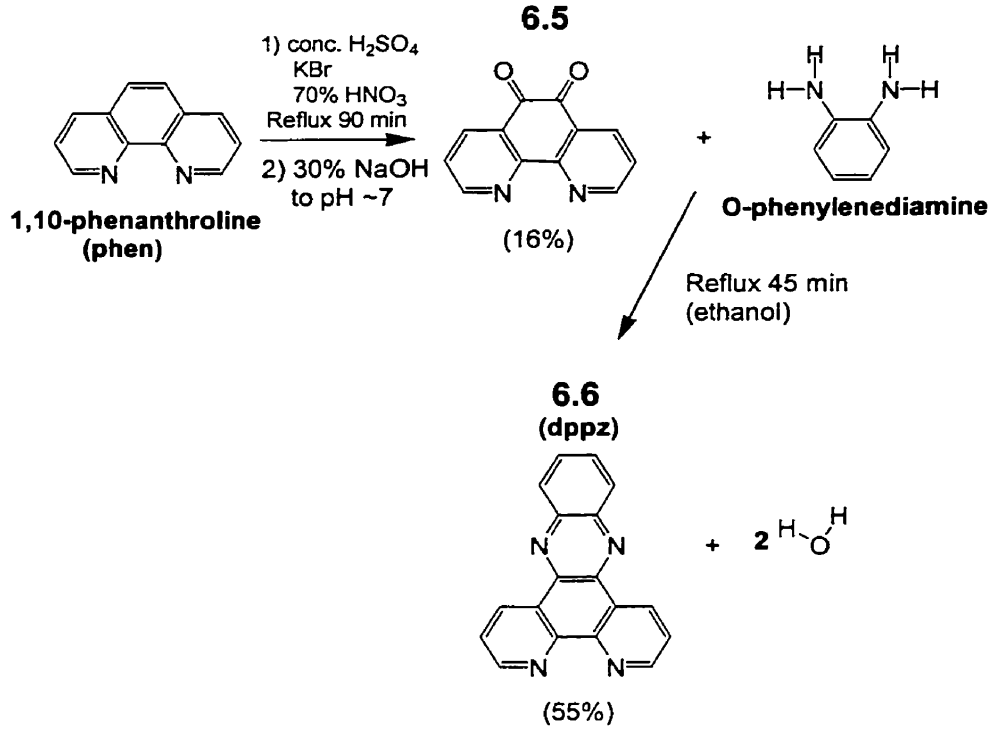

Figure 6-6. Outline for the synthesis of the dppz ligand.

2.1.2.1.1 Synthesis of 1,10-phenanthroline-5,6-quinone (*6.5*)

This synthesis is a slightly modified variant as reported by Hiort *et al* (1993). *Note: care should be taken with this reaction and should be performed behind a blast shield. It is not advisable to scale-up the reaction beyond this size otherwise it becomes quite volcanic.*

In a 100 – 150 ml round bottom flask, 5.02 g of 1,10-phenanthroline (phen) (25.3 mmole) was slowly added to 30 ml concentrated sulphuric acid. After dissolution, 2.55 g KBr was added. After the KBr is completely dissolved, 15 ml of 70% nitric acid was

slowly added. The solution was then slowly heated to reflux, and the temperature is maintained for 1.5 hours.

After the solution is cooled to room temperature, it was poured over ~180 g of ice. The green solution was then neutralized with 70% NaOH. During neutralization the solution goes yellow, then white and finally orange with light brown precipitate at neutral pH. The suspension was then allowed to sit overnight at room temperature. The solution was filtered, and the solid is extracted 2× with 100 ml boiling water. The extracts were then combined with the original filtrate.

The residual solid can be extracted with CH_2Cl_2 at this point to obtain 5-nitro-1,10-phenanthroline, this is the major bi-product of the reaction. This compound has been used in the synthesis of other ligands possessing 'tethers' (Murphy *et al,* 1993; Jenkins & Barton, 1992).

The combined aqueous extractions and filtrate above were repeatedly extracted with CH_2Cl_2 (7× 100 ml). The combined organic fractions were washed 2× 200 ml water, then dried over sodium sulphate. The sample was then reduced to dryness under vacuum. The residual orange product was crystallized from ~400 ml toluene, yielding 0.83 g of *6.5* (16% yield) as small orange crystals.

^{1}H NMR (400 MHz, $CDCl_3$): δ 8.79 (dd, 2 H), 7.98 (dd, 2 H), 7.35 (dd, 2 H).

2.1.2.1.2 Synthesis of DPPZ (*6.6*)

This reaction is essentially described by Dickerson & Summers (1970). To 20 ml anhydrous ethanol was added 472 mg *6.5* (2.25 mmole) and 470 mg O-phenylenediamine. The sample was then heated to reflux for 45 minutes then cooled to

4°C. The product crystallizes upon cooling. The fine yellow crystals were then collected by filtration and recrystalized from aqueous ethanol to give *6.6* (pentahydrate) as long yellow hair like fibers. The collected crystals weighed 460 mg (1.24 mmole) – (~55% yield).

^{1}H NMR (400 MHz, $CDCl_3$): δ 9.72 (dd, J = 8.1, 1.7 Hz, 2 H), 9.35 (dd, J = 4.7, 0.7 Hz, 2 H), 8.38 (m, 2 H), 7.96 (m, 2 H), 7.87 (dd, J = 8.12, 4.5 Hz, 2 H).

2.1.2.2 Synthesis of [Ru(dppz)(phen)(byp')]Cl_2

The route of synthesis used is outlined in figure 6-7

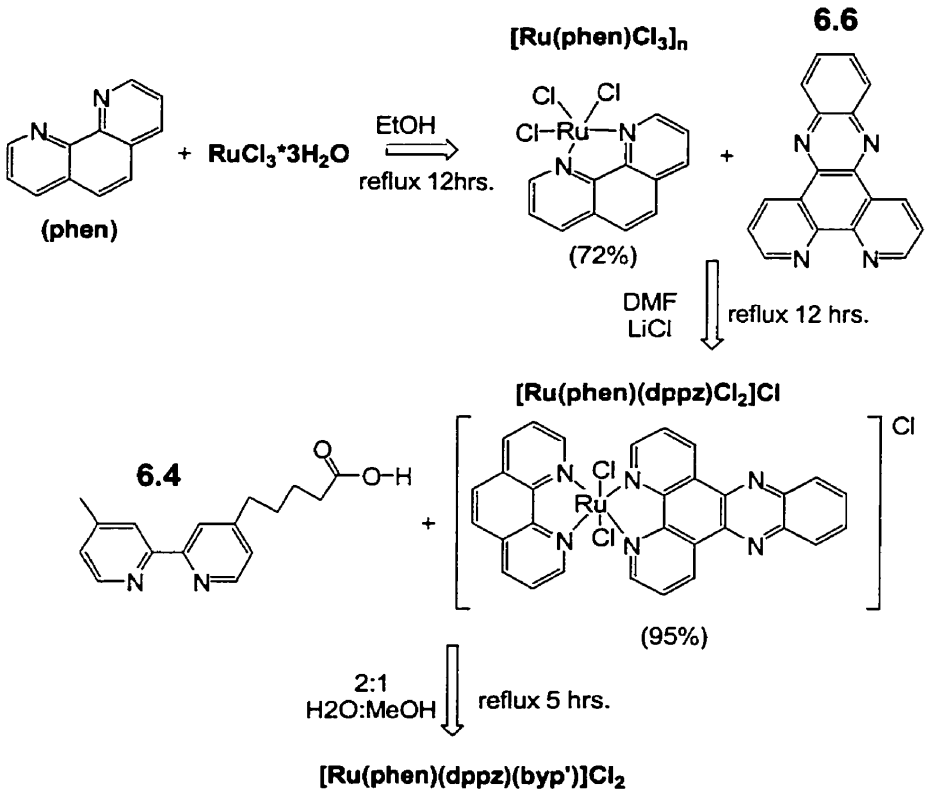

Figure 6-7. Synthetic outline for the synthesis of [Ru(dppz)(phen)(byp')]Cl_2.

2.1.2.2.1 Synthesis of $[Ru(phen)Cl_3]_n$

To 15 ml of anhydrous ethanol, 246 mg $RuCl_3 \cdot 3H_2O$ (0.940 mmole) (Pressure Chemicals) was added. The solution was heated to reflux until a green color was observed. At this point 170.9 mg phen·H_2O (0.862 mmole) dissolved in 7.5 ml anhydrous ethanol was added. The solution was allowed to continue to heat at reflux for 1 hour. After cooling the insoluble solid black mass of polymeric product if collected by centrifugation (too difficult to filter properly). Wash the insoluble pellet repeatedly with copious amounts of water, ethanol and acetone. The sample was then dried in the oven at 120°C then dried under high vacuum, resulting in 240 mg of $[Ru(phen)Cl_3]_n$ (0.620 mmole – 72% yield).

2.1.2.2.2 Synthesis of $[Ru(phen)(dppz)Cl_2]Cl$

To 3 ml DMF, 48.1 mg $[Ru(phen)Cl_3]_n$ (0.124 mmole) and 2.8 mg of LiCl are mixed. After some heating, 38.5 mg *6.6* (0.104 mmole) is added. The solution was then heated to reflux overnight. After cooling the sample was filtered to remove unreacted $[Ru(phen)Cl_3]_n$, the product was then precipitated by the addition of 13 ml acetone and placed at -20°C. The solid was collected by centrifugation and washed 2× with acetone and 1× with diethyl ether. The result was 62.7 mg of crude racemic $[Ru(phen)(dppz)Cl]Cl_2$ (95% yield). MOLDI-TOF: m/z $Ru(phen)(dppz)^{2+}$: 282.9 (calculated 281.3); $Ru(phen)(dppz)Cl^+$: 599 (calculated 599.03).

2.1.2.2.3 Synthesis of Ru(phen)(dppz)(byp) Cl_2

The synthesis of the final ruthenium(II) complex was accomplished by mixing 20.2 mg [Ru(phen)(dppz)Cl]Cl_2 (0.0318 mmole) and 17.1 mg of *6.4* (0.0633 mmole) into 3 ml H_2O: MeOH (2:1). The sample was heated to reflux. The reaction can be monitored as the insoluble reactant [Ru(phen)(dppz)Cl]Cl_2 disappears. The reaction can also be monitored and purity tested by TLC on silica plates using 1:1 200 mM NaCl: acetonitrile as solvent. The desired product has an Rf of ~0.30 and as the plate dries the orange spot should become fluorescent under long wavelength UV light, ie 366 nm. For this visualization drying is required as this compound is not fluorescent in water.

After the reaction was complete the sample is reduced in volume under vacuum. After removal of most of the methanol the sample is then made up to1 ml with water. The sample was extracted with 2× CH_2Cl_2 and 2× ether, in order to remove free ligands from solution. The sample was then loaded on a silica column and eluleted with the sample solvent as in TLC mentioned above. The fractions containing product were pooled then reduced in volume. To remove to the excess NaCl in solution two anion exchanges were done by selective precipitation, as described in section 2.1.1.2.1 for the purification of the rhodium (III) complex after column purification. The final dry product weighed 10.3 mg (35% yield). MOLDI-TOF: m/z Ru(phen)(dppz)(byp')$^{2+}$: 381.1 (calculated 381.4).

2.1.2.3 Preparation of Rutheium Labeled DNA (Ru-DNA)

The 5'-amino-DNA sequences are pre-treated as described for rhodium coupling procedure in section 2.1.1.3.

In a 0.5 ml eppendorf tube was added: 15 µl 1 mM [Ru(phen)(dppz)(byp')]Cl_2, 2.5 µl 1M MES (pH 5.75), 2.5 µl *N*-hydroxysulfosuccinimide sodium salt (25 µg/µl in H_20) and 2.5 µl of freshly dissolved EDAC (20 µg/µl in H_20). The sample was incubated at room temperature for 10-15 minutes. To the sample was added 15 µg 5'-amino-DNA as prepared above. After the addition of DNA, 2.5 µl of 50 mM $MgCl_2$ was added. The sample was then wrapped in aluminum foil and placed on a shaker overnight at room temperature.

The sample is then ethanol precipitated and rinsed 1× with 100% ethanol. The pellet is dissolved in 25 µl TE, then purified by reverse phase chromatography on a C-18 column as described above for the rhodium samples (section 2.1.1.3). After purification the samples are treated identically to that as the rhodium conjugates. The concentration of these samples can also be determined spectroscopically by determining the optical density at 440 nm (ε = 19,000) (Nunez *et al*, 1999).

2.1.3 Derivatization of DNA with Anthraquinone

To label a DNA with a 5' amino modification, with anthraquinone, we decided to directly couple an anthraquinone derivative with a carboxylic acid to a 5' amino group on the end of a C6 linker on the DNA. The coupling of anthraquinone-2-carboxylic acid (figure 6-8a) to the DNA's amino group is via peptide bond formation to give the final anthraquinone labeled DNA (AQ-DNA) as shown in figure 6-8(b).

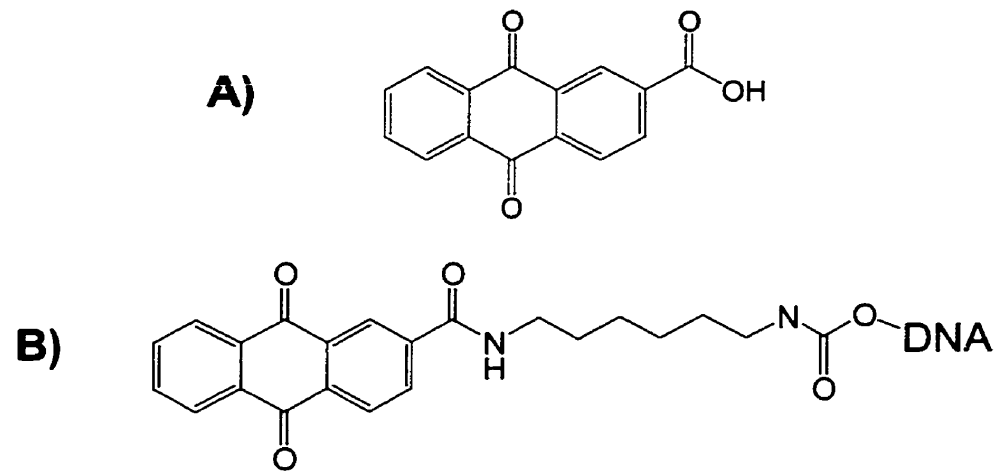

Figure 6-8. Modifying DNA with anthraquinone. a) Anthraquinone-2-carboxylic acid. B) DNA labeled to anthraquinone (AQ-DNA) through a peptide bond between the anthraquinone and a 5' amino group on a C6 linker.

2.1.3.1 Activation of Anthraquinone

To prepare anthraquinone-2-carboxylic acid for coupling to an amino group on the target DNA, it was made into the NHS ester as shown in figure 6-9. The procedure is slightly modified to that reported by Telser *et al.* (1989).

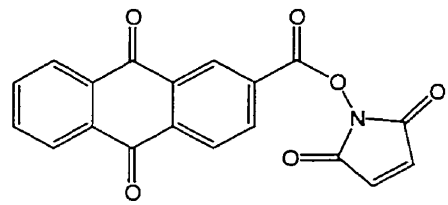

Figure 6-9. NHS ester of anthraquinone-2-carboxylic acid.

In a 50 ml round bottom flask 129 mg (0.51 mole) anthraquinone-2-carboxylic acid and 63.4 mg N-hydroxysuccinimide (NHS) (0.55 mmole) were dissolved in 8 ml dry dimethyl formamide (DMF) with stirring. The sample was cooled on an ice bath and then 114 mg 1,3-dicyclohexylcarbodiimide (DCC) (0.55 mmole) dissolved in 2 ml of dry DMF, was added drop wise with constant stirring. The solution was removed

from the ice bath and the solution was stirred at room temperature under a nitrogen atmosphere. TLC using silica gel F_{254} plates with diethylactate as solvent can monitor the reaction. The final product can be observed as a new spot with an Rf of ~0.8. After ~5 hours the reaction was completed.

The solution was then filtered to remove the dicyclohexyurea, and then the filtrate was dried under vacuum. The remaining solid was dissolved in chloroform ($CHCl_3$), filtered and allowed to crystallize by allowing $CHCl_3$ to slowly evaporate. The crude yellow crystals were collected by suction filtration and dried under vacuum, yielding 90 mg crude crystals (~0.26 mmole, 51%) of the anthraquinone NHS ester. The crystals were not further purified as the trace contaminants do not adversely affect the coupling to DNA and will be removed upon purification of the final AQ-DNA conjugate.

^{1}H NMR (400 MHz, $CDCl_3$): δ 9.08 (dd, J = 1.8, 0.5 Hz, 1 H), 8.51 (dd, J = 8.1, 1.8 Hz 1 H), 8.46 (dd, J = 8.1, 0.5 Hz, 1 H), 8.36 (m, 2 H), 7.86 (m, 2 H), 2.92 (s, 4 H).

2.1.3.2 Preparation of Anthraquinone Labeled DNA (AQ-DNA)

DNA with 5'-C6- amino label was purchased from University of Calgary Core DNA Services. Upon Arrival, the DNA is treated to remove nitrogenous contaminants from the DNA synthesis procedures as described in section 2.1.1.3 above.

The AQ-NHS ester (4.8 mg) was dissolved in 238 µl DMF. Aliquots are removed for each coupling reaction, 7 µl was added to 0.5 ml eppendorf tubes. To each sample was added 75 µl 100 mM sodium borate (pH 8.5) and 5-10 nmoles of prepared amino labeled DNA (typically 8-15 ul). The tube was covered in aluminum foil to keep

the sample dark and was placed on a shaker overnight at room temperature. The sample was then ethanol precipitated after the incubation by the addition of 27 µl 1M NaCl and 280 µl 100% EtOH. The sample was placed on dry ice and the pellet collected and washed as mentioned above. The pellet was suspended in the presence of 50 µl 100 mM triethylamine acetate and 100 µl $CHCl_3$. The uncoupled anthraquinone also precipitates and forms a large pellet. To fully suspend the DNA, the anthraquinone must be fully dissolved; this is why a two-phase solvent system was used to efficiently recover the DNA. After collecting the TEA aqueous solution, it was extracted 2× with 100 µl $CHCl_3$. The aqueous sample was then partially dried under vacuum to remove remaining chloroform. The DNA was then purified by reverse phase chromatography on an HPLC using a C18 Bondapack column (Waters).

HPLC protocols are identical to those described in section 2.1.1.3. Typical uncoupled DNA sequences have a retention time of 17 minutes, while the anthraquinone labeled DNA has a retention time of 23 minutes. Retention times vary somewhat for different sequences depending on base length. A typical elution profile is shown in figure 6-10, where absorbtion at 260 nm is seen as the major black trace and the almost background absorbtion at 334 nm is in gray.

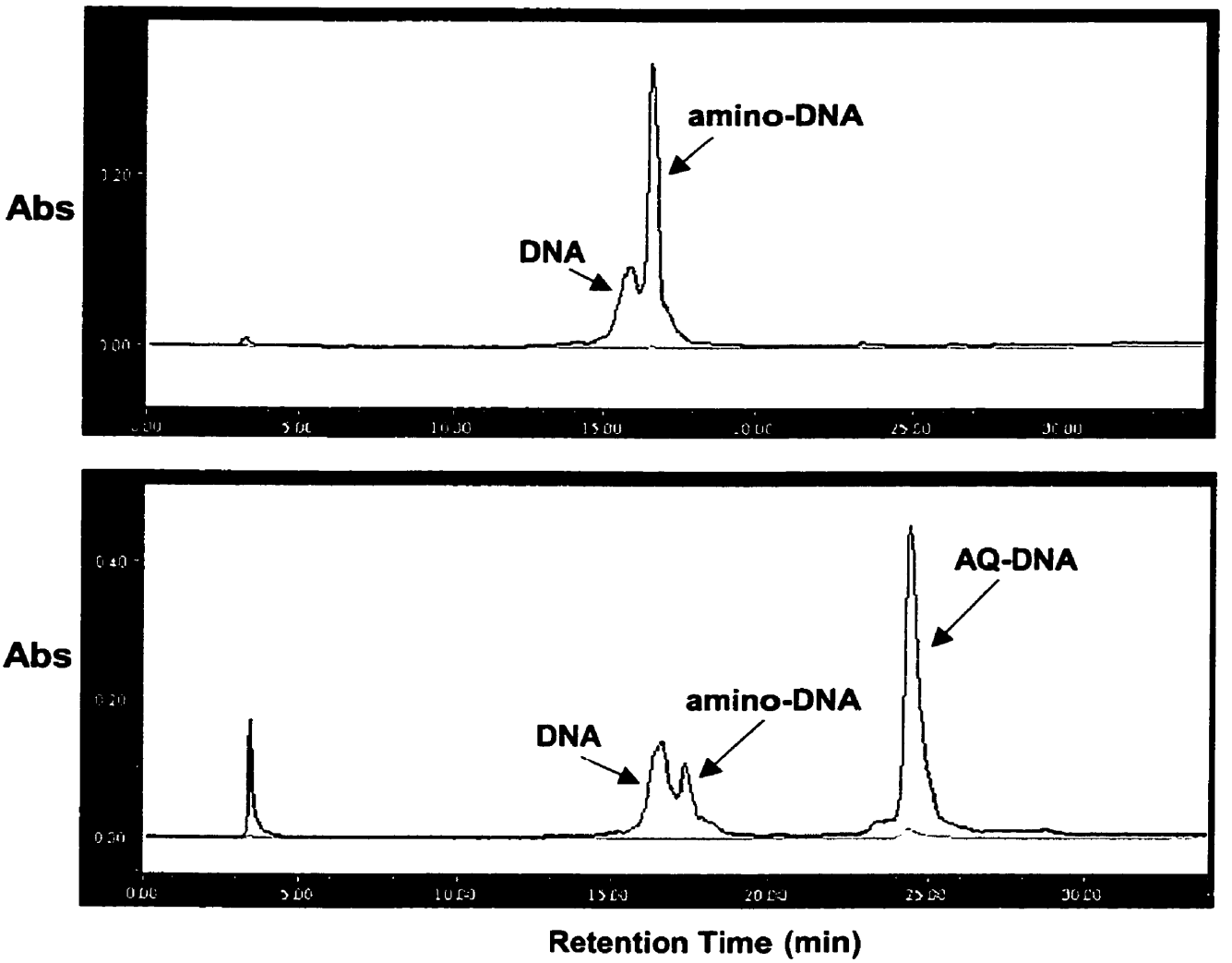

Figure 6-10. Elution profile of AQ-DNA purification monitored at 260nm and 335nm. Upper panel is DNA loaded alone as a control while lower panel is after the coupling reaction. A very minor peak at 334 nm (lower line) is observed with the coupled product (AQ-DNA), the extinction coefficient for the anthraquinone at 334 nm is less than 1% of the extinction coefficient at 260 nm for the conjugated DNA and anthraquinone. A major peak with a slightly shorter retention time than the amino-labeled DNA (amino-DNA), which remains unchanged in the two profiles is DNA that was not coupled to the C6 amino modification during synthesis (DNA).

After purification the samples are treated identically to that as the rhodium conjugates. The concentration of these samples can also be determined

spectroscopically. The absorbtion due to anthraquinone at 334 nm is too low ($\varepsilon < 4000$) to get an accurate measurement with the quantity of DNA being coupled (5-10 nmoles), so the sample is measured at 260 nm and an extinction coefficient is calculated for the conjugate using the following values for single stranded DNA ε(260 nm, $M^{-1}cm^{-1}$): adenine (A) = 15,000; guanine (G) = 12,300; cytosine (C) = 7400; thymine (T) = 6700; anthraquinone (AQ) = 29,000.

A typical yield of the AQ-DNA conjugates ranges from 50-85% depending upon the sequence and synthetic batch.

2.2 DNA Sequences

All DNA sequences used were ordered from the University of Calgary Core DNA services, which were gel purified upon arrival as described in previous chapters. (note: these sequences have been renamed from the original names used in my work. Old names are included in brackets so they can be identified in storage for individuals wishing to use these sequences)

Amino-1.2': 5'-amino-C6-AGTCTGCAGTTGAGACGCTGCTACCGGCTC
(amino-X.H')

2.3': 5'-GAGCCGGTAGCAGCGCGAGCGGTGGTTAGT
(H.Ri')

3.4': 5'-ACTAACCACCGCACGTGCAGGTTCCTTCTT
(Ri.B')

4.1': 5'-AAGAAGGAACCTGCATCTCAACTGCAGACT
(B.X')

2.1': 5'-GAGCCGGTAGCAGCGTCTCAACTGCAGACT
(H.X')

2.1'-2A: 5'- GAGCCGGTAGCAGCGAATCTCAACTGCAGACT

(H.X'-2A) –underlined bases are involved in the bulge in the bulged duplex.

A.B': 5'-AGTCTCGAACCATGCTCTCACCCACTGCTA

B.A': 5'-TAGCAGTGGGTGAGAGCATGGTTCGAGACT

2.3 Duplex and 4W-Junction Assembly

One sequence to be used in each construct is 5' end labeled with a ^{32}P-phosphate. A 100 pmole sample of the strand to be labeled is first heated at 90°C in a 100 µl piperidine solution. The sample was then dried under vacuum. The piperidine cleaves damaged and partially deprotected sequences. The DNA was then resuspended in 18 µl water then mixed with 5 µl forward reaction buffer, 1 µl T4 kinase and 1µl ^{32}P-γATP. The sample was then incubated at 37°C for 45 minutes, and then ethanol precipitated. The DNA was then purified on a 15% denaturing gel (0.5× TBE buffer). The bands are visualized by autoradiography, the gel containing the DNA is excised and passively eluted into 300 µl of 300 mM sodium acetate (pH 7.5). The DNA was finally concentrated by ethanol precipitation and suspended in 20 µl TE (10 mM Tris-Cl, pH 7.9, 0.1 mM EDTA).

A stock solution of 15 µl, containing 3 µM of each DNA (the end labeled strand is diluted with cold DNA to make a final concentration of 2.8 µM) sequence in 50 mM Tris-Cl (pH 8.0) and 50 mM NaCl, 0.1 mM EDTA was heated to 85°C for two minutes. The sample was then allowed to slowly cool to room temperature. After sitting at room temperature for at least 30 minutes, 4µl of non-denaturing loading buffer was added to the sample. The sample was then purified on a 7% non-denaturing gel (0.5× TB, 5 mM $MgCl_2$). The construct was visualized by autoradiography and the gel excised and the

DNA was eluted into a solution of 50 mM Tris-Cl (pH 7.9), 50 mM NaCl, 5 mM $MgCl_2$, 0.1 mM EDTA. The DNA was then concentrated using Microcon spin filters with a 10-kDa cutoff.

2.4 Photo-Irradiation and Guanine Oxidation Detection

DNA samples were diluted to a final concentrations of 0.3-0.5 μM DNA and 50 mM Tris-Cl (pH 7.9), 50 mM NaCl, 5 mM $MgCl_2$, 0.1 mM EDTA. Aliquots of 30 μl were placed into siliconized 500 μl eppendorf tubes and placed in a water bath at ambient temperature (either in a cold room or bench top). The samples were positioned such that they lined up directly under a handheld lamp (366nm peak wavelength) for typically 3.5 hour photo-irradiation. Various light sources (arc lamps and a nitrogen laser) have been tested as well as the use of bandpass filters (365 nm), but the best results were obtained with the small 366 nm hand held lamp and results were identical with or without filters with this light source.

After photo-irradiation, samples are precipitated by the addition of 3.5 μl 3M NaOAc (pH 7.5), 3 μl 100 mM EDTA, 2 μl 2 μg/μl glycogen, and 105 μl 100 % EtOH. The pellets were washed 2× with 70% EtOH, then resuspended in 100 μl 10% (v/v) piperidine. The samples were heated to 90°C for 30 minutes, and dried under vacuum. The samples were treated by two rounds of dissolving in 50 μl of water followed by drying under vacuum. Samples were finally dissolved in denaturing loading buffer and loaded on a 12% sequencing gel (8.4 M urea, 0.5× TBE). Gels were dried and visualized using a Molecular Dynamics Storm phosphoimager or a BioRad GS-350 phosphoimager.

3. Results and Discussion

Our objectives upon entering the field of charge transfer through DNA, were to examine the process in more complex DNA structures than in simple double helical DNA, upon which the bulk of the published work to date is based upon.

The system we originally decided on to monitor charge transfer was DNA covalently tethered with $Rh(phi)_2(byp')^{3+}$. With this rhodium compound, radical cations can be formed in the DNA by photo-irradiation at 350-390 nm (where only the rhodium complex absorbs). The determination of positions in the DNA where the charge can migrate to is performed by determining to positions where guanines form base-labile oxidized products. After synthesizing the rhodium complex and optimizing the coupling procedure, initial experiments were done to confirm we could obtain similar results with double helical DNA as has been previously reported (Hall *et al*, 1996).

Initial reproduction of the reported work was successful, where guanine oxidation could be detected along the length of duplex DNA upon photo-irradiation. When experiments were applied to DNA 4-way junctions, we observed unpredicted charge transfer down all arms of the junction (see below). After pursuing an explanation, we began to question the rhodium-based system and then decided to try another reported system where the photo-activated oxidizing agent was an anthraquinone derivative (Gasper & Schuster, 1997).

The following is a comparison of the results we observe in using the two systems while monitoring charge transfer through DNA 4-way junction, along with structural controls of double helices and double helices containing a 2 base (adenine) bulge.

3.1 Structure and Predicted Charge Transfer in 4-way junctions

As mentioned, the DNA structure of interest in this chapter for evaluating its ability to facilitate charge transfer is the immobile 4-way junction. As discussed in chapter 1), 4-way junctions adopt an 'X' like structure where the arms pair up into two co-axial stacks. With either parallel or anti-parallel 4-way junctions, each arm only has two potential pairing options for coaxial stacking. With the junction shown in figure 6-11, arm (I) can pair with either arm (II) or (IV). Reported literature on 4-way junctions has never found evidence for the stacking of the *diagonal* pairs (i.e. pairing of arms (I) & (III)). The determining factor for the preferential pairing of the helical arms is the identity of the bases at the junction. In most cases one form is energetically more favorable than the other, but in the cases where the sequences at the junction have symmetry, the two isomers form along with rapid isomerization between the two structures (Grainger *et al,* 1998; Miick *et al*, 1997). The sequences we have incorporated at the junction are known to highly prefer coaxial stacks between arms I & IV and II & III (Ducket *et al,* 1988) as shown in figure 6-11. This preferred conformation would result in a prediction that charge migration is to be observed down arms (I) and (IV) as shown by the dashed arrow in the figure.

During the course of our work, Barton's group had published a paper on immobile 4-way junctions using rhodium conjugated constructs (Odom *et al,* 2001). Their work indicates relatively identical charge migration down all four arms of the 4-way junction. Their results, which are counter intuitive to expectations, were suggested to be a result of conformational flexibility of the junction as charge transfer experiments

in double crossovers do not exhibit this promiscuity in charge transfer (Odom *et al,* 2000)

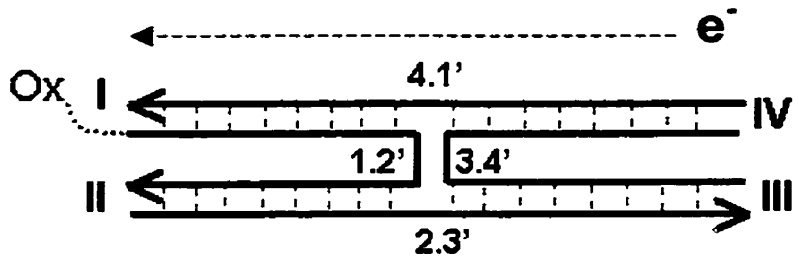

Figure 6-11. Schematic of the stacked 4-way junction tested. Ox indicates the photo-inducible oxidizing agent (either anthraquinone or $[Rh(phi)_2(byp')]^{3+}$. Double helical arms are numbered with roman numerals for reference. Positions of the single stranded DNA sequences 1.2', 2.3', 3.4' and 4.1' are indicated to show which arms of the junction they participate in.

With what is known about the conformational isomerization of 4-way junctions it is understood as mentioned above that each double helical arm can have two possible partners. In no reported cases has it been suggested that arms (I) and (III) can stack, which is an essentially 'forbidden' conformation. The only structural basis we could come up with that would allow charge transfer to arm (III) was if the rate of isomerization of the structure was on the same order of magnitude as the rate of charge transfer. In this scenario if a radical cation migrated to arm (IV) in figure 6-11, then a structural isomerization occurs such that arms (III) and (IV) stack, the radical cation could then migrate into arm (III). In essence this is possible, but all reported data suggests that charge migration is at least three orders of magnitude faster than the rate of conformational isomerization in the 4-way junction. The rate of isomerization of 4-way junctions is slow on the NMR time scale, resulting in an estimated rate of conversion to be the millisecond to second time scale. (Grainger *et al,* 1998; Miick *et al,* 1997). Even

if this occurrence is possible one would expect the magnitude of guanine damage down each duplex arm to be proportional to the extent that the junction prefers one conformation over the other.

To determine whether this phenomenon of promiscuous charge transfer was an artifact of using the rhodium conjugated complexes or was actually an indication of an unusual structure feature of 4-way junctions we continued our studies.

3.2 Assembly of Conjugated 4-Way Junctions

Before we commenced with charge transfer experiments with 4-way junction structures, we wanted to determine whether the structures could readily form with our modified sequences conjugated to either $Rh(phi)_2(byp')^{3+}$ (Rh-DNA) or anthraquinone (AQ-DNA).

Samples containing the ^{32}P-end labeled sequence 2.3' were mixed with the other sequences of the 4-way junction in a variety of combinations. These include: only the 3.4' strand; 3.4' and 4.1'; 3.4', 4.1' and AQ-1.2'; or 3.4', 4.1' and Rh-1.2' (AQ-1.2' & Rh-1.2' refer to the DNA sequences coupled to either the rhodium complex or anthraquinone). The samples were made to final concentrations of 1 μM of each strand and 1× folding buffer (50 mM Tris-Cl (pH 7.9), 50 mM NaCl, 5 mM $MgCl_2$, and 50 μM EDTA). The samples were heated to 90° C for two minutes, then allowed to slowly cool to room temperature over a 45 minute period. Aliquots of the samples (5 μl) were added to 1 μl non-denaturing-loading buffer then loaded on a 7% native gel (figure 6-12).

As can be seen in figure 6-12, every time an additional strand is added to a sample, a new, slower migrating species is formed. The observation of four distinct

species indicates that the slowest migrating species upon the addition of AQ-1.2' or Rh-1.2' incorporates all four DNA sequences. Taking Watson-Crick base pairing as the mode of association, the associated four strands will result in a 4-way junction. Similar experiments were done using an unmodified 1.2' sequence that resulted in identical results (data not shown).

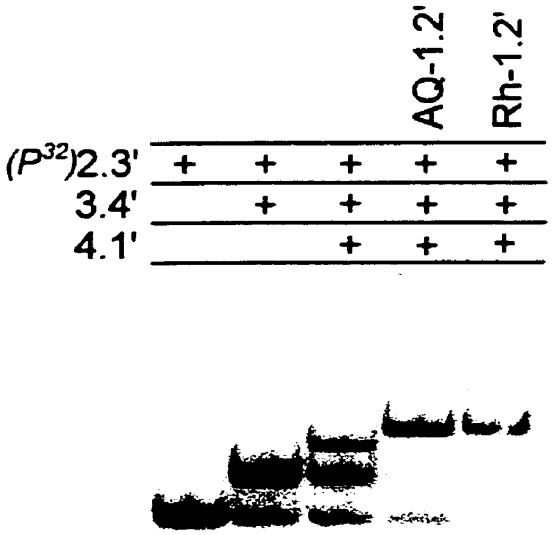

Figure 6-12. **Formation of conjugated 4W-junctions. Samples were mixed at a concentration of 1 μM of each indicated strand in folding buffer, heated to 90°C and cooled to allow annealing for 30 minutes. Samples were then loaded on a 7% non-denaturing gel (0.5×TB, 2 mM $MgCl_2$).**

3.3 Charge Through Immobile 4-Way Junctions

For experimentation to monitor charge transfer in the DNA constructs, 4-way junctions were assembled and gel purified as described in the materials and methods. Junctions containing the AQ-1.2' or Rh-1.2' strands were made that also contain either ^{32}P-end labeled 2.3' or 4.1' sequences. Using these two permutations of the location of the ^{32}P label, all four arms of the 4-way junction could be monitored. Labeled 2.3' will

detect charge migration to arms (II) and (III), while the end labeled 4.1' samples can detect charge migration in arms (I) and (IV).

Along with the above described 4-way junction samples, gel purified duplexes and duplexes containing a two base adenine bulge were formed with both Rh-1.2' or AQ-1.2' sequences, and the respective ^{32}P-end labeled 2.1' or 2.1'-2A sequences were prepared.

The gel-purified samples were photo-irradiated as described in the materials and methods at 366 nm for 210 minutes at 6-9° C. After this irradiation, samples were ethanol precipitated followed by hot piperidine treatment. Samples were then loaded on sequencing gels with appropriate ladders and dark controls. The dark controls are identically treated duplex samples that are not photo-irradiated to account for nonspecific DNA damage.

Figure 6-13 shows the results of the Rh-conjugated samples. As expected, there is observed cleavage at every guanine in the Rh-duplex, while similar cleavage is also observed in the duplex containing a 2 base adenine bulge. We originally were expecting duplexes possessing a bulge to act as a control for the effects of disrupting the base stacking of the duplex at that point. Analogous work by others (Gasper & Schuster, 1997), using duplexes with abasic sites have also observed similar results, indicating that the kink caused by the extra unpaired bases may still form a stacked structure.

As can be seen in the irradiated lanes for both the 2.3' and 4.1' 4-way junction samples, there is significant strand cleavage at all guanines with relatively similar intensities. This would suggest charge migration down all four arms of the junction as previously reported by Odom *et al,* (2001).

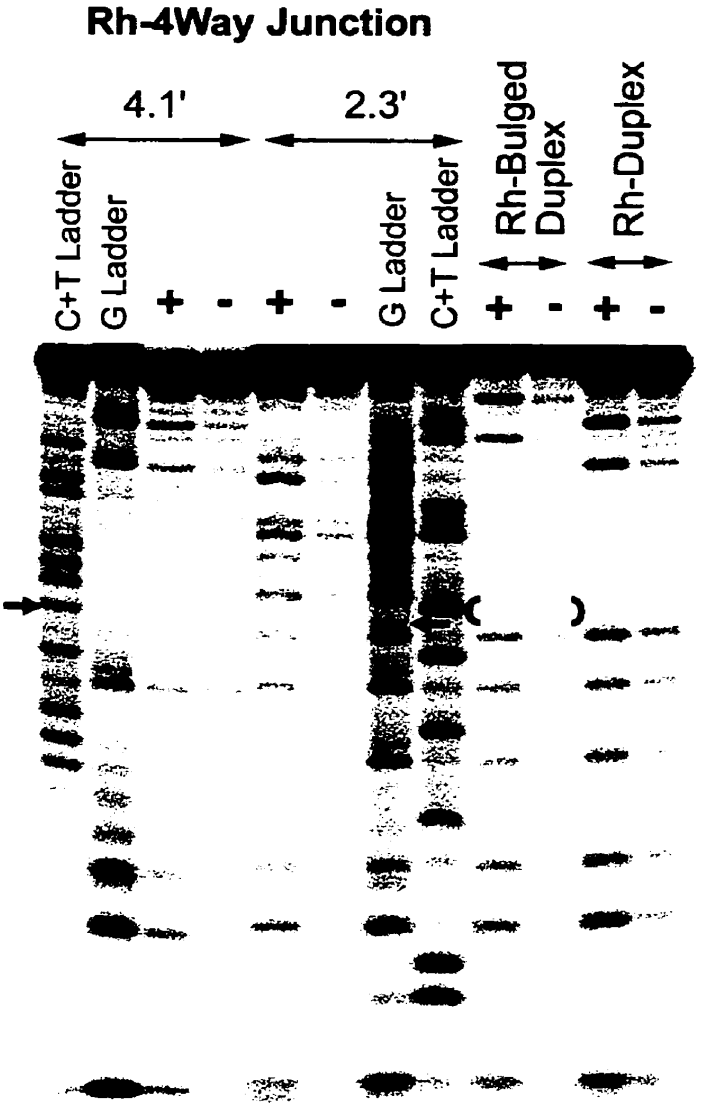

Figure 6-13. **Photo-induced guanine oxidation in rhodium conjugated DNA samples. Gel purified constructs were photo-irradiated at 366 nm for 210 minutes, (+) lanes, or left in the dark (-) lanes. Samples were then treated as described in the materials and methods and loaded on a 12% sequencing gel. Rh-duplex samples are double stranded DNA control, and the Rh-bulged duplex is the duplex containing a 2 base adenine bulge. The brackets indicate the position of the 2 extra bases. The arrows indicate the junction point in the 4-way junction on the 2.3' and 4.1' lanes.**

Significantly contrasting results are observed when the sample DNA constructs are conjugated with anthraquinone. As shown in figure 6-14, the double stranded control exhibits predicted cleavage throughout the duplex. DNA duplexes containing a bulge, also exhibits charge transfer through the entire helix indicated by the observable strand cleavage; still, a modest reduction is observed distal to the point of the double adenine bulge. The most glaringly observable difference between the Rh- and AQ-conjugated complexes is with the 4-way junction samples. When the 4.1' strand is labeled in a 4-way junction, strand cleavage is observed throughout the labeled strand. This indicates charge transfer between arms (I) and (IV) as indicated by our model in figure 6-11. When strand 2.3' is labeled in the context of the 4-way junction, no cleavage is observed anywhere along this sequence. This would suggest no charge transport occurs to arms (II) and (III). This observation fits the structural model of 4-way junctions, but is in disagreement with rhodium based results form Barton's group (Odom *et al,* 2001) and ours shown above.

To confirm this observation we performed the above-mentioned experiments again, but this time we used Rh- and AQ-4-way junctions containing 3.4' as the end labeled strand. In this case we would only expect to observe strand cleavage along the 3.4' sequence where it is involved in arm (IV) and not in the region involved in arm (III). Figure 6-15 shows the results of these experiments and the anthraquinone-conjugated samples behave as predicted as the 5' most guanine in a GG doublet located in arm (IV) exhibits reactivity.

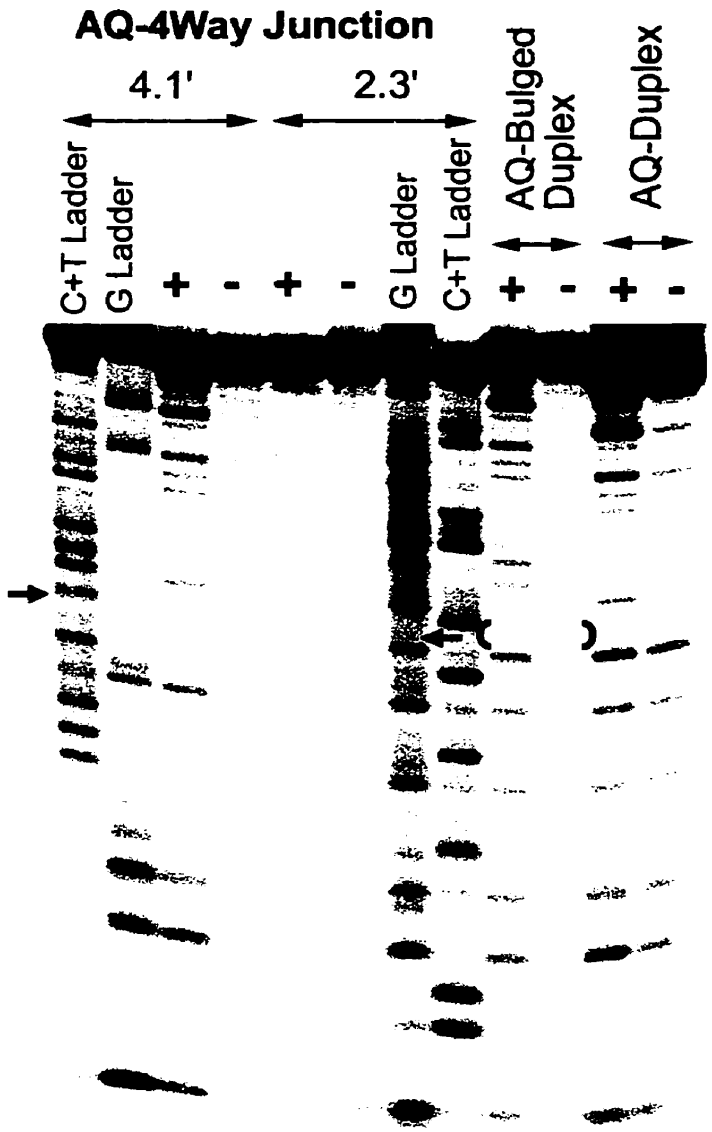

Figure 6-14. **Photo-induced guanine oxidation in anthraquinone conjugated DNA samples. Gel purified constructs were photo-irradiated at 366 nm for 210 minutes, (+) lanes, or left in the dark (-) lanes. Samples were then treated as described in the materials and methods and loaded on a 12% sequencing gel. AQ-duplex samples are double stranded DNA control, and the AQ-bulged duplex is the duplex containing a 2 base adenine bulge. The brackets indicate the position of the 2 extra bases. The arrows indicate the junction point in the 4-way junction on the 2.3' and 4.1' lanes.**

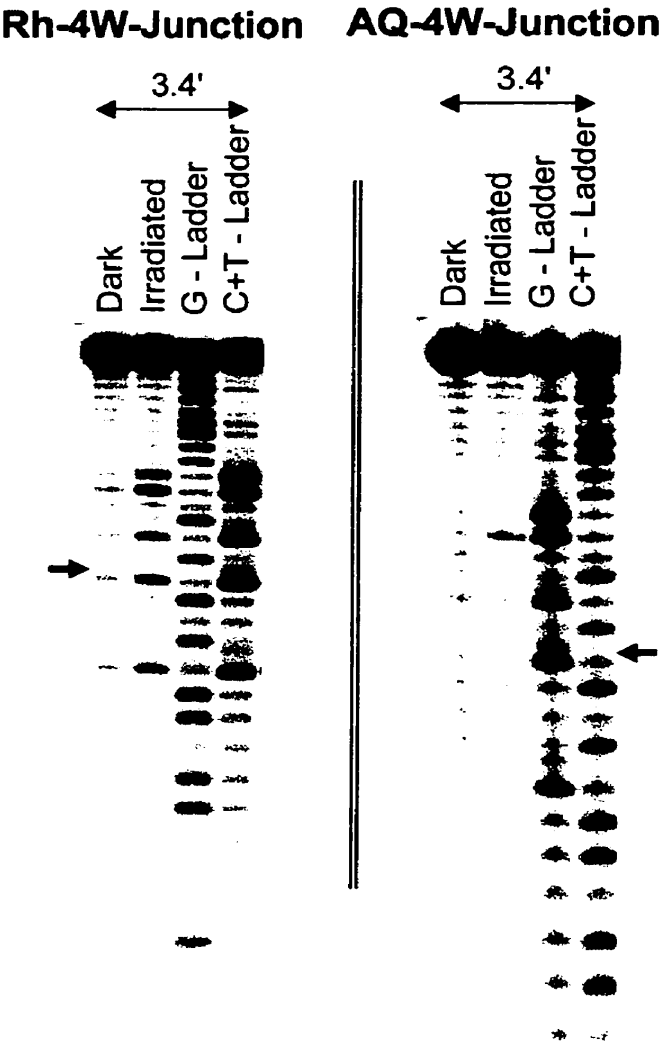

Figure 6-15. **Photo-induced guanine oxidation in the DNA strand 3.4'. Gel purified 4-way junction containing the end labeled 3.4' sequence and either Rh- or AQ-1.2', were photo-irradiated at 366 nm for 210 minutes. Lanes labeled dark are the non-irradiated dark controls. Samples were then treated as described in the materials and methods and loaded on to a 12% sequencing gels. Arrows indicate the junction point in the sequence that separates arms (III)** (lower) **and (IV)** (upper).

A summary of the observed cleavage patterns on the 4-way junction is shown in figure 6-16. Mapping the piperidine labile sites to the structure makes it obvious, that when using anthraquinone modified 4-way junctions, charge transfer is limited to arms

(I) and (IV). This is contrary to rhodium-modified junctions where cleavage is observed at all sites. This indicates an unpredicted event is occurring with the Rh-conjugated samples. We believe the Rh- samples are giving the anomalous results because the AQ- samples result in observations that concur with what is known about immobile 4-way junctions.

It can be ruled out that the radical cation can jump between the coaxial stacks because of differences in the redox potential of such cations formed by the two oxidizing agents. Once formed these radical cations should possess identical redox potentials regardless of how they were formed. Even if such radical cations could convey various potential energies, the redox potential of photo-activated anthraquinone is greater than that of the rhodium complex (2.18 eV and 1.4 -1.76 eV respectively, with value reported versus a standard carbon electrode (Armitage *et al,* 1994; Turro *et al,* 1996; Dandliker *et al,* 1998).

It has been ruled out that the tethered rhodium can intercalate into another 4-way junction molecule, because when non-radioactively labeled Rh-4-way junctions are photo-irradiated in the presence of ^{32}P-endlabeled 4-way junctions lacking a rhodium functionality, no observed strand cleavage is observed upon piperidine treatment. This observation has been made by us (data not shown) and by Barton's group (Odom *et al,* 2001).

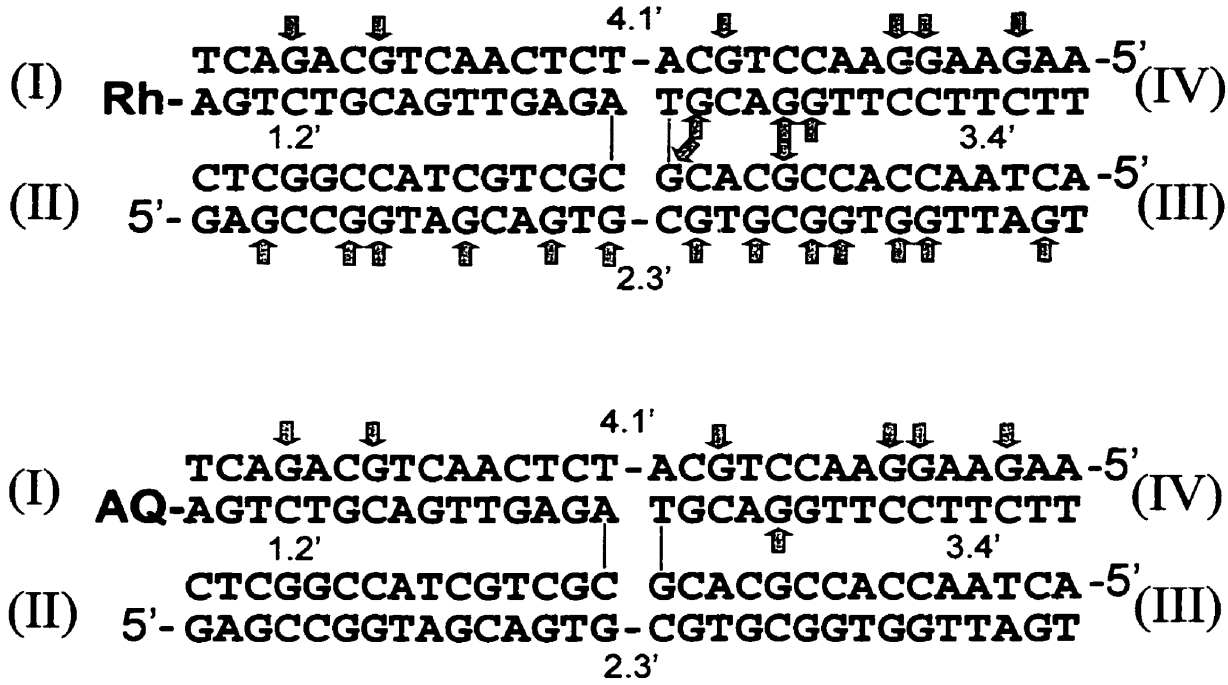

Figure 6-16. **Summary of results from charge transfer experiments with a 4-way junction. Arrows indicate sites of strand scission after photo-irradiation and hot piperidine treatment.**

3.4 Rhodium Intercalation

Another possibility we ruled out was the potential that the tethered rhodium on arm (I) could reach across the space and intercalate into arms (II) or (IV).

The $Rh(phi)_2(byp')^{3+}$ complex we have been using has the ability to cause direct DNA strand scission at the site of intercalation upon irradiation with shorter wavelength UV light (< 310 nm) (Hall *et al*, 1996). This ability to determine the intercalation site was one reason we originally chose to work with this compound.

Samples of Rh-conjugated 4-way junctions containing either 2,3', 3.4', or 4.1' ^{32}P-endlabeled sequences, along with a double stranded DNA control were prepared as described above. The samples containing ~0.4 μM DNA in 1× folding buffer were photo-irradiated with a 300 nm transilluminator through an optical filter that removes

light < 300 nm. After a 60-minute irradiation, the samples were lyophilized. The pellets were suspended in denaturing loading buffer then loaded on a 15% sequencing gel. As shown in figure 6-17, cleavage is only observed at the end of stem (I) as indicated by cleavage only observed in the 4-way junction when strand 4.1' is ^{32}P-endlabeled.

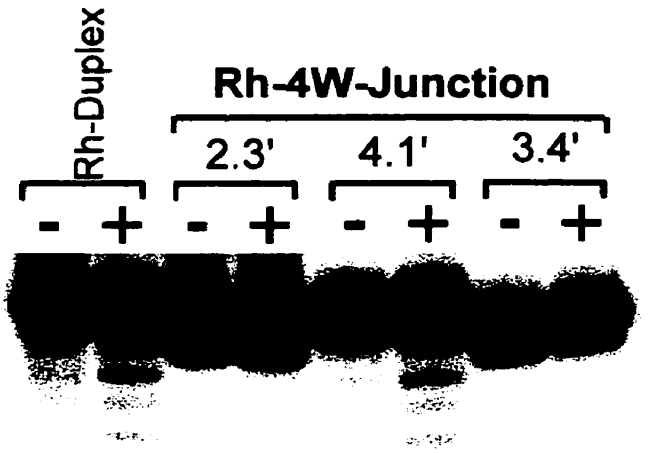

Figure 6-17. **Mapping the site of tethered rhodium intercalation. Gel purified Rh-conjugated 4-way junctions and double stranded DNA where photo-irradiated with 300-315 nm UV light for 60 minutes (+ lanes) or left untreated (- lanes). All samples where in 1× folding buffer at a concentration of 0.4 μM DNA.**

The above-mentioned observations have shed no light on the basis for the observed differences between using anthraquinone or rhodium conjugated DNA constructs. We have postulated other explanations such as the occurrence of a surface based reaction in the case of Rh- samples, as we have found that these samples are unusually 'sticky' in that they often adhere to surfaces. Further experimentation is

required to determine whether this or other processes are involved in the observed unpredictable nature of the tethered rhodium complexes.

3.6 Observations with Hexamine Cobalt

Conventional practices with immobile DNA junctions often use hexamine cobalt [$Co(NH_3)_6^{3+}$], as it is known to highly stabilize these structures (Welch *et al*, 1993; Grainger *et al*, 1998). Some initial tests were done with 4-way junction complexes that resulted in some anomalous results. I went back to examine the affect of hexamine cobalt and other salts we have on non-conjugated DNA duplexes.

Figure 6-18 demonstrates the effect of hexamine cobalt on the unmodified duplex made from sequences A.B' and B.A'. In this experiment duplexes (1 μM), in 1× folding buffer, were irradiated for 3 hours at 19° C as described in the materials and methods. As seen in the figure, the only situation where strand cleavage is observed is when DNA duplex samples are photo-irradiated in the presence of 100 μM hexamine cobalt followed by hot piperidine treatment. This treatment results in strand cleavage at three guanines within the sequence. All other combinations of conditions tested result in no observable affect to the DNA. It is noteworthy that only 5' guanines exhibit cleavage (one is the central guanine of the GGG triplet, but it is still 5' of another guanine).

No significant work has been done previously with experiments using cobalt compounds to create piperidine sensitive sites in DNA. There is some older work that describes some different cobalt(III) complexes being used to directly cleave DNA upon photo-irradiation with shorter wavelength UV light than used in this thesis to monitor

charge transport, i.e. less than 300 nm (Chang & Meares, 1982; Barton & Raphael, 1984).

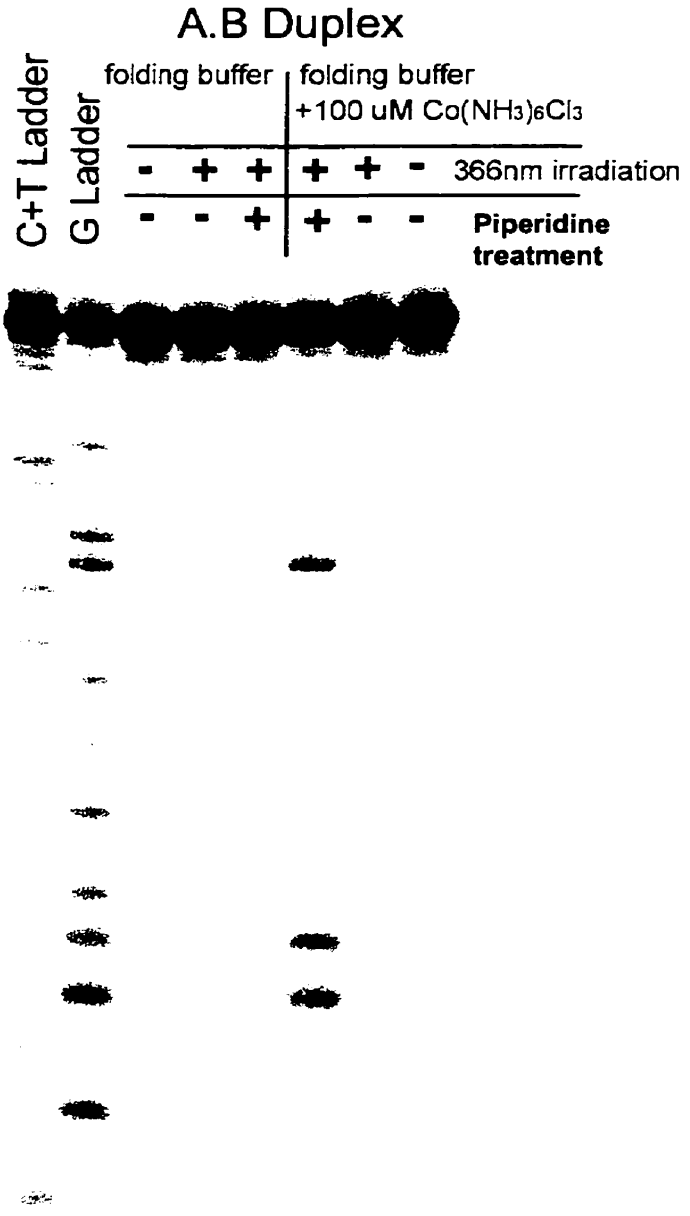

Figure 6-18. **Affect of hexamine cobalt on photo-irradiation of DNA. Samples containing 1 μM DNA in 1× folding buffer were treated as indicated then loaded on a 12 % sequencing gel.**

4. Conclusions

We have repeated the published work on charge transfer through immobile 4-way junctions as previously reported by Odom *et al* (2001). When we use DNA tethered with the organo-metallic rhodium complex, $Rh(phi)_2(byp')^{3+}$, we observe similar 'promiscuous' charge transfer down all 4 arms of the 4-way junction, as was reported. If the DNA is tethered with anthraquinone instead of the rhodium complex, contradicting results are observed. The anthraquinone based experiments result in observations that fit the known structure of DNA immobile 4-way junctions. Results using anthraquinone-conjugated DNA, indicates that the two coaxial base stacks formed between the double stranded arms of a folded 4-way junctions remain electrically uncoupled, such that they act as two non-interacting 'wires'.

This is the first report of a side-by-side comparison of the rhodium-based system to monitor charge transport by cation injection with another similar system. From our experimental data we have yet to define the process that is occurring with rhodium modified 4-way junctions, which results in experimental observations that are likely misinterpreted as long-range charge transport.

Chapter 7

DNA Based 'Electrical Switches'

1. Introduction

In chapter six we examined charge transfer through DNA junctions. These structures are relatively static in that they prefer a particular folded structure.

A question that we had since initially pursuing studies of electron transfer was whether DNA constructs could be designed that have a varying capacity for charge transfer that is modulated by some external signal. The idea arises from observations that disruptions to a double helix, such as a mismatch, reduce charge transfer efficiency (Kelly *et al,* 1997 & 1999; Giese & Wessely, 2000). It has also been shown that particular proteins that bind to double stranded DNA, disrupt base stacking, by kinking the helix and making some bases extra-helical also disrupt charge transport (Rajski *et al,* 1999; Wagenknecht *et al,* 2001). The proteins used in these studies were restriction enzymes that have been mutated, such that cleavage was inactivated but the DNA binding ability remained unaltered.

Instead of using a protein to disrupt the structure of a DNA duplex, we wanted to construct DNA structures that adopt different structures depending upon the presence of particular compounds in solution. The various structures that the DNA can adopt would be such that they either promote or inhibit charge transport. If this type of methodology proves successful it would open a new field where 'silicon chip' bound DNA 'sensors' could allow for immediate detection of particular target compounds.

1.1 Chapter Overview

This chapter presents two structural designs of DNA-'electrical switches' or 'electrical sensors' that are regulated by the presence of small molecules.

The two designs of DNA-based 'switches' we have constructed and tested are based upon a DNA aptamer that binds and recognizes adenosine and its variants (i.e. AMP, ATP etc.). Successfully demonstrating the ability to regulate charge transport by these aptamer based-'switches' would suggest that similar designs could be engineered from other aptamers targeting compounds of interest. If this is the case, devices could be developed for the rapid detection of drugs, hormones and other small molecules of medical significance.

2. Materials and Methods

2.1 Oligonucleotide Sequences.

All DNA sequences used were ordered from the University of Calgary Core DNA services and were gel purified upon arrival as described in previous chapters. The sequences used in the construction of 'switches' and control constructs are as follows:

ATP-aptamer sequences:

Amino-ATP-c: 5'-amino-C6-TTTAGCCAGGAGGAACCTTGAT

ATP-c: 5'-ATCAAGGTGGGGGATGGCTAAA

ds-ATP-c: 5'-ATCAAGGTTCCTCCTGGCTAAA

3W-aptamer sequences:

Amino-prATP2: 5'-amino-C6-AGTCTGCAGTTGAGATGGGGGATACCTTGGTAA

disATP2: 5'-TTACCAAGGTAGGAGGAAAGAGCGGTGGTTAGT

R.X': 5'-ACTAACCACCGCTCTTCTCAACTGCAGACT

Amino modified oligonucleotides were coupled to anthraquinone and purified as described in chapter 6. Rhodium complexes were not used because of the difficulties with this compound observed in chapter 6.

2.2 Aptamer Assembly

End labeled sequences were pretreated with piperidine and ^{32}P end labeled as described in chapter 6).

The DNA constructs were assembled by heating samples of constituent single stranded DNA sequences (1 μM ea) in 100 mM Tris-Cl (pH 8.0) and 100 mM NaCl, and 0.1 mM EDTA to 90°C for two minutes, then allowed to cool and anneal over a 45-minute period. The stock solution was then aliquoted to a number of tubes as required. To the aliquoted samples were added an equal volume of a 5 mM $MgCl_2$ solution containing adenosine, uridine or nothing (controls) depending on the sample being made. Final concentrations were: 0.5 μM DNA, 50 mM Tris-Cl (pH 8.0), 50 mM NaCl, 2.5 mM $MgCl_2$, 50 μM EDTA plus adenosine etc. The samples were then incubated for a minimum of 30 minutes before proceeding to photo-irradiation.

2.3 Photo-Irradiation and Detection of Oxidized Guanines

Irradiation of the samples was as described in chapter 6). After the photo-irradiation the samples where made up to 10× their original volume to a final concentration of 10% piperidine. The samples were heated to 90°C for 30 minutes, followed by drying under high vacuum. The samples were repeatedly (at least two times) suspended in 50 µl ddH_2O, then dried under vacuum. Samples were dissolved in denaturing loading buffer then loaded and resolved on a 12% denaturing gel (0.5× TBE) (note: load less than 20% of the total sample problems to avoid poor resolution of samples on the sequencing gel.) The gel was dried then visualized using a Molecular Dynamics Storm phosphoimager.

3. Results and Discussion

3.1 Electrical Switches modulated by Adenosine

The DNA structure in which we have based our designs of adenosine dependent 'switches', was the ATP-aptamer originally identified by *in vitro* selection by Huizenga & Szostack (1995). This aptamer has been shown to bind ATP, as well as adenosine and AMP analogs. Later work by Lin & Patel (1997) determined the NMR structure for the aptamer. Determination of the solution structure showed that the aptamer is a symmetrical internal loop that binds two adenosines; this point was missed in the original manuscript. A schematic for the structure is shown in figure 7-1, it has been determined that the double stranded flanking sequences are not important as long as a double helix is maintained. The basis of using the ATP-aptamer to regulate charge transfer, was that it can be accommodated in any DNA duplex sequence we wanted and like many RNA and

DNA aptamers, its binding site does not form in the absence of a ligand (see a review on RNA aptamer structures by Patel *et al,* 1997).

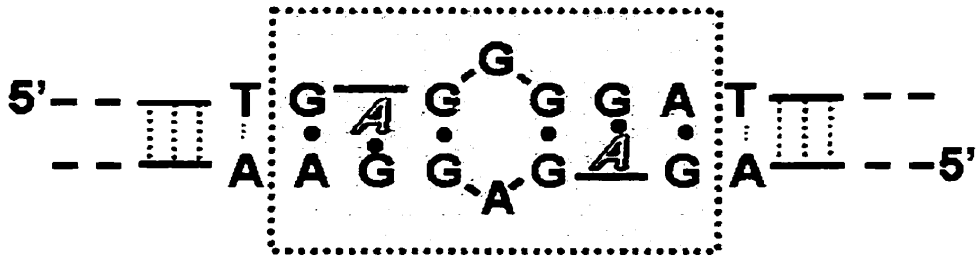

Figure 7-1. A schematic of the binding domain of the ATP aptamer. The outlined A's represent bound ATP or adenosine molecules.

3.2 A Through-Conduction Adenosine Switch

Reported work on the ATP aptamer, indicated that can be separated into two DNA strands by placing the binding domain in the context of duplex DNA as a symmetrical loop (Lin & Patel, 1997) allowed us to design the construct shown in figure 7-2. Short duplex sequences were added to either side of the aptamer domain. The first Watson and crick base pair on either side of the domain was maintained to that of the original reported sequence. The non-anthraquinone modified sequence (the one to be ^{32}P end labeled) contained two GG doublets. Each GG doublet was introduced to either side of the aptamer domain as indicator sequences for monitoring charge transfer.

The terminal duplex sequence where the anthraquinone interacts was based on the observation by Sanii & Schuster (2000) that the lack of a guanine in the first several base pairs increases the yield of distant guanine oxidation.

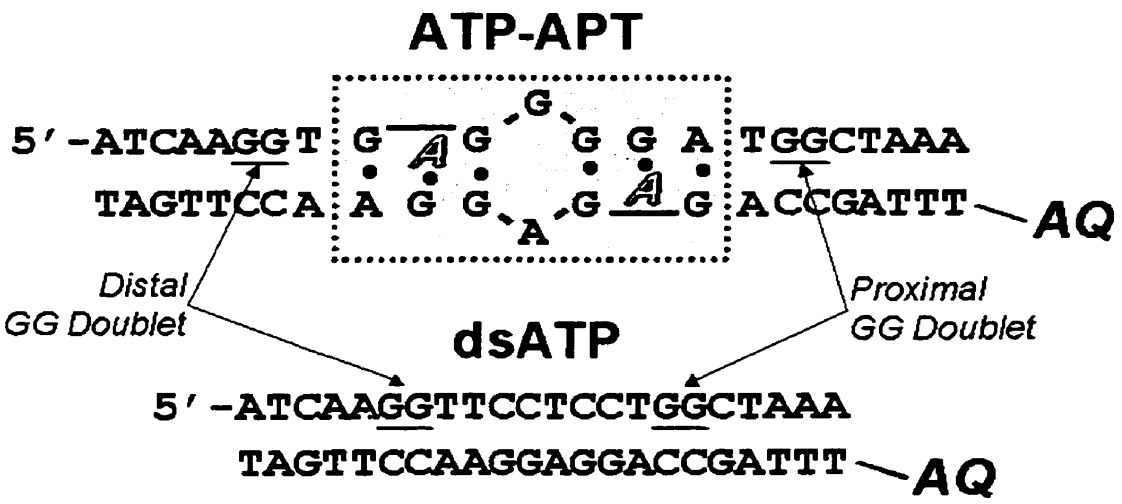

Figure 7-2. **DNA constructs used to test charge transfer through the ATP aptamer. Upper construct is the duplex containing the aptamer domain (shaded box). This construct contains GG doublets located proximally and distally relative to the aptamer domain, with respect to the linked anthraquinone (AQ). The doublets are used as indicators whether the electron hole can pass through the aptamer domain. The lower construct is the double stranded control that uses the same anthraquinone conjugated DNA sequences as the test construct.**

With this engineered ATP aptamer we hoped that the aptamer domain would exhibit a varying degree of resistance to charge transfer in response to adenosine binding. In this scenario the aptamer would in essence play the role of a ligand-dependent electrical on/off switch as depicted in figure 7-3.

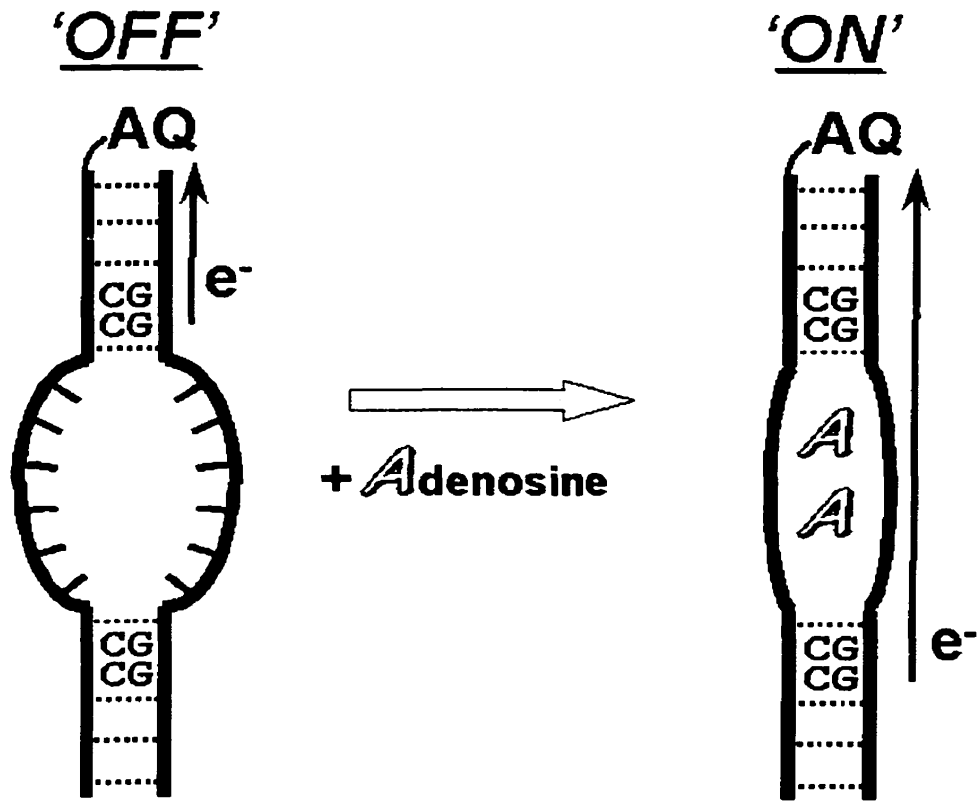

Figure 7-3. **Scheme for the modulation of charge transfer by the ATP aptamer. Upon binding of adenosine the folding of the aptamer domain is predicted to allow charge migration to occur to the distal GG doublet.**

3.2.1 Charge Transfer Modulation by Adenosine

Tests for the ability of the aptamer domain to regulate charge transfer through the DNA were done using adenosine. The original aptamer was selected to bind ATP but was also determined to tightly bind adenosine. Adenosine was chosen because of its lack of the charged phosphate groups that would otherwise bind the Mg^{2+} in solution. The use of adenosine allows the use of lower concentrations of Mg^{2+} in solution.

Figure 7-4 shows the results of experiments with both the double stranded control construct (dsATP) and the aptamer (ATP-APT). In these experiments DNA concentrations and the buffer and salt conditions were constant between all samples (1

μM DNA, 50 mM Tris-Cl (pH 7.9), 50 mM NaCl, 2.5 mM $MgCl_2$, and 50 μM EDTA). Irradiation alone induces some strand cleavage around the proximal GG pair of both DNA constructs (lane 2). This cleavage has been postulated to be the result of the formation of 8-oxoguanine, which can then undergo oxidative cleavage with further irradiation (Gasper & Schuster, 1997). Lanes 3-7 are samples after piperidine treatment. Lanes 3 show the results of dark controls, where DNA samples are treated with hot piperidine that were not photo-irradiated. These dark controls are to account for background levels of DNA damage. Lanes 4 of figure 7-4 show the result of photo-irradiated DNA constructs in the buffer solution alone. As can be seen, the dsATP control construct exhibits strand cleavage at both the proximal and distal GG pairs. In contrast to this, the ATP-APT exhibits strand cleavage at the proximal GG pair while only near background levels are observed at the proximal GG pair. This observation with the ATP-ATP construct, indicates that charge transfer can proceed down the DNA double helix that has the intimately associated anthraquinone, but the unstructured aptamer domain does not facilitate efficient charge transfer through itself.

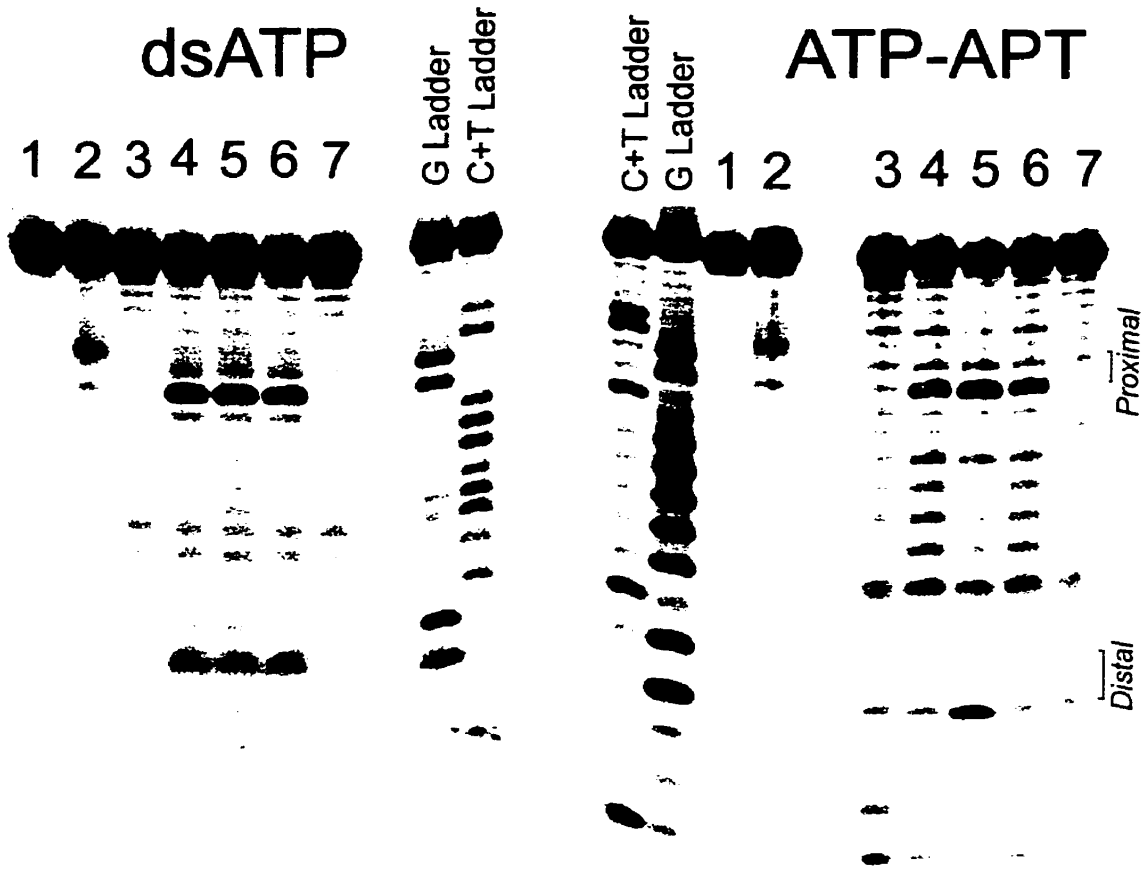

Figure 7-4. **Testing for charge transfer through ATP aptamer DNA constructs. Sequencing gels depicting sites of strand cleavage in the dsATP and ATP-APT DNA constructs. All samples contain 1 μM DNA, 50 mM Tris-Cl (pH 7.9), 50 mM NaCl, 2.5 mM $MgCl_2$, 50 μM EDTA. Lane 1 is the control untreated samples. Lanes 2 are of samples irradiated with the 366 nm lamp in the presence of 2.5 mM adenosine, but not treated with piperidine. Lanes 3 are non-irradiated dark control that has been piperidine treated. Lanes 4-7 have all been irradiated with the 366 nm lamp (45 min sdAPT, 90 min ATP-APT) followed by piperidine treatment. Lanes 4 contain no additions to the sample. Lanes 5 contain 2.5 mM adenosine. Lanes 6 contain 2.5 mM uridine. Lanes 7 are a combination of unlabeled (no ^{32}P) AQ-modified constructs (1 μM) and labeled constructs with no AQ-modification (1 μM). The mixed sample was also irradiated in the presence of 2.5 mM adenosine.**

The addition of adenosine to the sample to a final concentration of 2.5 mM causes a change to the 'conductivity' of the ATP-APT construct (lanes 5). Upon this addition photo-irradiation induces damage to the distal GG pair, suggesting that when the aptamer domain has bound the adenosine ligand, it adopts a structure that facilitates charge transfer. As expected, the addition of adenosine to the double stranded control has no effect on charge transfer in a normal DNA double helix.

To demonstrate that the observed adenosine dependent charge transfer is specific to adenosine, similar samples using uridine were tested. Lanes 6 are of samples that were photo-irradiated in the presence of 2.5 mM uridine. The two DNA constructs behave as predicted. The dsAPT control exhibits normal cleavage of the GG doublets indicating that uridine also has no affect on the process of charge transfer through a double helix. The ATP-APT construct behaves as if nothing was added; the cleavage patterns are identical to that of lane 4.

A final control was done to ensure that the observed oxidative damage to the GG doublets was from intra molecular reactions. Otherwise, observations that the anthraquinone on one DNA aptamer interacting with the bases on another DNA aptamer to result in the photo-induced oxidation of the GG doublets, would invalidate the above interpretation of the affect of the aptamer domain. Lanes 7 of figure 7-4 shows a sample containing a mixture of DNA constructs, one of which has conjugated anthraquinone but was not ^{32}P end labeled, and a second that was end labeled but did not have an anthraquinone functionality. In the case of an inter-molecular reaction, cleavage at the GG doublets would still be expected despite the labeled sequences not having anthraquinone modifications. As can be seen in lanes 7, both DNA constructs exhibit

only background amounts of strand cleavage, indicating that the process we are observing is in fact an intra-molecular reaction as originally predicted.

A difference between the experiments with the dsAPT and ATP-APT constructs was the irradiation time. The irradiation time required to get a significant amount of cleavage, while maintaining a maximum of one cleavage event per labeled strand was determined by photo-irradiation time dependence studies (data not shown). Prevention of over-cleavage ensures that samples are compared under conditions where there is a linear response (DNA damage) in relation to irradiation time.

Measured amounts of cleavage at the distal and proximal positions of both constructs are summarized in table 7-1.

	Proximal GG	Distal GG	Proximal/Distal
dsAPT	12.4%	2.9%	4.3×
ATP-APT	2.8(0.3)%	0.26(0.07)%	10.8
ATP-ATP + 2.5 mM adenosine	10.9(0.8)%	5.3(0.3)%	2.1×
(ATP-APT) Increase due to adenosine	3.9×	20.4×	

Table 7-1. Quantitative analysis of strand cleavage of dsATP and ATP-APT. Strand cleavage at proximal and distal GG doublets was measured for either 45 minute (dsAPT) or 90 minute (ATP-APT) photo-irradiation experiments under conditions described in the text. Values for ATP-APT are averages from three experiments, with errors given in brackets. Values for dsAPT are from an individual experiment.

As seen in table 7-1, the process of charge transfer appears more efficient in the dsAPT double stranded control, as it exhibits comparable amounts of cleavage with

irradiation times half that used for the ATP-ATP construct. Addition of adenosine to dsATP has no affect on levels of DNA cleavage. Examining the results for the ATP-APT construct indicates a dependence on strand cleavage for both the proximal and distal GG doublets. The observed adenosine modulation of the proximal GG doublet is likely a result of the unstructured nature of the aptamer domain in the absence of bound ligands, which could result significant dynamic motion in the region. The proximal GG doublet has a single A·T base pair separating it for the aptamer-binding domain so it is likely to experience some disruptions to base pairing as the end of the duplex 'breathes'. Being in a 'disrupted' state at some frequency would reduce the observed strand cleavage at the proximal GG doublet. A decreased reactivity of guanines near the ends of duplexes has been observed before in charge transfer experiments (Kan & Schuster, 1999).

Examination of proximal/distal cleavage ratios can be used to gain insight on the efficiency with which a charge can migrate through the intervening sequence. Comparing the ratios for dsAPT and adenosine bound ATP-APT (4.3 versus 2.1 respectively) indicates a remarkable result. Comparing these values suggests that when adenosine is bound the aptamer is as good as or better at allowing charge transfer to occur than our double stranded control.

Detectable cleavage at the distal GG double in the absence of adenosine (Table 7-1) indicates the migration of radical cations can still proceed through the 'vacant' aptamer domain. This partial 'conductivity' indicates that the aptamer does not behave as a true 'ON/OFF switch', but modulates the level of charge conduction. The increase of strand cleavage at the distal GG doublet is just over twenty-fold when 2.5 mM adenosine is present. The magnitude of regulation between the 'off' or 'high resistance' state (no

adenosine) and 'on' or 'low resistance' state (with adenosine) is adequate in providing a detectable signal. The remarkable point of this level of regulation is that this aptamer domain was never selected or designed to regulate charge transfer. By serendipity alone, the ATP aptamer can act as a modulating electrical switch. This observation holds a great deal of promise for future work in identifying DNA aptamers that regulate charge through *in vitro* selection methodologies.

3.2.2 Adenosine Dependence on Charge Transfer.

Studies were conducted to examine the concentration dependence on the oxidation of the GG doublets of the ATP-APT construct. The sensitivity of strand cleavage of both the proximal and distal GG doublets to adenosine allows the monitoring of charge transfer at both ends of the aptamer. Samples containing 1 μM ATP-APT in the standard buffer conditions described above, were irradiated for 90 minutes in the presence of varying amounts of adenosine. The titration curve in figure 7-5 shows the adenosine concentration dependence of both GG doublets. Values were corrected against a dark control. From the graph, it is observed that saturation is reached ~500 μM adenosine, indicating that the gel in figure 7-4 and the data in table 7-1 are at saturating concentrations of adenosine.

Analysis of the data indicates a different response to adenosine for the proximal and distal domains. If the data presented in figure 7-5 are used to calculate binding affinities for adenosine, concentrations of 51±9 μM and 160±30 μM adenosine result in one half maximal cleavage when monitoring the proximal or distal GG doublets respectively. The large discrepancy in values is likely the result of the aptamer binding to

two ligands. For the distal guanine doublet to be oxidized, we predict that both ligands must be bound to have a completely stacked structure to complete the 'circuit', so to speak. On the other hand, any ligand binding would promote increased guanine oxidation at the proximal guanine doublet. Upon binding one ligand, the aptamer domain would become more organized and stabilize the proximal duplex which would allow for more efficient charge transfer from the anthraquinone to proximal GG doublet.

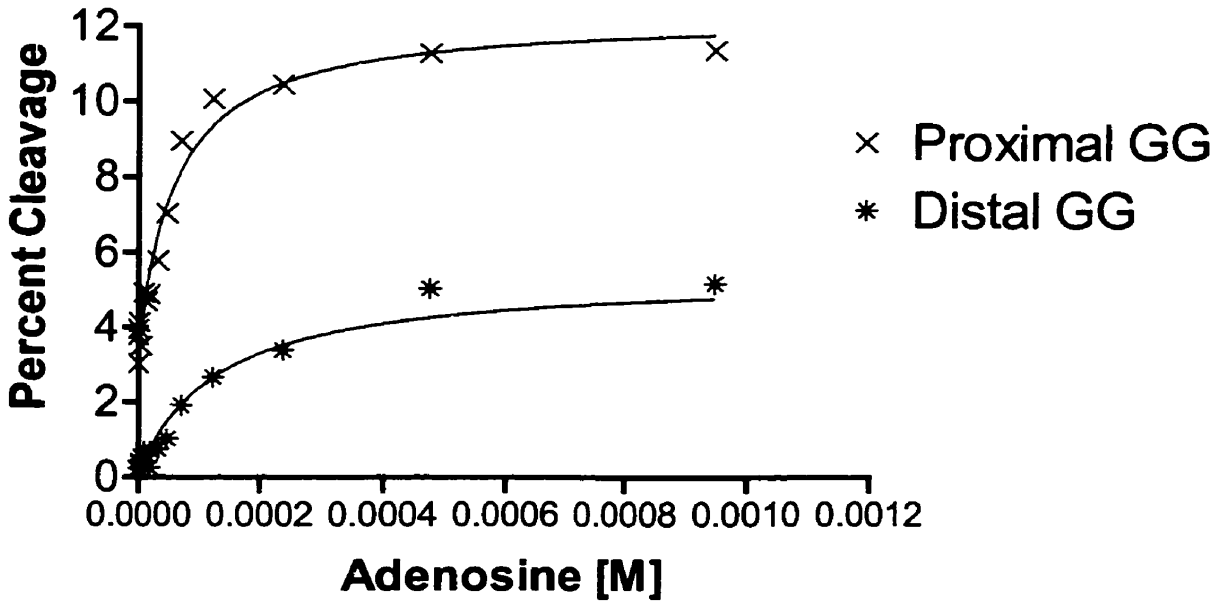

Figure 7-5. **Effects of adenosine concentration on guanine oxidation. Samples contained 1.0 µM DNA, 50 mM Tris-Cl (pH7.9), 50 mM NaCl, 2.5 mM $MgCl_2$, 50 µM EDTA. Plotted values are combined from two independent experiments. Concentrations of adenosine as high as 5 mM were tested but were omitted to allow for a less compressed view of the low adenosine concentration samples. Concentrations as high as 5 mM exhibit identical cleavage to those at 0.5 mM on the graph.**

Both adenosine concentrations determined for half maximal guanine oxidation and cleavage are significantly higher than that reported for the original ATP-aptamer.

The reported binding constant by Huizenga & Szostack (1995) was 6±3 uM for the original sequences under different buffer conditions than used here. Likely explanations for differences in affinities are the change of flanking sequences in our construct in comparison to the original aptamer, as well as difference in the buffer solutions.

A four state model in figure 7-6 is proposed for the binding of adenosine to the ATP aptamer. The aptamer has two binding sites that are denoted as A_1 and A_2 (they are within slightly different sequence contexts, but binding affinities may or may not be equivalent). Along with the fully bound and fully unbound states, exists two partially bound aptamers where either the A_1 or A_2 sites are occupied.

Effects on the proximal guanine doublet would be expected to be greater upon the occupation of site A_1 in comparison to site A_2, due to a more local influence on the structure.

The ability to simultaneously monitor the two different binding events in the ATP-aptamer was a completely unexpected observation, and may eventually lead to a way to examine some of the details of ligand binding by this aptamer. Unfortunately, due to time limitations, further examination and analysis to determine the characteristic of adenine binding where not pursued. Future work in this area may find that the process of charge transport in nucleic acids may be an invaluable tool in the examination of binding events and conformational changes of sequences of interest.

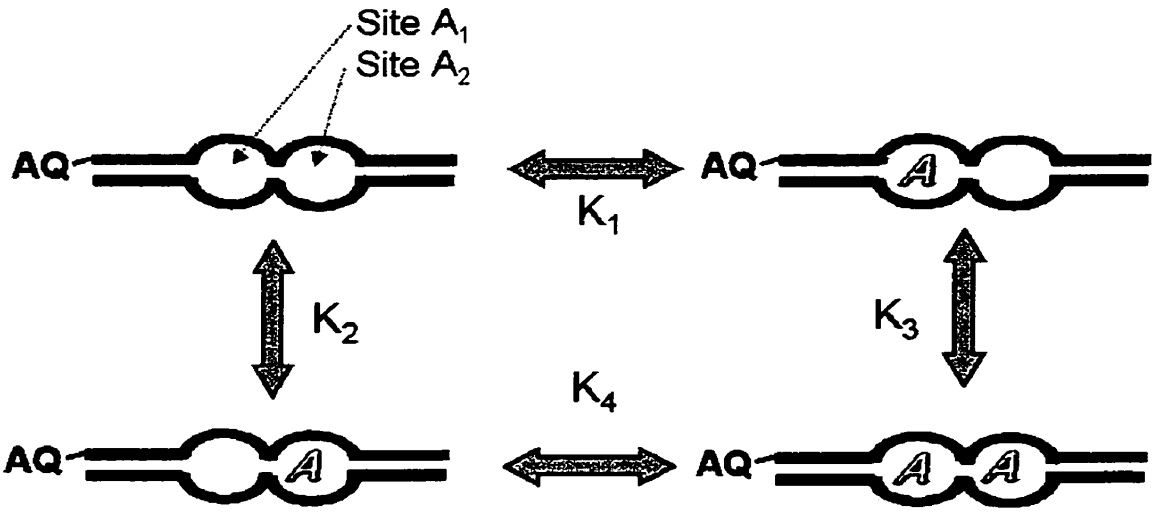

Figure 7-6. **Binding scheme for the ATP aptamer. Four binding constants are proposed because the binding affinity of site A_1 and A_2 may differ, as well there is a potential for 'positive' of 'negative' influences between the sites, i.e. does binding at one site influence the binding at the other. In the case of equal affinities for adenosine by the A_1 and A_2 sites, the scheme would be simplified with only two binding constant being observed as $K_1 = K_2$ and $K_3 = K_4$. If as well if there are no influences between the sites, then all binding would be described with a single binding constant K.**

3.3 A 3-Way Junction ATP Aptamer Switch

The above described observations that the ATP aptamer can facilitate charge transfer when bound to ligands were essentially a stroke of luck. Many aptamers cannot be used in the same fashion as we have used the ATP aptamer, this being a "through-conduction switch", as aptamers are not all formed from internal loops. The aptamers that are formed from internal loops may not form a conductive continual base stack, as with the ATP aptamer. We wished to determine whether we could develop a more universal design for electrically coupled sensors constructed from DNA.

A schematic shown in figure 7-7, shows a design of a DNA construct based upon the ATP aptamer that does not require electrical conduction through the aptamer domain. In this design the DNA has the connectivity of a 3-way junction. The aptamer is located near the junction site, such that when the aptamer binds ligands the structure collapses and a 3-way junction is formed. This type of design may be more applicable to other aptamer sequences, as it does not require the aptamer to be an electrical conductor nor is the sequence required to be an internal loop.

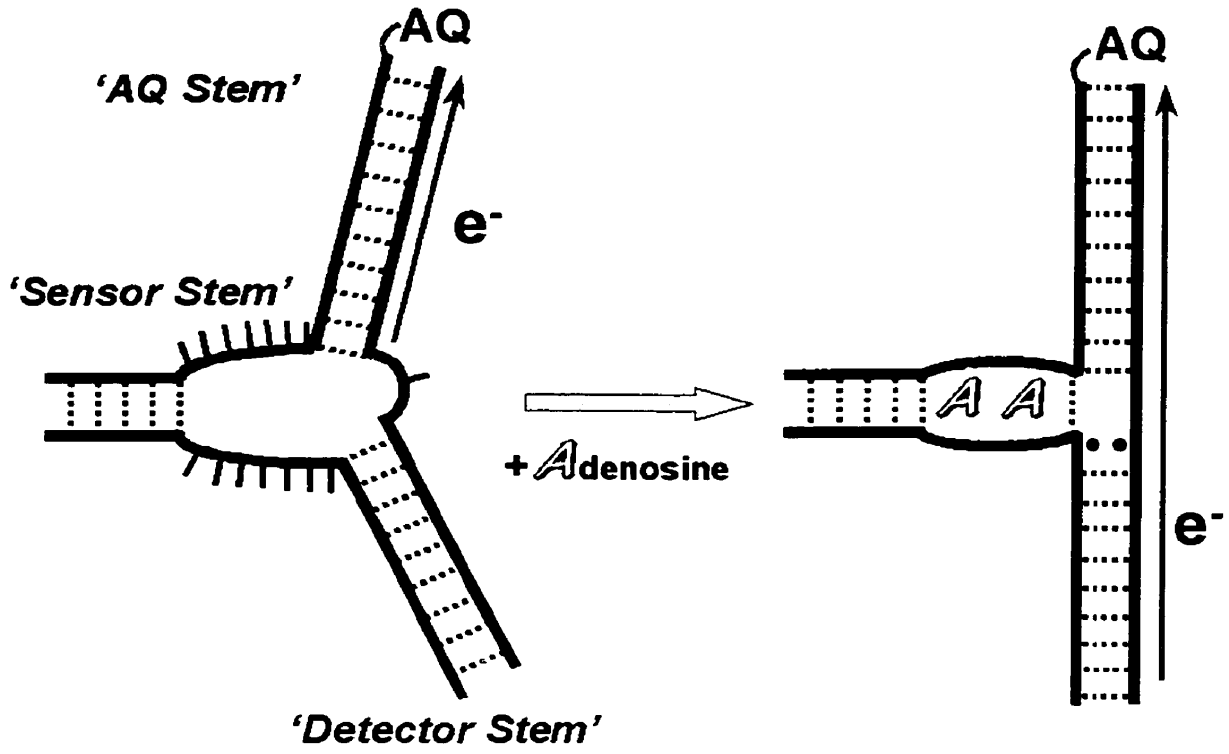

Figure 7-7. Design of a 3-Way junction ATP aptamer switch. In this design the absence of adenosine results in an open unstructured region at the core of the junction. This is predicted to result in charge transfer to occur down the AQ-stem as indicated by the arrow. The addition of adenosine is predicted to collapse the structure into a folded 3-way junction, allowing charge transfer to proceed down the detector stem. The • • indicates an A·G mismatch base pair.

3.3.1 Evaluation of Charge Transfer Regulation by the 3-Way Aptamer Construct.

As described in the materials and methods, 3W-ATP aptamer constructs were formed by annealing the three constituent DNA sequences; AQ-prATP2, disATP2, and R.X (1.0 μM ea.). The association of these three sequences is shown in figure 7-8. Samples containing the 3W-ATP aptamer were made to final concentrations of 0.5 μM DNA, 50 mM Tris-Cl (pH 7.9), 50 mM NaCl, 2.5 mM $MgCl_2$, and 50 μM EDTA. Test samples also contained 2.5 mM adenosine or 2.5 mM uridne. The prepared samples were then photo-irradiated for 3 hours at 8-10°C. In these samples, the single stranded sequence that partakes in the sensor and detector stems was ^{32}P-end labeled (strand disATP2). Following photo-irradiation samples were then ethanol precipitated, then piperidine treated as described in the materials and methods. Samples were then resolved on a 12% sequencing gel shown in figure 7-9.

As can be seen in figure 7-9, the presence of adenosine causes a significant enhancement to the reactivity of the 5' guanines in the two GG doublets located within the detector stem (G24 & G27) only in the presence of adenosine. A peculiar reactivity of an adenine (A18) also occurs in the sample containing adenosine. This adenine is in the single postulated base pair separating the ATP aptamer domain from the 3-way junction. A unique environment of the adenine at this point may allow the observed reactivity.

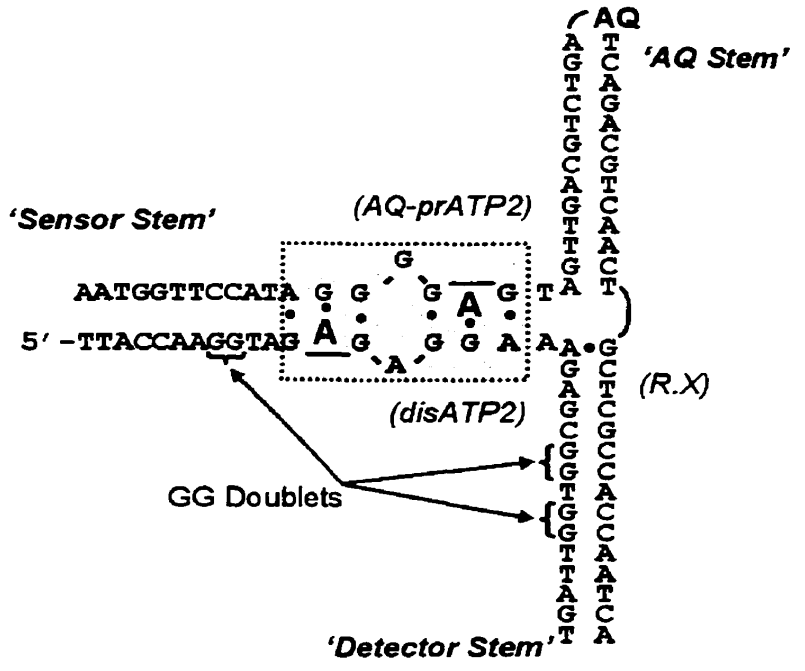

Figure 7-8. **The sequences and secondary structure of 3W-ATP aptamer. The ATP-aptamer binding domain is indicated by the shaded box. Names of the single stranded sequences are shown in brackets. Locations of the GG doublets that can be used to monitor charge transfer from the AQ stem.**

The lack of significant cleavage of the GG doublets in the control *sample (nothing added)* or the uridine-containing sample with respect to the dark control, suggests that this construct is in essence behaving as an adenosine-dependant electrical 'ON/OFF' switch. The signal in the 'on' state is significantly less than observed with the 'through-conduction adenosine switch' mentioned above, and the signal in the 'off' (no adenosine) state can be simply undetectable above background noise. With the low levels of reactivity in the control samples, an accurate/realistic measurement of the magnitude of signal modulation could not accurately be obtained.

Still, this 3W-ATP aptamer construct obviously exhibits an ability to modulate charge transfer between the two different DNA stems.

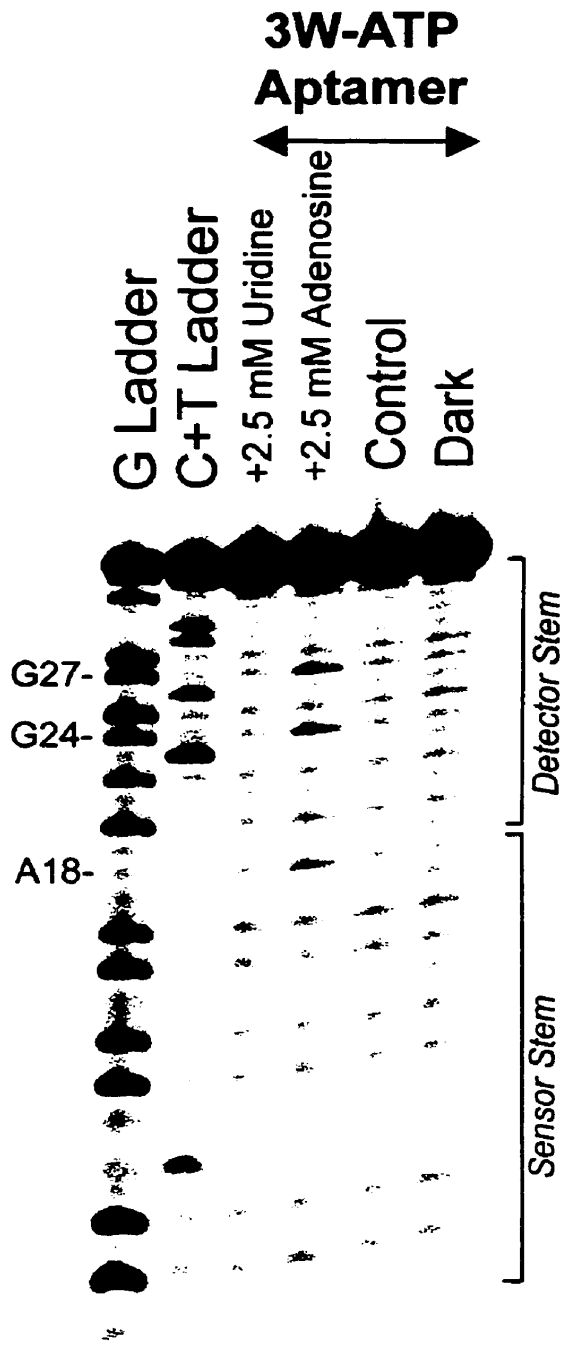

Figure 7-9. **Testing the 3-Way ATP aptamer. A 12% sequencing gel of 3W-ATP aptamer constructs piperidine treated after photo-irradiated for 210 minutes in the absence or presence of either 2.5 mM adenosine or uridine. All samples contain 0.5 μM DNA in 50 mM Tris-Cl (pH 7.9), 50 mM NaCl, 5 mM $MgCl_2$ and 50 μM EDTA.**

3.4 Future Directions

Demonstration of the capability of engineered DNA structures to modulate charge transfer by the presence of adenosine, is a proof of principle for the potential of using DNA in the development of electronic chemical sensors. As this is the first demonstration of DNA modulating an electrical signal upon 'sensing' a small target molecule, development in two key areas require significant investigation before this process may ever find practical applications.

A variety of DNA aptamer-based electrical switches or sensors will have to be constructed through rational design or *in vitro* selection. Ideally the next generation of sensors will target ligands of commercial or medical interest. Potential target ligands include various hormones, drugs, toxins, and aberrant metabolic products indicative of some physiological disorders. Development of 'electronic' DNA sensors could lead to rapid detection and diagnostic devices for medical screening.

A second aspect that also requires development, is the physical and electrical coupling of the DNA based switches to electronic surfaces *(chips)*. It is not feasible to develop methods for rapid detection using our protocols for detecting charge transfer. Ideally, one wants surface bound DNA that upon ligand binding, switches to an 'on' state. In this state, charge migration would occur through the DNA to the chip's surface. The use of appropriately designed chips would then allow for immediate detection of current flow. Currently this approach has been demonstrated for the detection of single stranded DNA and RNA, with the surface bound DNA sequence being complementary to target sequences (Kelly *et al,* 1999; Boon *et al,* 2000). In these applications the

formation of double helices facilitate charge transfer to the surface, thus allowing detection of the hybridization event.

4. Conclusions

This demonstration of modulating the process of charge transfer through DNA by the presence or absence of small molecules is a first.

We have demonstrated that through structural changes, DNA can modulate the efficiency of charge migration between two double helices. The example we used was the DNA ATP-aptamer, which folds and forms a binding pocket in the presence of an appropriate ligand (adenosine). We have successfully demonstrated application of two architectural designs that result in the modulation of charge transport upon a structural transition induced by ligand binding. This demonstration is likely applicable to the designing of other electrically coupled aptamers in the future designs of molecular sensors.

We have also made some observations that suggest a possibility that charge transfer could potentially be used as a new tool in the study of structure and function of nucleic acids.

Part V

Conclusions

If we knew what we were doing,
it wouldn't be called research, would it?
[Attributed]
- Albert Einstein, 1879-1955

Chapter 8

Conclusions

1. Synapsable DNA

The initial discovery of synapsable duplex by Venczel & Sen (1996), demonstrated the basic principles of the system, where G·G mismatches can facilitate the dimerization of DNA double helices in a cation dependent manner via the formation of G-quartets. Since this initial report, we have developed several aspects of this novel methodology for the association of double helices.

Initially our goal in exploring the potential of synapsable DNA, was to determine whether synapsable domains could be designed, such that they exhibit *self*-selectivity in mixed solutions. As described in chapter three, we were able to accomplish this task by spacing the G·G mismatches of synapsable domains into unique patterns by the incorporation of T·T mismatches as 'spacers'. We were also able to demonstrate that synapsable domains can effectively be integrated into more complex structures, while maintaining the property of *self*-selectivity. A potential problem was identified in designing some synapsable domains, structural symmetry. Strategies on how to surmount this problem have also been described in chapter three.

Beyond the accomplishments of our original goal, we have made several other key observations on the behavior of synapsable duplexes. A re-occurring structure we have seen, with long and flexible synapsable domains, is the formation of intra-molecular G- quartets, which results in a 'pinched' duplex.

The potential to form 'pinched' duplexes by some synapsable domains, results in either an inability to dimerize, or kinetically slow dimerization exhibiting an atypical

cation preference. Typically, we have perceived 'pinched' duplexes as simple kinetic traps preventing the formation of desired synapsed duplexes. We have recently begun to consider the formation of 'pinched' duplexes to be functional units unto themselves. Chapter four briefly discusses the potential of using domains incompetent in dimerization *(i.e. LMAT-3)* for cation dependent conformational changes

2. Catalytic DNA

By means of chemical probing and mutagenesis studies we have proposed a new secondary model for the cofactor independent DNAzyme, Na-8. The determination of the structure at this level as well as observations made with mutant enzymes, suggests opportunities to effectively minimize the enzyme and turn it into a true enzyme. Hopefully this newly proposed secondary structure will prove beneficial to future studies aimed at trying to determine how this enzyme catalyzes the hydrolysis of an RNA phosphodiester bond in the absence of a cofactor.

3. Charge Transfer

Of all of the work presented in this thesis, demonstration that DNA can act as 'electrical switches' is the most revolutionary. The ability to construct DNA structures that modulate the electron flow through induced conformational changes, promises enormous potential in the development of a new generation of sensors.

A typical property of nucleic acid aptamers of being 'unstructured' in the absence of ligands, suggests that our example will likely not be a rare case, as we have used this property that is shared by many of these ligand binding sequences. Opportunities to find

even better 'switches' than what can be achieved through rational design, exists as this methodology is applicable to *in vitro* selection techniques. Through *in vitro* selection, a variety structures that act as 'on'-switches or 'off'-switches, upon ligand binding may be developed.

In our work with examining charge transfer through DNA, we have found significant differences between two chemical functionalities that have been used in the literature to induce radical cation formation in DNA. The $Rh(phi)_2(byp')^{3+}$ compound exhibited some anomalous results when we examined charge transfer through immobile 4-way junctions, where guanine oxidation is detected down all four arms of the structure. This contrasted results from identical experiments when anthraquinone was used instead. We believe this contrast to be a result of some other event is occurring with the rhodium complex, which results in observations that could be misinterpreted as charge transfer, and not a result of differences in the mechanisms of charge transport. Still, we have not been able to determine the basis of the contradictory results observed.

References:

Aich, P., Labiuk, S.L., Tari, L.W., Delbaere, L.J.T., Roesler, W.J., Falk, K.J., Steer, R.P. and Lee, J.S. (1999) *M*-DNA: A complex between divalent metal ions and DNA which behaves as a molecular wire. *J. Mol. Biol.* **294**, 477-485.

Alivisatos, A.P. Johnsson, K.P., Peng, X. Wilson, T.E. Loweth, C.J. Bruchez, M.P. Jr. & Schultz, P.G. (1996) Organization of 'nanocrystal molecules using DNA. *Nature.* **382**, 609-611.

Amouyal, E. & Homsi, A. (1990) Synthesis and study of a mixed-ligand ruthenium(II) complex in its ground and excited states: Bis(2,2'-bipyridine)(dipyrido[3,2-a:2',3'-c]phenazine-N^4N^5) ruthenium (II). *J. Chem. Soc. Dalton Trans.* 1841-1845.

Aquilina, G. & Bignami, M. (2001) Mismatch repair in correction of replication errors and processing of DNA damage. *J. Cellular Physiology* **187**, 145-154.

Arkin, M.R., Stemp, E.D.A., R.E. Holmlin, Barton, J.K., Hormann, A., Olsen, E.J.C. and Barbara, P.F. (1996) Rates of DNA-mediated electron transfer between metallointercalators. *Science* **273**, 475-480.

Armitage, B., Yu, C., Devadoss, C., and Schuster, G.B. (1994) Cationic anthraquinone derivatives as catalytic DNA photonucleases: Mechanisms for DNA damage and quinone recycling. *J. Am. Chem. Soc.* **116**, 9847-9859.

Ban, N., Nissen, P., Hansen, J., Moore, P.B. & Steitz, T.A. (2000) The complete atomic structure of the large ribosomal subunit at 2.4 Å resolution. *Science* **289**, 905-920.

Barton, J.K. & Raphael, A.L. (1984) Photoactivated steriospecific cleavage of double-helical DNA by cobalt (III) complexes. *J. Am. Chem. Soc.* **106**, 2466-2468.

Basti, M.M., Stuart, J.W., Lam, A.T., Guenther, R. & Agris, P.F. (1996) Design, biological activity and NMR-solution structure of a DNA analogue of yeast $tRNA^{Phe}$ anticodon domain. *Nat. Struc. Biol.* **3**, 38-44.

Basu, S., Szewczak, A.A., Cocco, M. & Strobel, S.A. (2000) Direct detection of monovalent metal ion binding to a DNA G-quartet by ^{205}Tl NMR. *J. Am. Chem. Soc.* **122**, 3240-3241.

Behe, M. & Felsenfeld, G. (1981) Effects of methylation on a synthetic polynucleotide: The B-Z transition in poly (dG-m5dC).poly (dG-m5dC). *Proc. Natl Acad. Sci. USA* **78**, 1619-1623.

Benner, S.A., Ellington, A.P. & Tauer, A. (1989) Modern metabolism as a palimpsest of the RNA world. *Proc. Natl. Acd. Sci. USA* **86**, 7654-7656.

Bixon, M., Giese, B., Wessely, S., Langenbacher, T., Michel-Beyerle, M.E. & Jortner, J. (1999) Long-range charge hopping in DNA. *Proc. Natl. Acad. Sci. USA* **96**, 11713-11716.

Boon, E.M., Ceres, D.M., Drummond, T.G., Hill, M.G. & Barton, J.K. (2000) Mutation detection by electrocatalysis at DNA-modified electrodes. *Nature Biotech.* **18**, 1096-1100.

Borer, P.N., Pante, S.R., Kumar, A., Zanatta, N., Martin, A. Hakkinen, A. & Levy, G.C. C-13-NMR relaxation in 3 DNA oligonucleotide duplexes -- Model-free analysis of internal and overall motion. *Biochemistry* **33**, 2441-2450.

Braun, E., Eichen, Y., Sivan, U. & Ben-Yoseph, G. (1998) DNA-templated assembly and electrode attachment of a conducting silver wire. *Nature* **391**, 775-778.

Breaker, R.R. & Joyce, G.F. (1994) A DNA enzyme that cleaves RNA. *Chem. Biol.* **1**, 223-229.

Breaker, R.R. (1996) Are engineered proteins getting competition from RNA? *Curr. Opin. Biotech.* **7**, 442-448.

Breaker, R.R. (1997) DNA enzymes. *Nature Biotech.* **15**, 427-431.

Burrows, C.J. & Muller, J.G. (1998) Oxidative nucleobase modifications leading to strand scission. *Chem. Rev.* **98**, 1109-1154.

Cech, T.R. (2000) The ribosome is a ribozyme. *Science* **289**, 878-879.

Chang, C.H. & Meares, C.F. (1982) Light-induced nicking of deoxyribonucleic acid by cobalt (III) bleomycins. *Biochemistry* **21**, 6332-6334.

Chen, F.-M. (1992) Sr^{2+} facilitates intermolecular G- quadruplex formation of telomeric sequences. *Biochemistry.* **31**, 3769-3776.

Chen, F.-M. (1995) Acid-facilitated Supermolecular Assembly of G-quadruplexes in $d(CGG)_4$. *J. Biol. Chem.* **270**. 23090-23096.

Chen, J. & Seeman, N.C. (1991) Synthesis from DNA of a molecule with the connectivity of a cube. *Nature.* **350**, 631-633.

Crothers, D.M., Haran, T.E. & Nadeau, J.G. (1990) Intrinsically bent DNA. *J. Biol. Chem.* **265**, 7093-6

Cullis, P.M., Malone, M.E. & Merson-Davies, L.A. (1996) Guanine radical cations are precursors of 7,8-dihydro-8-oxo-2'-deoxyguanosine but are not precursors of immediate strand breaks in DNA. *J. Am. Chem. Soc.* **118**, 2775-2781.

Dandliker, P.J., Nunez, M.E. & Barton, J.K. (1998) Oxidative charge transfer to repair thymine dimmers and damage guanine bases in DNA assemblies containing tethered metallointercalators. *Biochemistry* **37**, 6491-6502.

Dandliker, P.J., Nunez, M.E. & Barton, J.K. (1998) Oxidative charge transfer to repair thymine dimmers and damage guanine bases in DNA assemblies containing tethered metallo intercalators. *Biochemistry* **37**, 6491-6502.

Debije, M.G., Milano, M.T. & Bernhard, W.A. (1999) DNA responds to ionizing radiation as an insulator, not as a 'molecular wire'. *Angew. Chem. Int. Ed.* **38**, 2752-2756.

Dickerson, J.E. & Summers, L.A. (1970) Derivatives of 1,10-phenanthroline-5,6-quinone. *Aust. J. Chem.* **23**, 1023-1027.

Dotse, A.K., Boone, E.K. & Schuster, G.B. (2000) Remote cis-syn thymine [2+2] dimers are not repaired by radical cations migrating in duplex DNA. *J. Am. Chem. Soc.* **122**, 6825-6833.

Duckett, D.R., Murchie, A.I.H., Diekmann, S., von Kitzing, E., Kemper, B. & Lilley, D.M. (1988) The structure of the Holliday junction, and its resolution. *Cell* **55**, 79-89.

Eley, D.D. & Spivey, D.I. (1962) Nucleic acid in the dry state. *Trans. Faraday Soc.* **58**, 411-415.

Ellington, A.D. & Szostak, J.K. (1990) *In vitro* selection of RNA molecules that bind specific ligands. *Nature* **30**, 818-822.

Fahlman, R.P. & Sen, D. (1998) Cation-regulated self-association of "Synapsable" DNA duplexes. *J. Mol. Biol.* **280**, 237-244.

Fahlman, R.P. & Sen, D. (1999) "Synapsable" DNA double helices: Self-selective modules for assembling DNA superstructures. *J. Am. Chem. Soc.* **121**, 11079-11085.

Fang, G. & Cech, T.R. (1993) Characterization of a G-quartet Formation Reaction Promoted by the beta Subunit of *Oxytricha* Telomere-binding Protein. *Biochemistry.* **32**, 11646-11657.

Faulhammer, D. & Famulok, M. (1997) Characterization and divalent metal-ion dependence of *in vitro* selected deoxyribozymes which cleave DNA/RNA chimeric oligonucleotides. *J. Mol. Biol.* **269**, 188-203.

Fink, H.W. & Schonenberger, C. (1999) Electrical conduction through DNA molecules. *Nature*, **398**, 407-410.

Fox, K.R. & Grigg, G.W. (1988) Diethylpyrocarbonate and permanganate provide evidence for an unusual DNA conformation induced by binding of the antitumor antibiotics bleomycin and phleomycin . *Nucleic Acids Res.* **16**, 2063-2075.

Friedman, A.E., Chambron, J-C., Sauvage, J-P., Turro, N.J. & Barton J.K. (1990) Molecular "light switch" for DNA: $Ru(byp)_2(dppz)^{2+}$. *J. Am. Chem. Soc.* **112**, 4960-4962.

Gasper, S.M. & Schuster, G.B. (1997) Anthraquinone linked to duplex DNA: The effect of gaps and traps on long-range radical cation migration. *J. Am. Chem. Soc.* **119**, 12762-12771.

Geyer, C.R. & Sen, D. (1997) Evidence for the metal-cofactor independence of an RNA phosphodiester-cleaving DNA enzyme. *Chem. Biol.* **4**, 579-593.

Geyer, C.R. (1998) Exploring the catalytic potential of nucleic acid enzymes. *Ph.D. Thesis.* Simon Fraser University.

Giese, B. (2000) Long-Distance charge transport in DNA: The hopping mechanism. *Acc. Chem. Res.* **33**, 631-636.

Giese, B. & Wessely, S. (2000) The influence of mismatches on long-distance charge transport through DNA. *Angew. Chem. Int. Ed.* **39**, 3490-3491.

Giese, B., Wessely, S., Spormann, M., Lindemann, U., Meggers, E. & Michel-Beyerle, M.E. (1999) On the mechanism of long-range electron transfer in DNA. *Angew. Chem. Int. Ed. Engl.* **38**, 996-998.

Gilbert, W. (1986) Origin of Life, The RNA World. *Nature* **319**, 618.

Gosh, P.K. & Spiro, T.G. (1980) Photoelectrochemistry of tris(bipyridyl)ruthenium(II) covalently attached to n-type SnO_2. *J. Am. Chem. Soc.* **102**, 5543-5549.

Grainger, R.J., Murchie, A.I.H., & Lilley, D.M.J. (1998) Exchange between stacking conformers in a four-way DNA junction. *Biochemistry* **37**, 23-32.

Gravholt, C.H., Friedrich, U., Caprani, M. & Jorgensen, A. L. (1992) Breakpoints in Robertsonian translocations are localized to satellite III DNA by fluorescence *in situ* gybridization. *Genomics*, **14**, 924-930.

Grinstaff, M.W. (1999) How do charges travel DNA? -An update on a current debate? *Agnew. Chem. Int. Ed.* **38**, 3629-3635.

Grozema, F.C., Berlin, Y.A. & Siebbeles, D.A. (2000) Mechanism of charge migration through DNA: Molecular wire behavior, single-step tunneling or hopping? *J. Am. Chem. Soc.* **122**, 10903-10909.

Guerrier-Takada, C., Gardiner, K., Marsh, T., Pace, N. & Altman, S. (1983) The RNA moiety of ribonuclease P is the catalytic subunit of the enzyme. *Cell* **35**, 849-857.

Guo, Q., Lu, M. & Kallenbach, N.R. (1992) Adenine affects the structure and stability of telomeric sequences.. *J. Biol. Chem.* **267**, 15293-15300.

Guo, Q., Lu, M., Markey, L.A. & Kallenbach, N.R. (1992) Interaction of the dye ethidium bromide with DNA containing guanine repeats.. *Biochemistry.* **31**, 2451-2455.

Hall, D.B., Holmlin, R.E. & Barton, J.K. (1996) Oxidative DNA damage through long-range electron transfer. *Nature* **382**, 731-735.

Hastie, N.D. & Allshire, R.C. (1989) Human telomeres: fusion and interstitial sites. *Trends Genet.* **5**, 326-331.

Henderson, P.T., Jones, D., Hampikian, G., Kan, Y. & Schuster, G.B. (1999) Long-distance charge transport in duplex DNA: The phonon-assisted polaron-like hopping mechanism. *Proc. Natl. Acad. Sci. U.S.A.* **96**, 8353-8358.

Herbert, A. & Rich, A. (1999) Left-handed Z-DNA: structure and function. *Genetica* **106**, 37-47.

Hiort, C., Lincoln, P. & Norden, B. (1993) DNA binding of Δ- and Λ-$[Ru(phen)_2DPPZ]^{2+}$. *J. Am. Chem. Soc.* **115**, 3448-3454.

Hoffman, T.A. & Ladik, J. (1964) *Adv. Chem. Phys.* **7**, 84-158.

Holmlin, R.E., Tong, R.T. & Barton, J.K. (1998) Long-range triplet energy transfer between metallointercalators tethered to DNA: Impotance of intercalation, stacking and distance. *J. Am. Chem. Soc.* **120**, 9724-9725.

Holmlin, R.E., Dandliker, P.J. & Barton, J.K. (1999) Synthesis of metallointercalator-DNA conjugates on a solid support. *Bioconjugate Chem.* **10**, 1122-1130.

Holliday, R. (1964) A mechanism for gene conversion in fungi. *Genet. Res.* **5**, 282-304.

Hsieh, P. & Panyutin, I.G. (1995) DNA branch migration. In *Nucleic Acids and Molecular Biology*, ed F. Eckstein, D.M.J. Lilley, **9**: 42-65. Berlin: Springer-Verlag.

Hud, N.V., Smith, F.W., Anet, F.A. &Feigon, J. (1996) The selectivity for K^+ *versus* Na^+ in DNA quadruplexes is dominated by relative free energies of hydration: a thermodynamic analysis by 1H NMR. *Biochemistry* **35**, 15383-15390.

Huizenga, D.E. & Szostack, J.W. (1995) A DNA aptamer that binds adenosine and ATP. *Biochemistry* **34**, 656-665.

Jaeger, L. & Leontis, N.B. (2000) Tecto-RNA: One dimensioal self-assembly through tertiary interactions. *Angew. Chem. Int. Ed. Engl.* **14**, 2521-2524.

Jaeger, L., Westhof, E. & Leontis, N.B. (2001) TectoRNA: Modular assembly units for the construction of RNA nano-objects. *Nucleic Acids Res.* **29**, 455-463.

Jaschke, A. & Seelig, B. (2000) Evolution of DNA and RNA as catalysts for chemical reactions. *Curr. Opin. Chem. Biol.* **4**, 257-262.

Jenkins, Y. & Barton, J.K. (1992) A sequence-specific molecular light switch: Tethering of an oligonucleotide to a dipyridophenazine complex of ruthenium (II). *J. Am. Chem. Soc.* **114**, 8736-8738.

Jeppesen, C. & Nielsen, P.E. (1988) *FEBS Letts.* **231**, 172.

Jeppesen, C. & Nielsen, P.E. (1989) Uranyl mediated photofootprinting reveals strong E. coli RNA polymerase- -DNA backbone contacts in the +10 region of the DeoP1 promoter open complex. *Nucleic Acids Res.* **17**, 4947-4956.

Johnston, W.K., Unrau, P.J., Lawrence, M.S., Glasner, M.E. & Bartel, D.P. (2001) RNA-catalyzed RNA polymerization: Accurate and general RNA-templated primer extension. *Science* **292**, 1319-1325.

Jortner, J., Bixon, M., Langenbacher, T. & Michel-Beyerle, M.E. (1998) Charge transfer and transport in DNA. *Proc. Natl. Acad. Sci. U.S.A.* **95**, 12759-12765.

Joyce, G.F. (1994) *In vitro* evolution of nucleic acids. *Curr. Opin. Struc. Biol.* **4**, 331-336)

Kan, Y. & Schuster, G.B. (1999) Long-range guanine damage in single stranded DNA: Charge transport through a duplex bridge and in a single-stranded overhang. *J. Am. Chem. Soc.* **121**, 10857-10864.

Kang, C., Zhang, X., Ratliff, R. & Moyzis, R. (1992) A rich crystal structure of 4-stranded *Oxytricha* telemetric DNA. *Nature* **356**, 126-131.

Katinka, M.D. & Bourgain, F. M. (1992) Interstitial telomeres are hotspots for illegitimate recombination with DNA molecules injected into the macronucleus of *Paramecium primaurelia. EMBO J.* **11**, 725-732.

Kelly, S.O., Holmlin, R.E., Stemp, E.D.A. & Barton, J.K. (1997) Photoinduced electron transfer in ethidium-modified DNA duplexes: Dependence on distance and base stacking. *J. Am. Chem. Soc.* **119**, 9861-9870.

Kelley, S.O., Boon, E.M. Barton, J.K. Jackson, N.M. & Hill, M.G. (1999) Single-base mismatch detection based on charge transduction through DNA. *Nucleic Acids. Res.* **27**, 4830-4837.

Khvorova, A., Kwak, Y-G., Tamkun, M., Majerfeld, I. & Yarus, M. (1999) RNAs that bind and change the permeability of phospholipid membranes. *Proc. Natl. Acad. Sci. USA* **96**, 10649-10654.

Kim, J., Cheong, C. & Moore, P.B. (1991) Tetramerization of an RNA oligonucleotide containing a GGGG sequence. *Nature,* **351**, 331-332.

Kimball,A., Guo, Q., Lu, M., Cunningham, R.P., Kallenbach, N.R., Seeman, N.C. and Tullius, T.D. (1990) Construction and analysis of parallel and antiparallel Holliday junctions. *Jour. Biol. Chem.* **265:** 6544-6547.

Kino, K. & Saito, I. (1998) Product analysis of G·G-specific photooxidation of DNA via electron transfer: 2-aminoimidazolone as a major guanine oxidation product. *J. Am. Chem. Soc.* **120**, 7373-7374.

Kinzler, K.W. & Vogelstein, B. (1990) The GL1 gene encodes a nuclear protein which binds specific sequences in the human genome. *Mol. Cell. Biol.* **10**, 634-642.

Knapp, S., Delle Karth, G., Friedl, J., Purtscher, B., Mitterbauer, G., Domer, P.H. & Jaeger, U. (1994) Guanine-rich (GGNNGG) elements at chromosomal breakpoints interact with a loop-forming, single-stranded DNA-binding protein. *Oncogene,* **9**, 1501-1505.

Kohwi-Shigematsu, T. & Kohwi, Y. (1992) Detection of non-B-DNA structures at specific sites in supercoiled plasmid DNA and chromatin with haloacetaldehyde and diethyl pyrocarbonate. *Methods Enzymol.* **212**, 155-180.

Kruger, K., Grabowski, P.J., Zaug, A.J., Sands, J., Gottschling, D.E. & Cech, T.R. (1982) Self-splicing RNA: autoexcision and autocyclization of the ribosomal RNA intervening sequences of *tetrahymena*. *Cell* **31**, 147-157.

Leontis, N.B., Kwok, W. & Newman, J.S. (1991) Stability and structure of three-way DNA junctions containing unpaired nucleotides. *Nucleic Acids Res.* **19**, 759-766.

Leontis, N.B., Hils, M.T., Piotto, M. Malhotra, A. Nussbaum, J. & Gorenstein, D.G. (1993) A model for the solution structure of a branched, three-strand DNA complex. *J. Biomol. Struct. Dyn.* **11**, 215-223.

Leontis, N.B. & Westhof, E. (2001) Geometric nomenclature and classification of RNA base pairs. *RNA* **7**, 499-512.

Lewis, F.D. Wu, T., Zhang, Y., Letsinger, R.L., Greenfield, S.R. & Wasielewski, M.R. (1997) Distance-dependent electron transfer in DNA hairpins. *Science* **277**, 673-676.

Li, Y., & Breaker, R.R. (1999) Deoxyribozymes: new players in the ancient game of biocatalysis. *Curr. Opin. Struc. Biol.* **9**, 315-323.

Li, Y., & Breaker, R.R. (1999b) Kinetics or RNA degradation by specific base catalysis of transesterification involving the 2'-hydroxyl group. *J. Am. Chem. Soc.* **121**, 5364-5372.

Lilley, D.M. (1995) Kinking of DNA and RNA by base bulges. *Proc. Natl. Acad. Sci. USA* **92**, 7140-7142.

Lin, C.H. & Patel, D.J. (1997) Structural basis of DNA folding and recognition in an AMP-DNA aptamer complex: distinct architectures but common recognition motifs for DNA and RNA aptamers complexed to AMP. *Chem. Biol.* **4**, 817-832.

Liu, F., Sha, R. & Seeman, N.C. (1999) Modifying the surface features of two-dimensional crystals. *J. Am. Chem. Soc.* **121**, 917-922.

Lorsch, J.R. & Szostak, J.W. (1996) Chances and necessity in the selection of nucleic acid catalysts. *Acc. Chem. Res.* **29**, 103-110.

Loweth, C.J., Caldwell, W.B., Peng, X., Alivisatos, A.P. & Schultz, P.G. (1999) DNA-based assembly of gold nanocrystals. *Angew. Chem. Int. Ed.* **38**, 1808-1812.

Lu, M., Guo, Q. & Kallenback, N.R. (1993) Thermodynamics of G-tetraplex formation by elomeric DNAs. *Biochemistry,* **32**, 598-601.

Ly, D., Kan, Y., Armitage, B. & Schuster, G.B. (1996) Cleavage of DNA by irradiation of substituted anthraquinones: Intercalation promotes electron transfer and efficient reaction at GG steps. *J. Am. Chem. Soc.* **118**, 8747-8748.

Mao, C., LaBean, T.H. Reif, J.H. & Seeman, N.C. (2000) Logical computation using algorithmic self-assembly of DNA triple-crossover molecules. *Nature.* **407**. 493-496.

Mao, C., Sun, W. & Seeman, N.C. (1997) Assembly of Borromean rings from DNA. *Nature* **386**, 137-138.

Mao, C., Sun, W. & Seeman, N.C. (1999) Designed two-dimensional Holliday junction arrays visualized by atomic force microscopy. *J. Am. Chem. Soc.* **121**, 5437-5443.

Mao, C., Sun, W., Shen, Z. & Seeman, N.C. (1999b) A nanomechanical device based on the B-Z transition of DNA. *Nature* **397**, 144-146.

Marsh, T. C. & Henderson, E. (1994) G-wires: Self-Assembly of Telomeric Oligonucleotide, d(GGGGTTGGGG), into Large Superstructures. *Biochemistry.* **33**. 10718-10724.

Maxim, A.M. & Gilbert, W. (1977) A new method for sequencing DNA. *Proc. Natl. Acad. Sci. U.S.A.* **74**, 560-564.

McCarthy, J.G., Williams, L.D. & Rich, A. (1990) Chemical reactivity of potassium permanganate and diethyl pyrocarbonate with B DNA: specific reactivity with short A-tracts. *Biochemistry* **29**, 6071.

Meggers, E., Kusch, D., Spichty, M., Wille, U. & Giese, B. (1998) Electron Transfer through DNA in the course of radical-induced strand cleavage. *Angew. Chem. Int. Ed. Engl.* **37**, 460-462.

Meggers, E., Michel-Beyerle, M.E. & Giese, B.J. (1998b) Sequence Dependent Long Range Hole Transport in DNA. *J. Am. Chem. Soc.* **120**, 12950-12955.

Miick, S.M., Fee, R.S., Miller, D.P. & Chazin, W.J. (1997) Crossover isomer bias is the primary sequence-dependent property of immobilized Holliday junctions. *Proc. Natl. Acad. Sci. U.S.A.* **94**, 9080-9084.

Mirkin, C.A., Letsinger, R.L., Mucic, R.C. & Storhoff, J.J. (1996) A DNA-based method for rationally assembling nanoparticles into macroscopic materials. *Nature.* **382**, 607-609.

Mitchell, G.P., Mirkin, C.A. & Letsinger, R.L. (1999) Programmed assembly of DNA functionalized Quantum Dots. *J. Am. Chem. Soc.* **121**, 8122-8123.

Mol, C.D., Parikh, S.S., Putnam, C.D., Lo, T.P. & Tainer, J.A. (1999) DNA repair mechanisms for the recognition and removal of damaged DNA bases. *Annu. Rev. Biophys. Biomol. Struct.* **28**, 101-128.

Mucic, R.C., Storhoff, J.J., Mirkin, C.A. & Letsinger, R.L. (1998) DNA-Directed synthesis of binary nanoparticle network materials. *J. Am. Chem. Soc.* **120**, 12674-12675.

Murphy, C.J., Arkin, M.R., Jenkins, Y., Ghatlia, N.D. Bossmann, S.H. Turro, N.J. and Barton, J.K. (1993) Long-range photoinduced electron transfer through a DNA helix. *Science* **262**, 1025-1029.

Murray, J.B., Seyhan, A.A., Walter, N.G., Burke, J.M. & Scott, W.G. (1998) The hammerhead, hairpin and VS ribozymes are catalytically proficient in monovalent cations alone. *Chem. Biol.* **5**, 587-595.

Nakatani, K., Dohno, C. & Saito, I. (1999) Chemistry of sequence-dependent remote guanine oxidation: photoreaction of duplex DNA containing cyanobenzophenone-substituted uridine. *J. Am. Chem. Soc.* **121**, 10854-10855.

Nakatani, K., Dohno, C. & Saito, I. (2000) Modulation of DNA-mediated hole-transport efficiency by changing superexchange electronic interactions. *J. Am. Chem. Soc.* **122**, 5893-5894.

Nissen, P., Hansen, J., Ban, N., Moore, P.B. & Steitz, T.A. (2000) The structural basis of ribosome activity in peptide bond synthesis. *Science* **289**, 920-930.

Nielsen, P. (1990) Chemical and photochemical probing of DNA complexes. *J. Mol. Recognition* **3**, 1-25.

Nuβbaumer, W., Gruber, H & Greber, G.F. (1988) Wasserphotolyse mit hilfe von funktionellen tris-(2,2'-bipyridin)ruthenium(II)-komplexon. *Monatshefte für Chemie* **119**, 1-15. *(German)*

Nunez, M.E., Hall, D.B. & Barton, J.K. (1999) Long-range oxidative damage to DNA: effects of distance and sequence. *Chem. Biol.* **6**, 85-97.

Odom, D.T., Dill, E.A. Barton, J.K. (2000) Robust charge transport in DNA double crossover assemblies. *Chem. Biol.* **7**, 475-481.

Odom, D.T., Dill, E.A. & Barton, J.K. (2001) Charge transport through DNA four-way junctions. *Nucleic Acids Res.* **29**, 2026-2033.

Ortiz-Lombardia, M., Gonzalez, A., Eritja, R., Aymami, J., Azorin, F. and Coll, M. (1999) Crystal structure of a DNA Holiday junction. *Nature Struct. Biol.* **6:** 913-917.

Park, S-J., Lazarides, A.A., Mirkin, C.A., Brazis, P.W., Kannewurf, C.R., & Letsinger, R.L. (2000) Electrical properties of gold nanoparticle assemblies linked by DNA. *Angew. Chem. Int. Ed.* **39**, 3845-3848.

Patel, D.J., Suri, A.K., Jiang, F., Jiang, L., Kumar, P.F.R.A. & Nonin, S. (1997) Structure, recognition and adaptive binding in RNA aptamer complexes. *J. Mol. Biol.* **272**, 645-664.

Porath, D., Bezryadin, A., de Vries, S. & Dekker, C. (2000) Direct measurement of electrical transport through DNA molecules. *Nature* **403**, 635-638.

Pörschke, D. & Eigen, M. (1971) Co-operative non-enzymic base recognition. *J. Mol. Biol.* **62**, 361-381.

Pyle, A.M., Chiang, M.Y. & Barton, J.K. (1990) Synthesis and characterization of physical, electronic, and photochemical aspects of 9,10-phenanthrenequinone diimine complexes of ruthenium (II) and rhodium (III). *Inorg. Chem.* **29**, 4487-4495.

Pyle, A.M. (1993) Ribozymes: a distinct class of metalloenzymes. *Science* **261**, 709-714.

Rajski, S.R., Kumar, S., Roberts, R.J. & Barton, J.K. (1999) Protein-modulated DNA electron transfer. *J. Am. Chem. Soc.* **121**, 5615-5616.

Roberts, C., Chaput, J.C. & Switzer, C. (1997) Beyond guanine quartets: cation-induced formation of homogenous and chimeric DNA tetraplexes incorporating iso-guanine and guanine. *Chem. Biol.* **4**, 899-908.

Robertson, D.L. & Joyce, G.F. (1990) Selection *in vitro* of an RNA enzyme that specifically cleaves single-stranded RNA. *Nature* **344**, 467-468.

Saito, I., Takayama, M., Sugiyama, H. & Nakatani, K. (1995) Photoinduced DNA cleavage via electron transfer: Demonstration that guanine residues located 5' to guanine are the most electron-donating sites. *J. Am. Chem. Soc.* **117**, 6406-6407.

Saito, I., Nakamura, T., Nakatani, K., Yoshioka, Y., Yamaguchi, K. & Sugiyama, H. (1998) Mapping of the hot spots for DNA damage by one-electron oxidation: efficacy of GG doublets and GGG triplets as a trap in long-range hole migration. *J. Am. Chem. Soc.* **120**, 12686-12687.

Sanii, L. & Schuster, G.B, (2000) Long-distance charge transport in DNA: Sequence-dependent radical cation injection efficiency. *J. Am. Chem. Soc.* **122**, 11545-11546.

SantaLucia, J.Jr. (1998) A unified view of polymer, dumbbell, and oligonucleotide DNA nearest-neighbor thermodynamics. *Proc. Natl. Acad. Sci. USA* **95**, 1460-1465

Sassanfar, M. & Szostack, J.W. (1993) An RNA motif that binds ATP. *Nature* **364**, 550-553.

Schleif, R. (1992) DNA looping. *Annu. Rev. Biochem.* **61**, 199-223.

Schuster, G.B. (2000) Long-Range charge transfer un DNA: Transient structural distortions control the distance dependence. *Acc. Chem. Res.* **33**, 253-260.

Schwogler, A., Burgdor, L.T., & Carell, T. (2000) Self-Repairing DNA based on a reductive electron transfer through the base stack. *Angew. Chem. Int. Ed.* **39**, 3918-3920.

Seela, F., Wei, C. & Melenewski, A. (1996) Isoguanine quartets formed by $d(T_4isoG_4T_4)$: tetraplex identification and stability. *Nucleic Acids Res.* **24**, 4940-4945.

Seelig, B. & Jaschke, A. (1999) A small catalytic RNA motif with Diels-Alderase activity. *Chem. Biol.* **6**, 167-176.

Seeman, N.C. (1982) Nucleic acid junctions and lattices. *J. Theor. Biol.* **99**, 237-247.

Seeman, N.C. (1985) Macromolecular design, nucleic acid junctions, and crystal formations. *J. Biomol. Struct. Dynam.* **3**, 11-34.

Seeman, N.C. (1998). DNA nanotechnology: Novel DNA constructions. *Annu. Rev. Biophys. Biolmol. Struct.* **27**, 225-248.

Seeman, N.C. (2000) In the nick of space: Generalized nucleic acid complementarity and DNA nanotechnology. *Synlett* **11**, 1536-1548.

Seidel, C.A.M., Schultz, A. & Sauer, M.H.M. (1996) Nucleobase-specific quenching of fluorescent dyes. 1. Nucleobase one-electron redox potentials and their correlation with static and dynamic quenching efficiencies. *J. Phys. Chem.* **100**, 5541-5553.

Sen, D. & Geyer, C.R. (1998). DNA enzymes. *Curr. Opin Chem. Biol.* **2**, 680-687.

Sen, D. & Gilbert, W. (1988) Formation of parallel four-stranded complexes by guanine-rich motifs in DNA and its implications for meiosis. *Nature* **334**, 364-366.

Sen, D. & Gilbert, W. (1990) A sodium-potassium switch in the formation of four-stranded G4-DNA. *Nature*, **344**, 410-414.

Sen, D. & Gilbert, W. (1992) Novel DNA superstructures formed by telomere-like oligomers. *Biochemistry*. **31**, 65-70.

Showalter, A.K. & Tsai, M-D. (2001) A DNA polymerase with specificity for five base pairs. *J. Am. Chem. Soc.* **123**, 1776-1777.

Simonsson, T. (2001) G-quadruplex DNA structures - Variations on a theme. *Biol. Chem.* **382**, 621-628.

Smirnov, I. & Shafer, R.H. (2000) Lead is unusually effective in sequence-specific folding of DNA. *J. Mol. Biol.* **296**, 1-5.

Soukup, G.A. & Breaker, R.R. (2000) Allosteric nucleic acid catalysts. *Curr. Opin. Struc. Biol.* **10**, 318-325.

Spassky, A. & Angelov, D. (1997) Influence of the local helical conformation on the guanine modifications generated from one-electron DNA oxidation. *Biochemistry* **36**, 6571-6576.

Steenken, S. (1997) Electron transfer in DNA? Competition by ultra-fast proton transfer? *Biol. Chem.* **378**, 1293-1297.

Steenken, S. & Jovanovic, S.V. (1997) How easily oxidizable is DNA? One-electron reduction potentials of adenosine and guanosine radicals in aqueous solution. *J. Am. Chem. Soc.* **119**, 617-618.

Stemp, D.A., Holmlin, R.A. & Barton, J.K. (2000) Electron transfer between metal complexes bound to DNA: variations in sequence, donor, and metal binding mode. *Inorg. Chim. Acta.* **297**, 88-97.

Stuhmeier, F., Welch, J.B., Murchie, A.I.H., Lilley, D.M.J. & Clegg, R.M. (1997) Global structure of three-way DNA junctions with and without additional unpaired bases: a fluorescence resonance energy transfer analysis. *Biochemistry* **36**, 13530-13538.

Suda, T., Mishima, Y., Asakura, H. & Kominami, R. (1995) Formation of a parallel-stranded DNA homoduplex by d(GGA) repeat oligonucleotides. *Nucleic Acids Res.* **23**, 3771-3777.

Sugiyama, H. & Saito, I. (1996) Theoretical studies of GC-specific photocleavage of DNA via electron transfer: Significant lowering of ionization potential and 5'localization of HOMO of stacked G bases in B-form DNA. *J. Am. Chem. Soc.* **118**, 7063-7068.

Szalai, V. & Thorp, H.H. (2000) Electron transfer in tetrads: Adjacent guanines are not hole traps in G-quartets. *J. Am. Chem. Soc.* **122**, 4524-4525.

Tarasow, T.M., Tarasow, S.L. & Eaton, B.E. (1997) RNA catalysed carbon-carbon bond formation. *Nature* **389**, 54-57.

Taton, T.A., Mirkin, C.A. & Letsinger, R.L. (2000) Scanometric DNA array detection with nanoparticle probes. *Science* **289**, 1757-1760.

Telser, J., Cruickshank, K.A., Morrison, L.E., Netzel, T.L. and Chan, K. (1989) DNA duplexes covalently labeled at two sites: Synthesis and characterization by steady-state and time resolved optical spectroscopies. *J. Am. Chem. Soc.* **111**, 7226-7232.

Tinoco, I.Jr. (1993) The RNA World. Editors Gesteland, R. F. and Atkins, J. F. Cold Spring Harbor Laboratory Press

Tirumala, S. & Davis, J.T. (1997) Self-assembling ionophores. An isoguanine-K^+ Octamer. *J. Am. Chem Soc.* **119**, 2769-2776.

Travascio, P., Bennet. A.J., Wang, D.Y. & Sen, D. (1999) A ribozyme and a catalytic DNA with peroxidase activity: Active sites versus cofactor-binding sites. *Chem. Biol.* **6**, 779-787.

Tuerk, C. & Gold, L. (1990) Systematic evolution of ligands by exponential enrichment: RNA ligands to bacteriophage T4 DNA polymerase. *Science* **249**, 505-510.

Turro, C., Evenzahav, A., Bossman, S.H., Barton, J.K. & Turro, N.J. (1996) *J. Inorg. Chem. Acta.* **243**, 101-108.

Turro, N.J., Barton, J.K. (1998) Paradigms, supermolecules, electron transfer and chemistry at a distance. What's the problem? The science or the paradigm. *J. Biol. Inorg. Hem.* **3**, 201-209.

Unrau, P.J. & Bartel, D.P. (1998) RNA catalysed nucleotide synthesis. *Nature* **395**, 260-263.

Venczel, E.A. & Sen, D. (1993) Parallel and antiparallel G-DNA structures from a complex telomeric sequence. *Biochemistry,* **32**, 6220-6228.

Venczel, E.A. & Sen, D. (1996) Synapsable DNA. *J. Mol. Biol.* **257**, 219-224.

Wagenknecht, H-A, Rajski, S.R., Pascaly, M., Stemp, E.D.A. & Barton, J.K. (2001) Direct observation of the radical intermediates in protein-dependent DNA charge transport. *J. Am. Chem. Soc.* **123**, 4400-4407.

Wang, J. (2000) From DNA biosensors to gene chips. *Nucleic Acids Res.* **28**, 3011-3016.

Wang, Y. & Patel, D.J. (1994) Solution structure of the *Tetrahymena* telomeric repeat $d(T_2G_4)_4$ G-tetraplex. *Structure* **2**, 1141-1156.

Wang, Y. & Patel, D.J. (1995) Solution structure of the *Oxytricha* telomeric repeat $d[G_4(T_4G_4)_3]$ G-tetraplex. *J. Mol. Biol.* **251**, 76-94.

Watson, J.D. & Crick, F.H.C. (1953) A structure for deoxyribose nucleic acid. *Nature* **171**, 737-738.

Welch, J.B., Duckett, D. & Lilley, D.M.J. (1993) Structures of bulged three-way junctions. *Nucleic Acids Res.* **21**, 4548-4555.

Welch, J.B., Walter, F. & Lilley, D.M. (1995) Two inequivalent folding isomers of the three-way DNA junction with unpaired bases: Sequence-dependence of the folded conformation. *J. Mol. Biol.* **251**, 507-519.

Wellinger, R. & Sen, D. (1997) The DNA structures at the ends of eukaryotic chromosomes. *Eur. J. Cancer,* **33**, 735-749.

White, H.B. III (1976) Coenzymes as fossils of an earlier metabolic state. *J. Mol. Evol.* **7**, 101-104.

Williams, T.T., Odem, D.T. & Barton, J.K. (2000) Variations in DNA charge transport with nucleotide composition and sequence. *J. Am. Chem. Soc.* **122**, 9048-9049.

Williamson, J.R. (1994) G-quartet structures in telomeric DNA. *Annu. Rev. Biophys. Biomol. Struct.* **23**, 703-730.

Williamson, J.R., Raghuraman, M.K. & Cech, T.C. (1989) Monovalent cation-induced structure of telomeric DNA: The G-quartet model. *Cell* **59**, 871-880.

Wilson, C. & Szostack, J.W. (1995) *In vitro* evolution of a self-alkylating ribozyme. *Nature* **374**, 777-782.

Wilson, E.K. (1997) DNA: Insulator or wire? *C&EN* Feb.24 33-39.

Winfree, E., Liu, F., Wenzler, L.A. & Seeman, N.C. (1998) Design and self-assembly of two-dimensional DNA crystals. *Nature.* **394**, 539-544.

Yarus, M. (1993) How many catalytic RNAs? Ions and the Cheshire Cat conjecture. *FASEB* **7**, 31-39.

Zhang, Y. & Seeman, N.C. (1994) The construction of a DNA truncated octahedron. *J. Am. Chem. Soc.* **116**, 1661-1669.